UC Santa Cruz

UC Santa Cruz Electronic Theses and Dissertations

Title

New Perspectives on the Composition and Cycling of Dissolved Organic Carbon and Nitrogen in the Ocean

Permalink

https://escholarship.org/uc/item/9793s6hj

Author

Broek, Taylor Alexander Borrius

Publication Date

2019

Peer reviewed|Thesis/dissertation

eScholarship.org Powered by the California Digital Library
University of California

UNIVERSITY OF CALIFORNIA
SANTA CRUZ

New Perspectives on the Composition and Cycling of Dissolved Organic Carbon and Nitrogen in the Ocean

A dissertation submitted in partial satisfaction
of the requirements for the degree of

DOCTOR OF PHILOSOPHY

in

OCEAN SCIENCES

by

Taylor A. B. Broek

March 2019

The dissertation of Taylor Broek is approved:

_____
Professor Matthew D. McCarthy, chair

_____
Adjunct Professor Thomas P. Guilderson

_____
Associate Professor Phoebe J. Lam

_____
Assistant Professor Brett D. Walker

_____
Lori Kletzer
Vice Provost and Dean of Graduate Studies

Copyright © by

Taylor A. B. Broek

2019

Table of Contents

List of Figures

List of Tables

Abstract

New Perspectives on the Composition and Cycling of Dissolved Organic Carbon and Nitrogen in the Ocean

Taylor A. B. Broek

Marine dissolved organic matter (DOM) is the largest pool of actively cycling organic carbon and nitrogen in the ocean. The amount of carbon in this pool is comparable to atmospheric CO_2 and represents a major capacitor in the global carbon cycle. However, despite the importance of DOM in biogeochemical cycles, our understanding of its composition and cycling dynamics is limited. This is in part due to the difficulty of isolating DOM for subsequent study, as well as the inherent selectivity of different isolation methods. Here we present a new approach to DOM isolation via a sequential combination of ultrafiltration and solid phase extraction. This approach allowed us to selectively isolate two fractions of material with different average molecular size and significantly different compositions and reactivities. By limiting the influence of reactivity mixtures, we were able to more directly investigate the composition and cycling dynamics of both labile and refractory DOM.

DOM fractions were isolated from four depths (surface, 400 m, 850 m, and 2500 m) in both the North Central Atlantic and North Pacific Subtropical Gyre. Measurements of a number of bulk isotopic ($\Delta^{14}C$, $\delta^{13}C$, $\delta^{15}N$) and compositional (C/N ratio, solid-state cross polarization ^{13}C and ^{15}N NMR) parameters confirmed the uniqueness of the two DOM fractions. The high molecular weight (HMW) fraction had younger average ages, was nitrogen rich, and was dominated by carbohydrate-like and protein-like molecules, consistent with more labile material. In contrast, the

low molecular weight (LMW) fraction had older average ages, was carbon rich, and was dominated by alicyclic carbon and heterocyclic nitrogen containing molecules, consistent with more refractory material. An investigation of the offsets in measured properties between ocean basins yielded a number of novel observations including the removal of refractory DOM and additions of fresh DOM to the deep ocean.

Our understanding of the composition and cycling dynamics of the nitrogen-containing fraction of DOM (DON) is even more limited. Spectroscopic evidence has shown that the composition of DON in the ocean is dominated by amide nitrogen, consistent with labile proteinaceous and biopolymeric material. Despite this, the significant concentrations of DON in both the biologically active and often nitrogen-limited surface ocean as well as the deep sea suggest that a large fraction of DON is resistant to degradation. However, the paradigm of a dominant labile, amide containing composition of DON is based on measurements of HMW DON alone. Measurements of isotopic ($\delta^{15}N$, amino acid $\Delta^{14}C$) and compositional (solid-state cross polarization ^{15}N NMR, amino acid D/L enantiomeric ratio) parameters of nitrogen-containing material in the LMW fraction collected for this study provided a new perspective on the composition and cycling of DON in the ocean. Amino acids within the LMW fraction had both old radiocarbon ages and high D/L ratios, suggesting that there is a bacterial mechanism capable of preserving proteinaceous material on millennial timescales. Further, NMR and nitrogen isotopic data demonstrated that LMW DON, representing a majority of the marine DON pool, is dominated by heterocyclic nitrogen-containing compounds, commonly understood to be present in intrinsically refractory molecular structures. These observations present

a new paradigm for the composition of marine DON and suggest a likely explanation for its long-term persistence in the ocean.

Dedication

~ For Mom ~

Acknowledgements

To Matt. I don't have the words to express my gratitude. Beyond the wisdom he has imparted and the experiences he has provided, I really owe it all to him. There is no way I would ever be Dr. Broek without him. He took a chance on a B- student. Someone who never liked school. Who was never very good at it. A former film major who broke down when he figured out he was going to spend more time writing about films than making them. Someone who wanted to drop out and find something else to do. Someone who managed to skate by on the fact that chemistry made sense to him.

A few years after he first took that chance on me, after finishing my Masters, Matt had seen enough that he wanted to keep me around. He needed funding if it was going to happen. The night before the NSF proposal was due that would eventually make that a reality, I got blasted by a 23-year-old in a Toyota Tacoma who had a few too many beers. A couple broken bones and a nasty concussion later, I was thrown into this thing. This beast of an undertaking that no one can fully understand until they are in it. Six years later, the night after I defended this degree, in some sort of freak accident that I still can't quite understand, my dog managed to head butt me hard enough to break my nose and rattle my brain again. It seems appropriate, somehow, that my PhD was bookended by head trauma, because it was a total blur. In the acknowledgments of *his* dissertation, Matt attempted to define what getting a PhD actually is, which out of a lack of creativity as I sit here writing this, combined with sleep deprivation and the mild brain trauma, I will quote directly: *"A PhD dissertation, at least in our field, is an odd thing. It is in part education, in part a job,*

at times more like purgatory. It grants you wide freedoms but limited direction, very limited pay, few milestones, and for the most part no ending point ever in sight. It blurs together the personal and professional for a long time in a way that likely never occurs again." That really stuck with me when I first read it a few years ago because I was deep into that purgatory, with no end in sight. Except here it is, the light at the end of the tunnel, hours away from emerging, mostly unscathed, as a completely different person. All thanks to that chance that Matt took and his continued belief in me.

However, it is the last part of that quote that I am focused on now. Because a lot of the people who helped me along the way were technically my co-workers, but that sure isn't how I will remember them. I am eternally grateful to everyone who made this a reality.

To Joe and Danielle. Who were the perfect friends for this journey. The distraction I so desperately needed.

To Tom. Who created opportunities and opened doors that have and will continue to change my life forever.

To Brett. Who embodied that blurring of professional and personal, providing a friend and colleague who I trusted. That I could look up to and learn from.

To Jessie. Who was my right hand during the cruise campaigns, plus my left hand, and at least one of my legs.

To Yamindira. Who maintained my sanity. There are the people who help you along the way and then there are the people who you literally couldn't do it without. I told someone once that if I deserve a PhD in oceanography, I should at least be

awarded an honorary Masters in cruise planning and logistics. If that happened, Yamindira would be my committee chair. She helped me through some of the most stressful moments of my life. When you go to sea, you need a plan B, C, and D. Without her I would be lucky to have a plan A. She does her job with a calm determination that I admire and aspire to have.

Finally, To Hilde. The butterfly's flap to my hurricane. She showed me how rad dinosaurs were and 11 years later I had a PhD. If she only knew.

Introduction

In the ocean, the amount of carbon (C) and nitrogen (N) stored in the dissolved, particulate, and sediment reservoirs directly controls the long-term cycling of nutrients and actively governs the magnitude and rates of primary production. Organic C and N in the dissolved phase represent the largest pool of reduced, biologically available, and actively cycling forms of these elements. The amount of C contained within the marine pool of dissolved organic matter (DOM) is comparable to the amount of C in atmospheric CO_2 and is therefore capable of significantly altering atmospheric CO_2 levels and global climate if perturbed.

Despite the size of the DOM pool and its ubiquitous presence throughout the water column in all areas of the global ocean, productivity in much of the surface ocean is limited by an absence of N and in nearly all of the deep ocean by the lack of biologically available organic C. This suggests that a significant portion of DOM is resistant to biological utilization. However, our understanding of the persistence of DOM under limiting conditions and its role in global biogeochemical cycles is lacking. This incomplete understanding is primarily because DOM is present in low concentrations in the ocean and is difficult to isolate from orders of magnitude more salt.

A number of isolation methods have been devised to concentrate and purify DOM for detailed analyses, however none have been able to recover the entirety of DOM from an individual water sample. As such, all isolation methods suffer from varying degrees of selectivity, be it chemical (in the case of solid phase extractions) or physical (in the case of filtration methods).

The first chapter of this dissertation elaborates on the limitations of current isolation methods and then describes and validates a new approach to recover large quantities of marine DOM for subsequent analyses. Two established isolation methods are combined, and size-based properties of DOM are exploited to selectively isolate both an actively cycling fraction as well as the persistent, biologically recalcitrant component. This approach was implemented in a shipboard field sampling campaign consisting of 46 sea days over 3 years in two major ocean basins in which a total of 51,330 L of water was collected for DOM isolation.

The second chapter of this dissertation presents compositional (C/N ratio; ^{13}C NMR) and isotopic ($\delta^{13}C$, $\Delta^{14}C$) data from measurements of these isolated samples to investigate the composition and cycling dynamics of marine DOM. This chapter focuses primarily on the recalcitrant pool of DOM and takes advantage of offsets in the properties of material recovered from the North Central Atlantic and North Pacific Subtropical Gyre to examine how this fraction of marine DOM changes over millennial timescales during deep ocean circulation.

The third chapter focuses in on the N-containing fraction of the DOM pool (DON) and begins this dissertation's investigation of the cycling of proteinaceous material in the ocean. Amino acids are the largest recoverable fraction of N-containing material in marine DOM and their well-established diversity of cycling dynamics represents a valuable tool for understanding different aspects of DOM composition such as degradation state and relative microbial influence. In this chapter, the enantiomeric ratios of amino acids are utilized to investigate the microbial sequestration of N via the production of refractory DON

The fourth chapter continues the investigation of proteinaceous DOM cycling in the ocean. A combination of preparatory high-pressure liquid chromatography and cutting-edge ultra-small sample radiocarbon analyses are used to make the first ever radiocarbon measurements of individual amino acids isolated from marine DOM throughout the water column. This chapter presents a number of incredibly novel and unexpected observations and suggests a new paradigm for the cycling of a major component of the nitrogenous material in the ocean.

Finally, the fifth chapter addresses the remainder of the N-containing material in the DOM pool. DON has historically been assumed to consist of structurally simple and labile biomolecules, such as the proteinaceous material discussed in the preceding chapters. However, its long-term persistence in the ocean suggests that it is highly resistant to biological utilization and degradation. In this chapter, the current paradigm regarding DON composition is challenged using a combination of isotopic ($\delta^{15}N$) and compositional (^{15}N NMR) analyses.

Chapter 1

Coupled ultrafiltration and solid phase extraction approach for the targeted study of semi-labile high molecular weight and refractory low molecular weight dissolved organic matter

The results presented in this chapter are published in Marine Chemistry as an article by Taylor A. B. Broek and co-authors as follows:

Broek T. A. B., Walker B. D., Guilderson T. P., and McCarthy M. D., 2017. Coupled ultrafiltration and solid phase extraction approach for the targeted study of semi-labile high molecular weight and refractory low molecular weight dissolved organic matter. *Marine Chemistry.* **194**, 146-157. http://dx.doi.org/10.1016/j.marchem.2017.06.007.

Abstract

Only a small fraction of dissolved organic matter (DOM) can be characterized at the molecular level by direct seawater analysis. Thus, the study of DOM requires isolation of extremely dilute organics from orders of magnitude greater concentrations of inorganic salts. Traditional isolation approaches have sought to isolate representative DOM fractions; however, currently available isolation methods all have selective chemical or physical biases. Recent work has indicated that DOM exists in a functional continuum of molecular size and ^{14}C age. High molecular weight (HMW) DOM is primarily composed of younger, semi-labile material, while much older, low molecular weight (LMW) DOM dominates the refractory background pool. Here we describe a new large volume DOM isolation approach that selectively isolates HMW and LMW DOM fractions with distinct ^{14}C ages, a proxy for reactivity. The method uses ultrafiltration (UF) to isolate HMW DOM (UDOM), and then solid phase extraction (SPE) to isolate LMW DOM permeating the UF system. We first assess two SPE sorbents (Agilent Bond Elute PPL and Diaion HP-20) for DOM chemical and isotopic selectivity. Second, we evaluate our UF/SPE

approach in the context of DOM recovery, elemental (C/N) and isotopic ($\delta^{13}C$, $\delta^{15}N$, $\Delta^{14}C$) composition of 8 HMW and LMW sample pairs, isolated from the North Central Pacific Ocean. Radiocarbon ($\Delta^{14}C$) analysis shows major differences in the $\Delta^{14}C$ value of HMW ($\Delta^{14}C$ = -37 to -380‰) and LMW ($\Delta^{14}C$ = -343 to -578‰) DOM fractions. We also observe elemental and stable isotopic offsets between HMW and LMW DOM at all depths. HMW UDOM (C/N = 11.5 to 13.1, $\delta^{13}C$ = -22.5 to -21.1‰, $\delta^{15}N$ = 6.2 to 7.1‰) has significantly lower C/N ratios and higher $\delta^{13}C$ and $\delta^{15}N$ values than LMW SPE-DOM (C/N = 24.2 to 28.5, $\delta^{13}C$ = -23.3 to -22.2‰, $\delta^{15}N$ = 3.1 to 4.0‰), with the exception of surface $\delta^{13}C$, which is equivalent in both size fractions. Together, these results indicate that our combined UF/SPE method successfully isolates separate young (semi-labile, HMW) and old (refractory, LMW) DOM fractions, each with distinct chemical and isotopic composition. Ultimately, by limiting the influence of DOM reactivity mixtures, our method provides an alternative approach for understanding DOM sources and cycling.

Introduction

Marine dissolved organic matter (DOM) represents the largest pool of actively cycling carbon and nitrogen in the ocean. The amount of carbon contained within ocean DOM is comparable in size to atmospheric CO_2, and therefore represents a major global reservoir, capable of altering atmospheric CO_2 levels if the balance of sources and sinks is substantially altered. Despite its importance in global biogeochemical cycles, it has remained difficult to characterize DOM at the molecular level. Only a small fraction of DOM exists as identifiable biomolecules, and most techniques for studying DOM composition require the isolation of dilute organics from high concentrations of inorganic salts (Benner, 2002).

Historically, DOM isolation methods have focused on maximizing recovery efficiency in order to isolate representative material at quantities sufficient for sample-intensive molecular and spectroscopic characterization approaches (Mopper et al., 2007). For example, solid phase extraction (SPE) using hydrophobic sorbents such as XAD and C_{18} recovers 20-50% of marine DOM. However, this approach is chemically selective, and the isolated material (SPE-DOM) is strongly biased against polar molecules (Amador et al., 1990; Green and Blough, 1994; Schwede-Thomas et al., 2005; Simjouw et al., 2005). As such, this SPE-DOM is poorly representative of total DOM (e.g., Town and Powell, 1993). New generations of hydrophobic styrene-divinylbenzene polymer based SPE sorbents have gained popularity for DOM isolation, generally achieving higher recovery efficiency than previous SPE (40 to 80%), with less reported molecular selectivity (Chen et al., 2016; Coppola et al., 2015; Dittmar et al., 2008; Green et al., 2014; Medeiros et al., 2015a; Stubbins et al.,

2012). However, relative to total DOM, this SPE-DOM is C-rich, primarily low molecular weight (LMW), and has slightly older average ^{14}C ages, suggesting that it too is not entirely representative of the total DOM pool (Coppola et al., 2015; Dittmar and Stubbins, 2014; Green et al., 2014).

Tangential flow ultrafiltration (UF) is another approach that has been widely used to isolate DOM (Benner, 2002; Benner et al., 1997; Guo et al., 1996; Santschi et al., 1995; Walker et al., 2011). UF uses semi-permeable membranes to retain only high molecular weight (HMW) DOM (UDOM). Whereas UDOM has C/N ratios similar to total DOM, it is dominated by a major reactive heteropolyscharide component (Aluwihare et al., 1997; Benner et al., 1997). In addition, the average ^{14}C age of UDOM is significantly younger than total DOC (Loh et al., 2004; Santschi et al., 1995; Walker et al., 2011; 2014), especially in the surface ocean. Further, most marine DOM (60-90%) is LMW (<1 kDa), and readily permeates a UF system (Benner and Amon, 2015).

Due to the operational nature of these isolation techniques, neither UDOM nor SPE-DOM is particularly representative of the total DOM pool. To date, no method consistently isolates total DOC across ocean depths and water masses, with most methods achieving substantially less than 100% recovery. More problematic than absolute recovery, however, is that all isolations suffer from varying degrees of selectivity. Incomplete recoveries and the inherent biases associated with different isolation mechanisms (size, hydrophobicity, etc.), can lead to broad process interpretations based on isolated sub-fractions, which likely represent very different compositional and functional DOM components.

Recent research suggests that a new approach to DOM isolation, focused on selective isolation of separate old and young fractions, may be more useful in investigating DOM composition and cycling. Specifically, multiple studies note trends in DOM composition, ^{14}C age, and reactivity, which are strongly linked to nominal molecular size (Benner and Amon, 2015; Walker et al., 2011; 2016a; 2016c). In general, HMW DOM is more biologically labile, biopolymer-rich, with younger ^{14}C ages, more identifiable biochemicals, and greater reactivity. In contrast, LMW DOM is generally more biologically recalcitrant, contains far fewer identifiable biomolecules, and has older ^{14}C ages at all depths (Amon and Benner, 1996; 1994; Benner et al., 1997; Benner and Amon, 2015; Kaiser and Benner, 2009; Walker et al., 2016c; 2016a; 2014; 2011). These observations expand upon the classical "two-pool" model of DOC cycling (Druffel et al., 1992; Williams and Druffel, 1987). In the two-pool model, a homogenous pool of "background" refractory DOM is present throughout the ocean, and is comprised of DOM with old ^{14}C ages (Beaupré and Aluwihare, 2010; Mortazavi and Chanton, 2004). Superimposed upon this background, refractory DOM is a pool of surface produced, "excess", semi-labile material with young ^{14}C ages (Carlson and Hansell, 2014; Walker et al., 2016c; 2011).

Here we evaluate a new DOM isolation approach, sequentially combining UF and SPE, in order to target two distinct, operationally defined DOM pools. The average MW of DOM retained by UF is a function of the concentration factor used (CF; ratio of volume filtered to final retentate volume), a high CF results in the retention of higher MW material (Kilduff and Weber, 1992; Walker et al., 2011). This

UF attribute allows for the targeted isolation of not only higher MW material, but also DOM with younger average ^{14}C ages (Walker et al., 2011). The DOM permeating a UF system is by definition LMW. Therefore, we hypothesize that SPE of seawater UF permeate will allow for the targeted isolation of LMW, refractory, background DOM.

We first test two formulations of SPE sorbent to evaluate the properties of SPE isolated material relative to total seawater DOM. We then apply our full UF/SPE method to selectively isolate HMW and LMW DOM from the surface to deep-ocean in the Central North Pacific Subtropical Gyre (NPSG). Finally, we evaluate our approach by comparing the elemental ratios (C/N), stable isotopic ($\delta^{13}C$, $\delta^{15}N$), and radiocarbon ($\Delta^{14}C$) properties of individual HMW and LMW DOM isolates. Overall, our main objective is not to optimize total DOM recovery, but rather to develop a method that can isolate large quantities of distinct operational fractions having bulk properties consistent with either semi-labile (excess) or refractory (background) DOM.

Materials & Methods

Definitions

Here we define "total DOM" to be all DOM passing a 0.2 μm filter. "HMW UDOM" represents the ≥2.5 kD material retained by the UF system. "SPE-DOM" represents material retained by the SPE sorbents. In the *SPE Sorbent Comparison* section, "PPL SPE-DOM" and "HP-20 SPE-DOM" are used to refer to DOM extracted from 0.2 μm-filtered seawater by PPL and HP-20 SPE sorbents

respectively. To distinguish SPE-DOM isolates of 0.2 μm-filtered seawater from material collected from ≤2.5 kD UF permeate using the combined UF/SPE method, we use "LMW SPE-DOM" for the ≤2.5 kD fraction. DOC and DON are used when discussing C or N specific properties of the DOM fractions.

Sample Collection

Samples were collected on two separate research cruises aboard the R/V Kilo Moana in August 2014 and May 2015. Sampling was conducted at the Hawaii Ocean Time Series Station ALOHA (A Long-Term Oligotrophic Habitat Assessment; 22° 45'N, 158° 00'W).

Significant precautions were taken to ensure ^{14}C-tracer free shipboard sampling. All laboratory spaces were cleaned floor-to-ceiling with 10% HCl followed by ethanol. Exposed surfaces (bench tops, walls, and ceiling) were covered and air vents redirected using plastic sheeting. ^{14}C swabs of lab spaces, outside deck areas, and sampling equipment measured during scheduled shipboard contamination monitoring swab tests by the University of Miami tritium laboratory (http://www.rsmas.miami.edu/groups/tritium) were reviewed prior to each cruse. More sensitive ^{14}C swipes were taken throughout the ship before and after each cruise and analyzed by accelerator mass spectrometry (AMS) to confirm a ^{14}C-tracer free sampling environment.

Surface water was sampled via the vessel's underway sampling system. The intake pipe is situated on the forward starboard hull section of the vessel approximately 7.5 m below the waterline. The laboratory seawater tap was allowed to

flush for 2 hours prior to each sampling. Seawater was pre-filtered through 53 μm Nintex mesh and pumped through a 0.2 μm polyethersulfone (PES) cartridge filter (Shelco Filters, Micro Vantage, water grade, 9.75" DOE, polycarbonate housing) prior to introduction to the ultrafiltration system. Large volume subsurface water samples were collected using successive casts of a rosette equipped with 12 x 24 L Niskin bottles. Sample water was transferred from the Niskin bottles via platinum cured silicone tubing to sample rinsed fluorinated high-density polyethylene (F-HDPE) carboys which were subsequently emptied into 1000 L HDPE intermediate bulk containers for storage. Subsurface water was similarly pumped through a 0.2 μm PES cartridge filter prior to ultrafiltration. All filters and storage containers were cleaned with 10% HCl prior to contact with sample seawater.

Experimental Design

Total DOM was separated into two distinct size fractions using a sequential combination of UF and SPE. A flow diagram of the isolation protocol is shown in Fig. 1.1. HMW UDOM was first isolated using a large-volume UF system; the permeate stream of this system (containing LMW DOM able to pass the UF membranes) was then collected, acidified in large batches to pH 2 and passed through the SPE sorbent. The eluted material from the SPE sorbent represents the LMW SPE-DOM fraction.

Tangential-Flow Ultrafiltration

The main UF system was constructed using a modified design of the system described in Roland et al. (2009) and expanded on by Walker et al. (2011). Briefly, the system was comprised of four-spiral wound PES UF membranes, having a nominal molecular weight cut off of 2.5 kD (GE Osmonics GH2540F30, 40-inch long, 2.5-inch diameter). The membranes were mounted in stainless steel housings, plumbed in parallel to a 100 L fluorinated HDPE reservoir, with flow driven by a 1.5 HP stainless steel centrifugal pump (Goulds Pumps, Stainless steel centrifugal pump, NPE series 1 x 1-1/4 -6, close coupled to a 1-1/2 horsepower, 3500 RPM, 60 Hz, 3 phase, Open Drip Proof Motor; 5.75 Inch Impeller Diameter, Standard Viton Mechanical Seals). All other system plumbing components contacting seawater were composed of polytetrafluoroethylene (PTFE) or stainless steel.

The system was run continuously at a membrane pressure of 40-50 psi, resulting in permeation flow rates of 1-2 L/min, depending primarily on the temperature of the feed seawater. Sample water was fed into the system using peristaltic pumps and platinum cured silicone tubing at a flow rate matched to the system permeation rates to ensure a constant system volume of approximately 100 L.

Seawater samples of 3000-4000 L were concentrated to a final retentate volume of 15-20 L, drained from the system into acid washed PC carboys and refrigerated (less than 12 hours at 2°C) until the next phase of processing. Samples requiring storage for longer than 12 hours were frozen and stored at -20°C. The UF system was then reconfigured to a smaller volume system, consisting of a single membrane having a smaller nominal molecular weight cutoff (GE Osmonics

GE2540F30, 40-inch long, 2.5-inch diameter, 1 kD NMWCO), and a 2.5 L PES reservoir for further volume reduction and subsequent salt removal (diafiltration). Using this smaller system, samples were reduced to 2-3 L under lower pressure (25 psi, permeation rate = 250 mL/min). Samples were then diafiltered using 40 L of 18.2 MΩ Milli-Q (ultrapure) water, adding water to the sample retentate reservoir at the same rate of membrane permeation. Reduced and diafiltered samples were stored in acid washed PC bottles at -20°C for transport. In the laboratory, samples were further concentrated by rotary evaporation using pre-combusted glassware (450 °C, 5 h). A molecular sieve and a liquid nitrogen trap were placed between the vacuum pump and rotovap chamber to ensure no contamination of isolated material by back streaming of hydrocarbons or other contaminants. After reduction to 50-100 mL, samples were dried to powder via centrifugal evaporation in PTFE centrifuge tubes. Dry material was homogenized with an ethanol cleaned agate mortar and pestle, transferred to pre-combusted glass vials, and stored in a desiccation cabinet until subsequent analyses.

Solid Phase Extraction

Solid phase extraction was conducted using PPL sorbent (Agilent Bondesil PPL, 125 µm particle size, part # 5982-0026) following the general recommendations of Dittmar et al. (2008) and Green et al. (2014), including loading rates, seawater to sorbent ratios, and elution volumes and rates. Between 300 and 500 g of sorbent was used for each extraction, depending on sample volume and DOC concentration, with average loading of 4.2 ± 1.4 L UF permeate per g sorbent representing 1.9 ± 0.6 mg DOC per g sorbent or a DOC to sorbent mass ratio of 1:600 ± 200. This is in line with

both the recommendations of Dittmar et al. (2008) and recent recommendations of Li et al. (2016). Permeate from the UF system was fed through PTFE tubing to a pair of 200 L HDPE barrels. The permeate water was then acidified in 200 L batches to pH 2 by adding 400 mL of 6 M HCl (Fisher Chemical, ACS Plus grade). Batch samples were mixed continuously during collection, acidification, and loading using a peristaltic pump and platinum cured Si and PTFE tubing positioned at the surface and bottom of each barrel. Acidified batches of seawater permeate were then pumped through the SPE sorbent. SPE flow rates were matched to UF permeation rates (1-2 L/min), such that a pair of 200 L barrels allowed one barrel to be filled while the contents of the other was passed through the sorbent.

Three custom SPE column configurations were used to contain the sorbent material. The column configuration was modified several times for ease of use on subsequent cruises. First, an open, gravity fed, large (49 mm ID x 1000 mm length, 1875 mL volume) glass chromatography column with 40 µm fritted disk and PTFE stopcock (Kimble-Chase™, Kontes™) was used. Next, we tested a custom-built high-pressure SS housing (10 cm ID x 3.5 cm bed height), and finally a parallel combination of 2 medium-pressure glass chromatography columns (Kimble-Chase™, Kontes™, Chromaflex LC, 4.8 mm ID x 30 cm, 543 mL volume). While all designs proved to be functionally equivalent, the latter parallel combination of 2 medium-pressure glass columns ultimately provided the best configuration in order to maximize flow rates while simultaneously optimizing the ratio of sorbent bed height to loading speed. Further, the commercial availability and ease of use associated with this configuration made it our preferred design.

Following sample loading, the SPE sorbent was desalted with 6 L of pH 2 ultrapure water at a low flow rate (250-300 mL/min). After desalting, the SPE sorbent was transferred to a glass chromatography column (75 mm ID x 300 mm length, 40 μm fritted disk, PTFE stopcock) with ultrapure water rinses to ensure quantitative transfer. Isolated organic material was then eluted from the sorbent with five to six 500 mL additions of methanol. The secondary all-glass and PTFE column was used to ensure that all wetted parts had strong chemical resistance to the methanol used during DOM elution. The eluted methanol solution was stored in pre-combusted amber glass bottles at -20°C for transport. Similar to UF samples, the methanol-eluted solutions were first reduced by rotary evaporation to 50-100 mL. Samples were then dried to powder via centrifugal evaporation in PTFE centrifuge tubes. Dry material was homogenized with an ethanol cleaned agate mortar and pestle, transferred to pre-combusted glass vials, and stored in a desiccation cabinet until elemental and isotopic analyses.

Small Volume SPE Comparisons

To compare sorbents, small volume SPE isolations were performed on 20 L sub-samples of the 0.2 μm-filtered UF feed water used for the larger volume surface and deep (2500 m) samples. Glass chromatography columns were packed with 50 g of either PPL or HP-20 sorbent (Supelco Diaion® HP-20, 250-850 μm particle size, 260 Å mean pore size, Sigma-Aldrich SKU: 13607) and experiments were conducted in parallel, with samples from the same seawater batch. Sample water was acidified to pH 2 with 40 mL of 6 N HCl in 24 L polycarbonate (PC) carboys and pumped

continuously through silicon tubing to the columns at a flow rate matched to the gravity flow (drain) rate for each column (100-200 mL/min). After loading the acidified 20 L samples, the sorbent was desalted with 600 mL pH 2 ultrapure water, and retained material was eluted with six 50 mL additions of methanol and collected in pre-combusted glass bottles. Methanol samples were stored at -20°C and dried to powder as described above.

Total DOM

Subsamples for dissolved organic carbon (DOC) and total dissolved nitrogen (TDN) concentration measurements were collected into pre-combusted 40 mL borosilicate glass vials following 0.2 μm-filtration. Samples were stored at -20°C until analysis. Subsamples for [DOC] and [TDN] were also taken from the UF system permeate to evaluate mass balance. An "integrated" permeate sample (e.g., Benner et al., 1997) was prepared by sampling and combining equal volumes (100 mL) collected at constant time intervals throughout the ultrafiltration. DOC and TDN concentration measurements were made using the high temperature oxidation method with a Shimadzu TOC-V in the Carlson lab at UCSB (https://labs.eemb.ucsb.edu/carlson/craig/services). DOC concentration measurement errors represent the standard deviation of n=3 replicate measurements. Total DON concentrations were determined by subtracting the sum of dissolved inorganic nitrogen (DIN) species (nitrate, nitrite, ammonia) from TDN. DIN concentrations were determined using a Lachat QuickChem 8000 Flow Injection Analyzer. Ammonia concentrations were below the limit of quantification (0.36 μM) for all

samples using QuickChem® Method 31-107-06-1-B. Nitrate and nitrite concentrations were measured as the sum of the two analytes using QuickChem® Method 31-107-04-1-C. The limit of detection for [NO3+NO2] using this method was 0.5 μM and the average precision of replicate standard measurements was ± 1.4 μM. In the case of [DON], measurement errors represent the propagated analytical uncertainty from the subtraction of [DIN] from [TDN]. DOC concentrations measurements were also determined via UV oxidation, cryogenic purification and manometric determination at UC Irvine. DOC concentrations were similar between the two methods and the presented values represent the error weighted mean of both measurements. For all sample depths, 0.2 μm-filtered seawater was also collected for C isotopic ($\delta^{13}C$, $\Delta^{14}C$) analysis into pre-combusted 1000 mL Amber Boston Round bottles, immediately frozen and stored at -20°C.

Elemental and Isotopic Analyses

Natural abundance radiocarbon ($\Delta^{14}C$) determinations of all isolated fractions were performed at the Lawrence Livermore National Laboratory, Center for Accelerator Mass Spectrometry (LLNL-CAMS) by AMS following standard graphitization procedures (Santos et al., 2007; Vogel et al., 1984). The $\Delta^{14}C$ signature of total seawater DOC (< 0.2 μm) was determined by UV-oxidation and AMS at the UC Irvine Keck Carbon Cycle AMS Lab (Beaupré et al., 2007; Druffel et al., 2013; Walker et al., 2016b). Results are reported as age-corrected $\Delta^{14}C$ (‰) for geochemical samples and have been corrected to the date of collection and are reported in accordance with conventions set forth by Stuiver and Polach (1977).

Isotopic ^{14}C results are reported as background and $\delta^{13}C$ corrected fraction modern (Fm; Supplemental Table 1), $\Delta^{14}C$ (Table 1), and conventional radiocarbon age (ybp; Supplemental Table 1).

Stable carbon ($\delta^{13}C$) and nitrogen ($\delta^{15}N$) isotope ratios were determined via elemental analyzer isotope ratio mass spectrometry (EA-IRMS) at the University of California, Santa Cruz, Stable Isotope Laboratory (UCSC-SIL; http://emerald.ucsc.edu/~silab/). Approximately 1 mg of each dry isolated DOM sample was weighed into tin capsules (Costec, 5 x 9 mm) for analysis. EA-IRMS analysis was conducted using a Carlo Erba CHNS-O EA1108-elemental analyzer interfaced via a ConFlo III device with a ThermoFinnigan Delta Plus XP isotope ratio mass spectrometer (Thermo Fisher Scientific). Standards, EA-IRMS protocols, and correction routines followed standard UCSC-SIL protocols. Analytical uncertainties of n=3 replicate measurements of isotopic standards ranged from ± 0.05 to 0.1‰ for both $\delta^{13}C$ and $\delta^{15}N$. Carbon to nitrogen elemental ratios were similarly determined by elemental analysis. The presented ratios are atomic ratios $(C/N)_a$ normalized to the mass of C and N, but have been abbreviated as C/N throughout.

Data Treatment and Reporting of Statistical Uncertainty

In most cases there are no significant offsets in the measured properties of samples collected on spring and summer time cruises from the same depth, and the average values of replicate measurements were generally indistinguishable within error between cruises. In cases where there were statistically significant offsets between cruises, the differences could be interpreted as either seasonal differences or

methodological variability (e.g. sample volume). In order to properly represent the potential spread of values, unless otherwise stated, all reported values represent the error-weighted average of replicate measurements (n=3) of material collected on both summer 2014 and spring 2015 cruises. The reported standard deviation represents the variance of the weighted mean, and accounts for the uncertainty from replicate measurements and the spread of values between cruises.

Results & Discussion

SPE Sorbent Comparison

To optimize our protocol for recovery of LMW DOM permeating the UF system, and to better understand potential for compositional bias, we first compare the elemental and isotopic properties of DOM isolated using two similar SPE sorbent formulations. We chose to evaluate Diaion HP-20 and Agilent PPL sorbents based on their application in recently published literature (Coppola et al., 2015; Green et al., 2014). These two sorbents have similar functional chemistry, but different bead size (250-850 μm for HP-20, 125 μm for PPL) and nearly an order of magnitude cost differential. The latter is an important consideration for any large-volume field application. Below we discuss the %DOC and %DON recoveries, C/N ratios, $\delta^{13}C$, $\delta^{15}N$, and $\Delta^{14}C$ values from replicate SPE experiments, placing them into the context of total DOM composition.

The PPL sorbent retains both more DOC and DON than HP-20. PPL recovered statistically identical proportions of DOC from both surface and deep water, representing 45 ± 4% (35 ± 2 μmol C/L) and 44 ± 4% (17 ± 1 μmol C/ L) of

total DOC respectively (average = 45 ± 3%) (Fig. 1.2, 1.3a). The HP-20 sorbent also has similar recoveries in the surface and at 2500 m (surface: 38 ± 1%, 30 ± 1 μmol C/L; deep: 34 ± 8%, 14 ± 5 μmol C/L; average = 35 ± 6%), but on average recovered significantly less DOC than PPL (two tailed t-test, DF= 5, t = 2.9, p = 0.03). As noted in the *Materials and Methods* section, the DOM loading (ratio of sorbent mass to DOM mass) was within the ranges recommended in the literature (Dittmar et al., 2008; Li et al., 2016). The HP-20 SPE-DOC recoveries are similar to those reported by a study of surface waters at Station M (43 ± 6%, Coppola et al., 2015). Our recoveries using the PPL sorbent are similar to values reported in several different ocean regions (Weddell Sea surface to bottom, 43 ± 5%, Dittmar et al., 2008; Atlantic Ocean surface to bottom, 41 ± 3%, Hertkorn et al., 2013) and within one standard deviation of the average of currently published open-ocean values (53 ± 13%, representing data from Dittmar et al., 2008; Green et al., 2014; Hertkorn et al., 2013; Medeiros et al., 2015a; Stubbins et al., 2012). We note that the recovery efficiency of PPL from open-ocean waters is generally lower than the average recovery efficiency from fresh water, estuaries, and coastal waters (68 ± 11%, representing data from Dittmar et al., 2008; Li et al., 2016; Medeiros et al., 2015b; Osterholz et al., 2016). This is consistent with well-known differences in SPE-DOC recovery efficiency between freshwater and seawater using other types of hydrophobic sorbents (Mopper et al., 2007).

In contrast to DOC, the difference in relative recoveries of DON between sorbent types is substantially larger; with PPL recovering 10-20% more total DON than HP-20 from both surface and deep water. The HP-20 sorbent recovers on

average 21 ± 7% of total DON, with little difference between surface and deep (21 ± 1% and 22 ± 10% respectively). PPL recovers far more DON (average PPL recovery = 34 ± 6%; two tailed t-test, DF= 5, t = 2.6, p = 0.045), with average recoveries more similar to those for DOC. The relative recovery of DON by PPL diverges between surface and deep isolations, with substantially higher %N recoveries in the deep ocean than the surface ocean (39 ± 3% vs. 30 ± 2%; two tailed t-test, DF= 10, t = 6.1, $p < 0.01$). Given the general chemical similarity of PPL and HP-20 sorbents, these differences are unexpected. While we do not have a mechanistic explanation, the higher relative recovery of N at depth by PPL suggests that the chemical properties of dissolved nitrogenous material in the deep sea make it substantially more amenable to isolation by PPL than HP-20.

The radiocarbon ($\Delta^{14}C$) values for both PPL and HP-20 isolated material suggest that DOC recovered by each sorbent approximates the average age of total DOC (Fig. 1.3f). In surface waters, however, both sorbents have a small but consistent bias toward collecting older DOC material, with this effect greater for HP-20 extracted material (surface PPL SPE-DOC $\Delta^{14}C$ offset from total DOC = 23 ± 14‰, two tailed t-test, DF= 2, t = 2.2, p = 0.16; HP-20 SPE-DOC offset = 52 ± 14‰, two tailed t-test, DF= 2, t = 5.3, p = 0.03). In contrast, the $\Delta^{14}C$ of SPE-isolated material at depth is indistinguishable from total DOC $\Delta^{14}C$ for both sorbents (PPL SPE-DOC offset, 12 ± 14‰, two tailed t-test, DF= 2, t = 1.0, p = 0.42; HP-20 SPE-DOC offset, 7 ± 10‰, two tailed t-test, DF= 2, t = 1.0, p = 0.44). Similar to the recovery values, the measured $\Delta^{14}C$ of our isolated material also compares well with limited published data. Specifically, the $\Delta^{14}C$ offset between total DOC and HP-20

SPE-DOC is similar to a previous study (total DOC = -299 ± 3‰, HP-20 SPE-DOC = -323 ± 15‰, offset = 24 ± 15‰, (Coppola et al., 2015). Likewise, previous $\Delta^{14}C$ measurements of PPL extracted material are also similar to total DOC $\Delta^{14}C$ values (Flerus et al., 2012; Lechtenfeld et al., 2014). Together with our data, these observations indicate that despite only recovering approximately half of total DOM, these SPE sorbents generally retain a representative age fraction of DOM from the deep ocean, which closely approximates total DOM $\Delta^{14}C$.

In most cases, however, SPE isolates have significantly different elemental and stable isotopic ratios than total DOM. The C/N ratios of SPE-DOM from the surface ocean are consistently higher than total DOM for both sorbents (Fig. 1.3c). However, as would be expected from DON recoveries, this difference is smaller for the PPL isolated material. For PPL SPE-DOM, the C/N values of surface samples are significantly higher than total DOM (18.4 ± 0.7 vs. 14.3 ± 0.8, two tailed t-test, DF= 2, t = 5.45, p = 0.03), while at depth C/N values converge, and become statistically indistinguishable (18.9 ± 1.3 vs. 19.5 ± 4.4, two tailed t-test, DF= 2, t = 0.18, p = 0.87). For HP-20 SPE-DOM, the offset is larger and similar in both surface and deep water (surface, 22.5 ± 0.7 vs. 14.3 ± 0.8, two tailed t-test, DF= 2, t = 10.9, $p < 0.01$; 2500 m, 27.4 ± 2.7 vs. 19.5 ± 4.4, two tailed t-test, DF= 2, t = 2.1, p = 0.16). We note that previously reported PPL SPE-DOM C/N ratios also show significant offsets from total DOM. For example, Green et al. (2014) report C/N ratios of 23 to 25 for PPL SPE-DOM, suggesting PPL does have a chemically selective bias against N-containing compounds. Overall, our high C/N ratios relative to total surface DOM are consistent with the low DON recoveries discussed above, as well as previous studies

which measure elevated C/N ratios in SPE-DOM, and with recent work showing SPE does not efficiently isolate N-rich or high O/C ratio molecules (Chen et al., 2016; Dittmar et al., 2008; Green et al., 2014; Hertkorn et al., 2013).

SPE-DOM $\delta^{13}C$ values are lower that total DOC $\delta^{13}C$ in the surface for both sorbents. HP-20 SPE-DOC has lower $\delta^{13}C$ values than total DOC throughout the water column (surface $\delta^{13}C$ = -22.3 ± 0.2‰ vs. -21.1 ± 0.4‰, two tailed t-test, DF= 2, t = 3.8, p = 0.06; 2500 m $\delta^{13}C$ = -22.5 ± 0.1‰ vs. -21.6 ± 0.2‰, two tailed t-test, DF= 2, t = 5.7, p = 0.03). PPL SPE-DOC $\delta^{13}C$ is similarly offset in the surface (-22.5 ± 0.7‰ vs. -21.1 ± 0.4‰, two tailed t-test, DF= 2, t = 2.46, p = 0.13), however, PPL SPE-DOC has similar $\delta^{13}C$ values to total DOC at depth (-22.2 ± 0.6‰ vs. -21.6 ± 0.2‰, two tailed t-test, DF= 2, t = 1.34, p = 0.31). The low SPE-DOC $\delta^{13}C$ for both sorbents is consistent with the SPE-DOC $\Delta^{14}C$ and C/N ratio offsets mentioned above. Specifically, hydrophobic, lipid-like components of the DOM pool likely to be retained strongly by SPE sorbents are C-rich and have lower $\Delta^{14}C$ and $\delta^{13}C$ (Hwang, 2003; Loh et al., 2004; Wang et al., 2001).

Because very few studies have measured the $\delta^{15}N$ of total DON, and none have measured it in the deep ocean, a directly analogous comparison of $\delta^{15}N$ between PPL and HP-20 SPE-DON is not possible. However, comparing published $\delta^{15}N$ values of surface DON from this ocean region (5.0 ± 0.5‰, Knapp et al., 2011), we find that PPL SPE-DON $\delta^{15}N$ (5.0 ± 0.2‰) more closely approximates that of total DON than HP-20 SPE-DON $\delta^{15}N$ (4.5‰; Fig. 1.3e). PPL and HP-20 SPE-DON $\delta^{15}N$ values both decrease with depth and remain consistently offset. Again, however,

without published deep total DON $\delta^{15}N$ data, it is not possible to evaluate this change relative to total DON.

Finally, we should note that it is possible that SPE sorbent blanks could contribute to these observed elemental and isotopic offsets. While we did not directly measure C blanks in this study, previous work, as well as isotope mass balance from our data indicate that this is highly unlikely as a major factor. One previous study evaluating the HP-20 sorbent for the purposes of $\Delta^{14}C$ measurements shows that no measurable carbon blank is introduced by the sorbent during processing (Coppola et al., 2015). Further, by direct measurement we find that both the PPL and HP-20 sorbent mediums used in this study have indistinguishable $\delta^{13}C$ values (27.4 ± 0.1‰), consistent with expected values for petroleum-based polymer sorbents. Based on these values, the SPE-DOC $\delta^{13}C$ offsets we observe compared to total DOC require that ~20% of our SPE-DOC be sorbent-derived blank in surface waters. This large amount of C cannot be reconciled with our relatively small $\Delta^{14}C$ offsets: a 20% contribution of sorbent C ($\Delta^{14}C$ =-1000‰) in the surface would result in SPE-DOC versus total DOC $\Delta^{14}C$ offsets of 170‰ and 145‰ for PPL and HP-20 DOC respectively. The small observed $\Delta^{14}C$ offsets also likely exclude the possibility of significant C-contamination from residual methanol, which is similarly depleted in ^{14}C due to petroleum-derived manufacturing processes.

Overall, our SPE-DOM recovery, elemental, and isotopic composition data indicate that both PPL and HP-20 do fractionate total DOM to some degree. As is expected for a hydrophobic sorbent, both select for C-rich components, which results in the extraction of material with depleted $\delta^{13}C$ and $\Delta^{14}C$ values. For the study of DON,

PPL isolates more representative material than HP-20. Where values can be compared, despite recovering only 30-40% of total DON, the $\delta^{15}N$ of PPL SPE-DOM approximates the $\delta^{15}N$ of total DON. At depth, the C/N ratio of PPL SPE-DOM is indistinguishable from total DOM C/N ratios. The consistent offsets in surface waters between SPE-DOM and total DOM suggests that some unknown fraction of younger, freshly produced DOM is not well retained by SPE. In contrast, the similarity between PPL SPE-DOM and total DOM elemental and isotopic properties at 2500 m suggests that PPL SPE-DOM is closely representative of the LMW material that dominates the deep ocean DOM reservoir. We therefore conclude that PPL represents an excellent choice for the targeted isolation of background DOM from LMW UF permeate.

Coupled UF/SPE: Recovery Efficiency

Given the above results, we use PPL in our combined UF/SPE approach. The UF/SPE method recovers a combined average of 37 ± 3% of total DOC, and 33 ± 7% of DON across all depths (Fig. 1.4). While the combined total recovery for both isolation steps is similar at all depths, there is also clear variation in the proportion of material retained by each system individually between the surface and subsurface. The UF system retains an average of 14 ± 2 μmolC/L in the surface and an average of 4 ± 1 μmolC/L from 400 m to 2500 m, representing 17 ± 1% and 9 ± 2% of total DOC respectively. SPE of the UF permeate retains a similar concentration of total DOC in the surface (15 ± 1 μmolC/L), and in the subsurface (12 ± 1 μmolC/L). As a percentage of total DOC, relative LMW SPE-DOC recovery therefore increases

dramatically from surface to subsurface depths (surface average = 19 ± 2%; average of 400 m to 2500 m = 29 ± 2%).

The decrease in both the absolute and percent recovery of HMW material from surface to deep is consistent with previous observations in all ocean regions (Benner and Amon, 2015). In contrast, the absolute recovery of SPE extractable LMW DOC is similar at all depths and therefore makes up an increasing percentage of total DOC with increasing depth. This trend counteracts the decreasing recovery of HMW UDOM, resulting in an essentially identical combined recovery at all depths (37 ± 3%). The similar absolute recoveries of LMW SPE-DOM from the surface and at depth is consistent with background DOM, hypothesized to exist at similar concentrations at all ocean depths in a classical two-pool model (Carlson and Hansell, 2014; Druffel et al., 1992).

When LMW SPE-DOC recoveries are considered relative to UF permeate DOC concentrations, the recovery of LMW SPE-DOC from the surface water UF permeate is significantly lower than PPL SPE-DOC extracted from surface total DOC (27 ± 1% vs. 45 ± 4%, two tailed t-test, DF= 6, $t = 11.7$, $p < 0.01$) (Fig. 1.5). In contrast, at 2500 m, LMW SPE-DOC % recoveries are equivalent to PPL SPE-DOC recoveries (PPL SPE-DOC recovery = 44 ± 4 %; LMW SPE-DOC recovery = 40 ± 3%; two tailed t-test, DF= 6, $t = 1.5$, $p = 0.18$). These differences in relative recovery between SPE-DOM and LMW SPE-DOM suggest that there is substantial overlap in the material recovered by the size-based and chemistry-based approaches. Specifically, in the surface, the UF system is removing a large portion of the material that SPE would otherwise have isolated from total DOM. At 2500 m, the difference in

relative recovery of SPE-DOC and LMW SPE-DOC is not statistically significant, consistent with the substantially lower proportion of HMW material that exists in the deep ocean (Benner et al., 1997; 1992).

Put another way, these observations indicate that PPL retains both HMW (younger) and LMW (older) material and is consistent with the $\Delta^{14}C$ data from the sorbent comparisons above. We note that published literature suggests some ocean HMW DOM may consist of aggregates of smaller molecules, bridged by inorganic cations (e.g., Chin et al., 1998; Hertkorn et al., 2006; Verdugo et al., 2004). While this could act to blur the boundaries between isolated HMW and LMW material and their respective ^{14}C ages, it should not significantly impact our overall operational isolation framework. Specifically, the concentration of HMW DOM isolated by UF is known to be dependent on ionic strength, potentially consistent with some influence of such aggregates (e.g., Walker et al., 2011), and yet UDOM is always much younger than LMW DOM (Loh et al., 2004; Santschi et al., 1995; Walker et al., 2016c; 2014; 2011). Finally, the depth related difference in the magnitude of overlap of UF and SPE isolated material also hints at chemical differences in the DOM pool, suggesting that there is a greater proportion of non-SPE isolatable DOM in the surface. This is also consistent with well-known changes in the functional character of HMW DOM with depth: specifically, while surface HMW DOM is dominated by polar biopolymers (in particular carbohydrates), deep ocean HMW DOM is dominated by carboxyl-rich aliphatic structures (CRAM) (Benner et al., 1992; Hertkorn et al., 2006; McCarthy et al., 1996).

Finally, it may seem somewhat surprising that the combined total % recovery of the coupled UF/SPE method is lower than the recovery of SPE-DOM from whole water alone. We hypothesize that the large seawater volumes, with the associated effects of high sorbent loadings and high CFs used in these experiments (in contrast with the smaller loadings used in the sorbent comparisons), are responsible for the lower recoveries. As noted previously however, our goal here is not to maximize total recovery, but rather to isolate large amounts of DOM fractions with distinct size (HMW vs. LMW) and reactivity (^{14}C age).

Coupled UF/SPE: Radiocarbon (Δ^{14}C) of HMW and LMW DOM

HMW UDOC Δ^{14}C values at each depth (-45 to -375‰) are significantly different than LMW SPE-DOC Δ^{14}C values (-350 to -575 ‰) (Fig. 1.6). At all depths sampled in the NPSG water column, the Δ^{14}C of total DOC is intermediate between the Δ^{14}C values of the two fractions, consistent with expectations based on our operational framework. In surface waters, the offsets are large, with HMW UDOC Δ^{14}C (-45 ± 10 ‰) significantly more positive than total DOC, and LMW SPE-DOC Δ^{14}C significantly more negative. In the deep ocean (400 m to 2500 m), LMW SPE-DOC Δ^{14}C offsets are smaller, with a constant negative Δ^{14}C offset (average offset = 37 ± 15 ‰) from total DOC (Fig. 1.8a). In contrast, HMW UDOC Δ^{14}C values remain substantially more positive than total DOC, with a similar average Δ^{14}C offset (175 ± 15‰) at all depths.

HMW UDOM Δ^{14}C values are similar to those obtained from prior isolations of HMW UDOM in this region using similar concentration factors (Walker et al.,

2011). Further, as has been observed by prior work, the ^{14}C ages of mesopelagic and deep ocean HMW UDOM (1600 – 3700 ybp) indicate the presence of an old DOC component. Compound class work on HMW UDOM indicates substantial diversity in the $\Delta^{14}C$ values of operationally defined biochemical fractions. While the main identifiable biochemical classes in deep UDOM appear semi-labile (as evidenced by their younger ^{14}C ages), a quantitatively smaller "lipid-like" fraction has extremely old ^{14}C ages (Loh et al., 2004). However, we note that even the oldest ^{14}C age of our bulk HMW UDOC (3700 ybp) is still significantly younger than both total DOC (6200 ybp) and LMW SPE-DOC (6800 ybp) at 2500 m.

The $\Delta^{14}C$ offsets from total DOC that we observe in both HMW UDOC and LMW SPE-DOC are consistent with previous observations about DOM size and age or reactivity (Amon and Benner, 1994; Benner and Amon, 2015; Walker et al., 2016c; 2014), and also expectations based on the relative abundance of relative size classes (Kaiser and Benner, 2009). Overall, these results indicate that this coupled method successfully isolates two separate operational fractions, dominated by either semi-labile or refractory DOM pools.

Coupled UF/SPE: Elemental Composition (C/N) of HMW and LMW DOM

The $\delta^{13}C$, $\delta^{15}N$ values and C/N ratios of HMW UDOM and LMW SPE-DOM (Fig. 1.7) allow a first examination of the information potential using our new isolation protocol. All bulk compositional values are dramatically different between our two fractions, reinforcing the contrasting biochemical composition of old versus young DOM pools.

The C/N ratio of LMW SPE-DOM is significantly higher (average of all depths: 26 ± 2) than HMW UDOM or total DOM, with no significant difference between surface and deep water (Surface C/N = 27.7 ± 0.4, average of 400 to 2500 m C/N = 26.1 ± 2.1; two tailed t-test, DF= 10, t = 1.3, p = 0.23). The elevated C/N ratios of LMW SPE-DOM suggest that older, LMW material at all depths is C-rich; consistent with highly unsaturated and aromatic structures proposed by studies using ultrahigh resolution mass spectrometry (Flerus et al., 2012; Hansman et al., 2015; Hertkorn et al., 2013; Medeiros et al., 2015a). Further, the invariant nature of LMW SPE-DOM C/N ratios with depth (Fig. 1.7) is again consistent with a background pool of chemically and isotopically homogeneous DOM (Druffel et al., 1992; Druffel and Beaupré, 2009).

HMW UDOM C/N ratios are substantially lower (average of all depths: 12 ± 1), also with no significant depth structure (Surface C/N = 12.4 ± 0.5, average of 400 to 2500 m C/N = 12.3 ± 0.6; two tailed t-test, DF= 10, t = 0.3, p = 0.8). The HMW UDOM C/N values reported here are somewhat lower than in some past work for the Central North Pacific (e.g., 17 ± 2, Benner et al., 1997). We hypothesize that the low C/N ratios and lack of depth trend are most likely related to the high CF used, which as noted above was chosen to maximize the isolation of the highest molecular weight material with the youngest ^{14}C ages. While prior elemental data on low concentration factor UDOM shows increases in C/N ratio with depth, more consistent with the C/N ratios of the total DOM pool (Benner, 2002), a high CF UF study by Loh and co-workers also observes no significant change in HMW DOM C/N with depth from a similar ocean region (Loh et al., 2004). Therefore, the unchanging C/N ratios with

depth suggest that the youngest, most labile fraction of the HMW DOM pool has a relatively uniform N-content throughout the entire Pacific water column, consistent with either non-selective degradation (McCarthy et al., 2004), or perhaps alternate surface-linked sources present at depth (Orellana and Hansell, 2012).

Surface water total DOM C/N ratios (14.1 ± 0.7) are slightly elevated compared to our HMW UDOM fraction, again consistent with expectations for our operational fractions within the two-pool model. At depth, the C/N of total DOM is substantially higher than UDOM (19 ± 5). However, because of the large errors associated with deep DON concentrations (i.e. when TDN and DIN are both high, e.g., McCarthy and Bronk, 2008), this trend is not statistically significant (two tailed t-test, DF= 4, t = 1.8, p = 0.15). We note that an overall increase in total DOM C/N with depth is expected based on relative proportions of HMW (low C/N) and LMW (high C/N) DOM in surface versus deep water. Overall, these HMW UDOM and LMW SPE-DOM C/N ratio offsets fit well within recent observations of broader trends between organic matter size, age, and elemental composition (Walker et al., 2016c; 2016a).

Coupled UF/SPE: Stable Isotopic Composition ($\delta^{13}C$, $\delta^{15}N$) of HMW and LMW DOM

In the surface, the $\delta^{13}C$ value of HMW UDOC and LMW SPE-DOC fractions are statistically indistinguishable (-22.5 ± 0.3 ‰ and -22.7 ± 0.2 ‰ respectively; two tailed t-test, DF= 10, t = 1.4, p = 0.2) (Fig. 1.7). Both values however, are lower than total DOC $\delta^{13}C$ (-21.1 ± 0.4 ‰). In the subsurface, the average $\delta^{13}C$ values of each fraction are offset from both each other and total DOM. There is no depth trend below

400 m in $\delta^{13}C$ within either fraction, leading to a constant offset between the two fractions (Fig. 1.9c). The $\delta^{13}C$ values of LMW SPE-DOM from ≥ 400 m are always lowest (average of 400 to 2500 m: -22.6 ± 0.4‰), the HMW UDOM always highest (average of 400 to 2500 m: -21.4 ± 0.4 ‰), and the total DOM values are intermediate between the two fractions (average: -22.1 ± 0.4 ‰).

The $\delta^{13}C$ results in the subsurface NPSG are consistent with expectations based on the relative functional composition of HMW and LMW pools. Specifically, LMW SPE-DOM likely contains more lipid-like and CRAM like structures (Hertkorn et al., 2006; Koprivnjak et al., 2009), consistent with both higher C/N and lower $\delta^{13}C$ values (e.g., Hayes, 2001). In contrast, the more abundant proteinaceous and carbohydrate compound classes in HMW UDOC are consistent with both lower C/N and higher $\delta^{13}C$ (Hayes, 2001). The intermediate $\delta^{13}C$ values of total DOC between LMW SPE-DOC and HMW UDOC for all depths (with the exception of the surface), further supports the conclusion that our method selectively isolates two operationally distinct fractions from different reactivity pools.

However, the large offset of both HMW UDOC and LMW SPE-DOC $\delta^{13}C$ from total DOC $\delta^{13}C$ in the surface (Fig. 1.7, 1.8) does not seem consistent with these ideas. This result could be linked to material not retained by either UF or SPE isolations. This would require the non-retained material to have similar $\delta^{13}C$ values to total DOC (average $\delta^{13}C$ value of approximately -20.8, by mass balance), and be composed of nominally low MW material (i.e., passes the UF membrane) that is also relatively polar (so as not to be retained by the hydrophobic sorbent). In addition, the average C/N value of the non-retained material (by mass balance) is ~14, and

therefore not consistent with expectations for ^{13}C-enriched proteinaceous material. Finally, the presence of this offset only in the surface samples, repeated in both seasonal cruises, suggests this non-retained DOM is fresh, labile, and disappears rapidly with degradation. However, this would seem to conflict with the average value for mass balance derived $\Delta^{14}C$ for the non-retained material (-240 ‰). An alternate explanation therefore, is that rather than missing material having an elevated $\delta^{13}C$, the HMW material isolated in the surface is skewed towards lower $\delta^{13}C$ values by the presence of a ^{13}C deplete component.

The $\delta^{15}N$ values of LMW SPE-DON (average of all depths: 3.5 ± 0.3 ‰) and HMW UDON (average of all depths: 6.6 ± 0.4 ‰) are significantly different throughout the water column (two tailed t-test, DF= 22, t = 21.4, $p < 0.01$) (Fig. 1.7). LMW SPE-DON $\delta^{15}N$ is significantly lower than HMW UDON $\delta^{15}N$ at all depths, with an increasing offset from surface to deep. Average surface LMW SPE-DON $\delta^{15}N$ is 4.0 ± 0.3‰ and decreases to a constant value in subsurface samples (average of all subsurface samples: 3.4 ± 0.1‰). HMW UDON $\delta^{15}N$ has the opposite behavior with depth: surface values average 6.3 ± 0.3‰, with higher average subsurface values of 6.7 ± 0.3‰. While the offset between HMW UDON and LMW SPE-DON $\delta^{15}N$ values are significant at all depths (average offset over entire water column = 3.1 ± 0.6 ‰), the offset also increases with increasing depth (Fig. 1.9d, surface offset = 2.2 ± 0.4 ‰, 2500 m offset = 3.4 ± 0.3 ‰, two tailed t-test, DF= 4, t = 4.1, p = 0.01).

Published values for bulk DON $\delta^{15}N$ in surface water for this region (5.0 ± 0.5‰, Knapp et al., 2011) are intermediate between the two isolated fractions (Fig. 1.7). In addition, the general direction of the offset with depth (i.e., HMW DON

having higher $\delta^{15}N$ values than LMW DON) is also consistent with the few prior observations in oligotrophic surface waters (Knapp et al., 2012). These novel data raise new questions regarding N-sources, and in particular what cycling processes over multi-centennial to millennial ocean mixing timescales could result in a similar $\delta^{15}N$ pattern at all depths in the North Central Pacific. While more detailed work will be required to address these questions, the difference in $\delta^{15}N$ value between our operational fractions in particular underscores the new potential of this approach to isolate separate DOM fractions with novel properties and distinct composition.

SPE-DOM vs. LMW SPE-DOM

As discussed in the *Coupled UF/SPE: Recovery Efficiency* section, recovery data indicates that there is substantial overlap in the material collected by UF and SPE. This is further supported by the differences in the elemental and isotopic properties of SPE-DOM compared to LMW SPE-DOM (Fig. 1.10). Whereas PPL SPE-DOM properties approximate total DOM in numerous cases (especially in the deep ocean), the properties of LMW SPE-DOM are consistently different than total DOC. LMW SPE-DOM is older, has higher C/N ratios, and lower $\delta^{13}C$ and $\delta^{15}N$ values that both SPE-DOM and total DOM at all depths. This suggests that there is some younger, lower C/N, higher $\delta^{13}C$ and $\delta^{15}N$ material which is isolated by SPE but is not isolated in the LMW SPE-DOM fraction because of prior removal by UF. The offset is greatest in the surface where there is the highest concentration of HMW DOM, further suggesting that the offsets are the result of partial collection of HMW DOM by SPE. Overall, this demonstrates that the removal of HMW DOM by UF is

required for the subsequent targeted isolation of refractory DOM via SPE.

Summary & Conclusions

We describe a new approach that targets the isolation of operational DOM fractions with strongly contrasting average age, molecular size, and bulk composition. We couple UF with SPE isolation from the UF permeate to selectively isolate HMW and LMW DOM respectively. The composition of the HMW UDOM samples is consistent with younger, more N-rich, semi-labile DOM, while the composition of LMW SPE-DOM isolates is consistent with older, C-rich, more refractory DOM. The contrasting properties of the individual isolates from surface to deep NPSG waters confirm that our MW partition is effective at isolating material with strongly distinct properties. Further, our large volume isolation protocol allows gram quantities of these DOM fractions to be isolated for subsequent analysis. The scalability of this approach further enables a wide range of detailed analyses, such as compound-specific stable or radio isotopic analyses, for which sample limitation can otherwise prohibit.

In order to optimize our coupled UF/SPE method, we performed a comprehensive set of tests with two SPE sorbents commonly applied in recent literature for DOM isolation; comparing the elemental ratios, stable isotope ratios, and radiocarbon age of SPE-DOM with the same properties in total DOM. These tests showed that PPL generally performs better than HP-20, with higher overall DOC recoveries and with elemental and isotopic compositions more representative of total DOM, especially in the deep ocean. However, our data also suggests that the

chemical and isotopic composition of SPE-DOM, in particular for nitrogenous organic material, is strongly depth-dependent. SPE of surface DOM discriminates strongly against organic nitrogen, and has $\Delta^{14}C$ and $\delta^{13}C$ values offset from total DOC, consistent with preferential isolation of hydrophobic, C-rich DOM. In contrast, PPL SPE-DOM in deep NPSG waters is statistically indistinguishable from total DOM for all elemental and isotopic properties we measure, including C/N ratios. This suggests that PPL is well suited to the study of the refractory, background DOM pool. However, it is also clear from isotopic and recovery efficiency data that PPL SPE-DOM isolates from any depth contain a mixture of both older, refractory DOM and a younger, semi-labile component. Therefore, the removal of the HMW young, semi-labile material by UF prior to SPE is required in order to isolate an older, more refractory component and limit the confounding influences of reactivity mixtures.

Together, our results underscore the compositional and isotopic heterogeneity of marine DOM and highlight the inherent problems with attempting to isolate truly representative DOM samples. We suggest that targeted isolation approaches, which exploit differences in DOM composition, can yield samples that allow more specific testing of multiple current hypotheses regarding the origin and composition of excess, semi-labile DOM and background, refractory DOM. The current era of DOM research is an exciting one, with multiple ideas suggested to explain refractory DOM persistence and biogeochemical cycling. Molecular diversity, dilution, microbial degradation, molecular size and composition, photo-oxidation, and micro-gel aggregation have all been suggested as key controls on refractory DOM formation (Arrieta et al., 2015; Chin et al., 1998; Dittmar, 2014; Flerus et al., 2012; Jiao et al.,

2010; Lechtenfeld et al., 2014; Walker et al., 2016a). This isolation approach represents a new tool for directly evaluating the composition of distinct DOM reactivity pools and allows for testing new hypotheses regarding DOM cycling in the ocean.

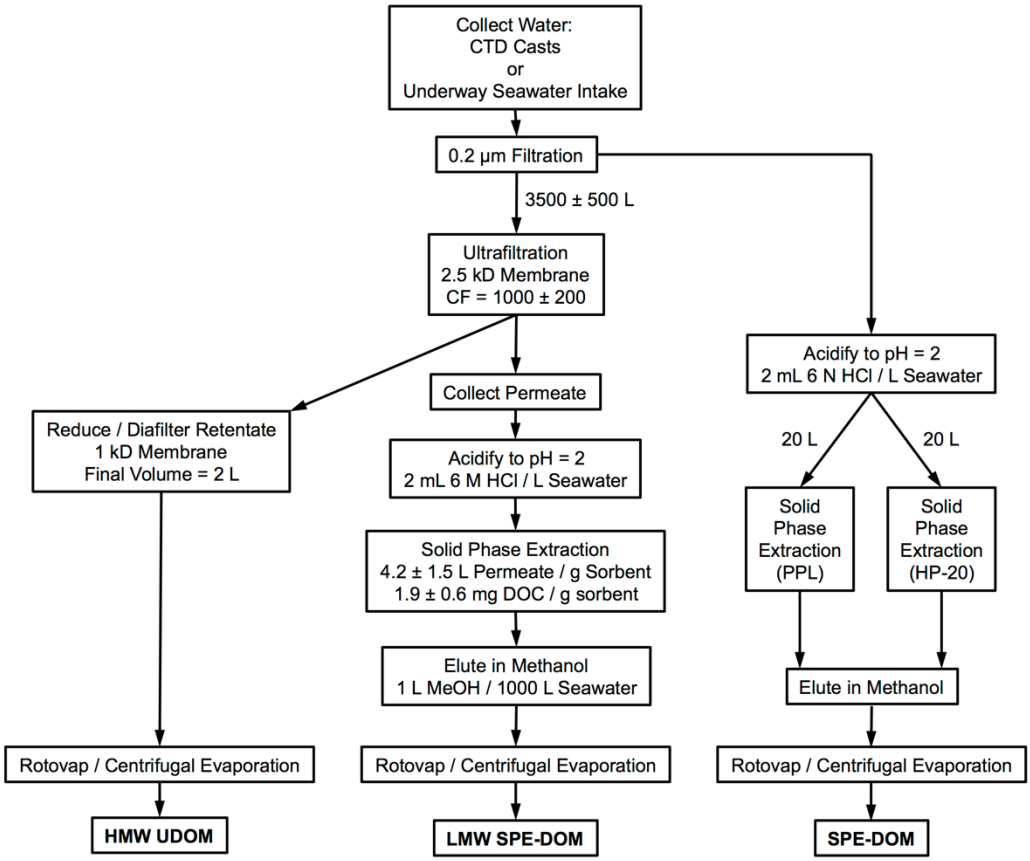

Figure 1.1 Flow chart detailing the steps involved in the isolation of high molecular weight ultrafiltered dissolved organic matter (HMW UDOM), low molecular weight solid phase extracted dissolved organic matter (LMW SPE-DOM), and traditional solid phase extracted dissolved organic matter (SPE-DOM). CF: concentration factor, ratio of volume filtered to final retentate volume.

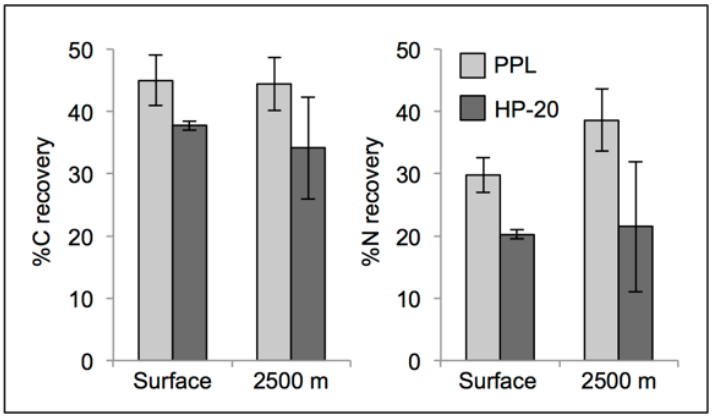

Figure 1.2 Comparison of relative recovery (%) of C and N isolated by PPL (light grey) and HP-20 (dark gray) SPE sorbents. Values represent error-weighted averages of material collected on two cruises and error bars represent 1σ standard deviation of these averages.

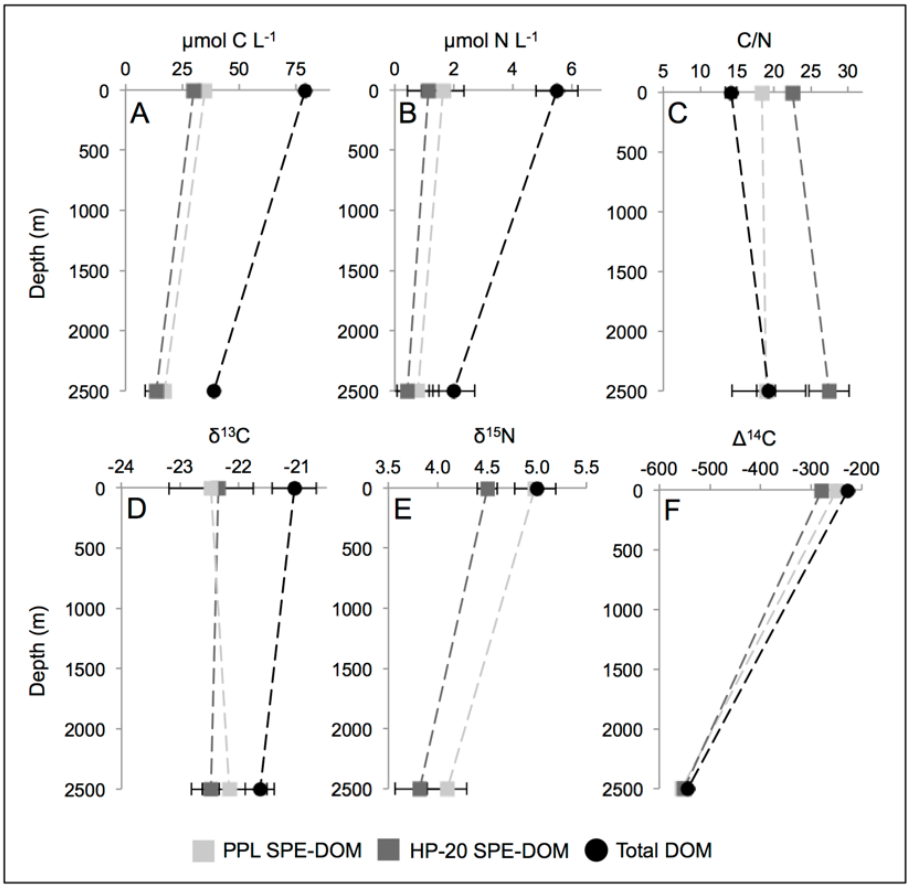

Figure 1.3 Carbon and nitrogen recovery, isotopic and elemental properties of SPE-DOM isolated by PPL (light grey squares) and HP-20 (dark grey squares) compared to measurements of total seawater DOM (black circles). Values represent error weighted averages of material collected on two cruises and error bars represent 1σ standard deviation of these averages. Where no error bars are visible, SD is smaller than symbols. A) µmolC L^{-1}, B) µmolN L^{-1}, C) C/N, D) $\delta^{13}C$, E) $\delta^{15}N$, F) $\Delta^{14}C$. Total DOM $\delta^{15}N$ value from Knapp et al. 2011.

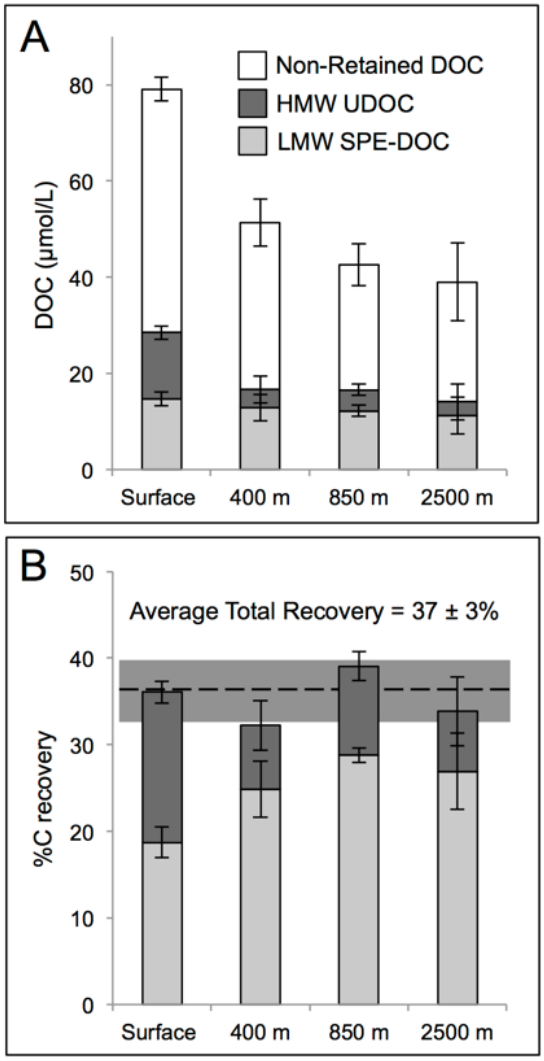

Figure 1.4 Total recovery of combined UF/SPE method, indicating relative proportions of DOC pool retained by SPE and UF steps with increasing depth. A) absolute C recoveries expressed as DOC concentration for the LMW SPE-DOC (light grey) and HMW UDOC (dark grey) isolations, compared to concentrations of non-retained DOC (white). B) relative recovery (%) of DOC by UF (dark grey) and SPE (light grey). Horizontal dotted line and grey bar represent average total recovery and SD of combined fractions. Values represent error-weighted averages of material collected on two cruises and error bars represent 1σ standard deviation of these averages.

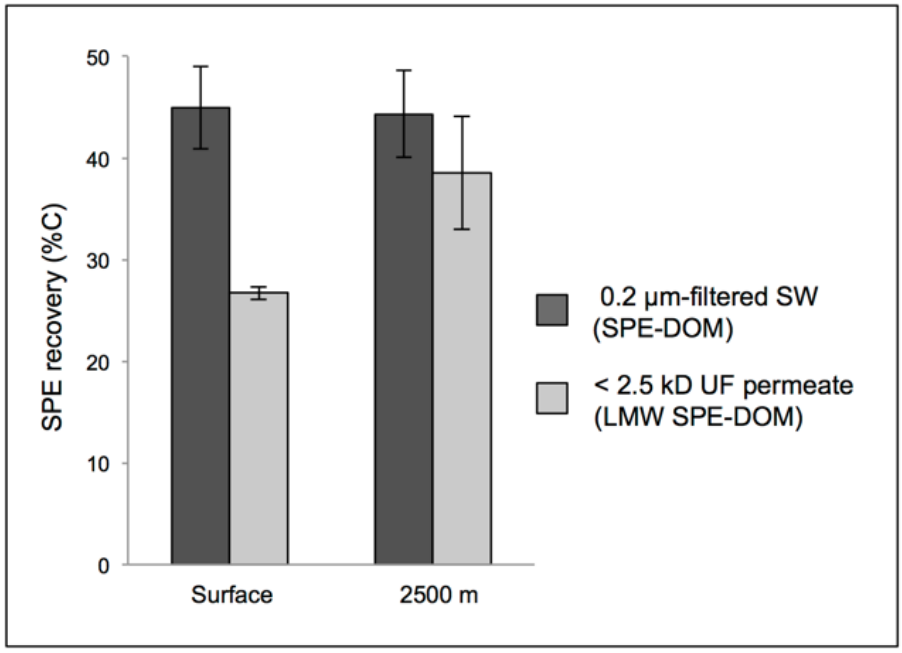

Figure 1.5 Relative recovery (%) of DOC from 0.2 µm-filtered seawater (PPL SPE-DOC; dark grey) and ≤2.5 kD UF permeate (LMW SPE-DOC; light grey).

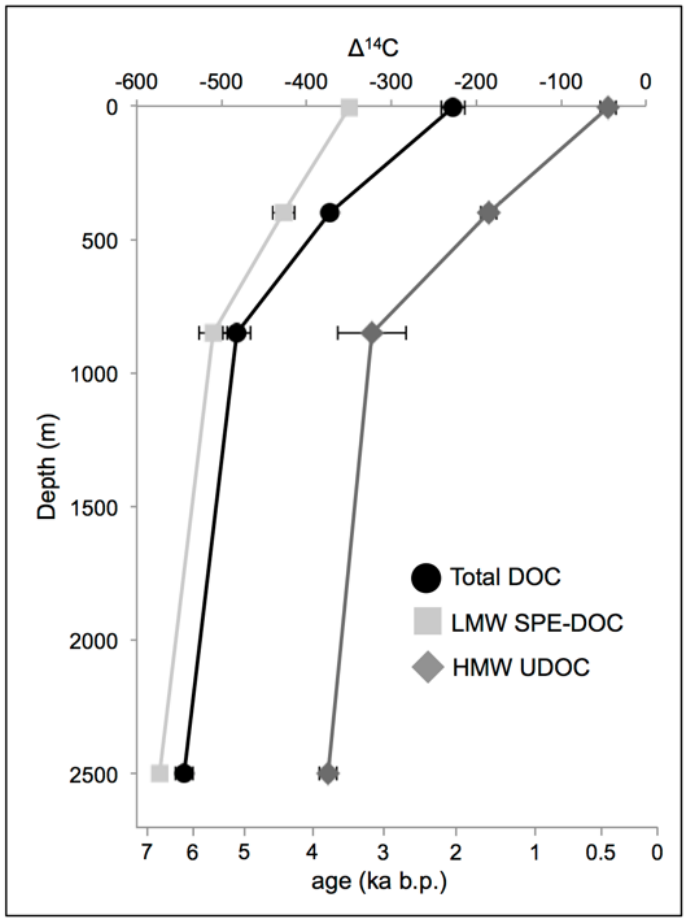

Figure 1.6 $\Delta^{14}C$ of total DOC (black circles) compared to LMW SPE-DOC (light grey squares) and HMW UDOC (dark grey diamonds). Bottom axis denotes the ^{14}C age in ka. Values represent error-weighted averages of material collected on two cruises and error bars represent 1σ standard deviation of these averages.

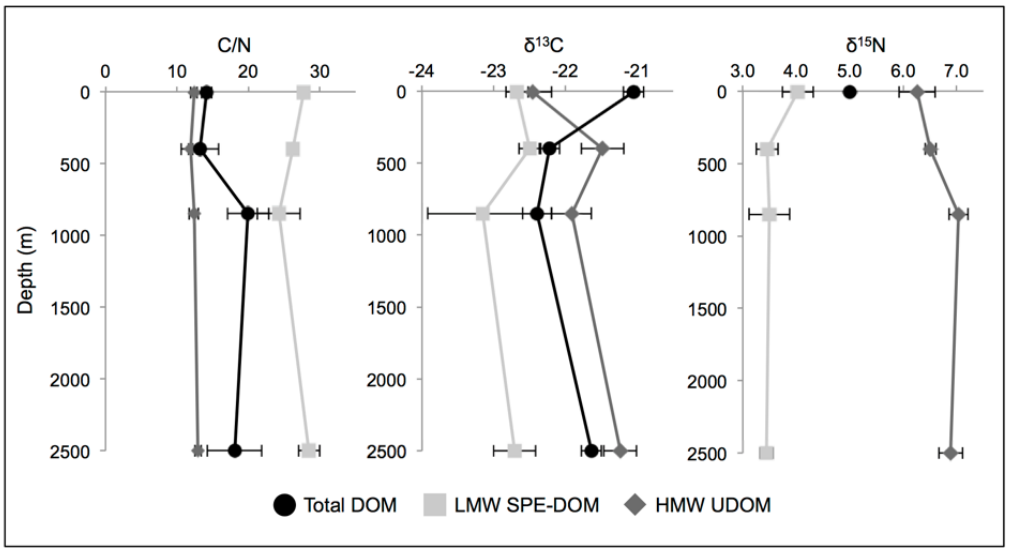

Figure 1.7 Depth profiles of elemental ratio (C/N), $\delta^{13}C$, and $\delta^{15}N$ values of total DOM (black circles) compared to LMW SPE-DOM (light grey squares) and HMW UDOM (dark grey diamonds). Values represent error-weighted averages of material collected on two cruises and error bars represent 1σ standard deviation of these averages. Total DOM $\delta^{15}N$ value from Knapp et al. 2011.

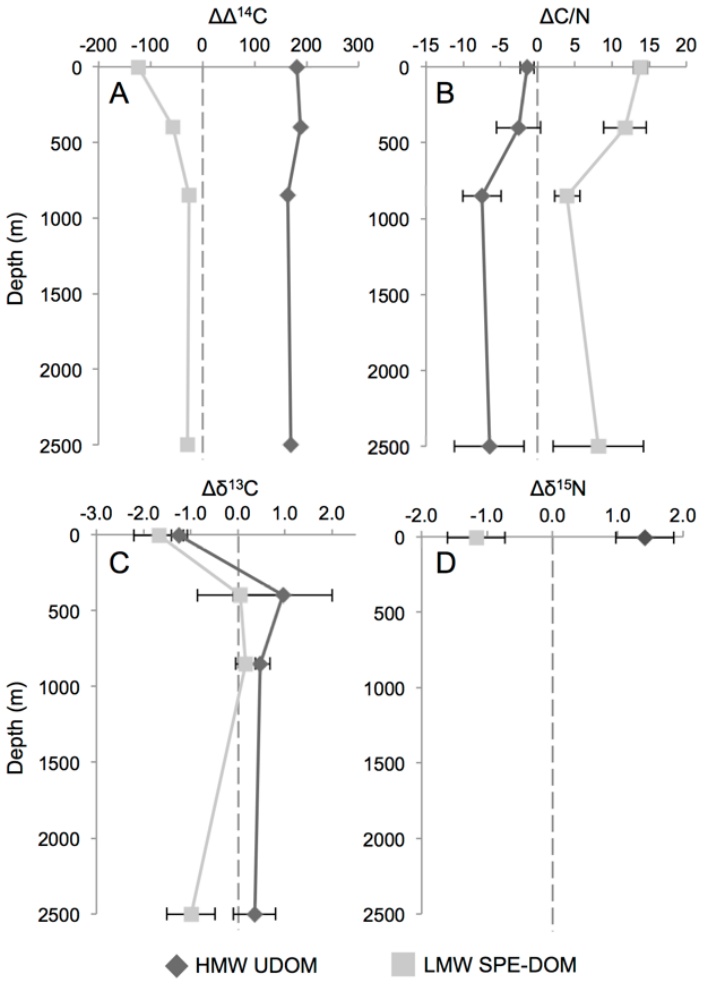

Figure 1.8 Elemental and isotopic properties of HMW UDOM (dark grey diamonds) and LMW SPE-DOM (light grey squares) fractions normalized to total DOM to show relative offsets of each fraction. Values calculated by subtracting the properties of total DOM from each fraction. A) $\Delta^{14}C$, B) C/N, C) $\delta^{13}C$, D) $\delta^{15}N$. Values represent error-weighted averages of material collected on two cruises and error bars represent 1SD of these averages. Where no error bars are visible, SD is smaller than symbols. Total DOM $\delta^{15}N$ value from Knapp et al. 2011.

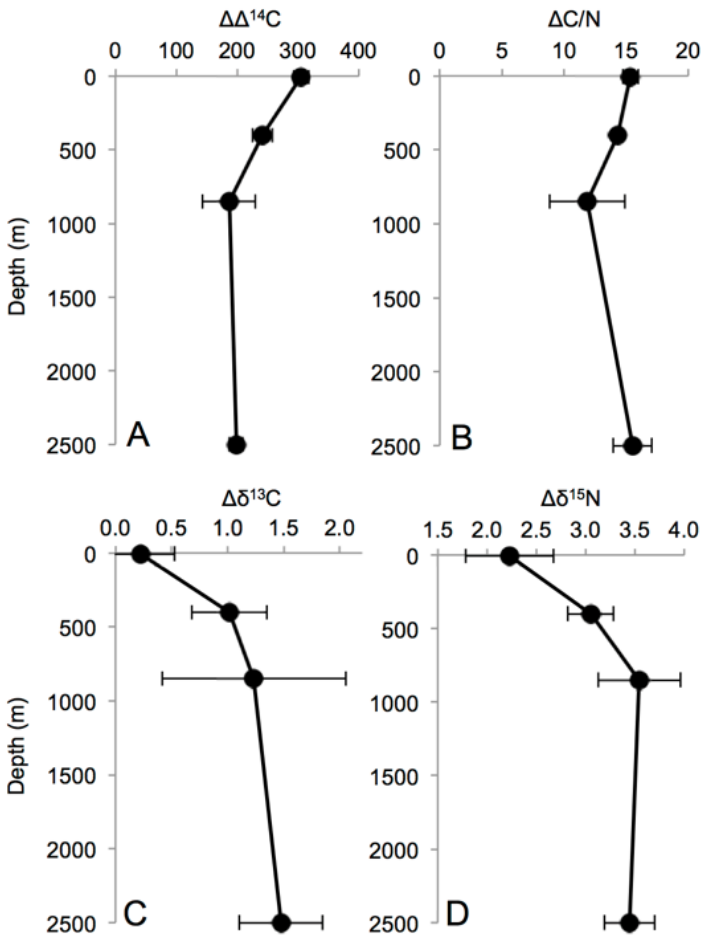

Figure 1.9 Absolute value of offset in elemental and isotopic properties between HMW UDOM and LMW SPE-DOM fractions. A) $\Delta^{14}C$, B) C/N, C) $\delta^{13}C$, D) $\delta^{15}N$. Circles are the absolute value of HMW UDOM minus LMW SPE-DOM. Values represent error weighted averages of material collected on two cruises and error bars represent 1SD of these averages. Where no error bars are visible, SD is smaller than symbols.

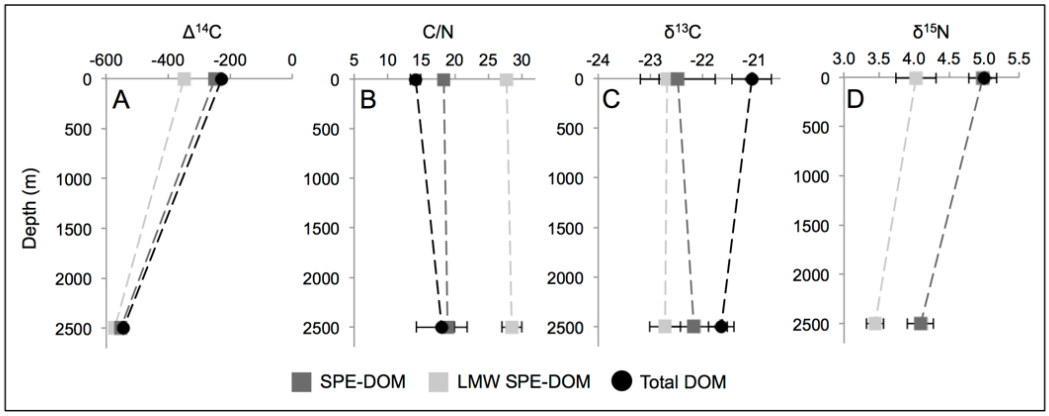

Figure 1.10 Isotopic and elemental properties of SPE-DOM (dark grey squares) compared to LMW SPE-DOM (light grey squares). The properties of total seawater DOM (black circles) are included for reference. Values represent error weighted averages of material collected on two cruises and error bars represent 1σ standard deviation of these averages. Where no error bars are visible, SD is smaller than symbols. A) $\Delta^{14}C$, B) C/N, C) $\delta^{13}C$, D) $\delta^{15}N$. Total DOM $\delta^{15}N$ value from Knapp et al. 2011.

Chapter 2

Low molecular weight dissolved organic carbon: aging, compositional changes, and selective utilization during ocean circulation

Abstract

Little is known about the cycling dynamics of marine dissolved organic carbon (DOC), particularly the refractory, low molecular weight (LMW) component that makes up the majority of this massive C pool. We measured stable isotopic ($\delta^{13}C$), radioisotopic ($\Delta^{14}C$), and compositional (C/N, ^{13}C solid-state NMR) properties of separately isolated high molecular weight (HMW) and LMW DOC fractions collected using a coupled ultrafiltration and solid phase extraction approach from throughout the water column in the North Pacific Subtropical Gyre and Central North Atlantic. The selective isolation of LMW DOC allowed the first investigation of the composition and cycling of the largest, previously elusive fraction of the DOC pool. The structural composition of the LMW DOC material closely matched that of carboxylic rich alicyclic material, which has been proposed as a major component of the refractory DOC pool. Examination of offsets in the measured parameters between the deep waters of the two basins provides the first direct assessment of changes in the composition of this material with ageing and utilization during ocean circulation. While our direct measurements largely confirm hypotheses regarding the relative cycling of HMW and refractory LMW DOC, we also demonstrate a number of novel observations regarding the removal of refractory DOC, additions of fresh DOC to the deep ocean, and compositional changes during global ocean circulation.

Introduction

Marine dissolved organic carbon (DOC) is the largest pool of reduced and actively cycling carbon in the ocean. Early measurements of the radiocarbon age of DOC compared to that of dissolved inorganic carbon demonstrated that at least a portion of DOC persists in the ocean on longer timescales than ocean circulation (Williams and Druffel, 1987; Druffel et al., 1992). These radiocarbon measurements combined with depth-based gradients in DOC concentration used to form a two-pool model of DOC cycling, with a pool of semi-labile material which is produced in the surface and degraded or utilized on timescales less than ocean circulation and a background pool of refractory material which cycles on millennial timescales with a relatively conservative distribution throughout the water column. The conservative behavior of DOC in the deep ocean has been utilized to investigate transit times of different water masses using offsets in radiocarbon age (Bauer et al., 1992; Hansell, 2013; Bercovici et al., 2018). However, DOC, even in the deep ocean, is a dynamic pool with constant removal and additions of new material (Smith et al., 1992; Hansman et al., 2009; Hansell and Carlson, 2013; Carlson and Hansell, 2014). Further, radiocarbon measurements of different components of the DOC pool have demonstrated a remarkable heterogeneity of $\Delta^{14}C$ values (Walker et al., 2011; Walker et al., 2014; Zigah et al., 2017; Broek et al., 2017) ranging from above modern (Druffel and Beaupré, 2009) to tens of thousands of years (Ziolkowski and Druffel, 2010; Coppola et al., 2015), suggesting significant variability in recalcitrance and cycling rates.

Increasing evidence has demonstrated a strong relationship between the average molecular weight of DOC, its radiocarbon content, and the relative recalcitrance of the material (Walker et al., 2011; Benner and Amon, 2015; Walker, et al., 2016a; Walker et al., 2016b; Broek et al., 2017). High molecular weight (HMW) DOC is primarily composed of recently produced material, containing intact labile biochemicals, whereas low molecular weight (LMW) DOC is old, degraded, biologically refractory, and dominates the background DOC pool which persists in the ocean on millennial timescales (Amon and Benner, 2015). The LMW fraction of the DOC pool is therefore a critical component that stores the vast majority of the ocean's dissolved organic carbon and nitrogen.

Until recently there has been no analytical approach to directly investigate this refractory LMW pool. The analyses that are possible in total seawater, primarily concentration measurements and bulk isotopic analyses, are limited and interpretations based on these measurements are complicated by the extreme heterogeneity of marine DOC. Material concentrated using ultrafiltration has been widely used for many DOC investigations. However, this is by definition HMW and therefore not representative of the refractory DOC pool. New generations of solid phase extraction (SPE) sorbents have more recently been used to isolate DOC that has been largely interpreted as primarily LMW material. However, it has been recently demonstrated that SPE-DOC isolated from whole seawater contains a significant fraction of younger, more labile HMW material (Broek et al., 2017). Coupled with ^{14}C ages that are comparable to total DOC (Flerus et al., 2012; Lechtenfeld et al., 2014), these new observations suggest SPE isolates are more similar to total DOC in

a number of properties than LMW DOC alone. Therefore, the issue of reactivity mixtures in SPE-DOM can confound interpretation of the composition and cycling behavior of this fraction (Broek et al., 2017).

An alternate approach to the study of LMW DOC has been indirect observations from the differences between ultrafiltered HMW DOC and total DOC. A number of studies have inferred some properties of the LMW DOC pool, such as ^{14}C age from these indirect calculations, however, these analyses are also severely limited by what it is possible to measure in whole seawater (Loh et al., 2004; Kaiser and Benner, 2009). Without a method to selectively isolate the LMW pool it has not been possible to directly apply many analyses with vast informational potential such as NMR and molecular level analyses requiring large sample sizes, limiting our understanding of the broad functional composition of DOC.

Here we present data from a new approach to DOC isolation utilizing a sequential combination of ultrafiltration and SPE, which has been developed and demonstrated as an effective means to specifically isolate large quantities of old, LMW DOC from both surface and deep water (Broek et al., 2017). By limiting the influence of DOC size and reactivity mixtures, this combined UF/SPE method provides a more direct approach than has previously been possible to investigate the composition, sources, and cycling of the most refractory material in the ocean. For the first time we measure the stable isotope ratios, elemental composition, and functional composition derived from solid-state NMR spectra of selectively isolated LMW DOC from throughout the water column in both the Atlantic and Pacific Ocean Basins. We interpret the results in the context of radiocarbon age and offsets between basins to

determine how the properties of this material change during deep ocean circulation. The properties of and changes to the LMW fraction are compared to the more commonly studied semi-labile HMW DOC material, which was collected from the same water, in order to investigate the relative behavior of different components of the DOC reactivity spectrum. Together these represent the first synoptic look at compositional changes of both semi-labile and refractory DOC with ageing and utilization during large scale ocean circulation.

Materials & Methods

Sample Collection

Samples were collected on four research cruises aboard both the R/V Kilo Moana in August 2014 and May 2015 and the R/V Atlantic Explorer in August 2015 and May 2016. Sampling was conducted at the Hawaii Ocean Time Series (HOT) Station ALOHA (A Long-Term Oligotrophic Habitat Assessment; 22° 45'N, 158° 00'W) in the North Pacific Subtropical Gyre (NPSG) and the Bermuda Atlantic Time Series Site (BATS; 31° 40'N, 64° 10'W) in the Central North Atlantic. Surface water was sampled via the vessels' underway sampling system with an inlet at approximately 7.5 m water depth on the R/V Kilo Moana and 2 m water depth on the R/V Atlantic Explorer. The laboratory seawater taps were flushed for approximately 2 hours prior to each sampling. Large volume subsurface water samples were collected from 400 m, 850 m, and 2500 m using successive casts of a rosette equipped with 24 x 12 L Niskin bottles. Seawater was pre-filtered through 53 µm Nitex mesh and pumped through 0.2 µm polyethersulfone (PES) cartridge filters prior to

ultrafiltration. All filters and storage containers were cleaned with 10% HCl and ultrapure water (Milli-Q; 18.2 MΩ) then flushed with seawater prior to sampling.

DOC Isolation

A detailed explanation of the DOC isolation protocol is described in Broek et al. (2017). Briefly, ultrafiltration was performed using a custom-built system consisting of four-spiral wound PES UF membranes (2.5 kD; GE Osmonics GH2540F30, 40-inch long, 2.5-inch diameter) mounted in stainless steel housings, plumbed in parallel to a 100 L fluorinated HDPE reservoir, with flow driven by a 1.5 HP stainless steel centrifugal pump. Seawater samples of 1000-4000 L were concentrated to a final retentate volume of 15-20 L, then further reduced to 2-3 L with a second custom-built ultrafiltration system with a single membrane of a smaller MW cutoff (1 kD GE Osmonics GE2540F30, 40-inch long, 2.5-inch diameter, 1 kD MWCO), Samples were then diafiltered by slowly adding 40 L of Milli-Q water at the same rate of membrane permeation. Samples were dried to powder with a combination of rotovap and centrifugal evaporator. LMW DOC permeating the UF system was isolated using PPL sorbent (Agilent Bondesil PPL, 125 µm particle size, part # 5982-0026) following the general recommendations of Dittmar et al. (2008) and Green et al. (2014), including loading rates, seawater to sorbent ratios, and elution volumes and rates. Permeate from the UF system was acidified in 200 L batches to pH 2 with HCl and pumped through the SPE sorbent contained in a parallel combination of 2 medium-pressure glass chromatography columns. Following sample loading, the SPE sorbent was desalted with 6 L of pH 2 ultrapure water and isolated

material was eluted with six 500 mL additions of methanol, which was similarly dried to powder via rotovap and centrifugal evaporation.

Total DOC ([DOC], [DON], $\Delta^{14}C$, $\delta^{13}C$)

Subsamples for dissolved organic carbon (DOC) and total dissolved nitrogen (TDN) concentration measurements were collected into pre-combusted 40 mL borosilicate glass vials following 0.2 μm-filtration. DOC and TDN concentration measurements were made via the high-temperature catalytic oxidation method using a Shimadzu TOC-V analyzer in either the Carlson lab at UCSB (https://labs.eemb.ucsb.edu/carlson/craig/services) or the Benner lab at the University of South Carolina (Benner et al., 1993). DOC concentrations measurements were also determined via UV oxidation, cryogenic purification, and manometric determination at UC Irvine. DOC concentrations were similar between the two methods and the presented values represent the error weighted average of both measurements. Total DON concentrations were determined by subtracting the sum of dissolved inorganic nitrogen (DIN) species (nitrate, nitrite, ammonia) concentrations, determined using a Lachat QuickChem 8000 Flow Injection Analyzer, from the measured TDN concentrations. Seawater samples for C isotopic analysis ($\delta^{13}C$, $\Delta^{14}C$) were collected in pre-combusted 1000 mL Amber Boston Round bottles, immediately frozen, and stored at -20°C.

EA-IRMS ($\delta^{13}C$, C/N)

Stable carbon isotope ratios ($\delta^{13}C$) and elemental ratios (C/N)a were determined via elemental analyzer isotope ratio mass spectrometry (EA-IRMS) at the University of California, Santa Cruz, Stable Isotope Laboratory (UCSC-SIL; http://emerald.ucsc.edu/~silab/) using a Carlo Erba CHNS-O EA1108-elemental analyzer interfaced via a ConFlo III device with a ThermoFinnigan Delta Plus XP isotope ratio mass spectrometer (Thermo Fisher Scientific). Standards, EA-IRMS protocols, and correction routines followed standard UCSC-SIL protocols. Analytical uncertainties of n=3 replicate measurements of the $\delta^{13}C$ of isotopic standards ranged from ± 0.05 to 0.1‰.

^{14}C-AMS ($\Delta^{14}C$)

Natural abundance radiocarbon ($\Delta^{14}C$) determinations of all isolated fractions were performed at the Lawrence Livermore National Laboratory, Center for Accelerator Mass Spectrometry (LLNL-CAMS) by AMS following standard graphitization procedures (Vogel et al., 1984; Santos et al., 2007). The $\Delta^{14}C$ signature of total seawater DOC (< 0.2 μm) was determined by UV-oxidation and AMS at the UC Irvine Keck Carbon Cycle AMS Lab (Beaupré et al., 2007; Druffel et al., 2013; Walker, Griffin, et al., 2016). Results are reported as age-corrected $\Delta^{14}C$ (‰) for geochemical samples and have been corrected to the date of collection and are reported in accordance with conventions set forth by Stuiver and Polach (1977). The isotopic values are reported as background and $\delta^{13}C$ corrected fraction modern (Fm), $\Delta^{14}C$, and conventional radiocarbon age (ybp).

Solid-state ^{13}C NMR

Solid state ^{13}C {1H} cross polarization magic angle spinning (CP/MAS) NMR spectra were collected on a Bruker Avance III spectrometer operating at 100.5474 MHz for 13C and 399.8285 MHz for 1H. A Bruker HXY MAS probe was used, along with 4mm ZrO2 rotors with Kel-F tips. The 1H π/2 pulse was 4μs, and cross polarization was achieved via a 70-100% power ramp on the 1H nucleus. Cross polarization contact time was 4ms, and the MAS rate was 10 kHz. The ^{13}C power (62.5 kHz)cand SPINAL-64 1H decoupling (225 kHz) were optimized using the peak intensity and peak widths of glycine, and ^{13}C chemical shifts were measured relative to the carboxylic acid group on glycine at ^{13}C = 176.49 ppm. A total of 16,384 acquisitions were collected for each sample with a 1 s pulse delay. 512 points were used for Fourier transform with a 10 μs dwell time. 100 Hz of line broadening was applied during processing.

The relative distribution of different functional groups was determined by integrating the area under the curve using the chemical shift ranges and assignments from Mao et al., (2012) as follows (Fig. 2.10): ketone, aldehyde, quinone (220-191 ppm); COO, NC=O (191-164 ppm); aromatic C-O (164-150 ppm); aromatics (150-117 ppm); OCO (94-60 ppm); OC (94-60 ppm); OCH3, NCH (60-45 ppm); CCH2C, CCHC (45-30 ppm); CCH2C, CCH3 (30-0 ppm). For some comparisons, including to previous data, regions were combined (as in Koprivnjak et al., 2009), resulting in four generalized groupings: carboxyl C (220-191 ppm), aromatic C (164-117 ppm), alkoxy C (117-60 ppm), and alkyl C (60-0 ppm).

Results

DOC Concentration and Recovery of High and Low Molecular Weight DOC Fractions

DOC concentrations in the Central North Atlantic are highest at the surface (average = 84 ± 14 μM) with significant offsets between Spring (94 ± 5 μM) and Summer (74 ± 8 μM) sampling (Fig. 2.1a). The concentration decreases through the upper 850 m to a relatively constant deep ocean concentration of 48 ± 2 μM (Average ≥ 850 m). In the NPSG, DOC concentrations are lower throughout the water column with an average surface concentration of 78 ± 3 μM decreasing to a deep ocean (2500 m) value of 37 ± 3 μM. There is some seasonal variability in surface ocean concentration, however, to a lesser degree than in the Atlantic Basin (Summer = 80 ± 1 μM; Spring = 76 ± 1 μM).

In the Central North Atlantic, ultrafiltration isolated an average of 10 ± 1 μmol-C L-1 in the surface and 5 ± 1 μmol-C L-1¬ in the subsurface (≥ 400 m), representing 12 ± 1% and 9 ± 1% of total DOC respectively (HMW UDOC; Fig. 2.1b). In the NPSG, ultrafiltration isolated 13 ± 1 μmol-C L-1 in the surface and 4 ± 1 μmol-C L-1¬ in the subsurface, representing 17 ± 1% and 9 ± 2 % of total DOC respectively.

SPE of LMW DOC permeating the ultrafiltration system isolated 22 ± 1 μmol-C L-1 from surface waters of the Central North Atlantic and an average of 17 ± 1 μmol-C L-1 from subsurface waters (LMW SPE-DOC; Fig 2.1c). The SPE approach isolated significantly less material from the NPSG, recovering 15 ± 1 μmol-C L-1 in the surface and an average of 12 ± 1 μmol-C L-1 in the subsurface.

Although the recovery in the surface was slightly higher than in the subsurface, as a result of the decreasing concentration of total DOC with depth, the relative % recovery is lower in the surface and higher at depth. In the Central North Atlantic this recovery represents 26 ± 3 % of total DOC in the surface and 34 ± 3 % in the subsurface (≥ 400 m). In the North Pacific the DOC recovery represents 18 ± 2 % of total DOC in the surface and 29 ± 2 % in the subsurface.

Radiocarbon ($\Delta^{14}C$) of total, HMW, and LMW DOC

In the Central North Atlantic the average surface $\Delta^{14}C$ value of total DOC is -186 ± 4 ‰ (1590 ybp) and decreases through the water column to a minimum value of -438 ± 4 ‰ (4570 ybp) at 850 m (Fig. 2.2a). There is a slight increase in $\Delta^{14}C$ at 2500 m ($\Delta^{14}C$ = -392 ± 4 ‰; 3930 ybp). NPSG $\Delta^{14}C$ of total DOC is lower (older ^{14}C age) at all depths, with an average surface value of -227 ± 14 ‰ (2000 ybp) decreasing to a minimum in the deepest samples (2500 m; -544 ± 10 ‰; 6240 ybp).

The $\Delta^{14}C$ of HMW UDOC is significantly higher (younger ^{14}C age) than that of total DOC throughout the water column in both basins (Fig. 2.2b) with an average value of -54 ± 15 ‰ (440 ybp) in the surface of the Central North Atlantic decreasing to a minimum in the deepest samples (2500 m; -278 ± 16 ‰; 2630 ybp). In the NPSG, average surface $\Delta^{14}C$ of HMW UDOC is similar to surface waters in the Central North Atlantic (-45 ± 10 ‰; 300 ybp), however, is lower throughout the rest of the water column, with a minimum of -375 ± 10 ‰ (3700 ybp) in the deepest samples (2500 m).

In contrast, the $\Delta^{14}C$ of LMW SPE-DOC is significantly lower (older ^{14}C age) than that of total DOC throughout the water column in both basins (Fig. 2.2c). In the Central North Atlantic, the $\Delta^{14}C$ value of LMW SPE-DOC mirrors that of total DOC with an average value of -323 ± 12 ‰ (3120 ybp) in the surface, decreasing to a minimum at 850 m (-467 ± 23 ‰; 5050 ybp), with a slight increase in the 2500 m samples ($\Delta^{14}C$ = -437 ± 37 ‰; 4530 ybp). In the North Pacific, the average $\Delta^{14}C$ of LMW SPE-DOC is lower than in the Central North Atlantic throughout the water column with an average surface value of -350 ± 9 ‰ (3380 ybp) decreasing to a minimum of -573 ± 6 ‰ (6770 ybp) in the deepest samples (2500 m).

Elemental (C/N) Composition

Carbon to nitrogen atomic ratios (C/N)a of total DOM, HMW UDOM, and LMW SPE-DOM are distinct from each other throughout the water column (Fig. 2.3a-c). The average C/N ratio of total DOM in all samples is 16 ± 4, however, within each sample the average standard deviation is high due to the compounded error associated with the high uncertainty of [DOC] and [DON] values (Fig. 2.3a). As a result, there is no statistically significant depth structure in either basin. However, in the deepest sample (2500 m) there is a significant offset between the two basins, with higher values in the North Pacific (18 ± 3) than the Central North Atlantic (11 ± 2). The C/N ratio of HMW UDOM is lower on average than total DOM and has a narrow range of values (11 to 14), with no significant depth structure or offsets between fractions (Fig. 2.3b). In contrast, the C/N ratio of LMW SPE-DOM is much higher than both total DOM and HMW DOM (Fig. 2.3c). The ratio is highest in the surface

and decreases through the upper water column. At 2500m there is a significant offset in the C/N ratio, with higher values in the NPSG (24 ± 2) than the Central North Atlantic (28.5 ± 1.5).

Stable Isotopic ($\delta^{13}C$) Composition

The $\delta^{13}C$ of total DOC has a narrow range of values (-22.7 to -21.1 ‰) which are statistically indistinguishable throughout the water column between the Central North Atlantic and North Pacific (Fig. 2.3e). There is some depth structure in both basins with the highest values in the surface (average of both basins = -21.1 ± 0.4 ‰) and lower values in the subsurface (average of all depths ≥ 400 m in both basins = -22.1 ± 0.4 ‰). Similar to total DOC, there are no significant offsets in HMW UDOC $\delta^{13}C$ values between basins (Fig. 2.3f). There is also significant depth structure, which follows the opposite trend of total DOC, with the lowest values in the surface (average of both basins = -22.4 ± 0.1 ‰) and higher values in the subsurface (average of all depth ≥ 400 m in both basins = -21.5 ± 0.25 ‰). In the surface, values are lower than that of total DOC whereas HMW UDOC values are higher than total DOC in the subsurface. In contrast, the $\delta^{13}C$ of LMW SPE-DOM has a very narrow range of values which are significantly lower than that of both total DOC and HMW UDOC throughout the water column with no significant depth structure or offsets between basins (Fig. 2.3g; average of all samples = -22.7 ± 0.2 ‰).

Functional Composition (Solid State ^{13}C-NMR)

The ^{13}C {1H} CP/MAS NMR spectra of HMW UDOC are dominated by peaks at ~110 ppm (acetal; O-C-O) and ~80 ppm (alkyl O-C-H) (Fig. 2.4a). The average ratios of O-alkyl to acetal C in HMW UDOC is 5.4 ± 1.0, consistent with the ratios of typical carbohydrates (Sannigrahi et al., 2005). This alkoxy component has the greatest relative abundance in the surface, comprising an average of 62 ± 3 % of the total signal, and is attenuated at depth (2500 m; 47 ± 2 %). The remainder of the signal is comprised of carboxyl (~175 ppm; 13 ± 5 %), and aliphatic (0-60 ppm; 31 ± 4 %) functional groups, with a minor aromatic (~135 ppm; ~1 %) component.

In contrast, the LMW SPE-DOC spectra are dominated by aliphatic (0-60 ppm; 62 ± 3 %) and carboxyl (~175 ppm; 16 ± 1 %) functionality (Fig. 2.4b). There is also a greater proportion of aromatic C (~135 ppm; 4 ± 1 %) in the LMW fraction. The signal in the alkoxy region (117-60 ppm; i.e. carbohydrate C in HMW DOC) comprises 17 ± 2 % of the LMW signal, however this is almost entirely O-alkyl C and so the ratio of the O-alkyl to acetal C is much higher (32 ± 12) than in the HMW fraction. Unlike the HMW material, there is little variability in relative proportion of functional groups with depth or between basins.

Discussion

Elemental and Isotopic Composition

The novel LMW DOC fraction recovered by our combined UF/SPE isolation approach allows for an examination of the composition of the refractory material which persists in the ocean on millennial timescales. While the LMW material

collected in the NPSG has previously been characterized (Broek et al., 2017), the addition of material from a second basin confirms a number of hypotheses that were suggested by more limited data, while also providing more mechanistic interpretations.

Radiocarbon analysis of the LMW material shows an average age that is significantly older than both the total DOC pool and the HMW UDOC fraction, indicating that it represents a significantly slower cycling component of marine DOC (Fig. 2.2). The LMW material has C/N ratios significantly elevated compared to the total pool, suggesting that LMW DOC throughout the water column is C-rich, consistent with expectations for the alicyclic and lipid derived material which has been hypothesized to account for a significant portion of recalcitrant marine DOC (Hwang, 2003; Hertkorn et al., 2006; Koprivnjak et al., 2009; Fig. 2.3c).

With the addition of the Central North Atlantic basin, we can now confirm a significant decrease in the C/N ratio of the LMW fraction through the upper water column (Fig. 2.3c). This finding is unexpected as it suggests that a nitrogenous component exists within the LMW pool which is actually more refractory than some portion of the non-N-containing material. However, while contrary to expectations based on common assumptions about the lability of N-containing materials, this observation is also consistent with the depth related changes in $\delta^{13}C$ of the LMW material (Fig. 2.3g). Overall, the $\delta^{13}C$ values of LMW DOC are lower than that of the total DOC pool in both basins, which was previously hypothesized to correspond to a contribution from ^{13}C depleted lipid-like material (Hayes, 2001; Broek et al., 2017). However, the $\delta^{13}C$ values are also variable through the water column in both basins

and there is a significant decrease with depth, coincident with the observed changes in C/N ratio. The relationship between $\delta^{13}C$ and C/N ratio is highly significant (R2 = 0.53) in both basins, especially when considered in each basin separately (Atl. R2 =0.94, Pac. R2 = 0.77; Fig. 2.9).

We hypothesize that these observations can be explained by changes in the relative contribution of different major compound types. Specifically, in contrast to the ^{13}C depleted values of lipid material, n-containing materials known to be present in the marine environment, such as peptides and tetrapyrroles compounds, all have elevated $\delta^{13}C$ compared to most other compound classes (Hayes, 2001). While there is no published data on N functionality of the LMW pool, there is at least some evidence to suggest that pyrrol and indol containing compounds may be more important than is currently recognized. For example, hydrolyzable amino acids make up most N in reactive surface DON, however these are a very small component of LMW DON (Kaiser and Benner, 2009; Benner and Amon, 2015). At the same time, solid state NMR of HMW DON indicates increasing heterocyclic-N functionality in the deep ocean (McCarthy et al., 1997; Aluwihare and Meador., 2008; Mao et al., 2012), representing old material where HMW and LMW structural compositions may begin to overlap. While somewhat circumstantial, this evidence suggests that refractory heterocyclic-N material may be an important component of LMW DON, and also that more rapid remineralization of a labile, C-rich, lipid-like material could be more important than is currently understood. Together, this could explain the observed trends in both the C/N ratio and $\delta^{13}C$ of the LMW fraction.

Finally, an additional implication of these observations is that there must be some amount of active cycling occurring within the LMW DOC pool, even in the subsurface ocean, despite its very old average ^{14}C age. This is also required, given the very significant ^{14}C depth trends observed within this fraction (Fig. 2.2c, 2.5b). The average ^{14}C age of LMW material in the surface ocean is thousands of years younger than LMW DOC in the deep ocean, clearly demonstrating that there is a significant fraction of more rapidly cycling LMW material in the surface ocean, which is not present in the deep ocean. However, given that in the subsurface ocean most DOC is LMW, this is not necessarily an unexpected observation.

In contrast, the bulk properties of the more commonly studied HMW UDOC material is unique relative to the LMW SPE-DOC fraction collected from the same water. As mentioned above, the average age of the HMW fraction is significantly younger than both the total DOC pool and the LMW fraction throughout the water column in both basins, demonstrating that this fraction represents a faster cycling component of the marine DOC pool (Broek 2017). This is consistent with both previous measurements of ultrafiltered material and expectations based on observed size-age relationships (Benner et al., 1997; Walker et al., 2011; Broek et al., 2017). The C/N ratio of the HMW material is also significantly lower than that of the LMW material, which was previously interpreted in the NPSG as evidence that the youngest, most labile fraction of the DOC pool has a relatively uniform N-content, likely due to rapid and non-selective remineralization (Broek et al., 2017). However, despite the lack of significant depth trend in C/N ratio within the HMW pool in either basin, there is a significant depth trend in $\delta^{13}C$ values. When looking at both basins

together, it is clear that this trend mirrors a similar trend in the LMW pool, with the lowest values in the surface and a significant increase with depth. The lower $\delta^{13}C$ value of HMW DOC in the surface was previously hypothesized to be evidence of a relatively labile HMW ^{13}C deplete component (Broek et al., 2017), but the low C/N ratios and lack of C/N depth trend in the HMW fraction is inconsistent with the C-rich nature of the most likely candidate compounds, such as lipids. However, because the $\delta^{13}C$ of lipid-like material can have very depleted values (Hayes, 2001) a small contribution from this material in the surface ocean could greatly skew the high $\delta^{13}C$ values of the HMW fraction but have very little effect on the C/N ratio. Because these more labile lipid compounds are likely to be actively degraded in the surface ocean, it is plausible that their components would be present as both HMW structures and LMW degradation products, potentially decreasing the $\delta^{13}C$ value of surface material in both MW fractions. Alternately, it is possible that the lack of C/N variability in the HMW fraction despite the $\delta^{13}C$ depth trends could be caused by a labile N-containing lipid component, such as lipopeptides which have been confirmed to be present in surface waters (Kaiser and Benner, 2008) and which would likely be HMW (Broek et al., 2019).

NMR functional composition

The solid-state ^{13}C NMR analysis is a powerful tool for determining the C functional composition of isolated DOC fractions. While both HMW UDOC (Benner et al., 1992; McCarthy et al., 1993; Sannigrahi et al., 2005; Hertkorn et al., 2006) and material isolated with electro dialysis reverse osmosis (ED/RO; Koprivnjak et al.,

2009; Mao et al., 2012) have been characterized by this approach previously, our isolated LMW DOC fraction provides a direct view of material that is either absent (in HMW UDOC), or likely to be obscured in a complex mixture by the presence of labile HMW material (in ED/RO material).

The functional composition of our LMW SPE-DOC fraction is significantly different from that of these previous solid-state NMR measurements. The signal is dominated by alkyl C, with a significant amount of highly saturated aliphatic functionality. There is also a large contribution from carboxyl C and a larger aromatic component than seen in HMW UDOC. There is some additional signal from alkoxy C, however, the high ratio of O-alkyl to acetal C suggests that this signal is almost certainly not derived from polysaccharides as is hypothesized for HMW DOC, but rather other more complex hydroxyl containing structures. When normalized to the total signal, the four LMW DOC spectra collected for this study, representing material from the surface and deep ocean (2500 m) in both Atlantic and Pacific Basins, are identical within the limits of this technique (Fig. 2.8b). This is strongly consistent with our ^{14}C data, indicating that in both the surface and deep ocean, our isolated LMW fraction represents a persistent refractory component with long oceanic residence times, which is well mixed throughout the water column and world ocean.

The functional composition of HMW UDOC from the same waters is generally consistent with previous measurements of ultrafiltered material (Fig. 2.11a; Benner et al., 1992; Sannigrahi et al., 2005), and provides useful contrast with our new LMW fraction. In the surface ocean, where the signal is dominated by alkoxy C thought to primarily represent polysaccharide containing compounds, spectra are

essentially identical to those published previously (Benner et al., 1992; McCarthy et al., 1993). There is a significant decrease in the relative proportion of the alkoxy C signal between the surface and deep ocean within the HMW fraction in both basins (Fig. 2.8a), also consistent with prior observations. This has been interpreted to represent a highly reactive labile fraction which is preferentially degraded (Repeta and Aluwihare, 2006). Further, the ratio of O-alkyl to acetal C of the material which is present in the surface but absent at depth is approximately 4 ± 1, confirming that the removed material is likely dominated by polysaccharides (Sannigrahi et al., 2005). There is no significant disappearance of other functional groups with depth, suggesting that the more refractory material within the HMW pool is dominated by alkyl C.

Direct NMR measurements of DOC isolated by ED/RO, which on average isolates far more material (70-80% of total DOC; Vetter et al., 2007) than either UF or SPE alone, show a composition intermediate between our two fractions (Fig. 2.11c; Koprivnjak et al., 2009; Mao et al., 2012). This is expected, as this material contains a larger fraction of total DOC and therefore represents a mixture of LMW and HMW material. Therefore, on a bulk structural level, the largest DOC fraction ever isolated is essentially a direct mixture of two compositionally very different pools, which our protocol has isolated directly. This observation, coupled with our radiocarbon and elemental composition data, arguably indicates that efforts to isolate the entire DOC pool are potentially unwarranted and can confound interpretations.

Beyond general composition, the specific functional distributions of our LMW SPE-DOC, dominated by alkyl and carboxyl peaks, is also remarkably similar to the

functional distribution of the proposed carboxyl-rich alicyclic molecules (CRAM) fraction of DOC (Hertkorn et al., 2006). CRAM is hypothesized to be distributed throughout the ocean at all depths, be present in all MW fractions, and represent a major refractory component of marine DOC. The proposed functional composition of this material was based on two different solid-state NMR based approaches. CRAM was first proposed by calculating the difference between deep ocean and surface UDOC spectra, which revealed a component dominated by carboxyl and alkyl C with a smaller contribution from aromatic C (Hertkorn et al., 2006), and later by a similar approach subtracting the spectra of UDOC from ED/RO spectra in order to visualize the component of the DOC pool not isolated by ultrafiltration (Koprivnjak et al., 2009). These visualizations closely matched that of the hypothetical CRAM fraction and suggested that CRAM is in fact a dominant component of the background refractory pool of DOC. More important, these subtractions resulted in spectra identical to that of our LMW fraction, providing further evidence that our LMW material is highly representative of the whole LMW DOC pool and demonstrating that our LMW DOC fraction allows the first direct means to investigate the composition and cycling of this major DOC pool. Our results clearly confirm the presence and dominance of CRAM material within the refractory LMW pool and is therefore consistent with the relative homogeneity of the functional composition our LMW DOC fraction at all depths and in both basins.

Finally, the identification of CRAM material within the HMW pool, both by previous studies and in this data (Fig. 2.12), combined with the dominance of CRAM in our LMW fraction shows that CRAM in fact spans a large range of MW.

Combined with the large range of ^{14}C ages of our DOC fractions and specifically the LMW material, this observation suggests that the CRAM material which dominates the background DOC pool is likely produced directly in the surface ocean, rather than being produced by successive microbial reprocessing and degradation throughout the water column as would be expected from size-age-reactivity continuum ideas.

Changes in deep ocean DOC during ocean circulation

If the deep waters of the Central North Atlantic and NPSG basins are interpreted as upstream and downstream endmembers of deep ocean circulation, differences in the concentration and properties of DOC between basins provides a direct means of investigating the utilization of DOC over millennial timescales.

At 2500 m there is a 11 ± 3 μM offset in total DOC concentration between basins, demonstrating deep remineralization of approximately 25% of total DOC during ocean circulation (Fig. 2.6a). This observation is very similar to independent prior estimates (e.g., ~14 μmol kg-1; Hansell, 2013). Within the individual fractions the offset is 1.3 ± 0.7 μM for HMW UDOC and 5.2 ± 0.7 μM for LMW SPE-DOM representing approximately 10% and 45% of the total remineralized DOC respectively. This indicates that a large proportion of the remineralized DOC in the deep sea is LMW, despite the expected recalcitrance of LMW material (Benner and Amon, 2015). However, given that LMW material makes up the majority of deep ocean DOC, this result and the prior observation of a significant concentration gradient requires that some portion of LMW be removed on the time scale of deep ocean circulation. When considered relative to the DOC concentration of the HMW

UDOM, LMW SPE-DOC, and non-retained fractions individually, the basin offsets correspond to an approximately 30% decrease in DOC in each fraction, apparently suggesting that all three pools are removed at generally similar rates despite the expected differences in reactivity. However, these basin offsets can only show the net change in DOC concentration and cannot differentiate removal from processes that might add material to the deep ocean DOC pool such as dissolution of particles, chemoautotrophy, or hydrothermal sources (e.g., Smith et al., 1992; McCarthy et al., 2010; Ingalls et al., 2006). If there were significant additions to an individual pool, the apparent utilization of that pool from concentration measurements could represent an underestimation of the actual removed material. Therefore, offsets in properties of each fraction between basins other than concentration must be used in order to deconvolute the influence of additions to the DOC pool from the removal of material.

The bulk $\Delta^{14}C$ of DOC represents an average of a heterogeneous pool of material. Despite this, barring any changes to the concentration or distribution of this material, the average $\Delta^{14}C$ of the total DOC pool will change as a function of time. However, because of the removal and potential additions of material with unique radiocarbon content during deep ocean circulation, ageing of the total DOC pool cannot be differentiated from these processes. Therefore, changes in the ^{14}C age of DOC inconsistent with expectations for aging can be interpreted as changes in the age distribution of the pool. If DOC was entirely conserved during ocean circulation the ^{14}C age difference between basins would be expected to approximately match the age difference of DIC. An age offset less than that of DIC would require fresh inputs of

younger material during deep circulation, whereas an age offset greater than DIC would require the selective removal of younger, more labile material.

There are significant ^{14}C offsets between the deep waters of the Central North Atlantic and NPSG in total DOC and in both HMW and LMW DOC fractions (Fig. 2.6b). The average $\Delta^{14}C$ offset at 2500 m is 150 ± 10 ‰ in total DOC, 90 ± 25 ‰ for HMW UDOC, and 140 ± 35 ‰ for the LMW SPE-DOC fraction; representing 2300 ± 200, 1100 ± 200, and 2200 ± 500 years respectively. When compared to the ^{14}C age offset in DIC at 2500 m at these same locations (1600 ± 200 years; GLODAP v2; Olsen et al., 2016) these offsets are suggestive of fundamentally different cycling, as well as potentially different relative sources and aging within each fraction (Fig. 2.7). Total DOC, LMW SPE-DOC, and the non-retained DOC all have apparent age offsets greater than that of DIC. This is consistent with the observed concentration offsets discussed above which show that LMW DOC material is being removed; and suggests that the removal includes a preferential utilization of younger DOC. In contrast, the apparent age offset of HMW UDOC is substantially less than that of DIC. This indicates an input of fresh HMW DOC to the deep ocean during circulation and demonstrates that the 30% decrease in HMW DOC concentration between basins is in fact an underestimation of the actual DOC removal, consistent with the higher expected lability of this pool relative to LMW DOC.

In addition to the $\Delta^{14}C$ offsets, the observed offsets in C/N ratios in the deep ocean are also consistent with selective utilization of more labile LMW material. In both the total DOC pool and in the LMW fraction there is a significant increase in the C/N ratio between the Central North Atlantic and NPSG (Total DOC offset = 7 ± 4;

LMW offset = 4 ± 2.5). This increase demonstrates that there is a preferential removal of N-containing material, consistent with expectations for the removal of fresher, less degraded material (Benner et al., 1992; McCarthy et al., 1993; Guo et al., 1996; Benner, 2002). In contrast, the lack of any corresponding offset in the HMW DOC fraction suggests that there is either no selectivity in degradation or utilization of HMW material, or as suggested from the ^{14}C age offsets between basins, that there is a relatively constant input of new, young, low C/N material to the HMW DOC pool.

Despite the lack of changes in elemental ratios of the HMW DOC pool, solid-state NMR difference spectra indicate some differences in the functional composition of this material in the deep ocean between the Atlantic and Pacific (Fig. 2.8c), although to a much smaller degree than the differences between surface and deep material (section 4.1.1). In the HMW fraction the primary difference between spectra corresponds to a higher relative proportion of alkoxy and carboxyl C in the deep waters of the Pacific. The apparent increase in alkoxy C during deep water transit is the opposite of the trend observed between surface and deep waters in both basins and suggests that rather than the removal of a more reactive carbohydrate-like fraction during deep ocean circulation, there is actually some amount of carbohydrate-like material added to the deep ocean HMW DOC pool. We note that the difference spectra also reveal significantly more alkoxy C in the surface waters of the NPSG than the surface waters of the Central North Atlantic (Fig. 2.8c). Since surface composition is linked to more rapid local processes, this difference between basins likely represents a difference in overall biogeochemistry at these two sites. Since highly oligotrophic, microbial loop dominated regions generally correspond with both

elevated DOC concentration and C/N ratio, this offset in bulk composition is likely due to the consistently oligotrophic nature of HOT site (Williams, 1995; Hansell and Carlson, 2001).

Finally, despite the clear removal of LMW DOC during ocean circulation, difference spectra indicate that there is essentially no change in the functional composition of this material during deep ocean circulation. This suggests that, in contrast to HMW DOM, the removal of LMW DOC is completely non-selective. This NMR-based conclusion corresponds to the traditional view of a refractory "background" pool, however at the same time is inconsistent with the significant $\Delta^{14}C$ and C/N offsets in LMW DOC between ocean basins. There are several possible explanations for this apparent contrast. First, it is possible that at the selective utilization of specific compound types cannot be determined at the functional group level of resolution provided by these NMR measurements. However, the changes in $\Delta^{14}C$ of this material combined with the functional similarity of LMW material in the surface and deep ocean, despite the large age gradient with depth, more likely demonstrates that both freshly produced LMW DOC and older LMW material which survives mixing into the deep ocean are compositionally essentially indistinguishable. This suggests that the pool of CRAM molecules is a heterogeneous mixture of compounds with different cycling rates but generally similar structures. Second, the increase in C/N ratio between basins, implying a selective loss of N-containing compounds, potentially demonstrates that N-containing material within the LMW pool has a generally similar functional composition as the bulk material. In other

words, this suggest that there is a significant amount of N-containing CRAM molecules in the deep ocean.

Summary & Conclusions

A combination of ultrafiltration and solid phase extraction was used to specifically isolate HMW and LMW DOC from throughout the water column in both the Central North Atlantic and NPSG Subtropical Gyre. The novel LMW fraction collected for this study represents a new and direct approach to investigate the composition and cycling of a large fraction of the DOC pool which dominates the refractory background pool of material which persists in the ocean for millennial timescales. Compared to the total DOC pool or the more commonly studied HMW DOC pool, the LMW DOC fraction isolated for this study is older, with lower $\delta^{13}C$ values, higher C/N ratios, and a composition dominated by alkyl and carboxyl functional groups

Although the LMW DOC fraction has significantly older average ^{14}C ages, implying much slower cycling rates, there is also clear evidence for active cycling within the LMW pool. In contrast to typical expectations for a homogeneous refractory background pool, there is a significant increase in ^{14}C age with depth which demonstrates a major pool of fresher LMW material in the surface ocean which is remineralized on timescales shorter than ocean circulation. We also observed significant changes in both the C/N ratio and $\delta^{13}C$ value of LMW DOC with depth, consistent with changes in the relative proportions of different compound types. These depth trends suggest that there is labile, C-rich material that dominates the

labile LMW DOC pool, likely a lipid-like component that is rapidly remineralized in the surface ocean. In addition, there is likely a more refractory N-containing component of the LMW DOC pool which is preserved in the deep ocean. There is also clear removal of LMW DOC in the deep ocean during overturning circulation, which is accompanied by a change in C/N ratio and a ^{14}C age offset consistent with the preferential utilization of a younger, more labile DOC component.

The first direct solid-state ^{13}C NMR analyses of LMW DOC demonstrates that its overall functional composition is essentially identical both throughout the water column and in both ocean basins, consistent with a uniform refractory background pool present throughout the world ocean. The specific distribution of functional groups is remarkably similar to the CRAM family of structures that has been proposed as a major component of refractory marine DOC. However, coupled with the clear shifts in LMW DOC elemental composition and increases in LMW DOC age with depth, there is evidence that material with this composition spans a range of reactivities and cycling rates. Specifically, our ^{14}C observations require that this material is produced rapidly in the surface ocean and is remineralized throughout the water column. Further, difference spectra indicating the presence of essentially indistinguishable CRAM material within the HMW pool indicates that CRAM spans a wide range of molecular sizes. This further supports the idea that CRAM material is likely produced in the surface ocean, perhaps in a wide distribution of related structures and sizes and is likely not derived from the microbial degradation of labile HMW structures.

Relative to the LMW DOC fraction, the HMW DOC isolated for this study has younger ^{14}C ages, higher $\delta^{13}C$ values, lower C/N ratios and a dominant carbohydrate like composition. In addition, in contrast to the clear net removal and elemental changes of LMW DOC, the HMW DOC fraction has unexpected cycling behavior in the deep ocean. While concentration offsets show clear removal of HMW DOC during overturning circulation, the ^{14}C age offset of this fraction between basins is less than can be accounted for based solely on ageing or the removal of a younger, more labile component. In addition, there is NMR spectroscopic evidence demonstrating an increase in carbohydrate-like material in the deep ocean during deep ocean circulation. Together, this indicates a source of fresh, carbohydrate-rich HMW material to the deep ocean HMW DOC pool. We hypothesize this new data represents a bulk structural signature resulting from the dissolution of sinking particles, with fresh carbohydrate material being added to the relatively small HMW DOC pool that survives in the deep ocean. This observation is wholly consistent with previous ^{14}C data suggesting a likely source of neutral sugars to the deep ocean from rapidly sinking particles (Repeta and Aluwihare, 2006). Our ^{14}C data and C/N ratios suggests that this input must be both relatively constant, and important in maintaining deep ocean HMW DOC concentrations. Overall, this suggests that the influence of particle input to the deep ocean HMW DOC pool may be more important than has been previously understood.

These first direct analyses of the LMW DOC pool and comparison to the more commonly investigated HMW DOC pool provided data consistent with many basic assumptions about both the differential cycling of different MW pools and the

presence of a refractory background pool dominated by CRAM like molecular structures. However, they also yielded a number of surprising results. Despite a generally invariable functional composition, LMW DOC is likely a more dynamic pool than was previously recognized, with properties implying a diverse, wide ranging family of CRAM like molecules in terms of molecular size, N content and relative reactivity. Our data also points to an unexpected influence of surface particle flux in both maintaining deep ocean HMW DOC concentrations and shaping its molecular composition. Future work should focus on the specific molecular structures of CRAM like material across a range of DOC molecular sizes and what properties potentially govern the differences in relative reactivity of the different structurally related compounds.

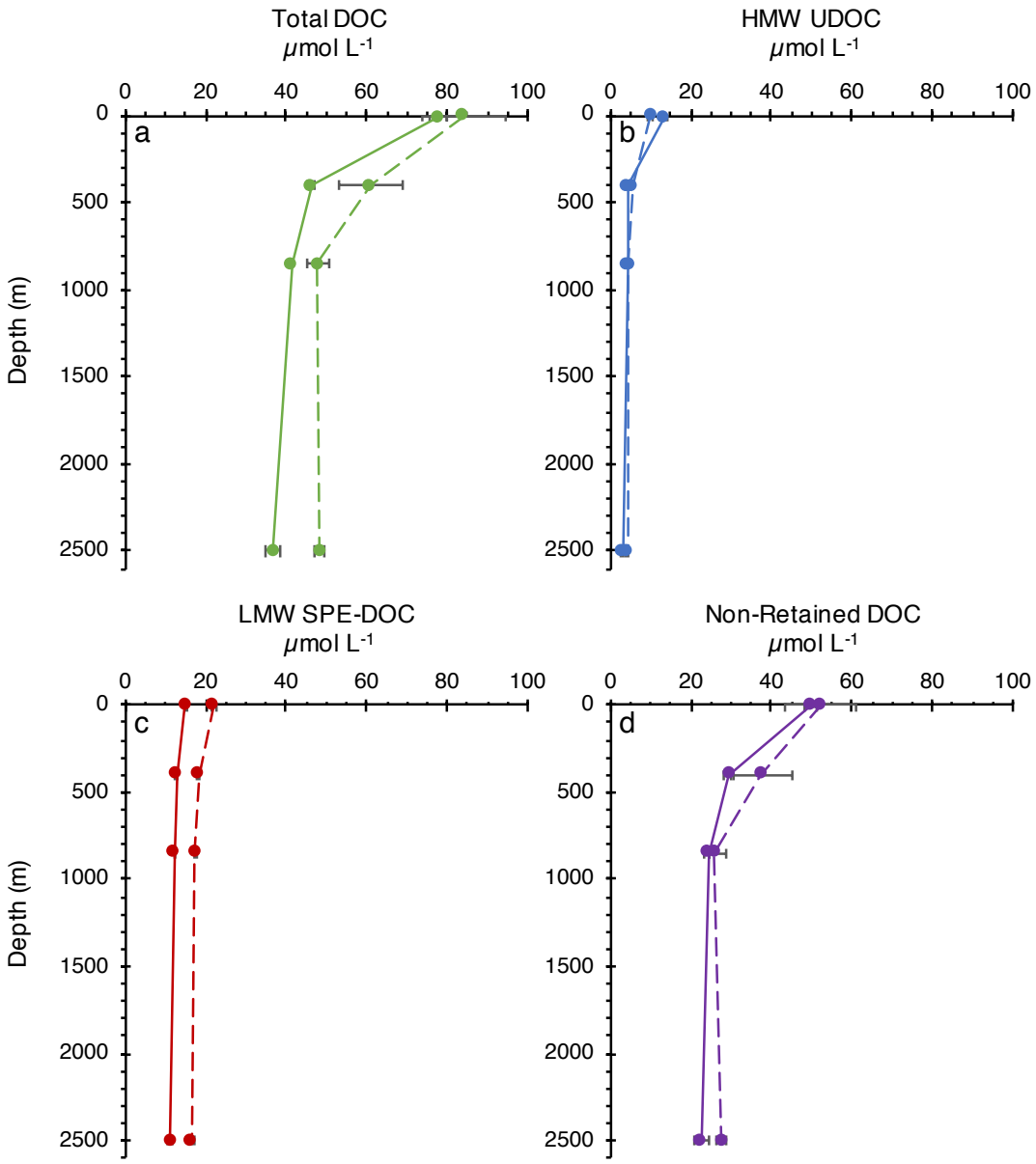

Figure 2.1 DOC concentration and material recovered with a combined UF/SPE approach. Depth profiles of (a) total DOC concentration (green), (b) DOC isolated by ultrafiltration (blue) and (c) solid phase extraction (red), and (d) non-recovered DOC (purple). Points connected by solid lines represent samples collected in the North Pacific Subtropical Gyre (HOT), and dotted lines represent samples collected in the Central North Atlantic. Points represent the error weighted average of values from 2 repeat cruise samplings in spring and summer, and error bars represent the standard error.

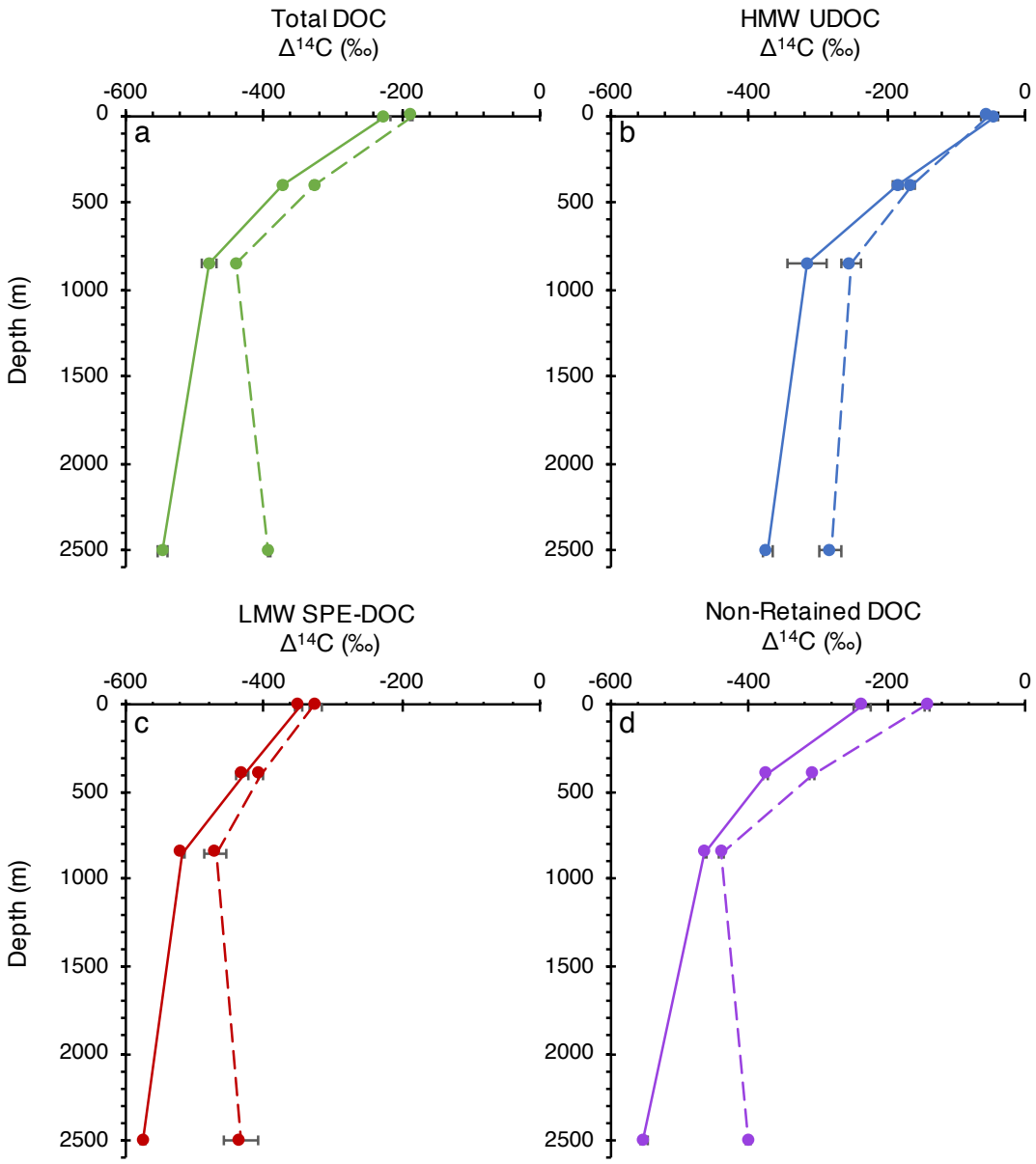

Figure 2.2 Radiocarbon content ($\Delta^{14}C$) of total DOC and material recovered with a combined UF/SPE approach. Depth profiles of (a) total DOC (green), (b) HMW UDOC (blue), (c) LMW SPE-DOC (red), and (d) the non-recovered material (calculated by difference). Points connected by solid lines represent samples collected in the North Pacific Subtropical Gyre (HOT), and dotted lines represent samples collected in the Central North Atlantic. Points represent the error weighted average of values from 2 repeat cruise samplings in spring and summer, and error bars represent the standard error.

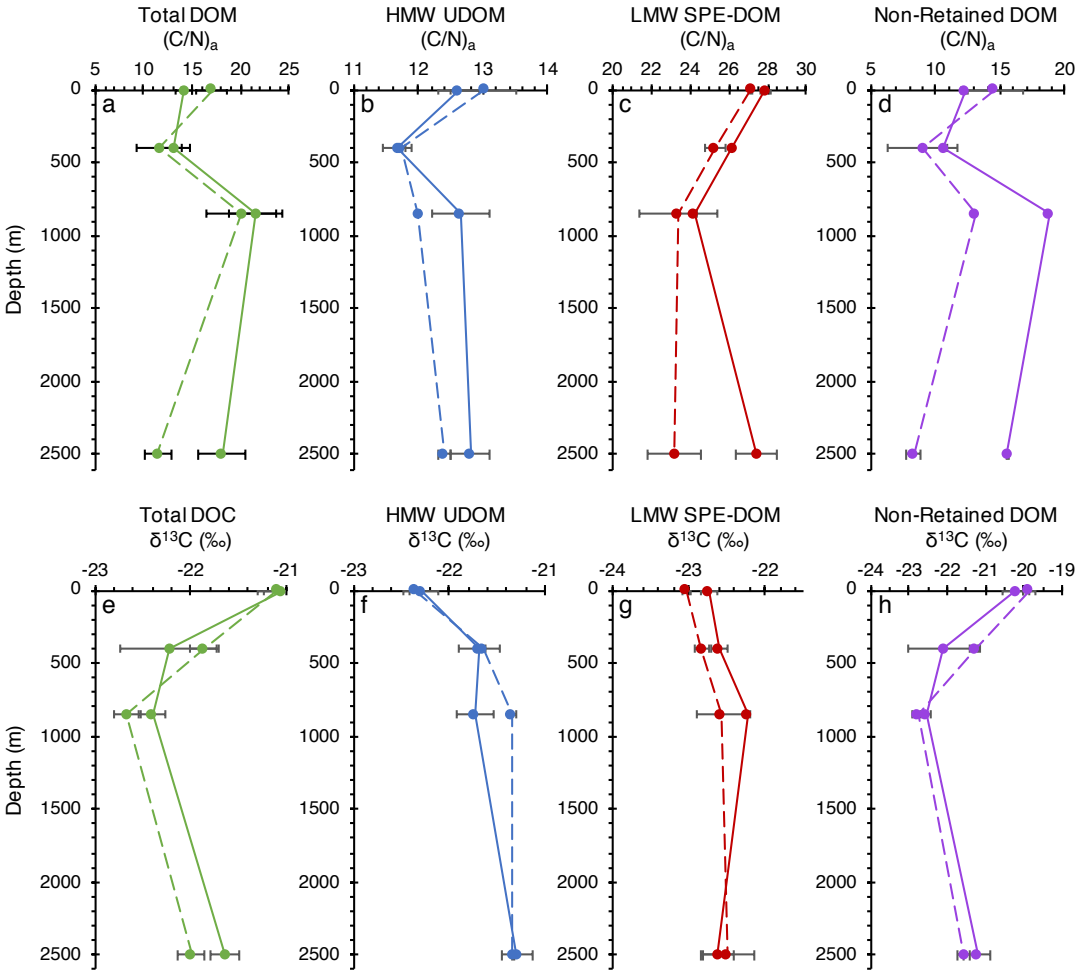

Figure 2.3 Carbon to nitrogen elemental ratios $(C/N)_a$ and stable C isotopes ($\delta^{13}C$) of total DOC and material recovered with a combined UF/SPE approach. Depth profiles of (a and e) total DOC (green), (b and f) HMW UDOC (blue), (c and g) LMW SPE-DOC (red) and (d and h) the non-recovered material (calculated by difference). Points connected by solid lines represent samples collected in the North Pacific (HOT), and dotted lines represent samples collected in the North Atlantic. Points represent the error weighted average of values from 2 repeat cruise samplings in spring and summer, and error bars represent the standard error.

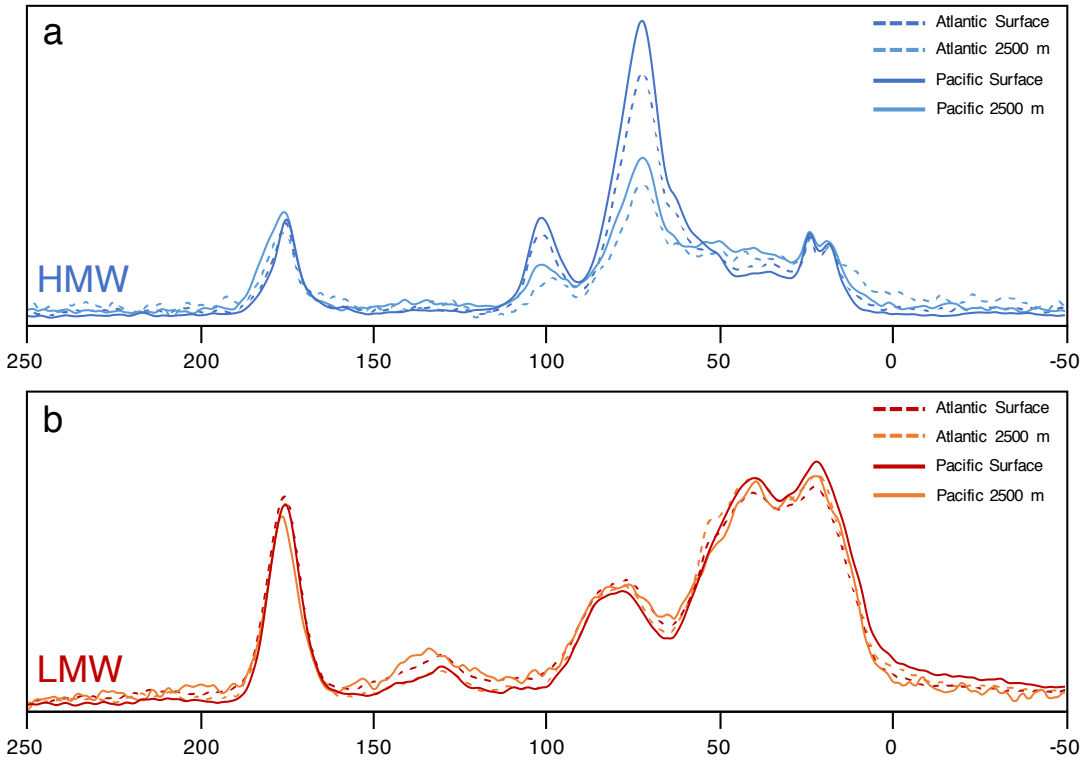

Figure 2.4 Solid-state ^{13}C NMR spectra of HMW UDOC and LMW SPE-DOC. (a) spectra of HMW UDOC collected in the surface (dark blue) and deep ocean (2500m; light blue) from the Central North Atlantic (dashed lines) and North Pacific Subtropical Gyre (solid lines). (b) spectra of LMW SPE-DOC collected in the surface (dark red) and deep ocean (2500m; orange) from the Central North Atlantic (dashed lines) and North Pacific Subtropical Gyre (solid lines). Spectral assignments are as follows: ketone, aldehyde, quinone (220-191 ppm); COO, NC=O (191-164 ppm); aromatic C-O (164-150 ppm); aromatics (150-117 ppm); OCO (94-60 ppm); OC (94-60 ppm); OCH_3, NCH (60-45 ppm); CCH_2C, CCHC (45-30 ppm); CCH_2C, CCH3 (30-0 ppm).

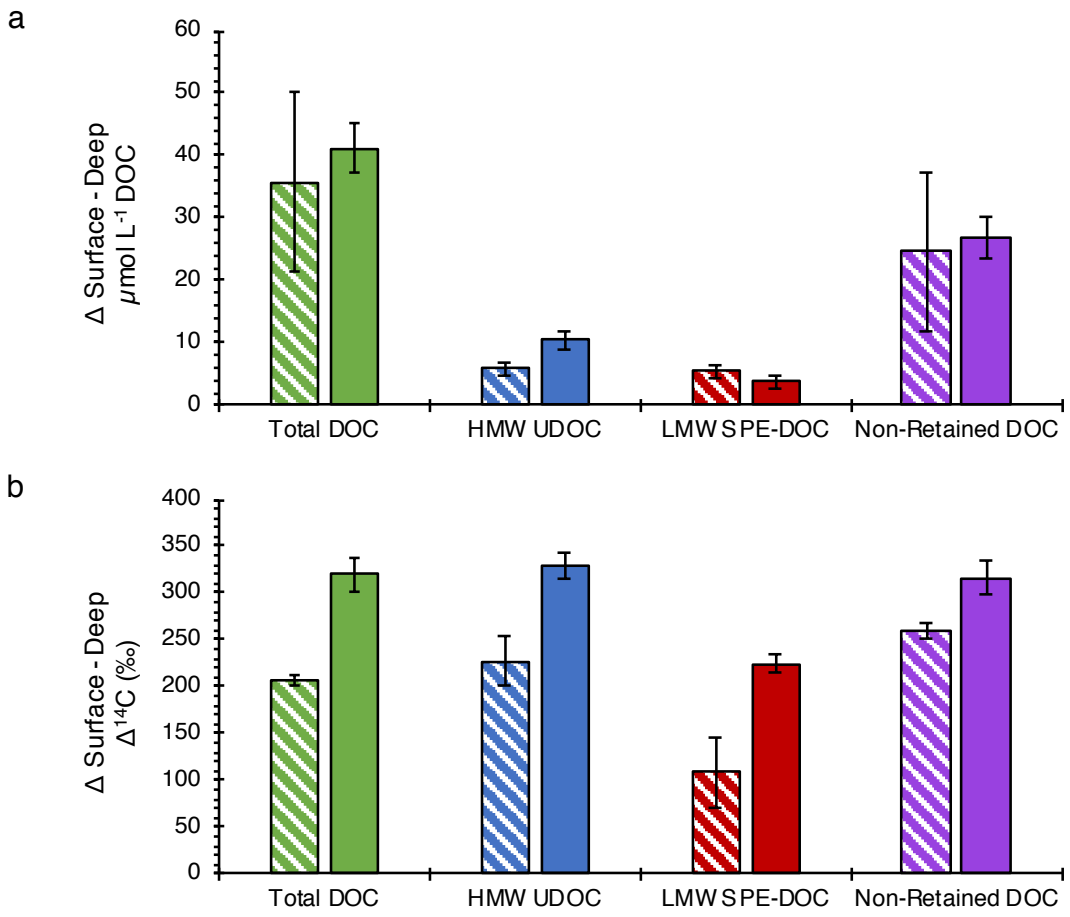

Figure 2.5 Offsets between the surface and deep ocean (2500 m) of the concentration (a) and radiocarbon content ($\Delta^{14}C$; b) of total DOC and material recovered with a combined UF/SPE approach. Solid bars represent the surface versus deep offset in the NPSG and striped bars represent the surface versus deep offset in the Central North Atlantic. Values represent the offsets between error weighted averages of values from 2 repeat cruise samplings in spring and summer, and error bars represent the propagated standard deviation of both sampling seasons and both depths.

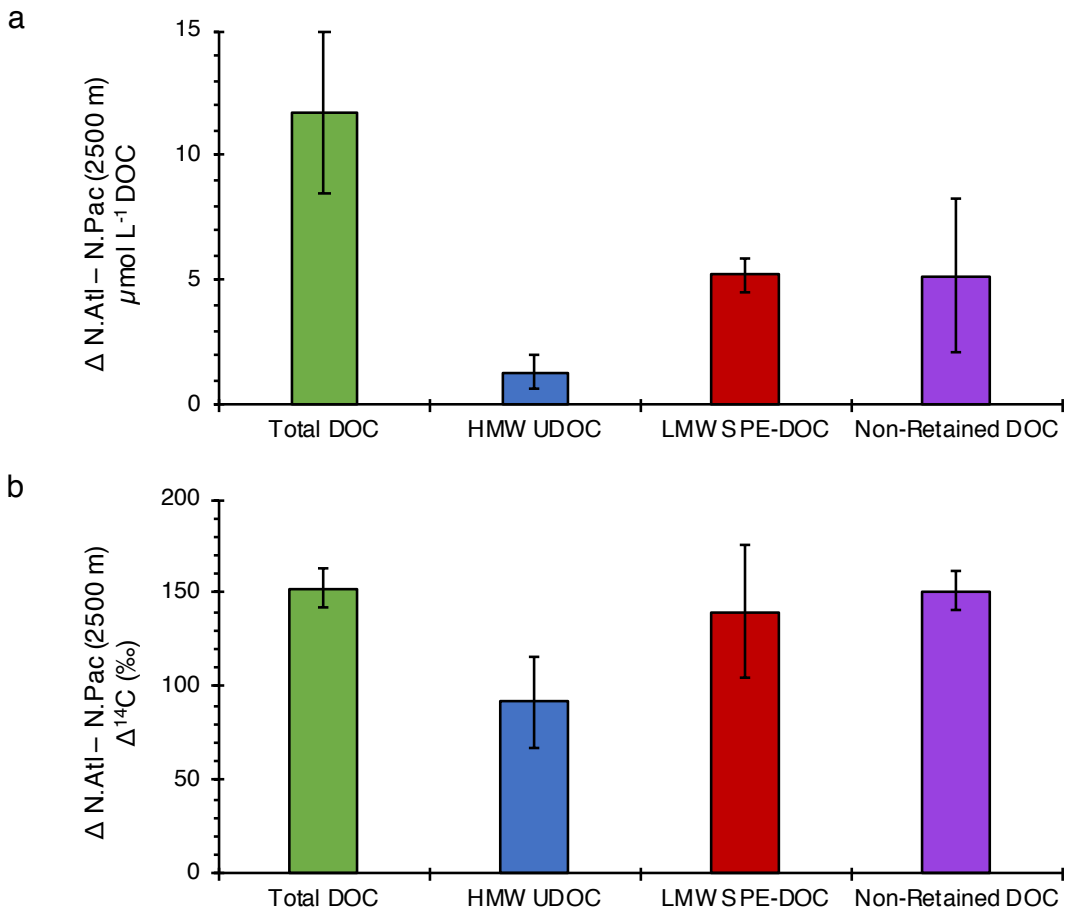

Figure 2.6 Offsets between Pacific and Atlantic basins of the concentration (a) and radiocarbon content ($\Delta^{14}C$; b) of total DOC and material recovered with a combined UF/SPE approach. Values represent the basin offsets between error weighted averages of values from 2 repeat cruise samplings in spring and summer, and error bars represent the propagated standard deviation of both sampling seasons and both basins.

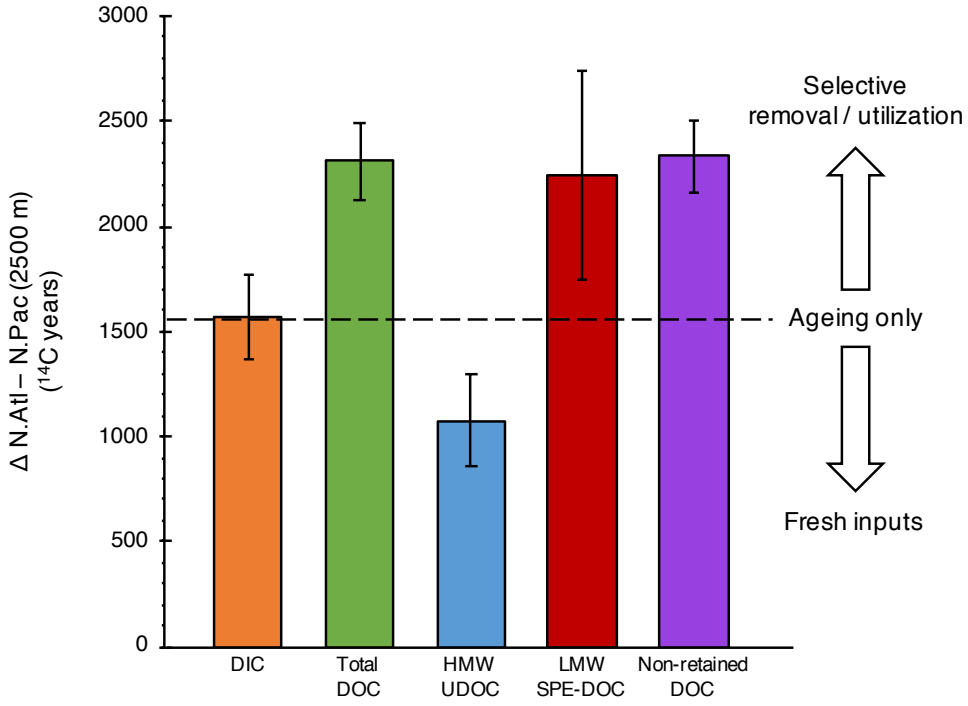

Figure 2.7 Offsets between Pacific and Atlantic basins in the radiocarbon age of DIC, total DOC, and material recovered with a combined UF/SPE approach. Values represent the basin offsets between error weighted averages of values from 2 repeat cruise samplings in spring and summer, and error bars represent the propagated standard deviation of both sampling seasons and both basins. Offsets within a DOC fraction greater than the DIC offset (dashed line) imply the selective removal of material of labile material with younger ^{14}C ages and offsets less than that of DIC imply additions to the deep ocean of fresher material with younger ^{14}C ages.

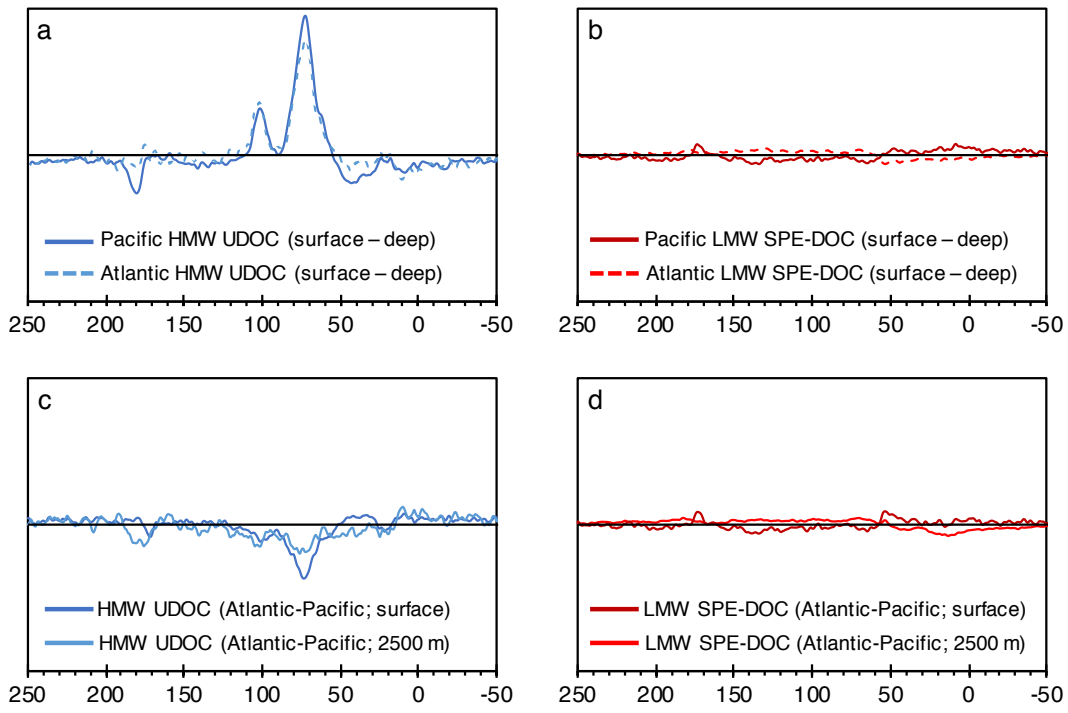

Figure 2.8 Solid-state ^{13}C NMR difference spectra from HMW UDOC and LMW SPE-DOC. (a) difference between surface and deep HMW UDOC material in the Pacific (solid dark blue line) and Atlantic (dashed light blue line). (b) difference between surface and deep LMW SPE-DOC material in the Pacific (solid dark red line) and Atlantic (dashed light red line). (c) difference between HMW UDOC material collected in the Pacific and Atlantic from surface (dark blue) and deep ocean (2500 m; light blue). (d) difference between LMW UDOC material collected in the Pacific and Atlantic from surface (dark red) and deep ocean (2500 m; light red). Values above the baseline demonstrate the removal of material with depth or between basins (from surface to deep or Atlantic to Pacific) and values below the baseline demonstrate the addition of material with depth or between basins (from surface to deep or Atlantic to Pacific).

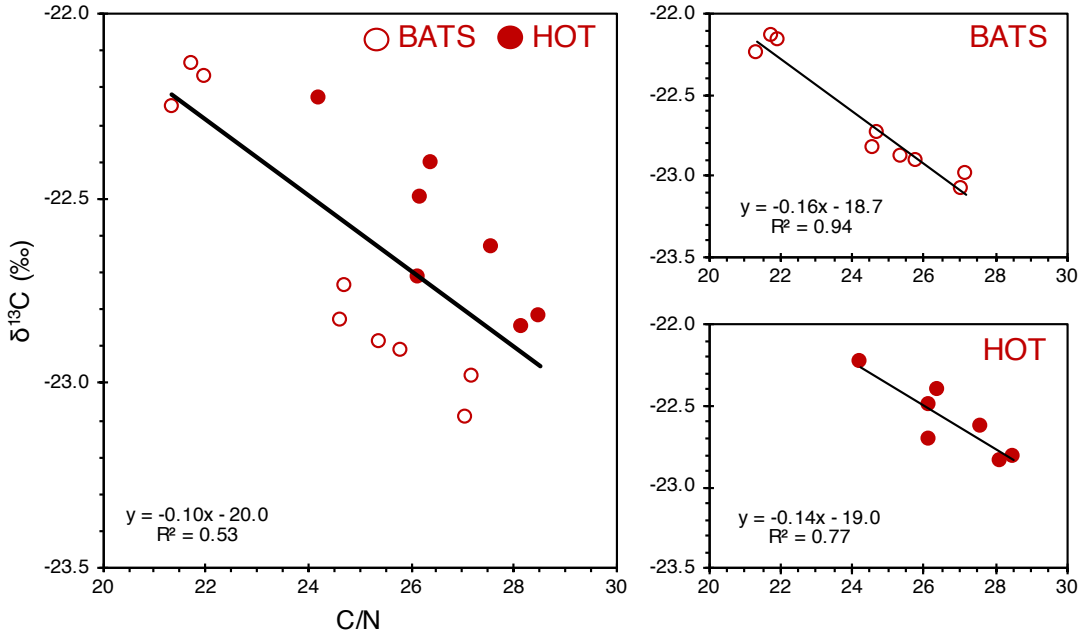

Figure 2.9 Liner relationship between $\delta^{13}C$ and C/N ratio within the LMW pool showing a significant correlation (R2 = 0.53) within the entire data set. The correlations are stronger within each individual basin (Central North Atlantic R^2 = 0.94; North Pacific Subtropical Gyre R^2 = 0.77). These correlations likely represent depth related changes in the relative distribution of different compound types, specifically the removal of a labile lipid-like material and persistence of a more refractory N-containing material.

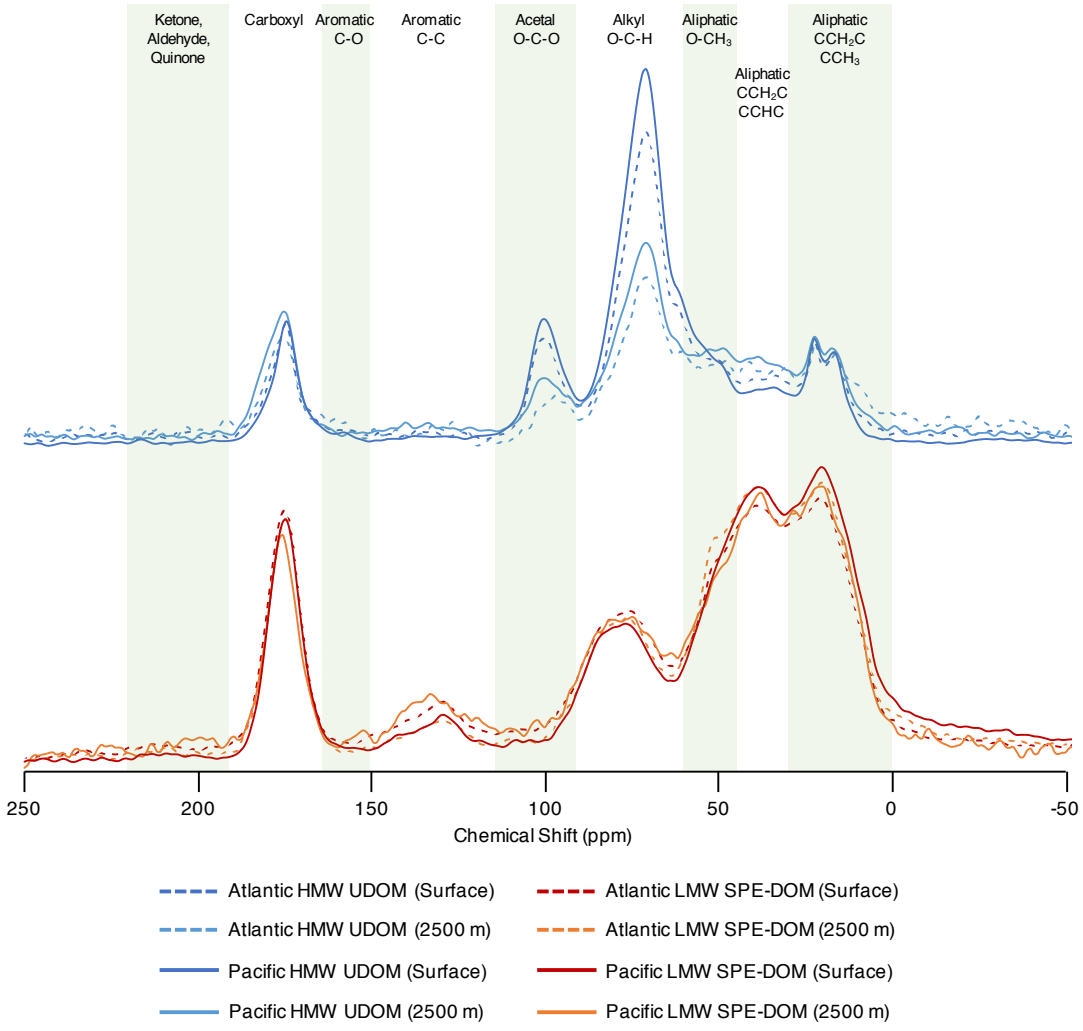

Figure 2.10 Solid-state ^{13}C NMR spectra of HMW UDOC and LMW SPE-DOC, showing spectral assignments of different functional groups. Assignments are as follows: ketone, aldehyde, quinone (220-191 ppm); COO, NC=O (191-164 ppm); aromatic C-O (164-150 ppm); aromatics (150-117 ppm); OCO (94-60 ppm); OC (94-60 ppm); OCH_3, NCH (60-45 ppm); CCH_2C, CCHC (45-30 ppm); CCH_2C, CCH3 (30-0 ppm).

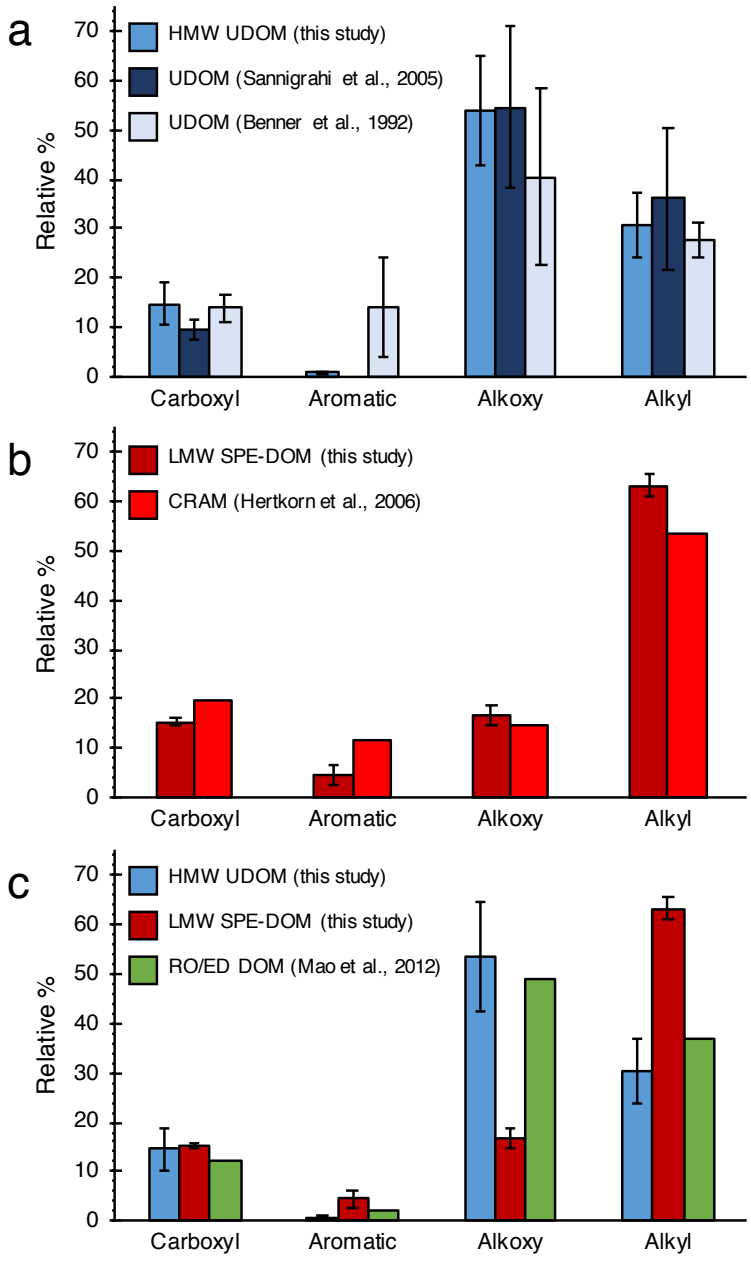

Figure 2.11 Solid-state ^{13}C NMR derived functional group distributions of HMW and LMW DOC compared to previous measurements or related material. (a) HMW UDOM from this study compared to UDOM measured in Benner et al., 1992 and Sannigrahi et al., 2005. (b) LMW SPE-DOM collected for this study compared to CRAM material from Hertkorn et al., 2006. (C) HMW UDOM and LMW SPE-DOM from this study compared to RO/ED DOM from Mao et al., 2012.

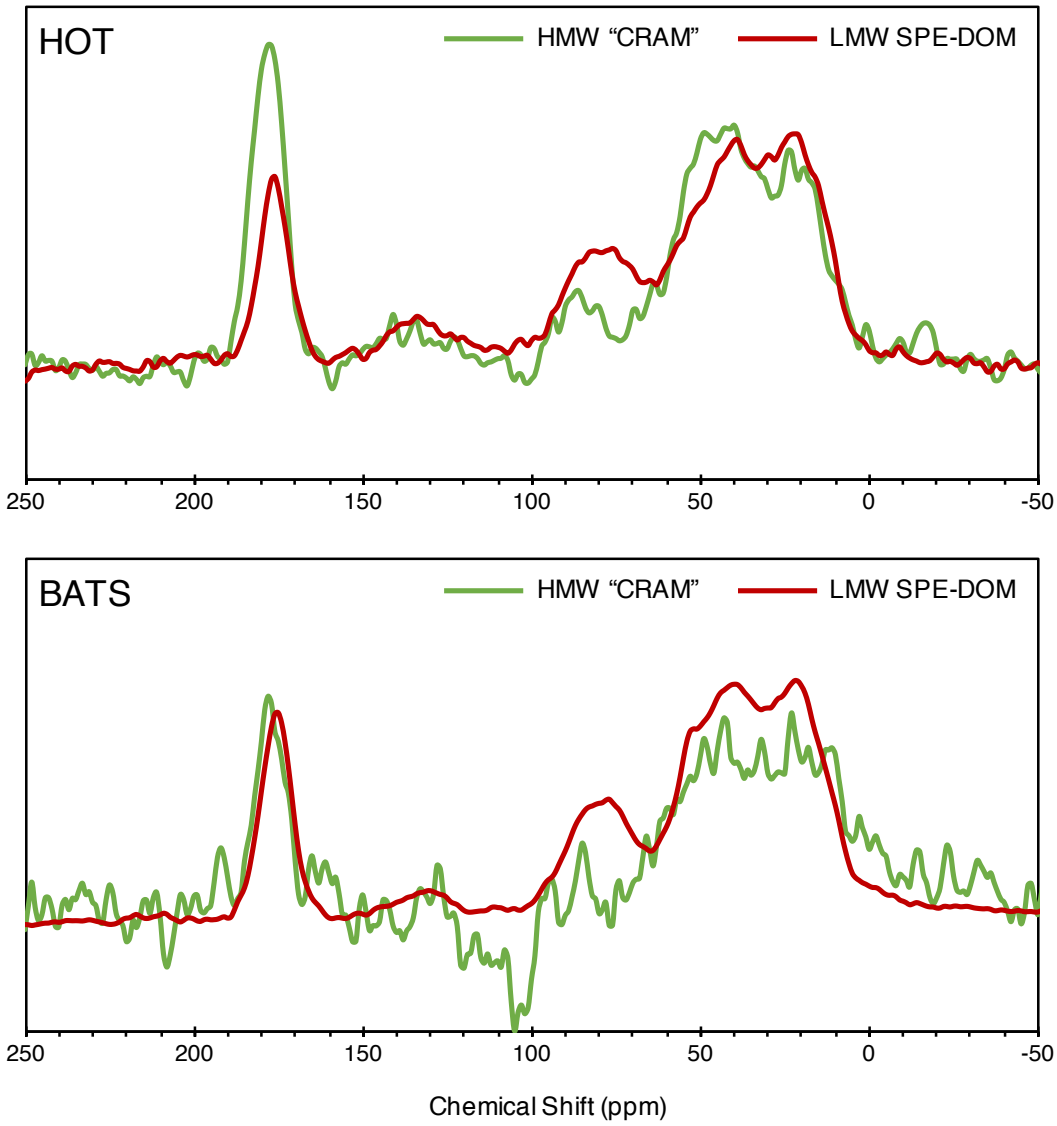

Figure 2.12 Hypothetical HMW CRAM spectra (green line) generated by subtracting surface minus deep HMW spectra (i.e., Fig. 2.8a) from deep HMW spectra (i.e., Fig. 2.4a; light blue) and LMW SPE-DOM spectra (red lines). Comparison shows presence of CRAM like material in both HMW and LMW DOC pools.

Chapter 3

Amino acid enantiomers in old and young dissolved organic matter: implications for a microbial nitrogen pump.

The results presented in this chapter are published in Geochimica et Cosmochimica Acta as an article by Taylor A. B. Broek and co-authors based on the data contained in the M.S. thesis of Amy L. Bour as follows:

Broek T. A. B., Bour A. L., Ianiri H. I., Guilderson T. P., and McCarthy M. D., 2019. Amino acid enantiomers in old and young dissolved organic matter: implications for a microbial nitrogen pump. *Geochimica et Cosmochimica Acta.* **247**, 207-219. https://doi.org/10.1016/j.gca.2018.12.037.

Abstract

Dissolved organic nitrogen (DON) represents the largest reservoir of fixed N in the surface ocean and a significant portion accumulates in the deep sea, where it can persist for millennial time scales. However, like the dissolved organic carbon (DOC) pool, the origin and composition of long-lived, refractory DON remains largely unknown. In recent years, the "microbial carbon pump" hypothesis has emerged from abundant evidence showing that microbial processes are primarily responsible for refractory DOC accumulation. However, a similar mechanism for DON has rarely been investigated. In the study of DON, spectroscopic evidence has indicated a primarily amide composition, implying a dominant contribution from peptides. Therefore, if an analogous "microbial nitrogen pump" controls refractory DON accumulation, the amino acid component should bear increasing signatures of microbial origin with increasing age. Here we investigate the microbial sequestration of N via the production of refractory DON, for the first time considering together DOM $\Delta^{14}C$ ages with amino acid (AA) molar abundance (Mol%) and D/L ratio (as a tracer for prokaryotic input). Measurements were made on a unique set of high and

low molecular weight (HMW, LMW) DOM isolates with $\Delta^{14}C$ ages and chemical compositions generally consistent with semi-labile and refractory DOM respectively. The samples were collected in the North Pacific Subtropical Gyre where deep waters contain some of the oldest DOC in the world ocean. We observe higher D/L ratios in older, LMW DOM isolates for almost all analyzed AAs. Using mass spectral data, we also quantify three D-AAs in all samples (D-valine, D-phenylalanine, and D-leucine), which have not previously been confirmed in ocean DOM. These newly identified D-AAs are concentrated in the LMW refractory DOM fraction and have oceanographically consistent depth profiles. Our results suggest that several novel D-AA subgroupings may be unique tracers for different prokaryotic source processes. D-Alanine appears to have largely independent cycling from the other D-AAs with a connection to the production of HMW DON, which we hypothesize is linked to water column peptidoglycan. In contrast, D-leucine, D-valine, and D-phenylalanine appear to be most strongly related to the production of LMW DON. Trends in both the HMW and LMW fractions suggest a linkage to sinking particles and local microbial transformations, implying that LMW DON has a direct biological source rather than originating from successive microbial reprocessing of HMW DON. Taken together, our observations are consistent with the dominant production of refractory LMW DON by prokaryotic organisms and suggests that different AA sub-groupings that can be used to track different processes within the DON pool.

Introduction

Marine dissolved organic matter (DOM) exerts a critical influence on climate, the microbial food web, and ocean nutrient regimes. This carbon (C) reservoir is comparable in size to atmospheric CO_2, and equivalent to more than five years of global net primary production (Woodward, 2007; Hansell et al., 2009). Ocean DOM likely originates almost entirely from marine primary production (Hansell et al., 2009), however only a small fraction is identifiable as common biomolecules (Benner and Amon, 2015). Despite major advances in techniques to study the DOM pool, most remains structurally unidentified at the molecular level (Repeta, 2014). This is particularly true in the subsurface ocean, where DOM is characterized by average radiocarbon (^{14}C) ages of 4000-6000 years (Williams and Druffel, 1987), and is dominated by low molecular weight compounds (Benner and Amon, 2015) with an enormous diversity of molecular structures (Koch et al., 2005).

Many explanations for the preservation of long-lived, or refractory DOM have been proposed, including non-marine origin, abiotic condensation reactions, microenvironments, particle interactions, photochemistry, and hydrothermal sources (Hedges, 1992; Nagata and Kirchman, 1999; Hedges et al., 2000; Kirchman, 2004; Eglinton and Repeta, 2006; Ziolkowski and Druffel, 2010; McCarthy et al., 2010; Arrieta et al., 2015; Benner and Ziegler, 1999). Recent work, however, has increasingly focused on microbial control of DOM cycling (Kaiser and Benner, 2008; Yamaguchi and McCarthy, 2018), showing that refractory DOM compounds are characterized by novel molecular structures and/or low concentrations that cause metabolic costs to outweigh the benefits of biological utilization (Hertkorn et al.,

2013; Dittmar, 2014; Arrieta et al., 2015). Bacteria not only degrade and metabolize OM, but can significantly contribute material to the bulk OM pool, for example: in DOM, marine snow, and sediments in lakes and oceans (Simon et al., 1990; Gweon and Fisher, 1992; Lehmann et al., 2002; Tremblay and Benner, 2006; McCarthy et al., 2007; Kaiser and Benner, 2008; Carstens and Schubert, 2012; Alkhatib et al., 2012; Niggemann et al., 2018). It has been clearly shown in laboratory experiments that heterotrophic microbes can produce refractory DOM from simple organic molecules and common biopolymers, characterized by increased structural complexity and decreased nutrient and energy content, (Ogawa, 2001; Benner and Amon, 2015; Lechtenfeld et al., 2015). The production of refractory DOM and associated carbon sequestration by bacteria, archaea, and viruses has, in recent years, been termed the "microbial carbon pump" (MCP; Jiao et al., 2010). The MCP idea represents a synthesis of a large number of prior studies which have examined the importance of microbial source and processes in the production of refractory molecules (Benner and Amon, 2015). Multiple specific mechanisms have been hypothesized as potential explanations for the formation of refractory DOM via an MCP, including the diversity of bacterial metabolic pathways, promiscuous exoenzymes, structural modification, and selective remineralization associated with microbial degradation (Jiao et al., 2010).

In contrast, the production of refractory DON and associated N sequestration via a microbial nitrogen pump (MNP; Yamaguchi and McCarthy, 2018) in many ways presents a greater puzzle. As with the more commonly explored MCP, this idea represents a shorthand to synthesize multiple past studies aimed at understanding

bacterial sources and transformations. However, in contrast to the enormous complexity of DOC chemical functionality, solid state ^{15}N-NMR analysis has indicated that DON is composed almost entirely of amide nitrogen (McCarthy et al., 1997; Mao et al., 2012; Sipler and Bronk, 2014). This observation strongly suggests that a very limited range of common biochemical structures, such as peptides and N-acetyl amino polysaccharides, are the dominant biomolecular components at all ocean depths (McCarthy et al., 1997; Aluwihare et al., 2005). These compound classes are among the most labile of all biochemicals (Cowie and Hedges, 1992; Jørgensen et al., 2014), and the amide linkage itself indicates relatively intact biopolymers (McCarthy et al., 1997). Nevertheless, deep ocean Δ^{14}C data suggests this same material survives over multiple ocean mixing cycles (Loh et al., 2004), while spectroscopic data has indicated rapidly diminishing amino sugar contribution in the subsurface ocean (Aluwihare et al., 2005). Together, these observations have suggested that proteinaceous material is the dominant subsurface compound class, even in refractory DON (McCarthy et al., 1997; McCarthy and Bronk, 2008). At the same time, primary production remains N-limited in the subtropical gyres despite the presence of micro-molar concentrations of DON (Moore et al., 2013; Sipler and Bronk, 2014). Taken together these observations present a conundrum: although both phytoplankton and heterotrophic bacteria can use DON (Bronk et al., 2007; Sipler and Bronk, 2014), and spectroscopic properties suggest that it is dominated by common, labile biochemical classes, relatively refractory DON is apparently produced in surface waters and persists for millennia in the deep ocean.

If the formation of refractory DON is in fact directly linked to microbial

source, then an MNP presumably depends largely on transformations of the combined amino acid (AA) fraction of the DOM pool (Yamaguchi and McCarthy, 2018). AAs are the largest identifiable component of DON and therefore represent the main biochemical class which could be used to investigate the microbial production of refractory DON at the molecular level (Eglinton and Repeta, 2006; McCarthy and Bronk, 2008). The structural diversity and differential utilization of AAs provides a wealth of molecular tracer potential. Molar percentage metrics have long been used as powerful indicators of relative degradation state and recalcitrance (Dauwe et al., 1999; Yamashita and Tanoue, 2003; McCarthy et al., 2004; Lechtenfeld et al., 2014; Lechtenfeld et al., 2015). However, for investigating direct bacterial source, the D-enantiomer of AAs (D-AAs) represent arguably the most powerful molecular tracer. The synthesis and incorporation of D-AAs into biochemicals is confined almost exclusively to prokaryotic organisms, making D-AAs among the few unambiguous proxies for bacterially derived molecules in the modern ocean (McCarthy et al., 1998; Kaiser and Benner, 2008; Radkov and Moe, 2014).

Finally, a growing body of recent research has shown that molecular size (and/or molecular weight) of dissolved organic matter is directly associated with both its reactivity and composition (reviewed by Benner and Amon 2015), and is also directly correlated with DOM ^{14}C age distributions (Walker et al., 2011; Walker et al., 2014; Walker et al., 2016). Specifically, observations of bulk molecular and isotopic properties suggest DOM exists in a continuum of size, age, and biological reactivity: high molecular weight (HMW) DOM is dominated by more freshly produced, semi-labile material, while lower molecular weight (LMW) DOM has far

older ^{14}C ages, contains fewer identifiable biomolecules, and is generally more biologically refractory (Walker and McCarthy, 2012; Benner and Amon, 2015; Walker et al., 2016; Broek et al., 2017). These sized based trends combined with the MCP conceptual framework suggest that successive microbial utilization and reprocessing corresponds with the production of smaller and increasingly refractory compounds. If microbial processes are primarily responsible for refractory DON formation, one might therefore expect a direct relationship between DOM molecular weight, ^{14}C age and abundance of bacterial tracers.

Here we directly examine these ideas using a novel approach coupling $\Delta^{14}C$ data with AA D/L enantiomeric ratios and relative AA molar abundance (AA-Mol%) measurements of separately isolated HMW and LMW DOM fractions from the North Pacific Subtropical Gyre. This site is the largest ocean biome on earth, and has deep waters which represent the endmember of overturning ocean circulation and contain the ocean's oldest DOM. Our main goal is to test the hypothesis that a linkage of D-AA with $\Delta^{14}C$ age would implicate bacteria as the direct sources for the progressive accumulation of refractory DON in the ocean. In addition, our large-volume DOM isolations allowed application of GC-MS analyses to identify an expanded suite of novel D-AAs not previously reported in marine DOM, but highly concentrated in the more refractory, LMW fraction. Together our results indicate that D-AA tracer potential in DOM is substantially greater than previously recognized. While our data strongly supports the basic MNP idea, it also suggests some surprising conclusions about the linkage of bacterial sourced refractory DON and molecular weight in the ocean.

Experimental Methods

Water Sampling

Our analyses were conducted on subsamples of the high molecular weight ultrafiltered DOM (HMW UDOM) and low molecular weight solid phase extracted DOM (LMW SPE-DOM) fractions previously described in Broek et al. (2017). These DOM samples were collected using a sequential sampling approach in which HMW DOM was first concentrated using a large-volume tangential-flow ultrafiltration (UF) system, at high concentration factor (CF; ~1000). LMW DOM which permeated the UF system was then isolated by solid-phase extraction (SPE). Broek and co-authors (2017) describe extensive testing and comparison of LMW resin isolates, showing that the isolated LMW material has isotopic ratios and bulk properties representative of total LMW DON (see additional discussion in section 4.1). Sampling was conducted at the Hawaii Ocean Time Series Station ALOHA (A Long-Term Oligotrophic Habitat Assessment; 22°45'N, 158° 00'W) aboard the R/V Kilo Moana cruises KM1418 (late Summer 2014) and KM1506 (Spring 2015). A full description of the sampling protocol and materials is presented in the appendix (appendix section 1.1) and is detailed elsewhere (Broek et al., 2017). The HMW ultra-filtered material represents 17 ± 1% and 9 ± 2% of total DOC in the surface (7.5 m) and subsurface (400-2500 m) respectively, and the LMW SPE-DOM represents 23 ± 2% of the remaining LMW DOC in the surface and 32 ± 2% in the subsurface. A thorough discussion of the extraction efficiency of the combined UF / SPE is presented in Broek et al., 2017.

Sample Preparation

Liquid-state acid hydrolysis was used to liberate individual AAs following the recommendations for reduction of racemization blanks (Kaiser and Benner, 2005). A 3.75 mg C subsample of HMW UDOM or LMW SPE-DOM material, representing approximately 20 L (surface) and 100L (mesopelagic and deep) of seawater for HMW UDOM, and 20-30 L of seawater for LMW SPE-DOM, were weighed into combusted vials (450°C/5 hrs.). 3 mL of 6 M HCl was added, vials were purged with N_2 and heated to 110°C for 20 hr. Acid hydrolysis completely deaminates asparagine (Asn) to aspartic acid (Asp) and glutamine (Gln) to glutamic acid (Glu), therefore the abbreviations Asx and Glx are used throughout to denote the combination of Asp/Asn and Gln/Glu respectively. HCl was removed under a stream of N_2, and the hydrolysates were re-dissolved in 1 mL of 0.1 M HCl. Hydrolysates were then purified using cation-exchange chromatography (Bio-Rad AG50W-X8, 200-400 mesh), following the methods of Takano et al., 2010. The ammonium hydroxide in eluted column samples was removed using the Jouan centrifugal evaporator (Société Jouan, Saint-Herblain, France) at a chamber temperature of 55 °C, and amino acids were then protonated by dissolving in 1 mL 0.1 M HCl. Trifluoroacetyl isopropyl ester derivatives were prepared following the general protocol of Silfer et al., 1991, with modifications discussed in Décima et al., 2017. AAs were further purified by solvent extraction followed by re-acetylation, as described by Décima et al., 2013 and samples were stored at -20°C for up to two weeks before analysis. Immediately before chromatography, samples were dried under a N_2 stream and re-dissolved in ethyl acetate.

GC-MS Analysis and Quantification

AA enantiomers were analyzed by gas chromatography-mass spectrometry (GC-MS; Agilent 7890A + 5975B) using a chiral column (Altech Chirasi-L-Val, 50 m length, 0.25 mm internal diameter, 0.16 μm film thickness). 1 μL of sample was injected through a splitless inlet at 200°C, using helium carrier (0.9 mL/min). Individual amino acids were separated using a 4-ramp, 57.5 min temperature program: 45°C start; 2°C/min to 75°C; 4°C/min to 110°C; 1°C/min to 125°C; 4°C/min to a final temperature of 200°C. Quantification was based on retention times for authentic D and L standards of each AA, coupled with ion peak areas obtained using single-ion monitoring, based on the following characteristic ion fragments (m/z): Alanine (Ala), 140; valine (Val), 168.1; threonine (Thr), 153; glycine (Gly), 126; isoleucine and leucine (Ile and Leu), 182.1; serine (Ser), 138; proline (Pro), 166.1; aspartic acid / asparagine (Asx), 184; glutamic acid / glutamine (Glx), 180; and phenylalanine (Phe), 190.1. Total amino acid yields, and relative abundance were quantified using mixed L-AA standards in a linear four-point calibration curve ranging from 1-1000 μmol/AA. For each AA, peak areas for both enantiomers were converted to molar quantities using the calibration curve for the corresponding ion fragment. Molar percentage abundance (Mol%) for each AA measured was calculated using the sum of the D and L enantiomers.

Racemization Corrections and Data Analysis

Measured AA enantiomeric ratios were corrected for racemization during sample preparation following the approach of Kaiser and Benner (2005). This

approach corrects for racemization during hydrolysis by combining the average racemization for free AAs and the AAs in a protein, measured by Kaiser and Benner (2005). Final racemization corrections consist of two main components: racemization during hydrolysis, and then subsequent racemization during derivatization. Since our hydrolysis conditions are identical to those examined in Kaiser and Benner (2005), we used their previously published hydrolysis corrections. However, we also independently quantified the racemization occurring under the analytical conditions used for this study, based on replicate measurements of the average %D-AA in a pure L-AA standard mixture. The racemization-corrected %D-AA we report considers both the hydrolysis and racemization blanks, calculated as described by Kaiser and Benner (2005). Finally, we also tested for potential racemization during our cation-exchange chromatography purification, a step which uses ammonium hydroxide to elute AAs that has not previously been included or tested in a D-AA analysis protocol. Similar to the racemization quantifications experiments discussed above, we used an L-AA standard mixture containing 9 AAs and measured the D/L AA ratio with and without this purification step. There was no observed increase in D-AA abundance beyond our racemization blanks for any of the analyzed AAs introduced by this process (Fig. 3.7).

Statistical analysis was conducted using the JMP statistical software package (SAS, Version 12). Statistical significance of the difference between means was determined using t-tests, with significance levels stated in the text. Relationships between variables are described using orthogonal least-squares regressions, with the ratio of the x and y measurement error variance determined from univariate variance

estimates of the x and y variables. Relevant p-values are noted in the text.

Results

Amino Acid Mol%

The relative molar abundance of AAs in our two DOM fractions (Fig. 3.1) is generally comparable to previous measurements in ocean DOM (McCarthy et al., 1998; Kaiser and Benner, 2009). Ala and Gly are the most abundant AAs in both HMW and LMW DOM; averaged across both fractions these AA make up 16 ± 5% and 22 ± 5% of the total AAs respectively. Asx and Glx are the next most abundant, with Mol% values of 13 ± 5% and 8 ± 2% respectively. The remaining AAs on average each represent 4 ± 1% of the total AA pool. However, there are also several clear differences in Mol% distributions between LMW and HMW fractions. Ala and Gly have the greatest Mol% offset between DOM size fractions (Fig. 3.1), however, the two AAs have opposite relationships with respect to MW. The Mol% of Ala is approximately 7% lower in the LMW fraction ($T = 3.45$, $df = 14$, $p < 0.01$), whereas Mol% of Gly is approximately 7% higher ($T = 3.06$, $df = 14$, $p < 0.01$).

In addition to the large Mol% offsets for Ala and Gly between fractions, there are smaller, but significant ($p \leq 0.05$), offsets in Mol% of Asx, Phe, Val, Thr, Ile, and Pro between the size classes. Among these AAs, Asx and Thr are elevated in the HMW fraction, whereas Phe, Val, Ile, and Pro are more abundant in the LMW fraction.

Amino Acid D/L ratios

The D/L ratios of the four D-AAs that have been widely reported in marine HMW DOM literature (Ala, Asx, Ser, and Glx) range from 0.2 to 0.7 (Fig. 3.2), consistent with previous measurements of similar HMW material (McCarthy et al., 1998; Kaiser and Benner, 2008; Fig. 3.8). The D/L ratios in the LMW fraction are generally higher than in the HMW fraction, with the exception of Ala, in which this this trend is the opposite. D-Ala also has the largest and most significant offset between HMW and LMW fractions of the 4 previously reported D-AAs (average offset = 0.21 ± 0.14, T = 4.38, df = 14, $p < 0.01$). The D/L ratio of Ala is also generally the highest of all the chiral AAs (Average D/L = 0.55 ± 0.16). The D/L ratios of all AAs other than Ala are always higher in the LMW fraction relative to HMW (average offset = 0.11 ± 0.05). The general offsets in D/L ratios are consistent at all depths sampled.

In addition to the D-AAs reported previously, we report here for the first time three additional D-AAs. These D-AAs (D-Leu, D-Val, and D-Phe) all have large and significant ($p > 0.01$) offsets in D/L ratios between HMW and LMW fractions (average offset = 0.12 ± 0.05), largely driven by the very low D/L ratios (average D/L = 0.05 ± 0.02) within the HMW fraction (Fig. 3.2). All three D-AAs were positively identified by GC-MS fragmentation patterns, and the reported abundance and D/L ratios were corrected for both racemization and derivatization blanks, as described previously (see experimental methods 2.4; appendix 2.0). Finally, it should also be noted that despite the large ^{14}C age offset between the HMW and LMW fractions, the observed offsets in D/L ratio between fractions cannot be due to abiotic racemization

alone. For example, in 3500 years (approximately the ^{14}C age offset between HMW and LMW fractions at 2500 m) abiotic racemization of Phe would be expected to increase its %D abundance by 1.4% (Bada, 1971), however the %D-AA of LMW Phe at that depth is approximately 50% higher than in the younger HMW material.

Water Column Structure of [D-AA], D/L ratio and AA Mol%

The concentration of individual D-AAs through the water column largely mirrors that of the total DOM pool, with the highest concentrations in the surface, decreasing with depth to a relatively constant value below 850m, consistent with expectations for a dominant surface derived source (Fig. 3.9). The average total D-AA concentration in the surface ocean is 9.4±0.1 nM in the HMW fraction and 3.0±0.2 nM in the LMW fraction. In the deep ocean (2500 m) the total D-AA abundance decreases to 2.4±0.1 nM and 1.2±0.1 nM in the HMW and LMW fractions respectively. Consistent with D/L ratio trends described above, D-Ala is by far the most abundant D-AA, with concentrations as high as 8 nM in surface HMW material. The three newly reported D-AAs (D-Phe, D-Leu, and D-Val) have the lowest concentration throughout the water column, with sub-nM concentrations in both MW fractions. Despite the oceanographic consistency of concentration profiles, there are some variations in the relative proportions of different AAs through the water column, most notably in excursions of the Mol% of Gly, Ala, Phe, and Leu at 400 m (Fig. 3.10). There is also notable depth variation in D/L ratio of select AAs, however, only the "new" D-AA (Leu, Val, and Phe) have significant changes in D/L ratio with depth, specifically Leu and Val, which have a clear structure with statistically

significant offsets between both surface and subsurface and HMW and LMW fractions (Fig. 3.3). For these AAs, D/L ratios are lowest in the surface, increasing to maximum values at 400, then decreasing again to apparently constant value in the deep ocean (i.e., similar values observed at 850m and 2500m). While these trends are generally consistent for both HMW and LMW fractions, the structure is exaggerated in the LMW fraction, based on a greater elevation of D/L ratio of both Leu and Val at 400m in the LMW SPE-DOM samples. There is also some depth structure in the D/L ratio of Phe (Fig. 3.3), however only in the more refractory LMW fraction, with a maximum Phe D/L ratio at 400 m decreasing to consistently lower values below 850 m, but no significant offset between the surface and 400 m. The lack of any significant depth structure in D/L ratio among the other D-AAs (Fig. 3.11) is consistent with previous published D/L measurements of Ala, Asx, Glx, and Ser in both HMW and total DOM (McCarthy et al., 1998; Nagata et al., 2003; Pèrez et al., 2003; Kaiser and Benner, 2008; Kaiser and Benner, 2009).

Relationships between D/L ratio, Mol% AA, and $\Delta^{14}C$

The D/L ratio and Mol% of individual AAs are directly linked across the entire size/age spectrum of marine DOM (Fig. 3.4). At the individual AA level, AAs with higher Mol% have higher contributions of their D-enantiomer, regardless of season, depth, or size class. This correlation is individually stronger within the HMW fraction ($R^2 = 0.86$) than in the LMW fraction ($R^2 = 0.69$) (Fig. 3.12), largely driven by the very high abundance and D/L ratio of Ala within the HMW fraction. However, even with Ala removed, a significant correlation between Mol% and D/L ratio remain

for all other AA ($R^2 = 0.47$; Fig. 3.13).

In contrast to Mol%, there was generally little linear correlation between D/L ratio of individual AAs and $\Delta^{14}C$ age of corresponding HMW or LMW DOM samples. However, there were clear offsets in AA D/L ratios between old and young material, corresponding to the ^{14}C ages in LMW and HMW DOM fractions respectively. When all samples are considered together, there are apparent significant correlations ($p < 0.05$) between the D/L ratio and $\Delta^{14}C$ for three AAs: Phe, Val, and Leu (Fig. 3.5; left panel). However, when considered within either HMW or LMW fractions individually these correlations are no longer statistically significant (Fig. 3.5; right panel), suggesting that change in D/L ratio of these AAs may not actually be linearly related throughout the entire age/size spectrum. Ala also had substantial offsets between D/L ratios in older LMW material and younger HMW material, however no statistically significant correlations within MW fractions (Fig. 3.5, 3.6). As noted above, D-Ala was also unique in that the D/L ratios were offset in the opposite direction compared to all the other D-AAs (i.e., more D-enantiomer in the younger, HMW material) (Fig. 3.6). Finally, for three AAs (Asx, Ser, and Glx) there were no correlations with DOM age, and no offsets between MW fractions (Fig. 3.14). Overall, for all D-AAs except for these three, there appears to be clear offsets in D/L ratio at all depths between the two MW fractions, however little evidence for a continuous relationship between DOM age and D/L ratio.

Discussion

Prokaryotic organisms dominate the synthesis and incorporation of D-AAs in the marine environment. D-AAs are a ubiquitous component of the peptide inter-bridge in bacterial peptidoglycans, providing one of the few unambiguous molecular tracers for bacterially synthesized AAs. As such, D-AAs are one of the most widely used tracers for bacterial influence in biogeochemical cycles and have been used as indicators of the contribution of bacterial carbon or nitrogen in a number of environments such as marine and lacustrine DOM and sediments (McCarthy et al., 1998; Grutters et al., 2002; Benner and Kaiser, 2003; Jorgensen et al., 2008; Carstens and Schubert, 2012; Carstens et al., 2012). Further, because D-AAs are contained within a major biochemical constituent of the DON pool, they can provide a more direct tracer for microbial contributions to the DON pool than extrapolations from DOC properties. Therefore, the significant ^{14}C age differences between our HMW and LMW DOM fractions combined with the elevation of D/L ratio across all D-AAs (except Ala) within the LMW fraction suggests that there is a larger prokaryotic contribution to LMW refractory marine DOM than the fresher HMW DON pool.

D-AA Comparison to Previous Measurements of HMW UDON and total LMW DON

The measured D/L ratios for the four D-AAs that have been widely reported in dissolved material (Ala, Asx, Ser, and Glx) correspond closely with previous direct measurements in HMW UDOM, and also with D/L ratios for LMW DOM previously calculated by difference (e.g., McCarthy et. al. 1998, Kaiser and Benner, 2008; Fig. 3.8). The similar D/L ratios in the HMW DOM pool are not unexpected, however this

comparison confirms that the specific protocol used here, including the new cation-exchange purification and our derivative-specific racemization corrections, yield results directly comparable with past approaches.

The similarity for the D/L ratios measured directly in our LMW SPE-DOM fraction and those previously calculated for total LMW DOM are more noteworthy. The prior LMW results (Kaiser and Benner, 2008) were derived by difference (total DON minus HMW UDON) for the entire operational LMW pool (~75-90% of total DON permeating a UF membrane). The fact that these values are identical within error to our direct measurements is somewhat remarkable, given the completely different sampling times, isolation and subsequent analysis conditions. Most important, this result suggests that our new coupled UF/SPE isolation protocol, despite directly recovering only 20-40% of LMW DOM, captures a representative fraction of the LMW AA pool. This conclusion is further supported by available $\delta^{15}N$ data, which suggests the portion of LMW DON we capture is also isotopically representative of the total LMW pool's $\delta^{15}N$ values (Broek et al., 2017). Together, this highlights a major advantage of our new method: because of the low concentration of D-AAs in deep ocean DOM, calculations that rely on mass balance to determine the properties of the LMW DOM pool are associated with high uncertainty. In contrast, direct measurements on large, organic–rich isolates can be far more precise, allowing a wider variety of direct molecular measurements compared to quantification at ambient concentrations.

Unique behavior of D-Ala: A potential tracer for peptidoglycan and labile HMW bacterial material

Ala emerged as unique across multiple aspects of our data set. D-Ala is the most abundant D-AA in all samples, and the relationship between the D/L ratio of Ala and DOM age and molecular weight is consistently the opposite from that of all other D-AAs (Fig. 3.2). These observations are also consistent with trends in Mol% (Fig. 3.1), together suggesting that D-Ala may be uniquely associated with highly labile bacterial source biochemicals with more rapid cycling than other D-AA containing compounds. This observation is also consistent with a maximum in Mol% Ala at 400 m in the HMW fraction (Fig. 3.10), suggesting that microbial processes in the water column contribute Ala predominantly to the HMW DOM pool. Multiple studies examining relative AA abundance changes with degradation have found that Mol% Ala generally increases with microbial alteration (Dauwe et al., 1999; Lee et al., 2000; Yamashita and Tanoue, 2003; Calleja et al., 2013). Within this framework, coupled with size-reactivity relationships, our results are unexpected. Past observations would predict that LMW DOM should be more degraded, and so might be expected to have both more total Ala and higher D/L Ala ratios. However, in our data, the higher D/L ratio and Mol% values in HMW DON compared to LMW DON suggests that biomolecules most enriched in D-Ala are concentrated in the HMW pool, and that D-Ala progressively grows into only the HMW pool with microbial processing.

We hypothesize that the most likely D-Ala source consistent with these observations is peptidoglycan, a structural polymer containing D-AAs, which is a

major component of bacterial cell walls (Schleifer et al., 1972; McCarthy et al., 1998). Peptidoglycan is a large polymerized macromolecule, which has been shown to be quite labile in seawater, with particularly rapid remineralization of the peptide component after hydrolysis (Nagata et al., 2003). Based on carbohydrate to D-AA ratios, previous work has indicated that intact peptidoglycan subunits likely constitute <0.1% of DON (Kaiser and Benner, 2008). While this might rule out the hypothesis of a main peptidoglycan source, there is evidence that degradation of peptidoglycan may obscure estimates based on molecularly identifiable sugar monomers. The work of Nagata and coauthors used radio-labeling experiments to show that intact peptidoglycan is rapidly broken into smaller molecular fragments during microbial degradation which are both resistant to further degradation, and importantly are no longer identifiable by standard chromatographic techniques (Kitayama et al., 2007). These direct marine degradation experiments suggest that peptidoglycan added to the dissolved phase would likely be rapidly degraded and structurally modified, such that intact D-Ala originally contained in peptide inter-bridges would not persist within the refractory LMW pool. It should also be noted that despite the dominance of D-Ala as a major component of peptidoglycan in cell walls, D-Ala also has other possible bacterial molecular sources such as lipopolysaccharides and lipopeptides (Kaiser and Benner, 2008). We therefore cannot exclude the possibility that other relatively labile, D-Ala rich microbial biomolecules could also contribute to these trends.

"New" D-AAs: potential tracers for refractory DON production

A novel aspect of our data is the identification of three D-AAs (D-Phe, D-Leu,

and D-Val) not previously identified in the DOM literature, but were present in all of the samples measured for this study. While some prior work has suggested the presence of minor amounts of these compounds in HMW DOM (McCarthy et al., 1998; Yamaguchi and McCarthy, 2018), reported abundances were both low and inconsistent, often indistinguishable from blanks. This is likely explained by the much lower abundance of these compounds in HMW UDOM samples compared to our LMW fraction. Further, earlier GC-FID or LCMS data was not able to make positive molecular identifications; DOM hydrolysate mixtures are notoriously complex, with multiple small and often overlapping peaks that cannot readily be identified based only on retention times (McCarthy and Bronk, 2008; Yamaguchi and McCarthy, 2018). In our data, GC-MS fragmentation data and quantification based on single-ion monitoring unambiguously shows that in addition to the four D-AAs widely measured in DOM previously, these three D-AAs are present in every DOM sample. Finally, the measurements of LMW DON D/L ratios of these D-AAs would likely not be possible with current instrumentation without the direct isolation and concentration of LMW DON used in our protocols.

The observations of strong enrichment of these D-AAs in LMW DOM relative to HMW DOM (Fig. 3.2), as well as the clear depth trends in the LMW fraction (including observed maxima at 400 m; Fig. 3.3), suggest these novel D-AAs are most strongly linked to the production of LMW, refractory DOM. While all D-AAs measured (except for D-Ala, as discussed above) were more abundant in older, LMW material, the relationships for D-Val, D-Leu, and D-Phe are clearly distinct. Of all 7 D-AAs we measured in this study, only these had clear and repeatable structure

in D/L ratio with depth between cruises. The synchronous depth structure for these compounds (Fig. 3.3) supports the hypothesis that they trace the same source material, with cycling in the upper water column distinct from the other D-AAs. More significantly, however, the variable behavior of AAs at 400m compared to the other depths suggests that local processes are resulting in active transformations within or additions to the LMW pool. This depth is within the "twilight zone" region of maximum particle flux attenuation, where sinking material from the euphotic zone is most rapidly remineralized by heterotrophic bacteria (Buesseler et al., 2007). While we do not have enough resolution to assess if 400 m in fact represents the exact maxima or minima in our measurements, we hypothesize that the offsets from surface to 400 m could be influenced by input of fresh, heterotrophic bacterial material. This demonstrates that despite the old average age of LMW DON, at least a portion of this material in the mesopelagic is involved in active cycling processes operating on timescales much shorter than that of ocean circulation. We also note that the waters around 400 m at Station Aloha are ventilated in the North Pacific outside of the subtropical gyre. Therefore, it is possible that the waters at this depth bear some unique signature of this other water mass. However, we have not observed any clear evidence for the influence of this water mass in other properties of our isolated DOM fractions (such as an inversion in ^{14}C age). Further, significant offsets in our measured properties between adjacent water masses would still be consistent with transformations of both the HMW and LMW fractions occurring on time scales much less than that of global ocean circulation.

To our knowledge, there are no currently known marine bacterial sources of

D-Leu, D-Val, and D-Phe. While future work will therefore be required to identify the molecular sources of these compounds, these observations suggest they trace the same, or perhaps very similar, classes of bacterial biomolecules. We hypothesize that these compounds may be useful new tracers for understanding microbial production of the most refractory DOM.

Finally, we note that Gly, despite being a major AA in HMW DOM (and dominating AA Mol% in LMW DOM), cannot be included in a similar analysis since Gly is non-chiral, and so has no D-enantiomer. However, its elevated Mol% within the LMW SPE-DOM fraction suggests that it might also be a useful AA for tracking the production of refractory LMW DON. This is consistent with the studies discussed in section 4.2 which demonstrated that Ala and Gly represent the most useful AAs for tracking microbial influence in total organic matter (Dauwe et al., 1999; Lee et al., 2000; Yamashita and Tanoue, 2003; Kaiser and Benner, 2012; Calleja et al., 2013). We hypothesize that measuring the $\delta^{15}N$ value of Gly might be one way to directly test this idea, since $\delta^{15}N_{Gly}$ has been shown to increase dramatically (+10 to +15 ‰ increase) during bacterial degradation of DOM (Calleja et al., 2013).

DOM ^{14}C age, MW fractions and D/L Ratios: Implications for a Microbial N Pump & DON size-reactivity "continuum"

This data set has allowed us to directly test the microbial N pump idea and investigate the hypothesis that microbes are directly responsible for the production of refractory DON and the associated sequestration of N within the marine DON pool. We hypothesized that a continuous relationship between AA-D/L ratio and DOC

$\Delta^{14}C$ would indicate a progressive increase in microbial influence along a size-reactivity continuum, with slopes reflecting relative rates of input for individual D-AA sources. In contrast, size-based discontinuities in slopes might indicate distinct sources for different D-AAs or unique degradation processes within the semi-labile and refractory DOM pools.

Our primary finding of higher overall D/L ratios in older, LMW material relative to younger HMW DOM strongly supports our basic hypothesis. However, the unexpected finding that there are little to no significant trends between D/L ratios and $\Delta^{14}C$ which apply across both MW fractions was in contrast to our original hypothesis. The apparent discontinuity between HMW and LMW in the $\Delta^{14}C$ regressions suggests that the behavior of these D-AAs might be more consistent with separate sources to HMW and LMW DON. This interpretation is an apparent departure from a size-reactivity "continuum" prediction, where LMW is derived from the degradation of HMW material. It would instead suggest a somewhat more complicated relationship, with more independent HMW and LMW DON pools, perhaps formed from different surface sources, or through different mechanisms. As mentioned above, the D-AA depth trends within the LMW material suggest it is being transformed on timescales much shorter than global ocean circulation, and the unique behavior of different AAs in each MW fraction demonstrates active cycling in both fractions. At the same time, the variation in distribution and apparent behavior of both fractions supports the idea that D-AAs likely have distinct microbial source biomolecules, as suggested by Kaiser and Benner (2008), as well as likely diversity in the cycling dynamics of the sources traced by each group.

The unified relationship between D/L ratio and molar abundance across all D-AAs (Fig. 3.4) was also an unexpected finding. Because of the greater number of D-AAs measured here, including the newly confirmed D-AAs that exist at low concentrations in both size classes, this relationship likely could not have been identified in past work. Overall, this apparent coupling of D/L ratio and molar abundance links bacterial source with relative AA concentration across all seven chiral AAs we now recognize in marine DOM, indicating that the most abundant AAs derive disproportionately from non-protein bacterial sources. This suggests that the relative abundance of all AAs within marine DOM is predominantly shaped by input from prokaryotic sources.

Summary and Conclusions

To test the "microbial N pump" hypothesis, we measured AA enantiomers and AA Mol% distributions in conjunction with ^{14}C ages for independently isolated HMW and LMW DOM fractions. D-AAs are direct biomarkers for prokaryotic source within the largest identifiable DON compound class and $\Delta^{14}C$ data provides an average age for each DOM fraction as a proxy for reactivity. Coupling these measurements allowed a first direct assessment of the prokaryotic contribution to different DON pools with greatly contrasting ages, recalcitrance, and bulk chemical properties, from the surface to the deep ocean in the North Pacific Subtropical Gyre.

When Ala is excluded, total D-AA abundances are highest in the samples with the oldest ^{14}C age, strongly supporting the idea that prokaryotic organisms represent a direct source of refractory DON. We observed similar D/L ratios as previously

published work for the four AAs widely reported in marine DOM (Ala, Asx, Glx, and Ser) in both HMW and LMW material. However, GC-MS analysis also allowed identification and quantification of three additional D-AAs (D-Leu, D-Val, and D-Phe) present at all depths in all samples, although strongly concentrated in LMW DOM. Despite the lower concentrations of these newly confirmed D-AAs, their concentration profiles show oceanographically consistent trends within and between size fractions, confirming that they are real compounds with unique tracer potential. We observed consistent and unique relationships between D/L ratio, AA-Mol%, and $\Delta^{14}C$ among different AAs, suggesting that a number of key D-AA subgroupings may represent unique proxies for specific bacterial sources.

D-Ala emerged as unique within almost all aspects of our data set. Consistent with previous reports, D-Ala was the single most abundant D-AA in our DOM samples. However, in contrast to the relationship between D/L ratio and ^{14}C age for all the other D-AAs, we observed lower D/L ratios of Ala in the older, refractory, LMW DOM fraction, and higher D/L ratios in the younger, semi-labile, HMW fraction. This distinct relationship was accompanied by analogous Mol% trends, with significantly lower Mol% Ala in refractory DOM compared with semi-labile DOM. We therefore hypothesize that D-Ala cycling is linked to the input and subsequent degradation of semi-labile peptidoglycan material. This apparently contrasts with other D-AAs, which may have more diverse bacterial origins and slower degradation rates.

Aside from Ala, the offset in D/L ratios between semi-labile HMW and refractory LMW DOM was largest for the newly confirmed D-AAs, suggesting these

may be the best D-AA tracers for bacterial contribution to the refractory DON pool. Further, the depth trends in both AA Mol% and D/L ratio are nearly identical for these AAs, suggesting that they may trace the same microbial source materials. The minimum and maximum of AA Mol% and D/L ratio respectively in the upper mesopelagic also suggest a potential linkage to sinking particle sources. Future work will be required to investigate the most likely biomolecular sources for these D-AAs, however we hypothesize that together D-Val, D-Leu, and D-Phe have potential as new tracers for the most refractory bacterial material accumulating in the ocean's DON pool. Overall, our data suggests that within the expanded group of 7 D-AAs now identified, subgroups of D-AAs trace individual microbial sources with unique cycling rates and demonstrates a significant expansion of tracer potential for D-AAs in ocean DOM.

Together, our data set strongly supports a microbial N pump, however, not necessarily one that operates exactly as expected from the current interpretation of a DOM size-age "continuum". While the D-AA enantiomers are generally concentrated within the refractory LMW pool, the lack of continuity in D/L ratio across a ^{14}C age spectrum raises the possibility that although refractory LMW DON has a clear microbial source, it is not necessarily derived from microbial degradation of semi-labile HMW DON, but rather from independent microbial sources in the upper ocean. We caution, however, that this interpretation is in part based on the assumption that trends in DON or AA ^{14}C ages generally follow those of total DOM, and also that they are mostly surface derived. While this seems very likely based on past work (Loh et al., 2004) as was well methodological tests with both ultrafiltration (Walker et

al., 2011) and SPE sorbents (Flerus et al., 2012; Broek et al., 2017), we suggest that future work aimed at both determining exact ages of purified AAs in the ocean, coupled with an expanded understanding of specific molecular sources of different D-AAs, could lead to a far more detailed mechanistic understanding of how different bacterial communities contribute to the formation of refractory DON in the oceans.

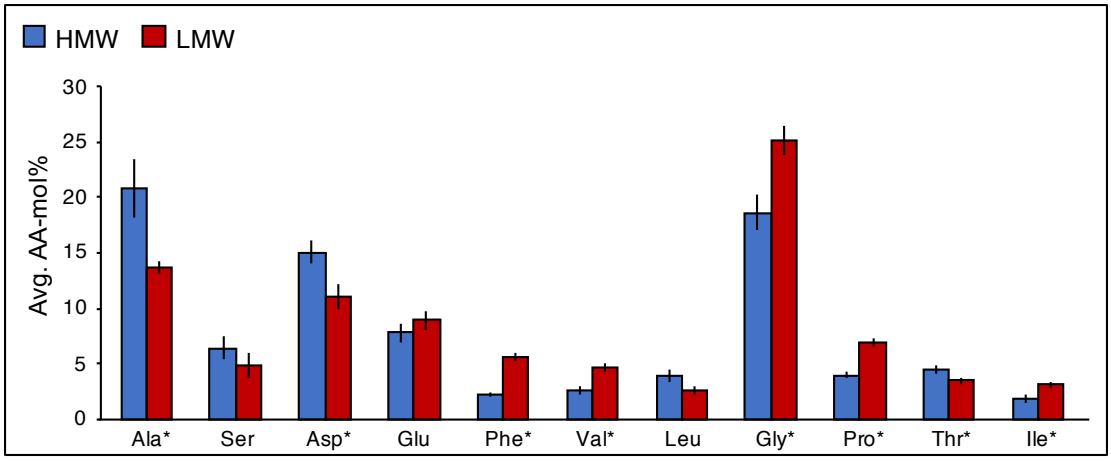

Figure 3.1 Average AA Mol% in HMW Semi-Labile and LMW Refractory DOM Fractions. The relative distribution of most AAs is generally similar for both fractions. Ala and Gly are the most abundant AAs in both HMW and LMW DOM; averaged across both fractions these AA make up an average of 16 ± 5% and 22 ± 5% of the total AAs respectively. However, Mol%-Ala is highest in HMW DOM while Mol%-Gly is highest in LMW DOM. In addition, the relative Mol% of Asx and Thr are higher in HMW DOM, whereas Phe, Val, Pro, and Ile have higher relative abundance in LMW DOM. Blue bars = AA-Mol% distribution in HMW UDOM, red bars = AA-Mol% distribution in LMW SPE-DOM. Error bars represent the standard error of the mean AA-Mol% across depth- and cruise-averaged values (n=8). Stars (*) indicate AAs for which the Mol% offset between fractions is significant (t-test, $p \geq 0.05$)

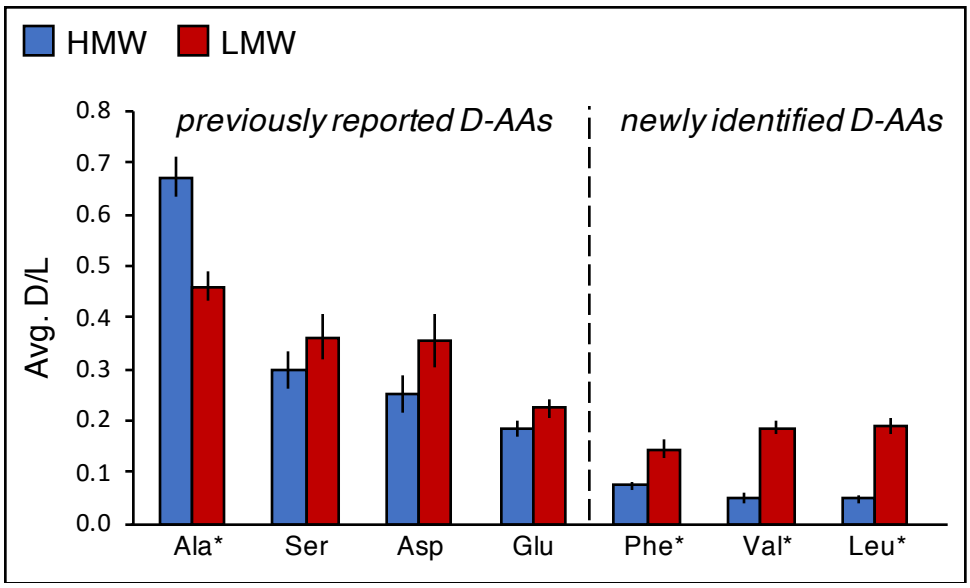

Figure 3.2 Average AA D/L Ratio in HMW Semi-Labile and LMW Refractory DOM Fractions. The average AA D/L ratio is higher in the LMW refractory DOM fraction compared to HMW semi-labile DOM for all AAs except for Ala. "Previously reported" refers to D-AAs that have been commonly identified in the literature in both HMW and total DOM. "Newly identified" refers to D-AAs confirmed in DOM here for the first time, based on GC-MS fragmentation patterns. Blue bars = D/L ratio in HMW UDOM, red bars = D/L ratio in LMW SPE-DOM. Error bars represent the standard error of the mean D/L ratio across depth- and cruise-averaged values (n=8). Stars (*) indicate AAs for which the D/L offset between fractions is significant (t-test, $p \leq 0.01$).

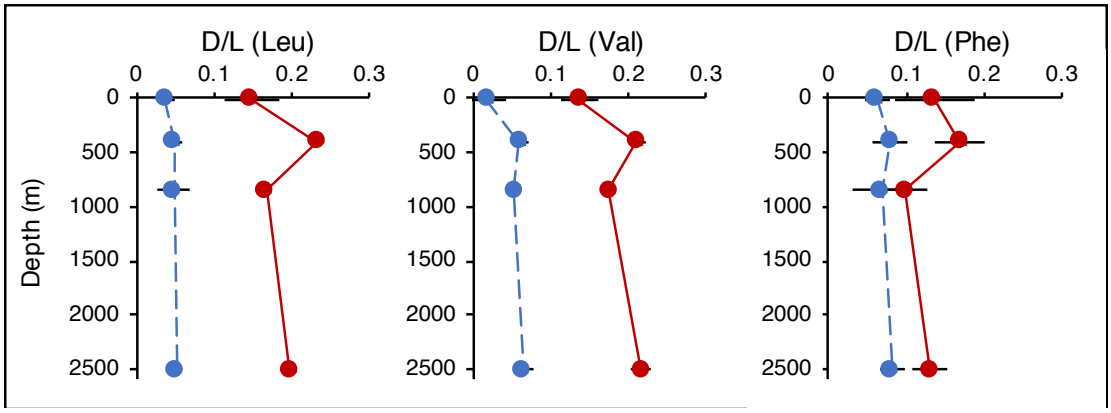

Figure 3.3 AA D/L Ratio Depth Profiles in HMW Semi-Labile and LMW Refractory DOM Fractions (Leu, Val, Phe only). All three of the "newly identified" D-AAs (Leu, Val, and Phe) have significant changes in D/L ratio with depth within the LMW fraction, specifically Leu and Val fraction, which have a clear structure with statistically significant offsets between surface and subsurface and maxima at 400m. Each point represents the average value of duplicate sampling seasons. Blue symbols, dashed line = HMW DOM; red symbols, solid line = LMW SPE-DOM. Error bars represent the propagated standard error associated with racemization corrections and season-averaged D/L ratios.

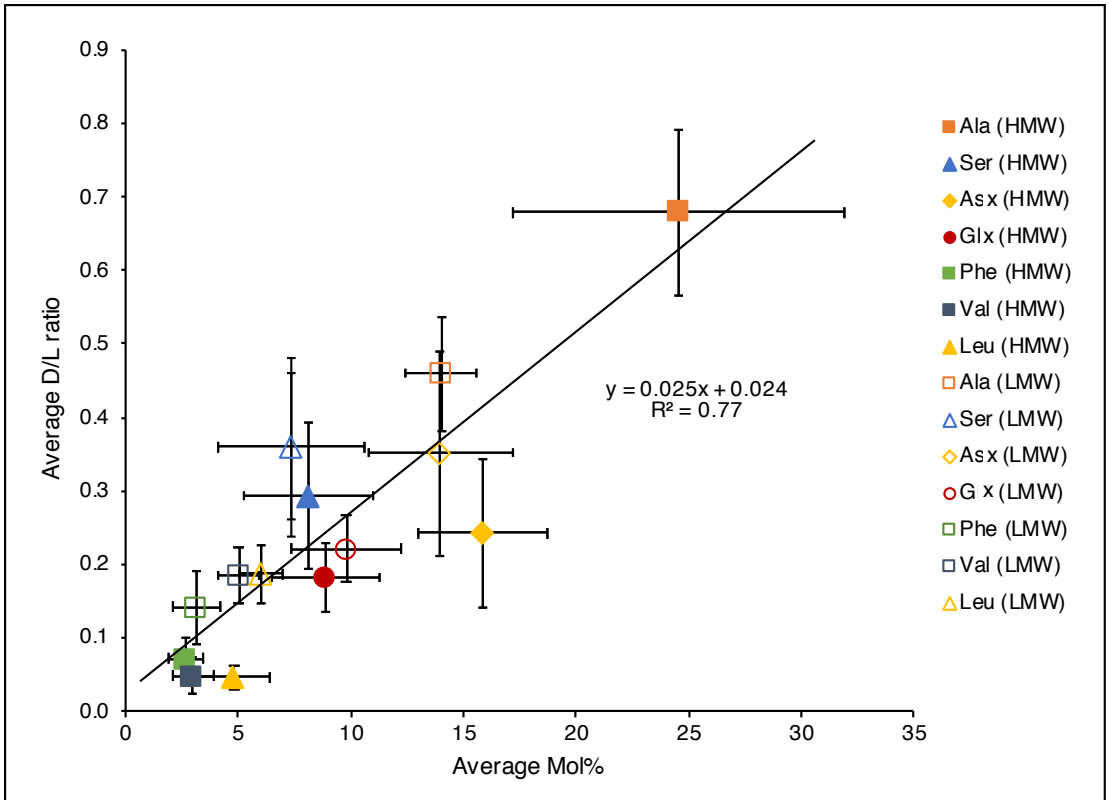

Figure 3.4 Positive Correlation Between AA-Mol% and D/L Ratio Across All Amino Acids in Both HMW Semi-Labile and LMW Refractory DOM Fractions. Each point represents the average Mol% and D/L ratio of all samples for each AA, error bars represent the standard deviation of all samples (n=8). $R^2 = 0.77$, $t = 6.4$, $df = 14$, $p > 0.01$.

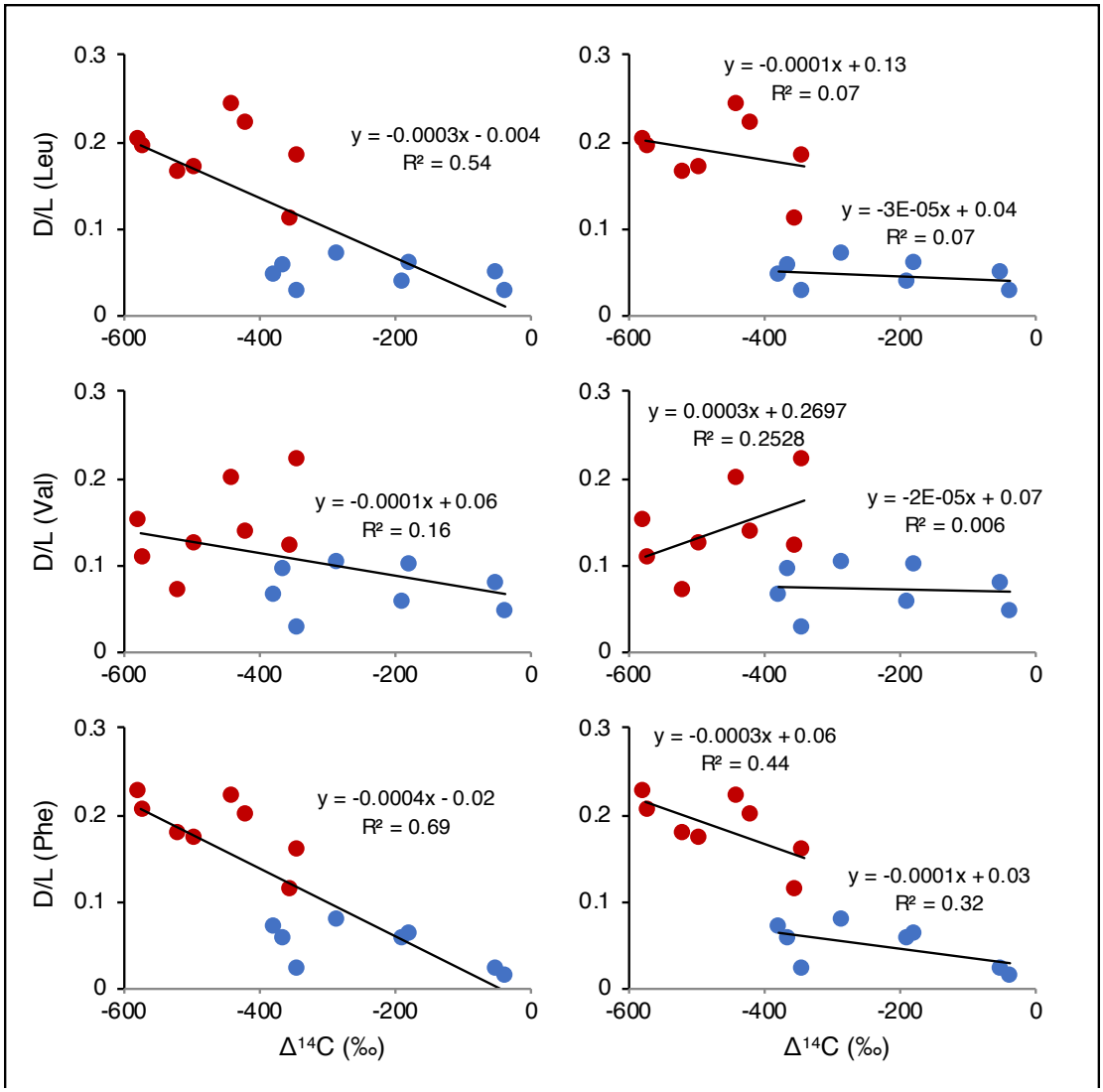

Figure 3.5 D/L ratio vs. $\Delta^{14}C$ of AAs with significant D/L offsets between fractions (Leu, Val, Phe). The three "newly identified" D-AAs (Leu, Val, and Phe) have significant offsets in D/L ratio between HMW semi-labile and LMW refractory DOM fractions. As a result, when all samples are considered together, there are significant correlations ($p < 0.05$) between the D/L ratio and $\Delta^{14}C$ (left panel). However, when considered within either HMW or LMW fractions these correlations are no longer statistically significant (right panel), suggesting that change in D/L ratio of these AAs may not actually be linearly related throughout the entire age/size spectrum. Each point represents a single sample. Red symbols = LMW SPE-DOM, blue symbols = HMW UDOM.

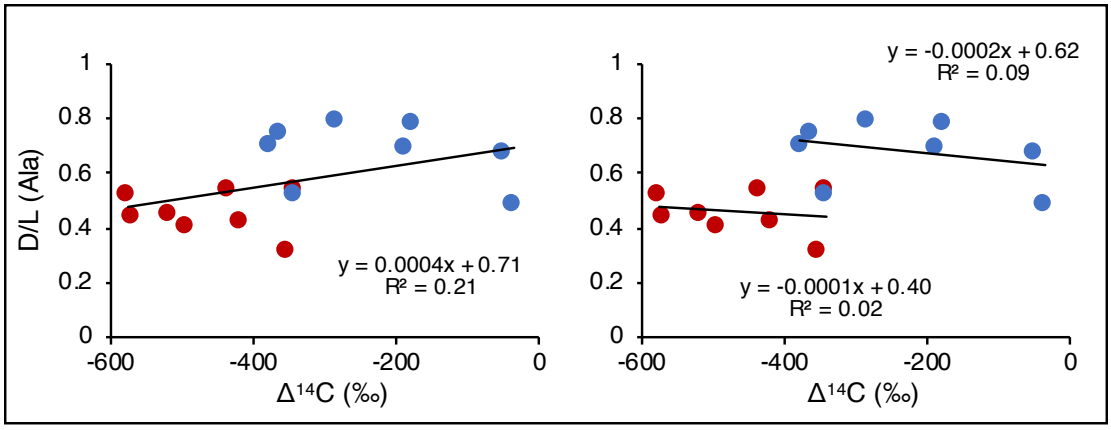

Figure 3.6 D/L ratio vs. $\Delta^{14}C$ of Alanine. Similar to Leu, Val, and Phe, the average D/L ratio of Ala is significantly different between HMW semi-labile and LMW refractory DOM fractions. As a result, when all samples are considered together, there are significant correlations ($p < 0.05$) between the D/L ratio and $\Delta^{14}C$ (left panel). However, when considered within either HMW or LMW fractions these correlations are no longer statistically significant (right panel), suggesting that change in D/L ratio of these AAs may not actually be linearly related throughout the entire age/size spectrum. Each point represents a single sample. Red symbols = LMW SPE-DOM, blue symbols = HMW UDOM.

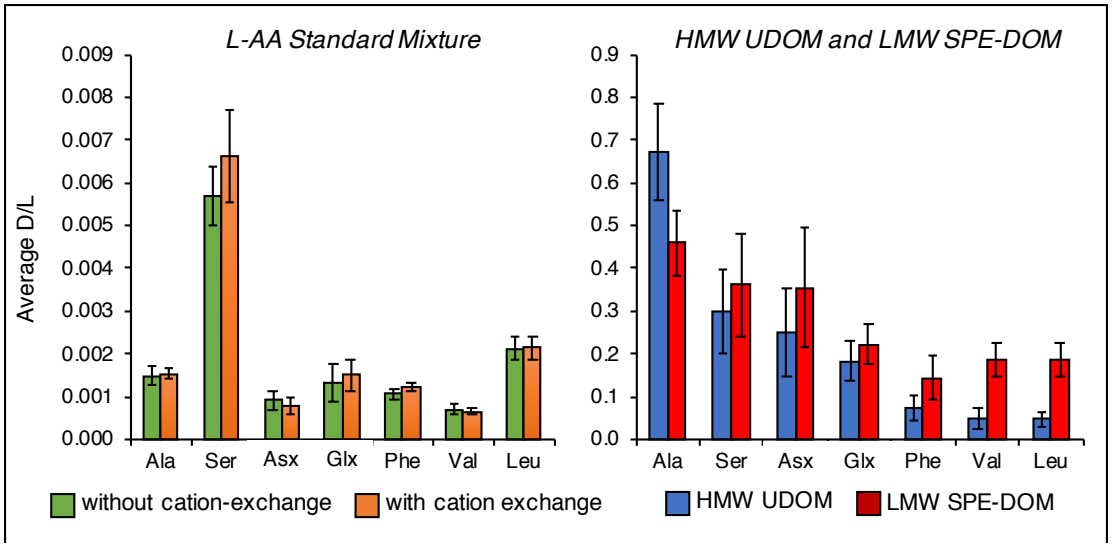

Figure 3.7 AA racemization during sample prep. Left panel: Comparison of D/L ratio of L-AA standard following derivatization with (orange bars) and without (green bars) cation-exchange purification step showing no significant difference. Error bars represent the standard deviation of n=3 samples. Right panel: Average D/L ratio of HMW UDOM (blue bars) and LMW SPE-DOM (red bars) fractions for reference, highlighting the very minor contribution of racemization produced D-AAs compared to the high D/L ratio of isolated DOM fractions. (nb: y-axis of the right panel is 2 orders of magnitude larger than the left panel). Error bars represent the standard error of the mean D/L ratio across depth- and cruise-averaged values (n=8).

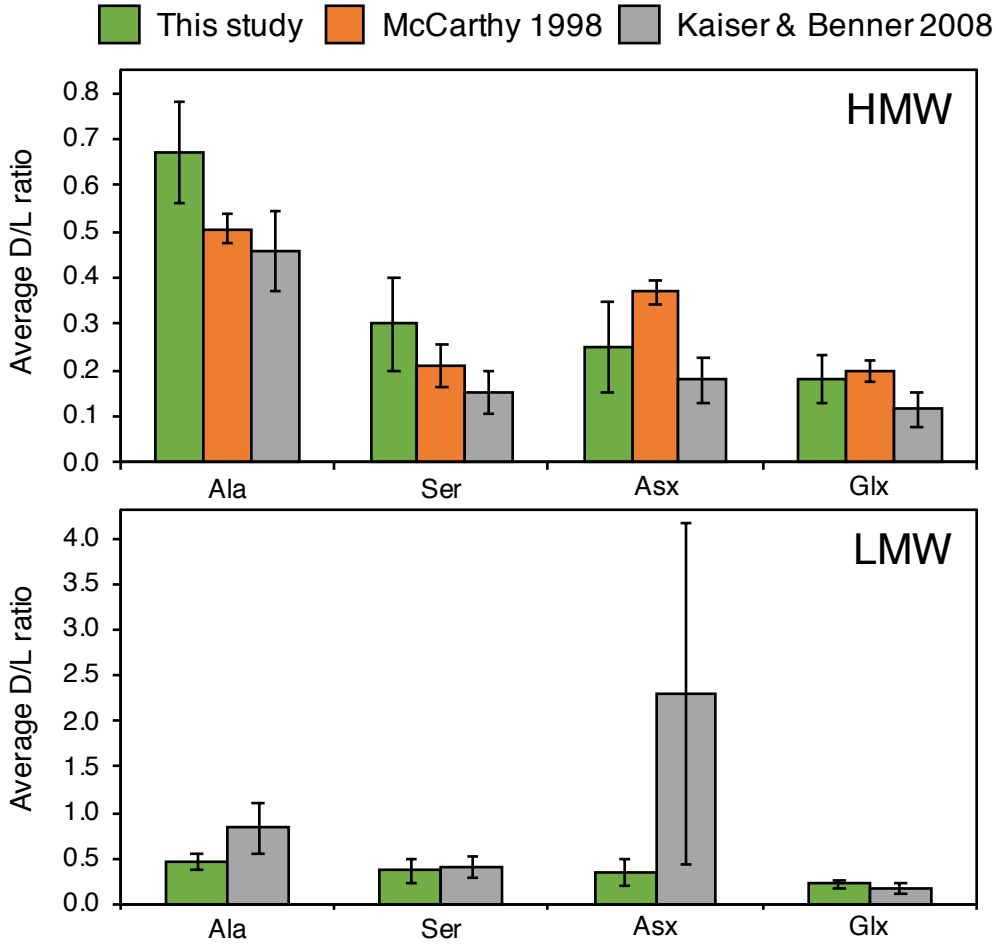

Figure 3.8 D/L ratio: comparison to previous work. Comparison of measured D/L ratios to previously published data. Top Panel: Average measured D/L ratios of HMW DOM compared to two previous studies (McCarthy et al., 1998; Kaiser & Benner, 2008). Bottom panel: Average measured D/L ratios of LMW SPE-DOM compared to previously published D/L ratios calculated by subtracting HMW from total DOM (Kaiser and Benner, 2008). Calculated LMW D/L ratios from Kaiser and Benner represent the average and standard deviation of all measurements made in the upper 300 m of the water column. Below 300 m the error in calculated values is high due to select AAs (or specific enantiomers of each AA) below the limit of detection. Because of the lack of D/L variability throughout the water column for these AAs, the use of only upper ocean samples for this comparison is valid.

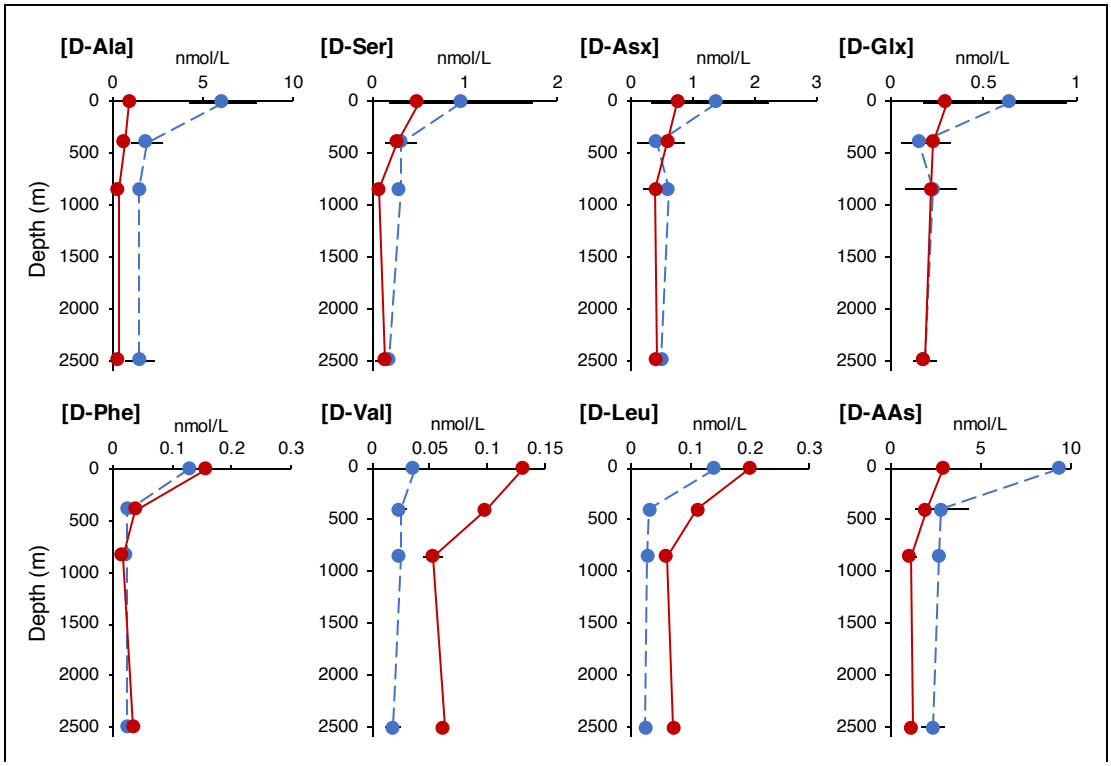

Figure 3.9 D-AA concentration depth profiles. Depth profiles of D enantiomer concentration [D-AA] for all AAs generally follows the distribution of total DOM, with the highest concentration in the surface ocean, decreasing to a relatively constant value in the deep ocean. Each point represents the average value of replicate sampling seasons. Blue symbols, dashed line = HMW DOM, red symbols, solid line = LMW SPE-DOM. Error bars represent the propagated standard error associated with racemization corrections and season-averaged D/L ratios.

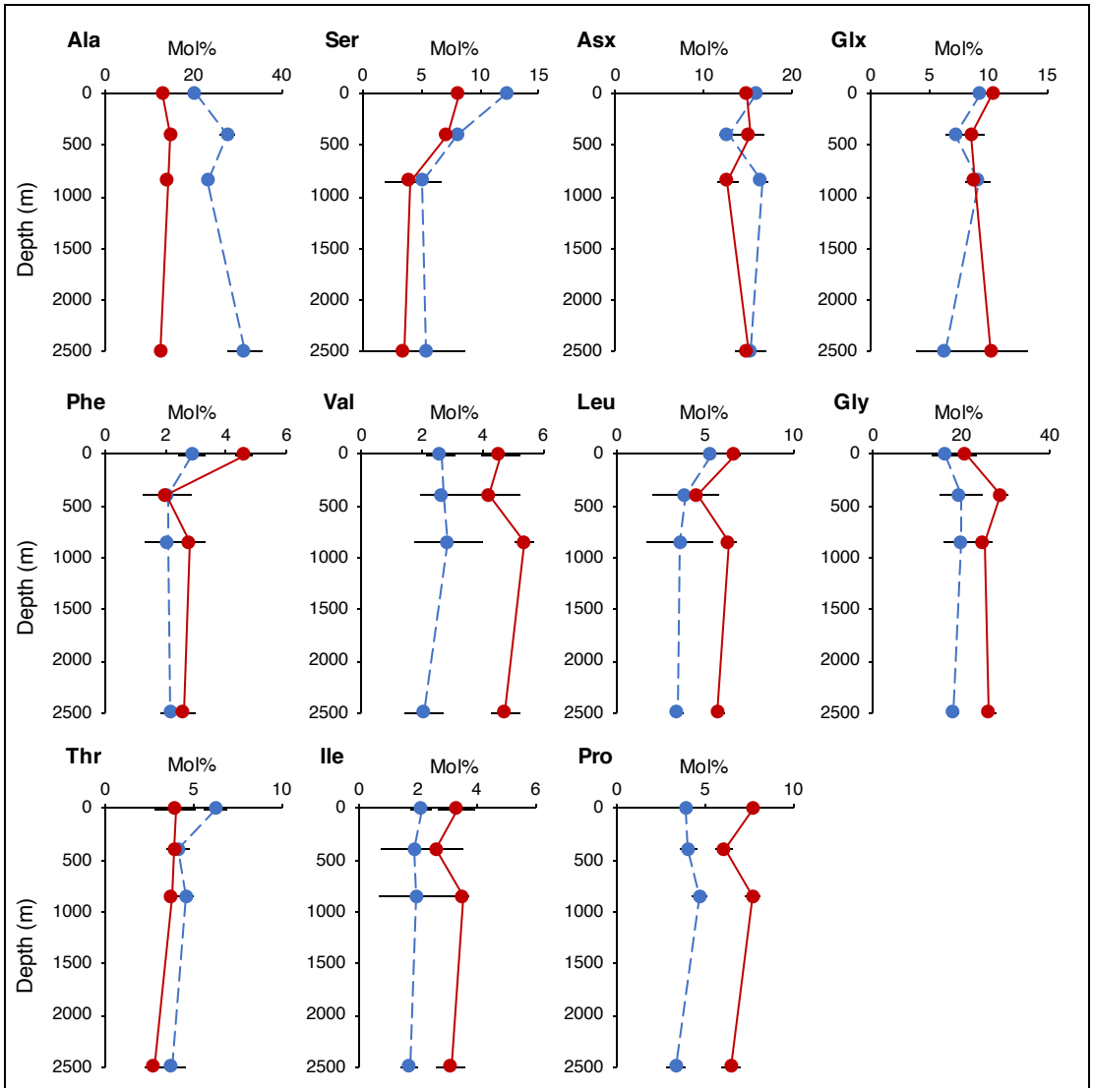

Figure 3.10 AA-Mol% depth profiles. There are variations in the relative proportions of select AAs through the water column, most notably in excursions of the Mol% of Gly, Ala, Phe, and Leu at 400 m within specific fractions. Each point represents the average value of replicate sampling seasons. Blue symbols, dashed line = HMW DOM, red symbols, solid line = LMW SPE-DOM. Error bars represent the propagated standard error associated with racemization corrections and season-averaged D/L ratios.

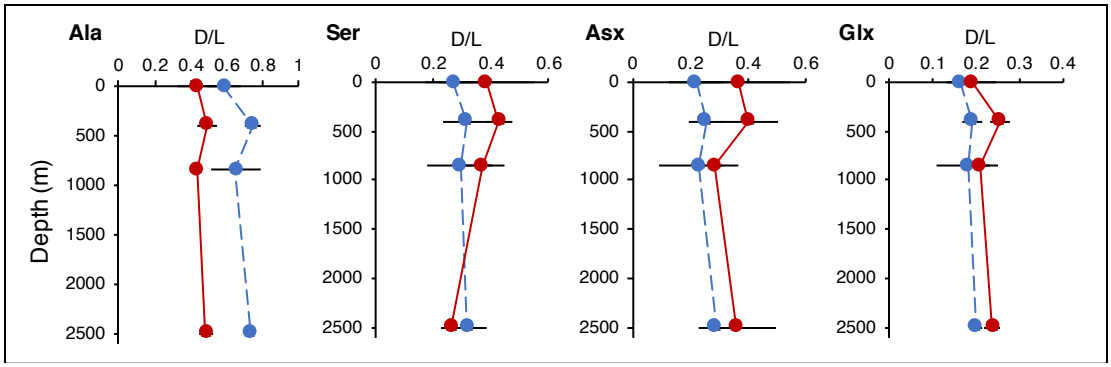

Figure 3.11 D/L ratio depth profiles. The depth profiles of the "previously reported" AAs (not included in Fig. 3.3) show no significant structure throughout the water column. Each point represents the average value of replicate sampling seasons. Blue symbols, dashed line = HMW DOM, red symbols, solid line = LMW SPE-DOM, Error bars represent the propagated standard error associated with racemization corrections and season-averaged D/L ratios. AA abbreviations are as defined in the text.

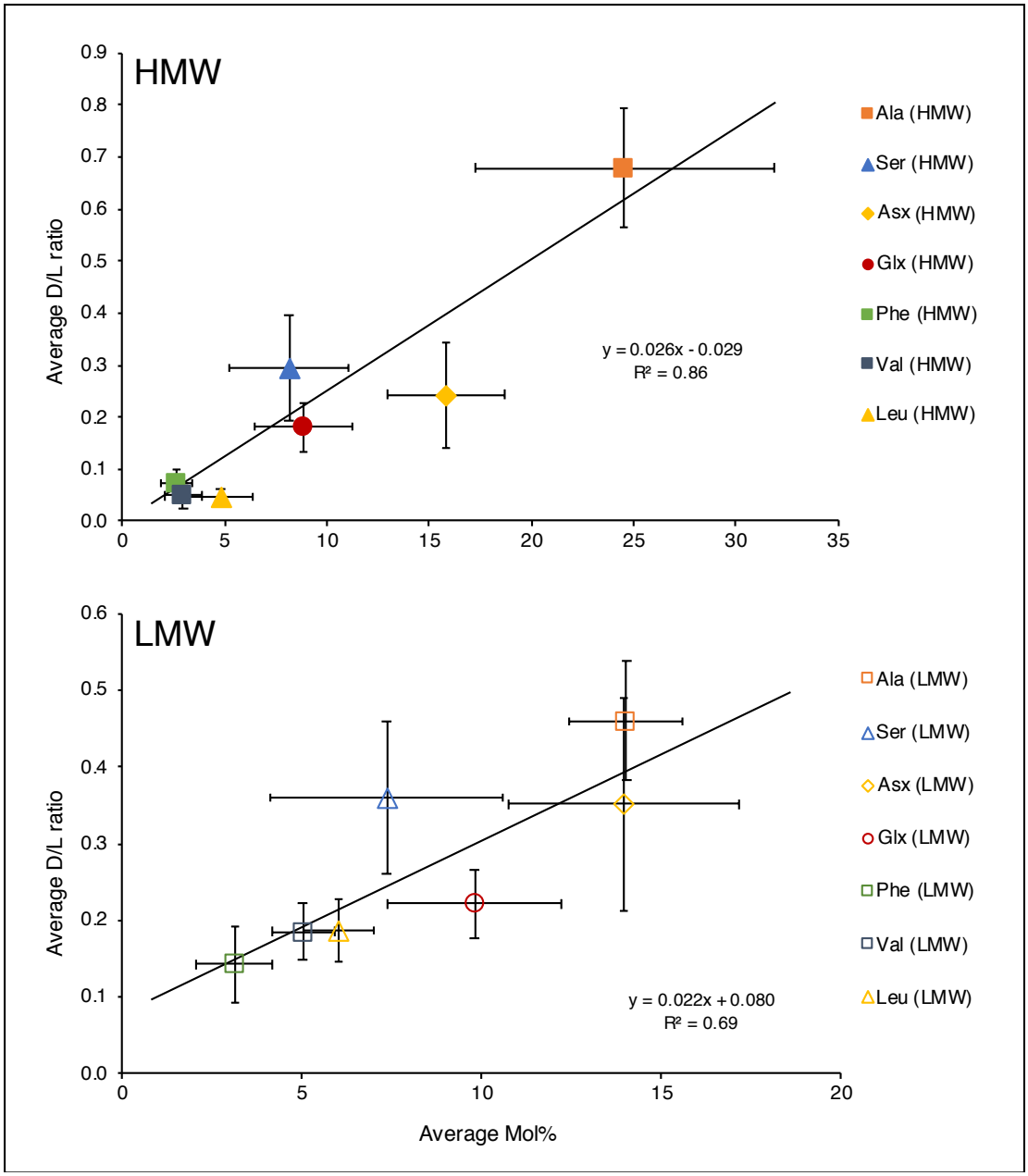

Figure 3.12 Positive Correlation Between AA-Mol% and D/L Ratio Across All Amino Acids in Separate HMW Semi-Labile and LMW Refractory DOM Fractions. Each point represents the average Mol% and D/L ratio of all samples within each DOM fraction for each AA, error bars represent the standard deviation of all samples (n=8). HMW: $R^2 = 0.86$, t = 5.6, df = 6, p > 0.01. LMW: $R^2 = 0.69$, t = 3.3, df = 6, p > 0.01.

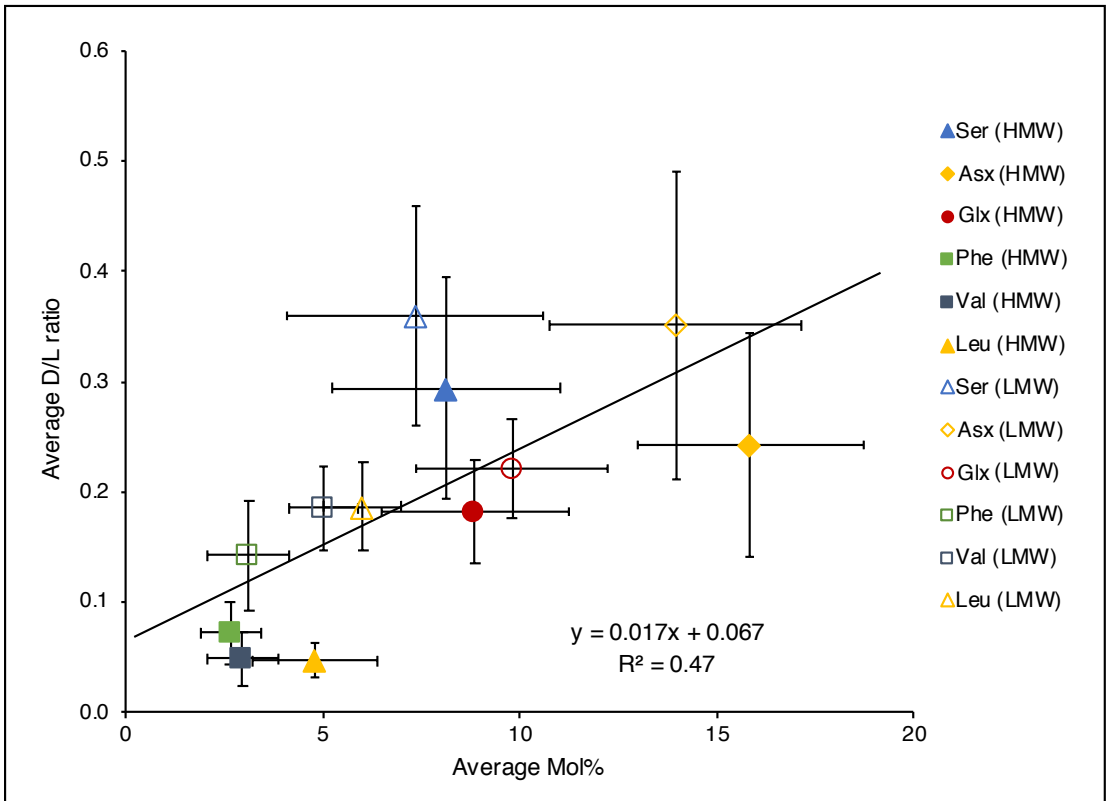

Figure 3.13 Positive Correlation Between AA-Mol% and D/L Ratio Across All Amino Acids, excluding Alanine, in Both HMW Semi-Labile and LMW Refractory DOM Fractions. Demonstrates that the correlation between average D/L ratio and Mol% is significant even without the influence of Ala. R2 = 0.47, t = 3.0, df = 12, p = 0.005.

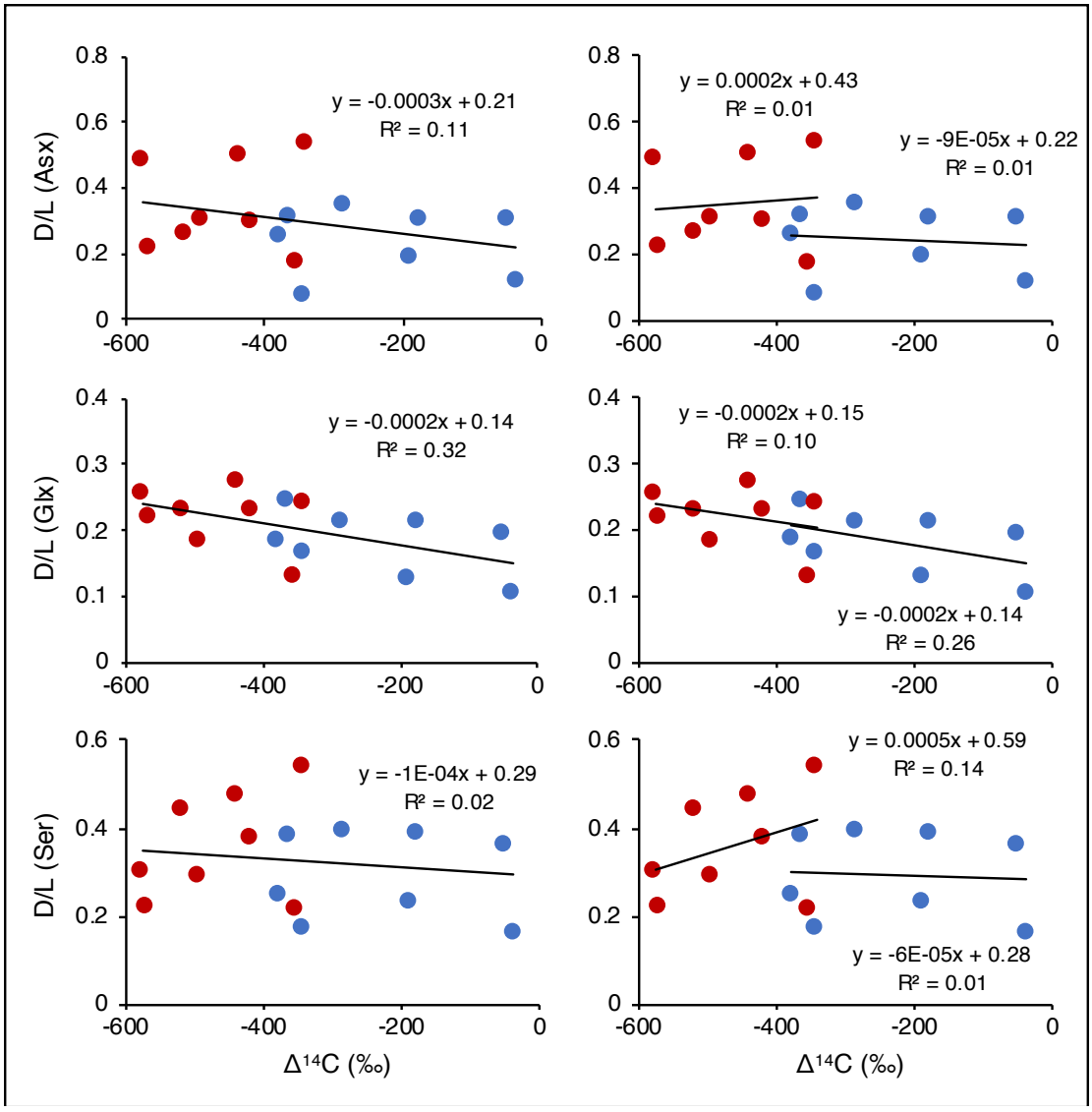

Figure 3.14 D/L Ratio vs. $\Delta^{14}C$ of the AAs without Significant D/L Offsets Between Fractions (Asx, Glx, and Ser). The average D/L ratio of Glx, Asx, and Ser are equivalent within error in HMW semi-labile and LMW refractory DOM fractions. Correlations of $\Delta^{14}C$ and D/L ratio for these AAs are insignificant; both between fractions (left panel) and within fractions (right panel). Each point represents a single sample. Red symbols = LMW SPE-DOM, blue symbols = HMW UDOM.

Chapter 4

Radiocarbon analysis of individual amino acids in marine dissolved organic matter: implications for the cycling of proteinaceous material in the ocean

Abstract

Dissolved organic nitrogen (DON) is one of the largest global reservoirs of biologically available nitrogen, yet its cycling dynamics remain poorly understood, largely due to a lack of isotopic data specific to N-containing biomolecules. Here we present the first radiocarbon analysis of individual amino acids (AAs), the largest molecularly identifiable DON component, isolated from the proteinaceous marine DON pool. In contrast to past assumptions of a relatively homogenous pool, our new data reveals a remarkable heterogeneity in the ^{14}C age of individual AAs, ranging from modern to thousands of years old in both surface waters and the deep ocean. This data suggests a fundamentally new view of marine DON cycling and demonstrates that proteinaceous material throughout the ocean is an extraordinarily diverse and actively cycling pool. Further, this data implies that different AAs trace different AA-containing compounds with significantly different sources, reactivities, and cycling dynamics.

Introduction

Marine dissolved organic nitrogen (DON) is the largest pool of reduced and actively cycling N in the ocean, however, little is known about its composition, sources, and role in biogeochemical cycles. In large part this is due to the lack of N-specific compositional and isotopic data. One of the major unanswered questions regarding ocean DON is its reactivity and overall cycling rates, in particular compared with the broader dissolved organic carbon (DOC) pool. The sources and cycling rates of DOC are far better constrained because both stable and radioisotopic measurements can be made directly on seawater DOC at ambient concentrations (Williams and Druffel, 1987). Bulk radiocarbon (^{14}C) measurements of DOC traditionally suggested that the vast majority of ocean DOC is a refractory and uniform, well mixed reservoir (Druffel et al., 1992). Limited radiocarbon measurements of operationally defined DOM components challenged this view, demonstrating an unexpected diversity in the cycling of different compound types (Loh et al., 2004). However, because there is no established method to selectively and exclusively isolate all N-containing material from DOM, it is unclear how nitrogenous material would be expected to cycle relative to other DOM.

Detailed information regarding DON sources and cycling must therefore rely on analysis of N-containing biomarkers. Amino acids (AAs) are the largest recoverable nitrogenous molecular component of DOM at all ocean depths (McCarthy and Broek, 2008), and therefore represent the most informative compound class for understanding DON reactivity. Past attempts to directly constrain DON cycling rates have come from radiocarbon analysis of an operationally defined

"protein-like" fraction isolated from high molecular weight (HMW) DOM samples (Loh et al., 2004). This data indicated that the protein-like material was younger than both total DOC and HMW DOC, implying that DON may cycle at significantly faster rates than other DOM. At the same time, the operational protein-like fraction had ^{14}C ages in excess of 3000 years in deep waters of the North Pacific. This study, combined with spectroscopic evidence demonstrating that the same HMW isolates are dominated by amide containing (likely proteinaceous) material at all depths (Aluwihare et al., 2005; McCarthy et al., 1997) with little variation in AA distributions (Broek et al., 2019; Kaiser and Benner, 2009; McCarthy et al., 1996), suggested that subsurface DON is a homogeneous pool which persists in the ocean on timescales longer than global ocean circulation. However, these old ages are puzzling given the expected lability of proteins and other amide containing compounds.

While this study provided compelling information regarding the variable cycling of different DOM components, the supposed proteinaceous material on which these radiocarbon measurements were made was not pure AAs, but rather an operationally defined fraction. Therefore, it is possible that these values reflect more than just N-containing proteinaceous material and are skewed by the presence of a potentially complex mixture of other organic compounds. In addition, the HMW ultrafiltered material from which the protein-like fraction was isolated represents a small fraction of the total DOM pool (generally 5-25%; Benner et al., 1992; Broek et al., 2017; Walker et al., 2011). Additionally, it is now widely recognized that on average the HMW fraction of DOM represents a more rapidly cycling component with more recognizable biomolecules than the remaining low molecular weight

(LMW) material (Amon and Benner, 2015; Walker et al., 2011; 2016a; 2016b). It is therefore possible that the LMW DON pool contains modified or degraded proteinaceous material (Kaiser and Benner, 2009), with potentially much slower cycling rates than DON in the HMW pool.

The only way to definitively quantify DON cycling rates is through radiocarbon measurement of fully purified DON components. However, due to the difficulty of isolating individual compounds from complex DOM matrices and low concentrations which require challenging low-level AMS techniques, no such measurements have been published. Here we present the first radiocarbon analysis of individual amino acids (AAs), purified independently from both younger HMW and older LMW DOM fractions. Both HMW and LMW DOM were extracted from the surface and deep (2500 m) waters of the North Pacific Subtropical Gyre (NPSG) using an inline combination of ultrafiltration and solid phase extraction (Broek et al., 2017). These separately isolated DOM size fractions were further purified using a cation-exchange chromatography method to obtain a fraction comparable to the previously studied protein-like fraction (Loh et al., 2004; Takano et al., 2010). Individual AAs were subsequently isolated from the HMW and LMW protein-like fractions using an established preparatory scale high pressure liquid chromatography (HPLC) method (Bour et al., 2016; Broek et al., 2013; Broek and McCarthy, 2014). These samples collected from the deep waters of the NPSG contain the oldest DOM in the world ocean and therefore represent ideal material for investigating the cycling and long-term preservation of proteinaceous material in the deep ocean.

Methods

The study was conducted using subsamples of the HMW ultrafiltered DOM and LMW solid phase extracted (SPE) DOM fractions described in Broek et al. (2017), collected using a sequential combination of large-volume tangential-flow ultrafiltration (UF) and SPE of the LMW UF permeate using Bond Elute PPL sorbent. The specific samples used for this study were collected from surface (7.5 m) and deep ocean (2500 m) waters at the Hawaiian Ocean Time-Series (HOT) Station ALOHA (A Long-Term Oligotrophic Habitat Assessment; 22°45' N, 158° 00' W) aboard the R/V Kilo Moana cruises KM1418 (late Summer 2014) and KM1506 (Spring 2015).

The protein-like fraction was isolated using a cation-exchange chromatography method following liquid-state acid hydrolysis. Approximately 60 mg of dry HMW UDOM or LMW SPE-DOM material was weighed into 8 ml glass vials with 5 mL of 6 N HCl, flushed with N2 gas and heated to 110°C for 20 hrs. Resulting hydrolysates were dried under N2 gas, re-dissolved in 2 mL of 0.1 N HCl, and purified using cation-exchange chromatography (Bio-Rad AG50W-X8, 200–400 mesh) following the methods of Takano et al. (2010). Individual AAs were isolated following cation-exchange chromatography using an HPLC method described in Broek et al., (2013) Broek and McCarthy (2014), and Bour et al., 2016.

Dry AA isolates were transferred to 6 mm quartz tubes with 100 uL of 60°C milliQ water and dried under vacuum via centrifugal evaporation. Closed tube combustion, graphitization, and radiocarbon analyses were conducted following the

procedures described in Bour et al., 2016 and Walker and Xu, 2019

Results & Discussion

The radiocarbon ages of the protein-like material extracted from the HMW DOM samples are generally comparable to past measurements (Loh et al., 2004), confirming that our sampling and isolation protocols can reproduce prior results. As expected, the protein-like fraction has slightly younger ages than bulk HMW material (Fig. 4.1; surface Δ-$\Delta^{14}C$ = 19 ± 5 ‰, 160 ± 40 years; 2500 m Δ-$\Delta^{14}C$ = 33 ± 3 ‰, 400 ± 40 years), however, the previously measured offsets were slightly larger (average Δ-$\Delta^{14}C$ = 90 ± 20%; 970 ± 510 years; Loh et al., 2004), likely due to the older average age of the bulk HMW DOM in that study, which was isolated by a UF system with a smaller nominal MW cutoff, resulting in a sample with lower average MW (Broek et al., 2017; Walker et al., 2011).

The protein-like fraction isolated from LMW material is novel, with no comparable values in the literature. Similar to the HMW fraction, the radiocarbon age of the LMW protein-like fraction is younger than the bulk LMW material with offsets from the bulk material that are slightly greater than the HMW offsets (Fig. 4.1; surface Δ-$\Delta^{14}C$ = 49 ± 3 ‰, 575 ± 40 years; 2500 m Δ-$\Delta^{14}C$ = 38 ± 3 ‰, 690 ± 45 years). However, in contrast to HMW isolates, the LMW protein-like material has old ages in both the surface and deep ocean (surface $\Delta^{14}C$ = -294 ± 3 ‰, 2735 ± 30 years; 2500 m $\Delta^{14}C$ = -540 ± 3 ‰, 6170 ± 30 years).

Together, these observations are consistent with the prior suggestions that the operational protein-like material represents a faster cycling DOM component (Loh et

al., 2004), not only in HMW semi-labile material, but throughout the entire DON pool. However, the novel LMW data also demonstrates that there is a very slowly cycling proteinaceous component of the DOM pool, which persists throughout the water column for millennia. These very old ages at all depths therefore raise the question of how proteinaceous material might persist on long time scales, escaping degradation even in the biologically active surface ocean.

While the implications of the very old LMW protein-like fraction are compelling, as discussed previously, these values cannot unambiguously be interpreted as representing purely proteinaceous material given the lack of molecular level specificity of the operational isolations and could be skewed by the presence of older, non-proteinaceous material. In fact, the HPLC method used to isolate the AAs analyzed for this study clearly indicates that the protein-like fraction contains a significant amount of non-AA material (Fig. 4.2). In both the HMW and LMW fractions, the chromatographic regions where AAs are expected to elute contain well separated AA peaks in the relative proportions expected from previous measurements of the AA abundance of these samples (Broek and Bour et al., 2019; Ianiri et al., unpublished?). However, outside of the AA analytical windows, there are a significant number of non-AA peaks in both MW fractions. This is particularly evident in the LMW material, where there is a large baseline increase with a total area representing more material than the sum of all eluting AAs (Fig. 4.2a). These chromatographic results likely indicate a significant contribution of non-AA C in the protein-like fraction, which could substantially impact $\Delta^{14}C$ values.

While the HPLC chromatographs provide a convincing suggestion that the protein-like fraction contains a significant amount of non-proteinaceous material, radiocarbon analysis of individual AAs provides the only direct means to investigate the purity of the protein-like fraction and verify the interpretations based of this operationally defined material. The first such measurements of the $\Delta^{14}C$ values of individual AA isolates confirm that the prior protein-like data is in error. Comparison of a relative molar abundance (Mol%) weighted radiocarbon content ($\Sigma AA\text{-}\Delta^{14}C$) of individually purified AAs from each MW fraction to the protein-like material shows that the true age of proteinaceous material is significantly younger than the operational defined material in all samples (Fig. 4.1; HMW average $\Delta\text{-}\Delta^{14}C = 95 \pm 22$ ‰, 910 ± 400 years; LMW $\Delta\text{-}\Delta^{14}C = 107 \pm 70$ ‰, 1230 ± 450 years). An alternate explanation for this result could be additional proteinaceous AAs not measured in this study (e.g. methionine, histidine, lysine, arginine), which would have depleted enough $\Delta^{14}C$ values to skew the protein-like age older. However, both the HPLC chromatograms from this study and previous Mol% measurements of the same material used in this study (Broek and Bour et al., 2019) demonstrate that those AAs are in most cases below the limit of detection, suggesting that this is highly unlikely. Overall, these millennial scale offsets in ^{14}C age between the protein-like fraction and the combined AAs clearly demonstrates that the protein-like fraction contains a significant amount of non-protein material and demonstrates that this operational fraction is not valid for interpreting the cycling rates of proteinaceous material in the ocean. However, perhaps more significant, while the ΣAA ages are younger than the operationally defined fraction, this AA pool still has a very old ages in the deep ocean

(Fig. 4.1; 2500 m; HMW ΣAA-$\Delta^{14}C$ = -222 ± 35 ‰, 2000 ± 420 ybp; LMW Δ-$\Delta^{14}C$ = -482 ± 30 ‰, 5260 ± 490 ybp).

While the summed age of all measured AAs presents a number of intriguing new implications for the cycling of proteinaceous material in the ocean, the ability to measure individual AA $\Delta^{14}C$ values provides a means to go significantly beyond the average age of proteinaceous material and investigate any differences or patterns in individual AA $\Delta^{14}C$ as evidence of variable cycling within the proteinaceous DON pool.

In fact, there is a significant amount of variability in the $\Delta^{14}C$ of individual AAs within each DOM fraction (Fig. 4.3, 4.4). As is suggested from the HMW ΣAA $\Delta^{14}C$ values, within the HMW pool all AAs in the surface ocean have modern ^{14}C ages (≥ 0‰), demonstrating that they are entirely derived from freshly produced POM. The ^{14}C content of AAs in the surface ocean pool has a narrow span of values, ranging from +20 to +124 ‰. This is consistent with expectations for freshly produced HMW protein, derived from primary productivity and POM (Druffel et al., 1992). In contrast, in the deep ocean the ^{14}C content of HMW DOM AAs has a significantly larger range of values (Fig. 4.3, 4.4; $\Delta^{14}C$ = -415 to -120 ‰; ^{14}C age of 970 to 4240 ybp). Because a number of AAs in the deep ocean HMW DOM pool are actually older than the timescale of ocean circulation, it is likely that some proportion of older AAs must also be present in the surface ocean. A simple mass balance calculation leads to $\Delta^{14}C$ values of +80 to +345 ‰ for the excess AAs in the surface ocean. This demonstrates that surface AAs contain substantially more bomb ^{14}C than

average values show (Beaupré and Druffel, 2009), suggesting that some fraction AAs in the surface HMW DOM pool were produced within the last ~60 years.

The $\Delta^{14}C$ values of individual AAs in deep sea HMW pool provide novel evidence of a direct biogeochemical linkage to the surface ocean. Specifically, the youngest AA in the deep ocean HMW DOM pool is alanine (Ala; 970 ybp; $\Delta^{14}C$ = -121 ± 12 ‰), which is significantly younger than the remainder of the AAs, as well as the bulk HMW DOM pool. Its ^{14}C age is substantially less than a single ocean mixing cycle, suggesting that a major sinking particle source is required (Smith et al., 1992), as opposed to production by heterotrophic microbial processes in situ from other DOM or being mixed into the deep Pacific with DOM carried via overturning circulation. This conclusion is consistent with the higher concentration of Ala in the deep ocean HMW DOM pool relative to other AAs (~30 Mol%; Broek and Bour et al., 2019), as well as the high D/L ratio of Ala within the deep ocean HWM DOM pool (Ala D/L = 0.7; Broek and Bour et al., 2019).

The remainder of measured AA ages in the deep ocean HMW DOM pool are significantly older than Ala (Fig. 4.3, 4.4). While some contribution from particle flux for these AAs cannot be ruled out based on average $\Delta^{14}C$ values, the older values overall suggest that even in the HMW pool other AAs have old ages due to either direct ageing of recalcitrant AA-containing material, or from deep heterotrophic or chemoautotrophic production. However, in most cases, the ^{14}C ages of AAs in the deep ocean HMW DOM pool are significantly older than DIC and therefore cannot be derived solely from chemoautotrophic production (Fig. 4.5).

Within the LMW DOM AA pool, the ^{14}C ages of individual AAs are significantly older than the HMW DOM AAs, with a wide range of values in both the surface and deep ocean. The ^{14}C ages of AAs in the surface ocean LMW DOM pool range from 260 to 2620 ybp ($\Delta^{14}C$ = -40 to -284 ‰). Glycine (Gly) and serine (Ser) stand out as significantly younger in the surface ocean than the remainder of the AAs. These younger surface ages suggest that there is a direct source of freshly produced Gly and Ser to the surface LMW DOM pool. Ser in the surface ocean LMW pool also has a high D/L ratio (D/L = 0.4; Broek and Bour et al., 2019), suggesting that the source is likely linked to microbial utilization and transformation of recently produced algal material. Although Gly does not have an enantiomer to assess the microbial influence of this fresh material, Gly is often associated with bacterial production (Dauwe et al., 1999; Calleja et al., 2013; Kaiser and Benner, 2012; Lee et al., 2000; Yamashita and Tanoue, 2003). The high relative abundance of Gly in surface ocean LMW DOM (Mol% = 20%) is also consistent with fresh bacterial production. Further, both of these observations demonstrate that rather than being a unified pool of degraded material, there is active cycling of proteinaceous LMW DOM in the surface ocean.

In the deep ocean, the ^{14}C ages of AAs in the LMW DOM pool are significantly older, with a narrower range of values (4130 to 6760 ypb; $\Delta^{14}C$ = -407 to -572 ‰) which are more similar to the bulk LMW DOM material than in the surface ocean. As with most HMW DOM AA, all AAs within the LMW DOM pool are significantly older than DIC, ruling out a major deep ocean chemoautotrophic source for any of these compounds (Fig 4.5). However, in contrast to the deep ocean

HMW DOM AA pool, there are no AAs with significantly younger ^{14}C ages which might suggest a sinking particle source.

Overall, the average ^{14}C ages of AAs in the deep ocean are much older than would be expected for this labile compound class, particularly within the LMW DON pool. The old average ages in the deep ocean have two possible mechanistic explanations. First, there are significant gradients in the concentration of DOM in the deep ocean (Hansell, 2013), and while there are likely numerous abiotic and biotic sinks for this material, the significant abundance of heterotrophic prokaryotes in the would suggest that biotic utilization and remineralization plays a role in deep ocean DOM removal (Carlson and Hansell, 2014). Therefore, it is possible that proteinaceous material with highly depleted $\Delta^{14}C$ vales is produced by heterotrophic microbes in the deep ocean using C derived from local DOM. In this case, the AAs would appear old because they were synthesized in situ from a pre-aged starting material. If true, this data would provide some of the first direct evidence for the microbial utilization of refractory DOM in the deep ocean. Alternately, recalcitrant AA containing compounds could be produced in the surface ocean and aged during ocean circulation. Although the exact mechanism for producing refractory proteinaceous material is not known, one study has shown that there is an accumulation of deaminated peptides in marine sediments (Abdullah et al., 2017). The deamination of peptides would render them resistant to the degradation by a number of microbial exoenzymes and could be a potential pathway for the preservation of proteinaceous material. This is consistent with mechanisms that have been proposed for preservation of other components of DOM pool, such as microbial

modification or direct microbial production of intrinsically stable structures (Dittmar, 2014; Jiao et al., 2010).

While surface production of refractory proteinaceous material and deep heterotrophic production are not mutually exclusive, we can use ancillary data to constrain the most likely reason for the old AAs in the deep ocean. Previous AA enantiomeric data has demonstrated a significant microbial influence on the proteinaceous DOM pool, particularly within LMW DOM (Broek and Bour et al., 2019). This is most consistent with microbial modification of peptides leading to increased recalcitrance. Further, it has been shown that there are no significant trends between $\Delta^{14}C$ and D/L ratio, demonstrating that the microbial influence on the DOM pool does not increase through time (Broek and Bour et al., 2019), ruling out constant direct microbial production during ocean circulation. Finally, despite the higher D/L ratios within the LMW pool compared to the HMW pool, there is no evidence from either radiocarbon or nitrogen stable isotopes which shows a clear connection between the two pools, suggesting that instead of LMW material being produced from the degradation of HMW material, these two fractions are largely separate pools of material, produced in the surface ocean with different cycling dynamics.

Conclusions & Implications

Overall, these results fundamentally challenge previous expectations for a relatively uniform composition of the proteinaceous DOM pool, and suggest instead that different AAs may be unique tracers for a diverse range of AA-containing compounds having equally unique reactivities and cycling dynamics. The tracer

potential for specific AAs has now been demonstrated in numerous studies (Dauwe et al., 1999; Calleja et al., 2013; Kaiser and Benner, 2008; Yamashita and Tanoue, 2003), including a recent publication of AA enantiomeric ratios using the same samples measured for this study (Broek and Bour et al., 2019). However, while these past studies and AA based indices can provide information about the degradation state of DOM and the level of microbial influence, the ^{14}C age of specific AAs can potentially provide the first direct and quantitative assessments of the recalcitrance and cycling rates of specific compounds.

More broadly, this new data suggests that our understanding of the nature and cycling of proteinaceous material in the ocean must be reevaluated. Although the absolute concentration of AAs has long been observed to decreases with depth (Kaiser and Benner, 2008; McCarthy et al. 1996), the relative molar distribution of AAs is also generally consistent throughout the water column (Broek and Bour et al., 2019; Kaiser and Benner, 2009). Together with similar ^{15}N NMR spectra from HMW isolates, this has suggested that what is typically interpreted as proteinaceous material in the ocean is largely a homogeneous and well-mixed pool. If this were the case, one would expect generally similar AA ^{14}C ages representing a well-mixed, average cycling rate. In contrast, the strong diversity of ages we see in individual AA data strongly suggest a very different paradigm. We suggest that some combination of unique molecular sources or different production pathways at different ocean depths are required to produce such ^{14}C diversity. Together with evidence for a dominant microbial source (refs), this raises the possibly that much of the AA pool in the ocean

does not trace proteinaceous material at all, but rather derives from a far more diverse collection of bacterial amino containing compounds.

While there are multiple possible explanations for the old AAs, we observe in both HMW and LMW pools, we suggest that microbial transformations of surfaced-produced algal material which render it resistant to further degradation is the most likely explanation. The older AA ages within the LMW DON pool measured in this study combined with high AA D/L ratios within this pool (Broek and Bour et al., 2019) suggest that surface microbial processes are a key factor in the long-term preservation of proteinaceous material, providing persuasive evidence for a microbial N pump, analogous to the microbial C pump (Jiao et al., 2010). Ultimately, proteinaceous material in the deep ocean is likely derived from a number of different sources including chemoautotrophic production, heterotrophic microbial production, dissolution of sinking particles, as well as vertical mixing during deep water formation. Regardless of the specific sources, this data provides a new view of the cycling dynamics of proteinaceous material in the ocean. Instead of a relatively homogenous pool of material with uniform cycling rates, this study demonstrates that proteinaceous DON in the ocean is a dynamic pool of actively cycling material with a significant heterogeneity of reactivity and cycling rates.

Overall, this data provides a new view of the cycling dynamics of an important component of marine DON. However, they also pose the question of how far they can be extrapolated to understand cycling of the entire DON pool. This data only directly provides information regarding the age and dynamics of proteinaceous or AA-containing material, and while proteinaceous material within the HMW pool should

be mostly representative of the all HMW DON based on the amide and amine dominance of this fraction (Aluwihare et al., 2005; McCarthy et al., 1997), the concentration of recoverable of AAs in LMW material is much lower, suggesting that proteinaceous compounds are a minor fraction of the LMW DON pool. More significantly, new evidence has demonstrated that the LMW DON pool is far more complex than the HMW pool and dominated by heterocyclic-N containing compounds with a very minor contribution from amide material (Broek et al, submitted). Individual extracted compounds such as AAs are commonly used to interpret the origin and cycling of the larger OM pool from which they are derived, even if (for example with lipid biomarkers) they directly represent only small fractions of total material. However, potential interpretation of LMW DON cycling based on AA ^{14}C ages depends on the assumption of approximately similar sources and cycling behavior despite having very different chemical compositions. Given the apparent heterogeneity of cycling rates of different chemical constituents of the DOM pool revealed by this and previous studies this is perhaps unlikely. While the accuracy of this assumption is not known, we suggest that it now represents one of the central questions of ocean DOM biogeochemistry. Ultimately, future work aimed at identifying specific non-proteinaceous N-containing compounds within the DON pool, specifically in the LMW pool, will be required to gain a comprehensive understanding of the cycling of DON in the ocean.

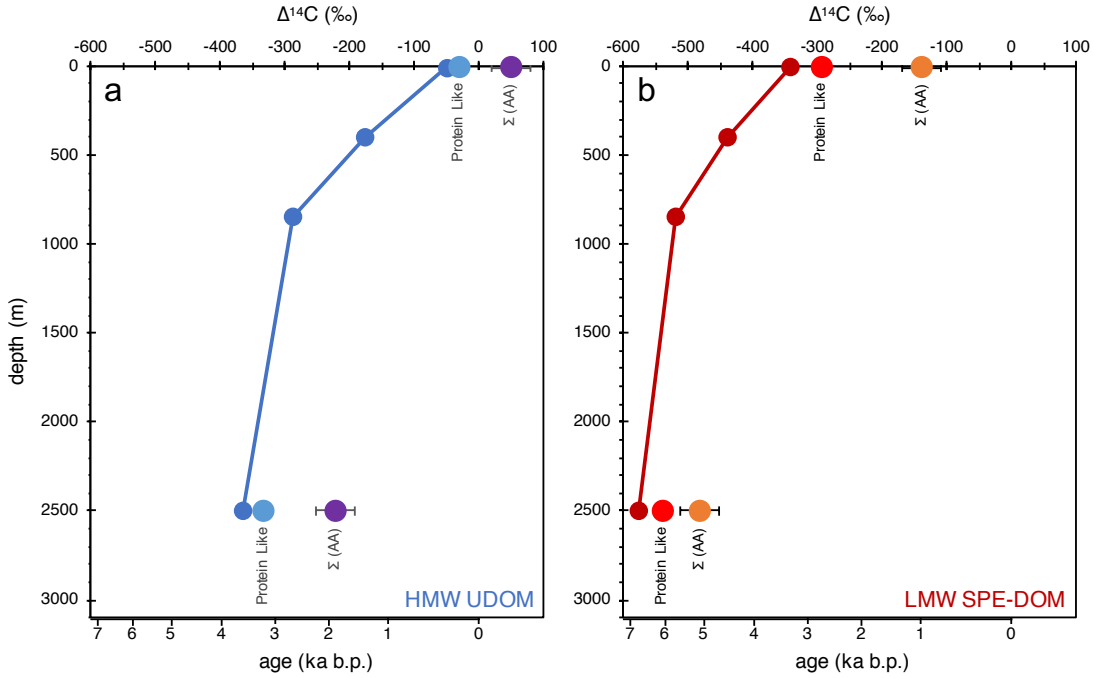

Figure 4.1 Radiocarbon content ($\Delta^{14}C$ and ^{14}C age) of bulk HMW UDOM (a; blue line), LMW SPE-DOM (b; red line), and the protein-like fraction (light blue; light red) and Mol% weighted average of AAs (ΣAA; purple; orange) isolated from each DOM size fraction. ΣAA error bars represent the propagated standard deviation of AA $\Delta^{14}C$ values.

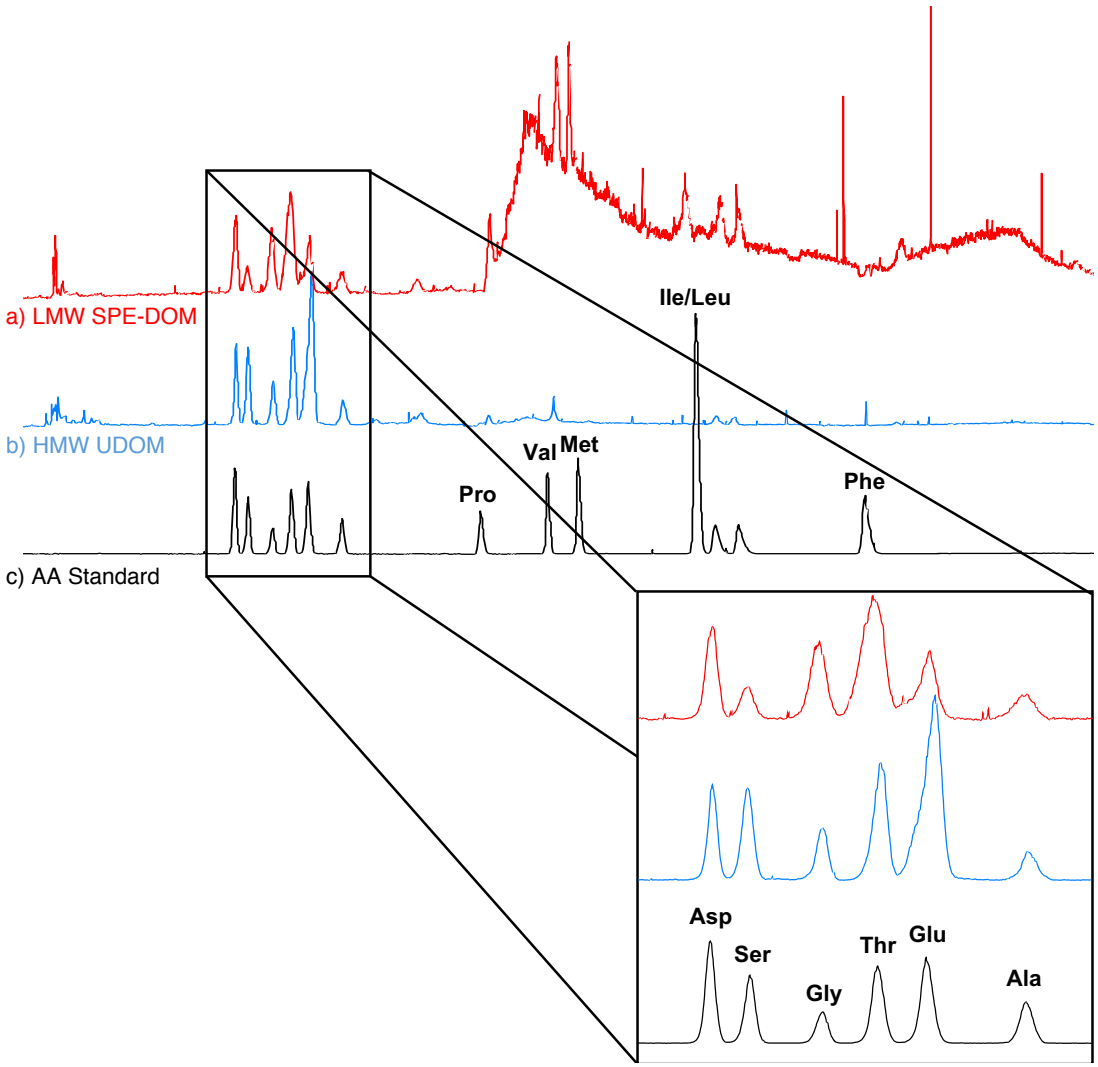

Figure 4.2 HPLC-ELSD chromatograms of LMW SPE-DOM (a), HMW UDOM (b) and an equimolar amino acid standard mixture (c).

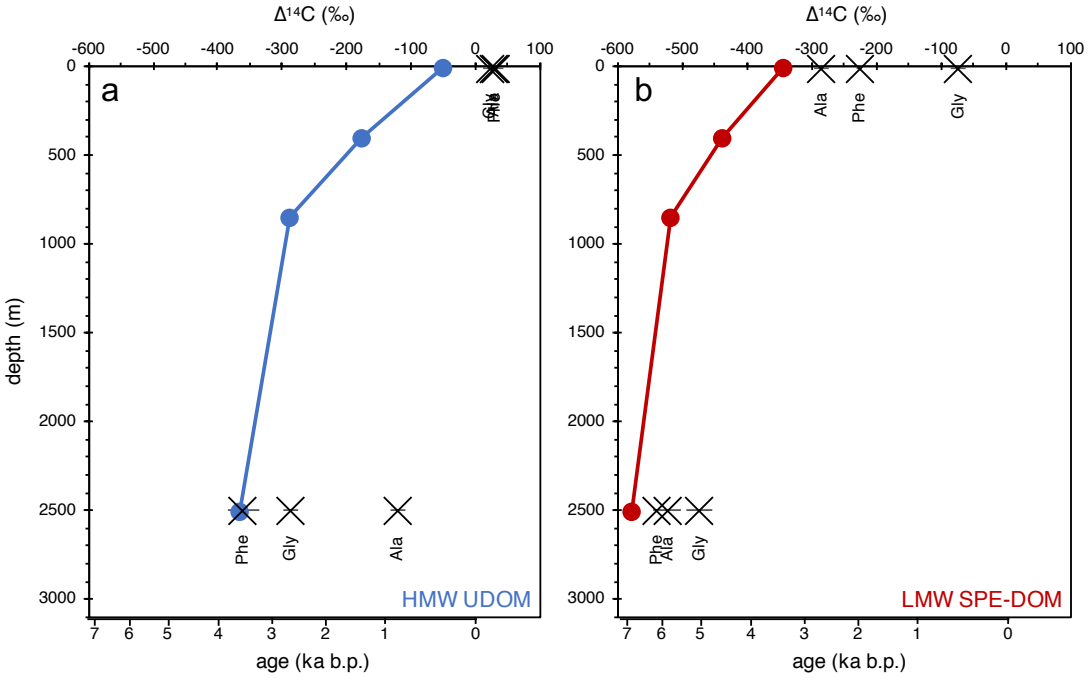

Figure 4.3 Radiocarbon content ($\Delta^{14}C$ and ^{14}C age) of bulk HMW UDOM (a; blue line), LMW SPE-DOM (b; red line), and the three AAs isolated from all 4 samples (alanine, Ala; glycine, Gly; phenylalanine, Phe). AA error bars represent the analytical uncertainty of measured $\Delta^{14}C$ values.

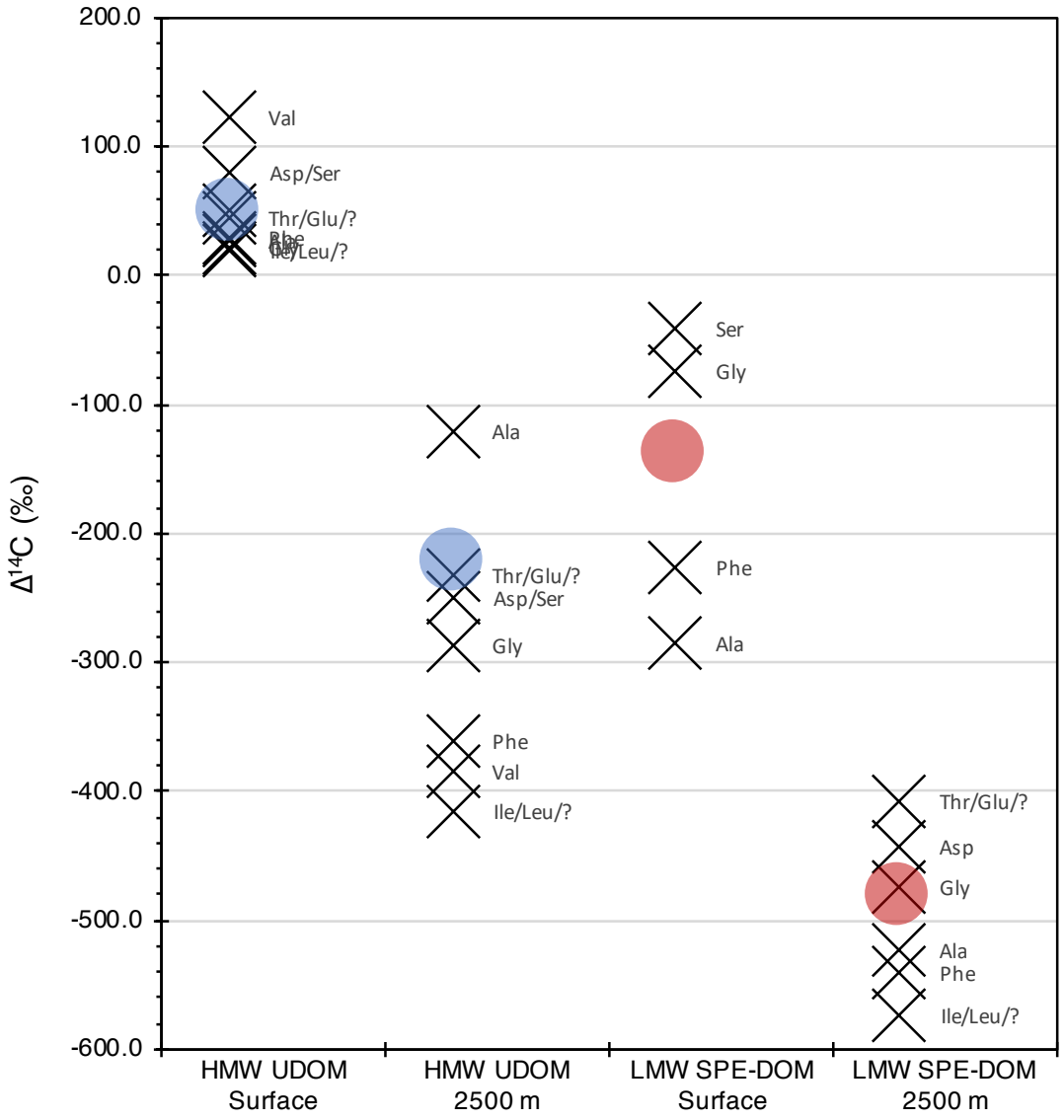

Figure 4.4 Radiocarbon content ($\Delta^{14}C$) of all AAs isolated from bulk HMW UDOM and LMW SPE-DOM from the surface and deep (2500 m) ocean. Abbreviations are as follows: alanine (Ala), aspartic acid (Asp), glycine (Gly), glutamic acid (Glu), isoleucine (Ile), leucine (Leu), phenylalanine (Phe), threonine (Thr), and valine (Val). Red and Blue circles represent the Mol% weighted average of all AAs (ΣAA).

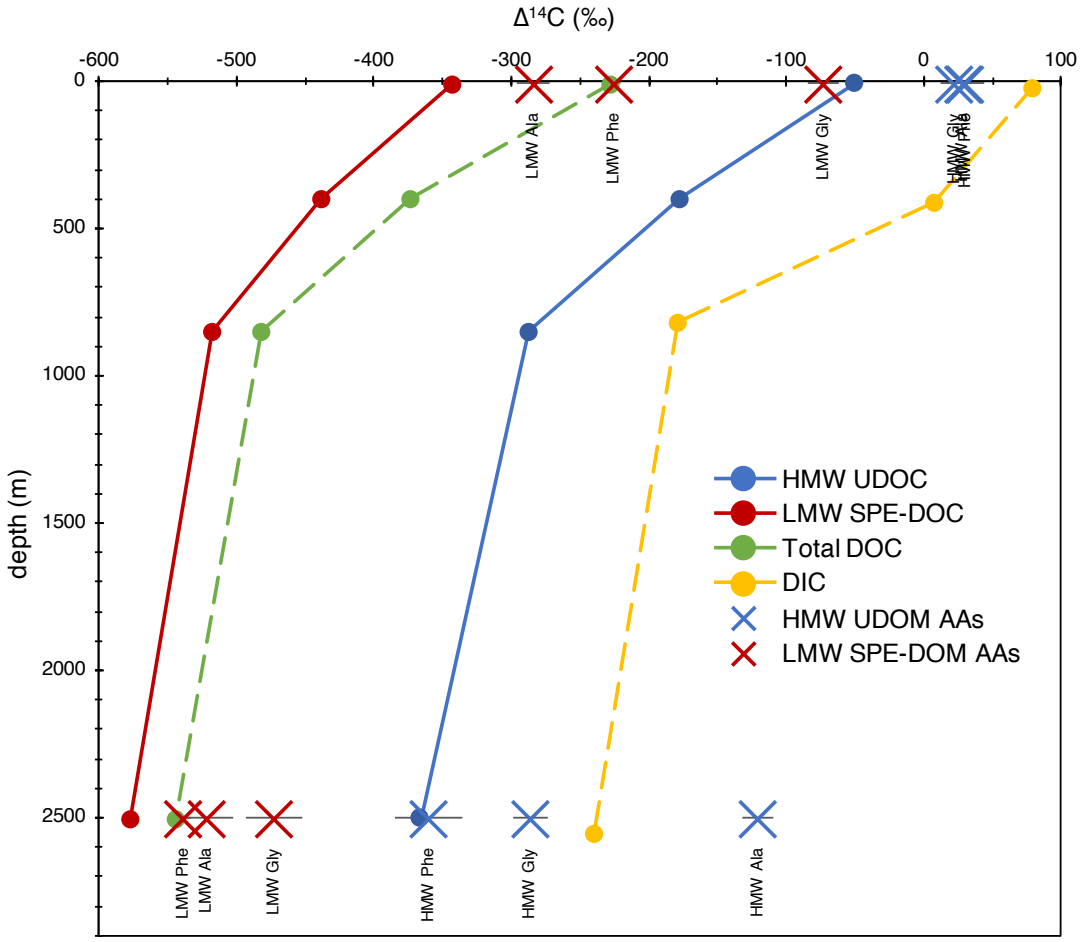

Figure 4.5 Radiocarbon content ($\Delta^{14}C$) of bulk HMW UDOM (blue), LMW SPE-DOM (red), and the three AAs (alanine, Ala; glycine, Gly; phenylalanine, Phe) isolated from all HMW (blue Xs) and LMW (red Xs) samples compared to total DOC (green) and DIC (yellow). AA error bars represent the analytical uncertainty of measured $\Delta^{14}C$ values.

Chapter 5

The dominant heterocyclic composition of marine dissolved organic nitrogen.

Abstract

Marine dissolved organic nitrogen (DON) represents one the largest global reservoirs of fixed nitrogen. However, its molecular composition and dynamics remain poorly understood. We report the first solid-state ^{15}N NMR compositional analysis and nitrogen isotopic ratio ($\delta^{15}N$) measurements of selectively isolated low and high molecular weight (LMW, HMW) DON collected from the surface to deep ocean in the subtropical North Atlantic and Pacific Oceans. HMW DON is primarily amide everywhere with elevated $\delta^{15}N$ values, consistent with prior data. In contrast, LMW DON is universally dominated by heterocyclic N with far lower $\delta^{15}N$ values, converging on constant deep ocean $\delta^{15}N$ values in both basins. Because LMW material makes up the large majority of DON, these observations require a dramatic shift in our understanding of marine DON composition. Further, these observations are inconsistent with the production of LMW material from degradation of labile HMW DON, and the different $\delta^{15}N$ values of each size fraction are likely diagnostic of their unique biochemical composition. This data indicates that a major, previously unrecognized aromatic N component dominates recalcitrant DON throughout the water column, and further suggest that HMW and LMW DON are fundamentally distinct reservoirs with independent sources and cycling.

Introduction

DON is the largest reservoir of organic nitrogen (N) in the ocean and is the most abundant form of fixed N in the surface ocean. At the same time, primary production in much of the ocean is N limited, suggesting that most DON is resistant to utilization. Therefore, refractory DON (RDON) at all depths represents a major control on ocean productivity and biogeochemical cycling of N. However, despite its importance in the global N cycle, little is known about RDON composition, sources, or cycling dynamics.

The limited understanding of RDON molecular composition is largely linked to analytical limitations imposed by low concentrations relative to salts and inorganic N. At most, ~20% of marine DON can be measured as identifiable biochemicals in bulk seawater (McCarthy and Bronk, 2008). As a result, most chemical and isotopic methods for elucidation of unknown material rely on isolation methods to concentrate and desalt dissolved organics such as ultrafiltration (UDOM; Aluwihare et al., 2005; Benner et al., 1992; 1997; McCarthy and Bronk, 2008; McCarthy et al., 1997; 1996). Compositional information from NMR suggests a dominant amide composition, most likely from polymeric amino acids and amino sugars (Aluwihare et al., 2005; McCarthy et al., 1997). These UDOM isolates have many bulk characteristics similar to total DOM (Benner et al., 1992; McCarthy and Bronk, 2008), leading to a paradigm that most DON in the ocean is dominated by amide-N. However, the relative structural simplicity and expected lability of most amide containing compound classes has posed a major conundrum for understanding the long-term persistence of RDON.

In recent years, however, it has become increasingly clear that the operationally defined HMW material isolated by ultrafiltration is dominated by the most labile portion of the standing DOM pool and represents only 5-30% of total DOM (Aluwihare and Meador, 2008). Multiple studies have demonstrated a relationship between MW, biological reactivity, and ^{14}C age, all indicating increased recalcitrance and older ^{14}C ages with decreasing size (Benner and Amon, 2015; Walker et al., 2016; 2011). Given this observation and the fact that LMW material makes up the vast majority of dissolved material (Benner and Amon, 2015), the molecular composition of LMW DON likely holds the key to understanding the persistence of RDON.

Here, for the first time, we investigate the composition and cycling of separate HMW and LMW DON fractions collected throughout the water column in the subtropical North Pacific and Atlantic Oceans. Samples were isolated using a novel approach based on molecular weight separation, combining sequential ultrafiltration and solid phase extraction (SPE) to selectively recover semi-labile HMW and refractory LMW material (Broek et al., 2017). While this approach was developed to specifically target endmembers of the DOM size-reactivity continuum, our data represents the largest fraction of the total ocean DON pool ever directly characterized.

Results & Discussion

Radiocarbon content of these fractions confirmed major differences in the average ages and cycling rates of the HMW and LMW material (Fig. 5.4), with total

LMW material on average 2700 ± 400 years older than HMW (Broek et al., 2017). This is consistent with the relative reactivity of the two fractions: with HMW material representing a faster cycling pool and LMW isolates representing refractory material with average ages encompassing multiple ocean mixing cycles. While the bulk ^{14}C ages of these DOM fractions may not exactly match the average age of the nitrogenous material, these samples nevertheless provide the first direct view of RDON composition and isotope ratios throughout the water column.

Solid-state ^{15}N cross polarization magic angle spinning (CP-MAS) NMR can identify the nitrogen functional composition of geochemical samples, representing a powerful approach to characterize complex materials where most compounds cannot be identified at the molecular level (Aluwihare et al., 2005; Cardoza et al., 2004; Knicker, 1996; Knicker et al., 1993; McCarthy et al, 1997). Similar to previous findings, HMW DON spectra at all depths are dominated by amide-N functionality (~120 ppm; Fig. 5.1), with some amine-N (~30 ppm), consistent with an almost entirely biopolymeric composition (e.g., polypeptides, N-acetal amino polysaccharides). In contrast, the LMW DON ^{15}N NMR spectra indicate a completely different composition. LMW DON samples are dominated by aromatic (heterocyclic-N) functional groups at all depths, with far more complex spectra characterized by numerous overlapping peaks in the region of ~130-170 ppm (e.g., pyrrole, indole).

Integration of deconvoluted peaks provides an estimate of the relative N functional composition of the two fractions (Fig. 5.1, 5.5). In the HMW fraction of both surface and deep DON, amide and amine-N represent essentially the entire signal (90-95 %). In contrast, aromatic heterocyclic-N comprises the large majority

(80-85%) of the LMW DON signal at all depths, with a weak shoulder indicating the presence of some amide-N. However, it is important to note that these directly integrated aromatic-N contributions are likely underestimates. Signal intensity from different functional groups in CP-MAS NMR is linked to proton density, so relative response for aromatic-N will always be lower than amide or amine-N (Smernik and Baldock, 2005). The actual proportion of aromatic nitrogenous compounds in LMW DON are likely even greater than our integrated values indicate.

Heterocyclic-N containing compounds are common and encompass a range of biomolecules including pigments as well as purines and pyrimidines (Ohkouchi and Takano, 2014). The intrinsic stability of aromatic ring structures often leads to recalcitrance, and there is abundant evidence from multiple environments for the relative stability of heterocyclic-N compounds. In the ocean, pigment degradation products (e.g., porphyrins and tetrapyrroles) are resistant to further bacterial degradation. For example, intact porphyrins have been recovered from ancient geological samples, including oil shales and Precambrian rocks (Ohkouchi and Takano, 2014). In soils, heterocyclic-N is a major refractory component and is hypothesized to play a role in the long-term stability of soil ON (Knicker, 2007, 2004). While there are also potential abiotic sources of heterocyclic-N (e.g., combustion products or hydrothermal inputs), these should be extremely minor relative to surface production. Further, the heterocyclic-N composition we observe across all depths, coupled with elevated surface LMW DON concentrations (Broek et al., 2017), requires a fresh surface source for most LMW heterocyclic material. Overall, the starkly different N compositions of old LMW DON compared with

younger HMW material strongly suggests differences in molecular structure as the central factor controlling the relative recalcitrance of marine nitrogenous material.

Different bimolecular classes have diagnostic isotopic offsets from bulk cellular material based on their metabolic pathways (Hayes, 2001; Ohkouchi and Takano, 2014): proteinaceous material is more positive and heterocyclic-N compounds are isotopically light. Large offsets between these classes are seen in fresh biomass and detrital material (Batista et al., 2014; Higgins et al., 2011; Yamaguchi et al., 2018). If HMW and LMW DON are composed of these different biochemical groups, then one would expect a characteristic offset in $\delta^{15}N$ values. Our data shows this exact pattern: at all depths in both ocean basins the $\delta^{15}N$ value of the proteinaceous HMW DON fraction is higher, with an average offset of 2.6 ± 0.7 ‰ from heterocyclic LMW DON (Fig. 5.2). This offset represents an independent confirmation of the NMR structural information.

An alternate explanation could be fractionation related to DON cycling. A prior study reported generally similar LMW versus HMW $\delta^{15}N$ offsets in oligotrophic surface waters but interpreted this as evidence that HMW DON is either progressively fractionated during hydrolysis in forming the LMW pool, or that both HMW and LMW DON are degraded with similar fractionation, albeit utilized differently (Knapp et al., 2012). However, if HMW and LMW pools were directly linked via the first mechanism, then LMW DON would necessarily be comprised of degradation products of HMW biopolymers. However, the compositional difference we observe rules out this explanation, at least for the material isolated by our approach. While heterocyclic- N can be produced from other N-containing compounds by high heat

(Knicker, 2010), there is no plausible mechanism for transformation of amide-N into heterocyclic-N at the cold temperatures and geochemically short timescales associated with ocean circulation. Similarly, the idea that degradation of diverse heterocyclic-N compounds and simple peptides would proceed with identical isotopic fractionation is extraordinarily unlikely.

The different compositions of HMW and LMW DON, coupled with concentration gradients in the upper ocean, instead suggest a surface source of both HMW (amide) and LMW (heterocyclic) DON. Incubation experiments demonstrate that marine bacteria can generate complex mixtures of refractory LMW DOC, rich in aromatic compounds (Lechtenfeld et al., 2015). While no analogous studies have yet focused on N-containing compounds, these results provide an intriguing paradigm for production of chemically distinct DON sources in the surface ocean, consistent with a microbial origin of most marine DOM (Yamaguchi et al., 2018). At the same time, there may be direct algal sources of heterocyclic-N to the refractory DON pool (Zhao et al., 2017). The pyridine signal present only in our surface LMW NMR spectra supports the idea that a more diverse range of heterocyclic-N types may cycle rapidly in the surface ocean.

The HMW and LMW DON $\delta^{15}N$ profiles and offsets between basins have implications for DON cycling. HMW DON $\delta^{15}N$ profiles in both basins are lowest in the surface, increasing with depth to maxima at 850 m (Fig. 5.2). At all depths, the Pacific has higher HMW $\delta^{15}N$ values. Together these observations are consistent with a semi-labile pool of amide-N material undergoing progressive degradation during ocean circulation (Hansell, 2013; Silfer et al., 1992). In contrast, LMW DON $\delta^{15}N$

values in both basins are identical within error (0.2 ‰) despite a 2600 ± 500 year difference in DOM ^{14}C age. This is consistent with the lack of isotopic fractionation of recalcitrant heterocyclic compounds on ocean circulation timescales.

A more direct way to evaluate the relationship between HMW and LMW DON cycling is to examine the relationship between $\delta^{15}N$ and $\Delta^{14}C$ within each fraction, as an indicator of the relative change in $\delta^{15}N$ values with progressive DOM aging (Fig. 5.3). We observe a large distribution of ^{14}C ages within each isolated fraction, as well as significant overlap between HMW and LMW isolates (Fig. 5.3). If LMW and HMW material were predominantly linked via a continuum of progressive aging and degradation with associated $\delta^{15}N$ fractionation, one would expect a generally progressive relationship between $\delta^{15}N$ values and DOM $\Delta^{14}C$. However, despite substantial overlap in ^{14}C content there is essentially no overlap in $\delta^{15}N$ values (Fig. 5.3). The two MW fractions appear as distinct groupings and within each individual MW pool the relationship between $\Delta^{14}C$ and $\delta^{15}N$ is consistent with fundamentally different cycling: HMW material shows a correlation consistent with ocean transport, while the LMW pool shows no relationship. Consistent with their very different molecular level compositions, these observations support the idea that LMW and HMW pools are not directly linked via degradation, but rather are two largely independent pools.

Conclusions & Implications

Our results point to a fundamentally new paradigm for DON composition and cycling, leading to a new explanation for the major mechanisms regulating most

DON. Our data demonstrates that the longstanding idea of marine DON as functionally simple amide-containing biochemical classes likely only applies to a small portion of the DON pool (Aluwihare et al., 2005; McCarthy and Bronk, 2008; McCarthy et al., 1997). Our results indicate a very different compositional story, showing that refractory LMW DON is dominated by ^{15}N-depleted heterocyclic-N compounds originating from surface biological production. Further, the ^{14}C ages of LMW DOM supports the recalcitrance of these compounds, suggesting a major refractory heterocyclic-N pool throughout the water column, which persists over multi-millennial timescales.

Because the UF/SPE approach used here was designed to target the endmembers of the DOM age and reactivity spectrum, this poses the question of how far these results can be extrapolated. One thing is certain: our directly recovered DON (27 ± 6% of the total pool) represents the largest proportion of ocean DON ever directly isolated for molecular characterization. Combined, the two fractions represent more than double the typical recoveries of the ultrafiltered material that was previously used to infer DON composition. In addition, both the isotopic and molecular level similarity observed for these LMW SPE isolates compared to total LMW DON strongly suggest that our LMW DON fraction is representative of most LMW DON throughout the ocean's water column. Because LMW material makes up ~90% of DON these results likely extend to much of the DON reservoir.

Together our results indicate that the dominant composition, origin, and cycling of the ocean's DON reservoir is substantially different than has been previously understood. A larger implication is that the cycling dynamics of the N-

containing fraction of DOM may depart from typical expectations for the total DOM pool (Amon and Benner, 2015; Jiao et al., 2010). While LMW DON is clearly older and more refractory than HMW DON, our data strongly suggests that LMW material does not derive from HMW DON. These data are most consistent with two largely independent pools, having very different molecular compositions and isotopic signatures. We hypothesize that refractory, heterocyclic LMW DON compounds are produced in the surface ocean concurrently with more labile amide dominated HMW material, rather than from successive reprocessing and degradation of this material. Future research into the sources and recalcitrance of heterocyclic ON, in particular those produced by algae vs. heterotrophic bacteria, may represent the most important direction to finally gain a comprehensive understanding of the ocean's DON pool.

Supplemental Information

Extended Methods and DON Recovery

The coupled ultrafiltration (UF) and solid phase extraction (SPE) approach used to collect the samples analyzed for this study was designed to target endmembers of the DOM size-age-reactivity continuum. The high molecular weight cutoff (2.5 kD) UF membranes used and high concentration factors ensure collection of the highest MW, most labile material possible, but also results in lower average recoveries than UDOM isolated at low concentration factors (Walker et al., 2011). The final combined recovery from the two-step isolation approach is ~ 30% of the total DON pool. This represents a much larger fraction of DON than was examined in prior isotope and NMR studies based on ultrafiltration. However, the larger

significance is that major fraction also appears representative at both bulk isotope and molecular level of most LMW DON (see next section).

Representativeness of LMW SPE-DOM

Detailed consideration of the chemical and isotopic properties of UDOM and SPE isolates (Broek et al., 2017) shows that the LMW results presented in this study extend beyond our directly isolated LMW material, and likely to the majority of the LMW DON in the ocean. While our LMW SPE isolates are somewhat biased towards older material with higher C/N ratios, ancillary results at both the bulk and molecular level demonstrate that the LMW SPE fraction is more representative of the LMW material permeating the ultrafiltration system than SPE of total seawater is of total DOM (Fig. 5.7). For example, the average ^{14}C age of the LMW SPE-DOM fraction is similar the that of the total LMW pool (i.e. Total DOM – HMW UDOM), with an average offset of 600 ± 450 years (45 ± 40 ‰). In contrast the HMW UDOM fraction is 3400 ± 2000 years (440 ± 80 ‰) younger than the LMW pool. Specific to DON, at both BATS and HOT the $\delta^{15}N$ of surface LMW SPE-DON is statistically indistinguishable from the LMW DON pool (Total DON – HMW UDON), whereas the $\delta^{15}N$ of HMW UDON at HOT is significantly higher than LMW DON. At the molecular level, the enantiomeric ratios of amino acids in our LMW SPE-DOM fraction is indistinguishable from previous measurements of the D/L ratio of LMW DON calculated from the difference of HMW and Total DON (Broek and Bour et al., 2019). Together these observations strongly suggest that our LMW DON is very likely to be generally representative of most LMW DON throughout the ocean's

water column, but in particular in the deep sea. Overall, the data strongly indicate that most LMW (and therefore most DON in the ocean) is far more similar to what we isolated by SPE than the HMW amide-dominated material isolated by ultrafiltration on which previous DON compositional studies are based.

These observations also highlight the ability of the selective LMW vs. HMW isolation approach to more clearly determine composition, as opposed to more common isolation methods that strive to isolate the largest possible fraction of DOM (e.g., RO/ED, SPE of total seawater). The removal of HMW DON, which we have shown to be isotopically and compositionally very different from total DON, allows direct observation of LMW DON without any confounding influence from the HMW material. Further, as mentioned in the main text, ^{15}N NMR likely actually underrepresents heterocyclic-N. Therefore, NMR of material from less selective isolations approaches (e.g., RO/ED and SPE of *total* seawater) would likely not be able to definitively identify the aromatic component because of the dominance of the amide signal.

^{15}N CP-MAS NMR Spectra and Relative Distribution of N Functionality

Integration of deconvoluted peaks compared between samples provides an overall indication of the relative differences in compositional distribution (Fig. 5.5). The HMW material signal is dominated by amide and amine functionality throughout the water column with some depth-based variability (average = 95%; surface = 98%; 2500 m = 92%). The remaining signal represents a small contribution from heterocyclic-N (average = 5%; surface = 2%; 2500 m = 8%). These functional group

distributions for HMW DOM are similar to previous measurements for UDOM (McCarthy et al., 1997; Aluwihare et al., 2005). A small contribution from heterocyclic-N in HMW DOM was also recognized in previous studies, with one suggesting that up to 15% of marine DON could be composed of this material (Aluwihare and Meador, 2008). Another estimate from a coastal ecosystem found heterocyclic-N to be as high as 25% of the total N (Maie et al., 2006). However, this study suggested that this material likely derives from soot and charring of terrestrial materials.

In contrast, the LMW fraction is dominated by heterocyclic-N functionality throughout the water column with some depth-based variability (average = 76%; surface = 80%; 2500 m = 72%). The remaining LMW signal arises from amide and amine-N (average = 25%; surface = 20%; 2500 m = 28%). However, these are almost certainly also minimum estimates. In solid state NMR the signal intensity from different functional groups in is linked to proton density, so different functional groups can give very different levels of signal response. For example, one previous study which attempted to quantify the relative signal from different functional groups in solid state NMR found that the signal from heterocyclic-N could be as low as 20% of the signal from amide-N (Smernik and Baldock, 2005). If this is considered, the actual average heterocyclic-N content could be as high as 95% in the LMW fraction, and up to 20% in HMW DON.

Comparison of surface and deep HMW DON spectra show a slight decrease in the relative proportion of primary amines in the deep ocean (i.e., increase in amide/primary amine ratio), suggesting either selective removal of labile amine

containing compounds or the modification of biomolecules resulting in conversion of amine to amide N. There is a larger proportion of aromatic-N in surface waters due to the presence of a significant pyridine component (~ 10% of the total signal) which appears to be entirely absent in the deep ocean. This potentially represents a labile LMW heterocyclic component which is produced in the surface and is degraded on timescales much less than global ocean mixing. Candidate pyridine containing biochemical classes expected to be relatively labile include nucleic acids, vitamins, and metabolites (Ohkouchi and Takano, 2015).

Together, these observations suggest that there are likely more than two pools of functionally distinct DON in the ocean. Within the HMW biopolymeric pool there is likely both semi-labile proteinaceous material as well as a more refractory pool dominated by modified biopolymers which are more resistant to enzymatic degradation. Within the LMW heterocyclic pool there is likely both very refractory material which persists on timescales greater than ocean circulation with a generally conservative distribution throughout the water column and a separate labile heterocyclic component which is produced and rapidly consumed or degraded in the surface ocean.

$\delta^{15}N$ of Proteinaceous and Heterocyclic Nitrogen

Different bimolecular classes have diagnostic isotopic offsets from bulk cellular material based on their metabolic pathways (Hays, 2001). Amino acids and detrital proteinaceous material are universally elevated in ^{15}N relative to bulk cellular N, as observed both in cultures and in multiple ocean ON pools including plankton

tows, sinking particles, and HMW DON (Yamaguchi et al., 2018; Batista et al., 2014). In contrast, available data for biological aromatic N compounds suggests these are universally strongly *depleted* in ^{15}N compared to bulk cellular N. For example, multiple studies have shown that the $\delta^{15}N$ of chloropigments in both algae and bacteria are 5-7 ‰ lower than the $\delta^{15}N$ of total cellular N in culture (Higgins et al., 2011; Sachs et al., 1999). Finally, similar offsets are also observed in detrital material, with pigments and unsaturated N degradation products substantially depleted in ^{15}N relative to bulk sedimentary ON (reviewed in Oukouchi and Takano, 2015).

Surface Cycling and Isotopic Fractionation of DON

As noted in the text, a previous study demonstrated similar, but in fact somewhat smaller, offsets between the $\delta^{15}N$ of HMW and LMW DON in oligotrophic surface waters (where DON $\delta^{15}N$ can be measured directly in the absence of DIN (Knapp et al., 2012). In the absence of structural information, these authors proposed two stead state model cases, based on different hypothesized pathways and fractionation factors for production, degradation, and uptake of LMW DON, tuned to mathematically reproduce the $\delta^{15}N$ offsets observed. All scenarios, however, assume that both LMW and HMW DON pools are composed of amide material.

One scenario is that LMW DON would could come primarily from the degradation of HMW DON with attendant strong isotope fractionation. The fractionation factors required for degradation of HMW DON would be similar to those measured for peptides (5-6 ‰). This match, coupled with the fact that proteinaceous material must by definition be hydrolyzed to smaller (LMW) units

before uptake and utilization, as well as previous literature on size-composition-reactivity trends in the ocean (Benner and Amon, 2015), might generally make this the expected scenario.

A second model scenario posits that LMW DON results from direct breakdown of POM, again assuming it is amide and so also with a subsequent strong isotope effect associated with its remineralization, however with the addition of selective re-uptake of LMW DON by primary producers. In order to reproduce the observed offset between HMW and LMW DON $\delta^{15}N$ values, an addition pathway must also be added for the re-uptake of LMW DON by primary producers, having a much lower fractionation value. This model scenario also assumes that since LMW is also amide, the fractionation associated with remineralization of LMW DON is essentially identical to that for HMW material and peptides (~5 to 6 ‰).

However, the fundamental structural difference between HMW and LMW material we report rules out both these explanations. As noted in the text, there is no reasonable mechanism by which HMW peptides could be transformed into LMW heterocyclic-N compounds. Further, recent molecular level isotope data clearly shows that HMW proteinaceous material in the central Pacific has individual amino acid isotope patterns inconsistent with this scenario for producing elevated $\delta^{15}N$ values of HMW DON (Yamaguchi et al., 2018). Instead the amide material which NMR shows as dominating HMW DON appears to instead to be directly produced by bacteria. Further, molecular evidence for nitrate source at the base of the deep chlorophyll maximum further suggests in fact elevated $\delta^{15}N$ values in HMW DON are due to nitrate source values, not fractionation with degradation.

Again, the compositional differences we report, as well as the lack of any isotopic offset in our LMW DON data with remineralization between ocean basins, make this also seems implausible for the fractions we have isolated. First, it is highly unlikely that the remineralization of LMW heterocyclic-N compounds would have identical, or even similar fractionation, as peptide hydrolysis. $\delta^{15}N$ fractionation during protein degradation is based on selective cleavage of C-N bonds, as large biopolymers are progressively cleaved into smaller units and then monomers (Silfer et al., 1992). It is not associated with the uptake of the LMW products into biota (an expectation in fact also implicitly included in both steady state model versions). Therefore, given the dominant heterocyclic composition of LMW material, a similar large fractionation to peptide hydrolysis would not be expected, as selective cleavage of aromatic N bonds would seem highly unlikely. Instead the LMW unsaturated N monomers would be far more likely be taken up directly, with little or no attendant ^{15}N fractionation expected. This expectation is exactly what is observed in the lack of any $\delta^{15}N$ change with slow degradation of the LMW DON between ocean basins.

Rapid Surface Cycling of LMW DON

Recent data, as well as our surface LMW ^{15}N NMR spectra, suggest that surface ocean sources and cycling of LMW DON in the upper most biologically active surface layer may also be more complex, and could also include more diverse major compound types, than is currently understood. For example, Knapp et al. (2018) recently showed that DON $\delta^{15}N$ values are strongly linked to chlorophyll, oxygen, and DON concentrations in shallow oligotrophic ocean surface waters (> 50

m only), consistent with either direct algal sources or with unsaturated N sources from tightly coupled microbial production. Heterocyclic ON with characteristically of lower $\delta^{15}N$ values may also account for these correlations. As noted above, our NMR spectra of only surface LMW DON samples show a significant contribution of pyridine-N in both ocean basins, resonance which is absent in lower depth samples, suggestive of rapid cycling. While pyridines are common moieties, this potentially represents greater importance of labile biomolecules such as metabolites and vitamins that would likely have low $\delta^{15}N$ values. Finally, recent reports of pigment derived N in the deep sea also suggest possible greater importance for surface produced, algal unsaturated N compounds (Zhao et al., 2017).

Relationship between $\Delta^{14}C$ and $\delta^{15}N$ in HMW and LMW DOM

While as noted in the text there is no overall relationship between all ^{14}C and ^{15}N data across MW fractions (Fig. 5.3), there are strong relationships within *only* the HMW fraction (Fig. 5.6). $\delta^{15}N$ and $\Delta^{14}C$ regressions within the semi-labile HMW DON fraction have significant negative slopes within both basins ($R^2 = 0.32$, $t = 2.6$, $df = 14$, $p = 0.01$), indicating a small increase in $\delta^{15}N$ with increasing age (decreasing $\Delta^{14}C$). This is consistent with offsets expected for progressive slow hydrolysis of proteinaceous material, as discussed in the main text.

In contrast, there is no significant relationship ($R^2 = 0.09$, $t = 1.1$, $df = 13$, $p = 0.15$) between $\delta^{15}N$ and $\Delta^{14}C$ within refractory LMW DOM between ocean basins, demonstrating that average DOM age is not a predictor of the $\delta^{15}N$ value in refractory DON cycling (Fig. 5.6a). The lack of relationship between $\delta^{15}N$ and $\Delta^{14}C$ in the

refractory LMW DON, together with similarity of deep ocean values, suggest that there is either very little alteration of the LMW material during overturning ocean circulation, or that LMW DON degradation is not associated with ^{15}N fractionation. Nitrogen isotopic fractionation during molecular degradation is strongly dependent on both chemical composition and specific mechanism, related to specific N bond breakage (Ohkouchi and Takano, 2014). For example, as noted above proteins have clearly demonstrated fractionation related to amide bond hydrolysis, but amino sugars may have none, since the hydrolysis of these compounds does not involve N bond breakage (Yamaguchi et al., 2018). While we are not aware of data specifically for fractionation of heterocyclic DON compounds during environmental degradation, given the expectation of LMW is not composed of biopolymers, as noted above a lack of any fractionation is plausible and in fact likely what would be expected.

Separated by location, however, the $\delta^{15}N$ and $\Delta^{14}C$ correlations of the LMW refractory fraction have small *opposite* slopes in each basin (Fig. 5.6b), suggesting that slightly different surface-derived $\delta^{15}N$ LMW values from each basin must converge on an equivalent value in the oldest samples. The opposite slopes combined with the remarkable isotopic homogeneity of deep ocean LMW DON matches expectations based on a measured ^{14}C age encompassing multiple meridional overturning circulation cycles and likely represents a global averaging of the different source $\delta^{15}N$ signals via physical mixing.

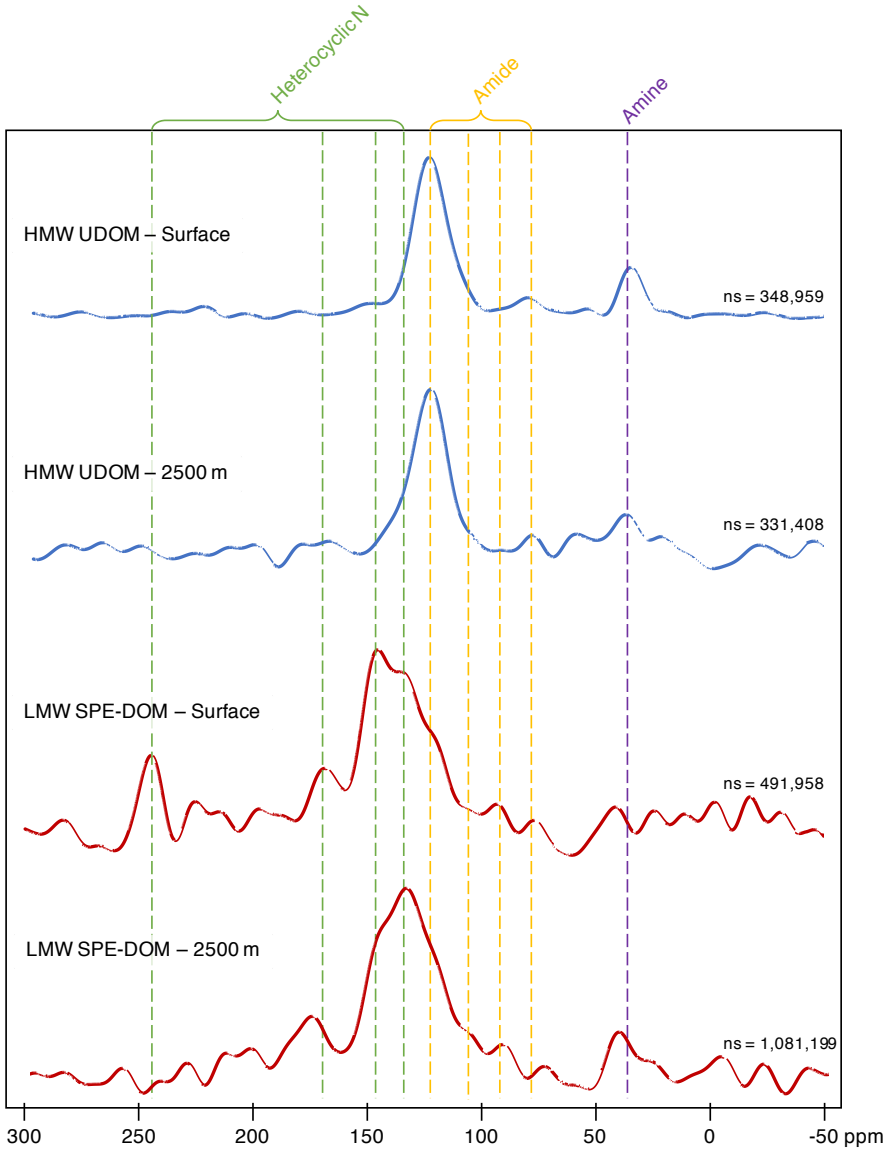

Figure 5.1 ^{15}N CPMAS NMR Spectra of HMW and LMW DON fractions from surface and deep ocean (2500 m) waters collected in the North Central Pacific. Peak centers are marked with dashed lines at chemical shifts of 240, 170, 145, 130 (pyridine, indoles, pyrroles; green), 120, 105, 90, 70 (amides; yellow), and 35 (amine; purple) ppm. The HMW spectra are dominated by signal from amide and amine N representing on average 95% of the total signal. In contrast LMW spectra are dominated by signal from various forms of heterocyclic-N which make up an average of 76% of the total signal.

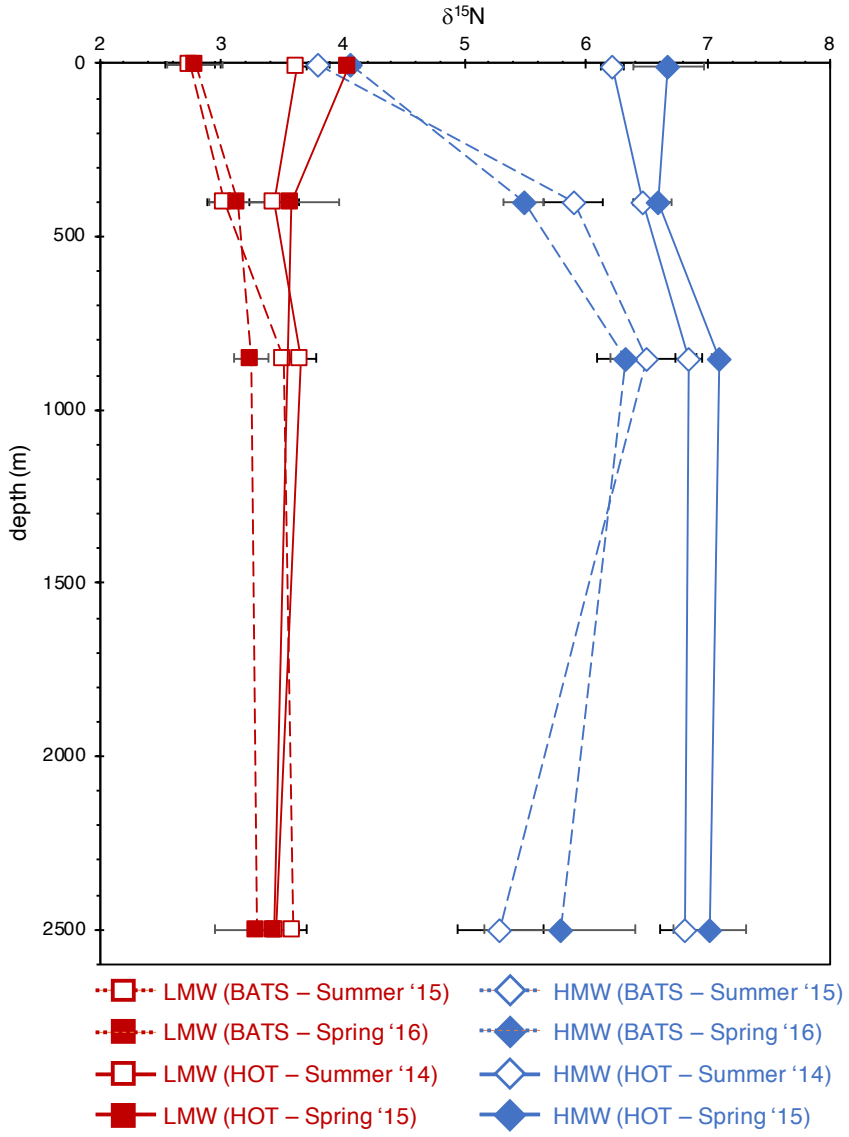

Figure 5.2 $\delta^{15}N$ depth profiles of HMW UDOM (blue diamonds) and LMW SPE-DOM (red squares) DON collected in the N. Pacific (HOT; solid lines) and N. Atlantic (BATS; dotted lines) between the Summer of 2014 and the Spring of 2016. Open symbols represent samples collected in the summer, filled symbols represent samples collected in the spring. Sampling depths are surface, 400 m, 850 m, and 2500 m. Error bars represent the standard deviation of n=3 $\delta^{15}N$ measurements of each sample and range from 0.01 to 0.5 ‰. Within each basin, the $\delta^{15}N$ of HMW UDON is always higher than that of LMW SPE-DON. The $\delta^{15}N$ offset between HMW and LMW DON collected from the same water is statistically significant in all cases, with an average offset between fractions of 2.6 ± 0.7 ‰.

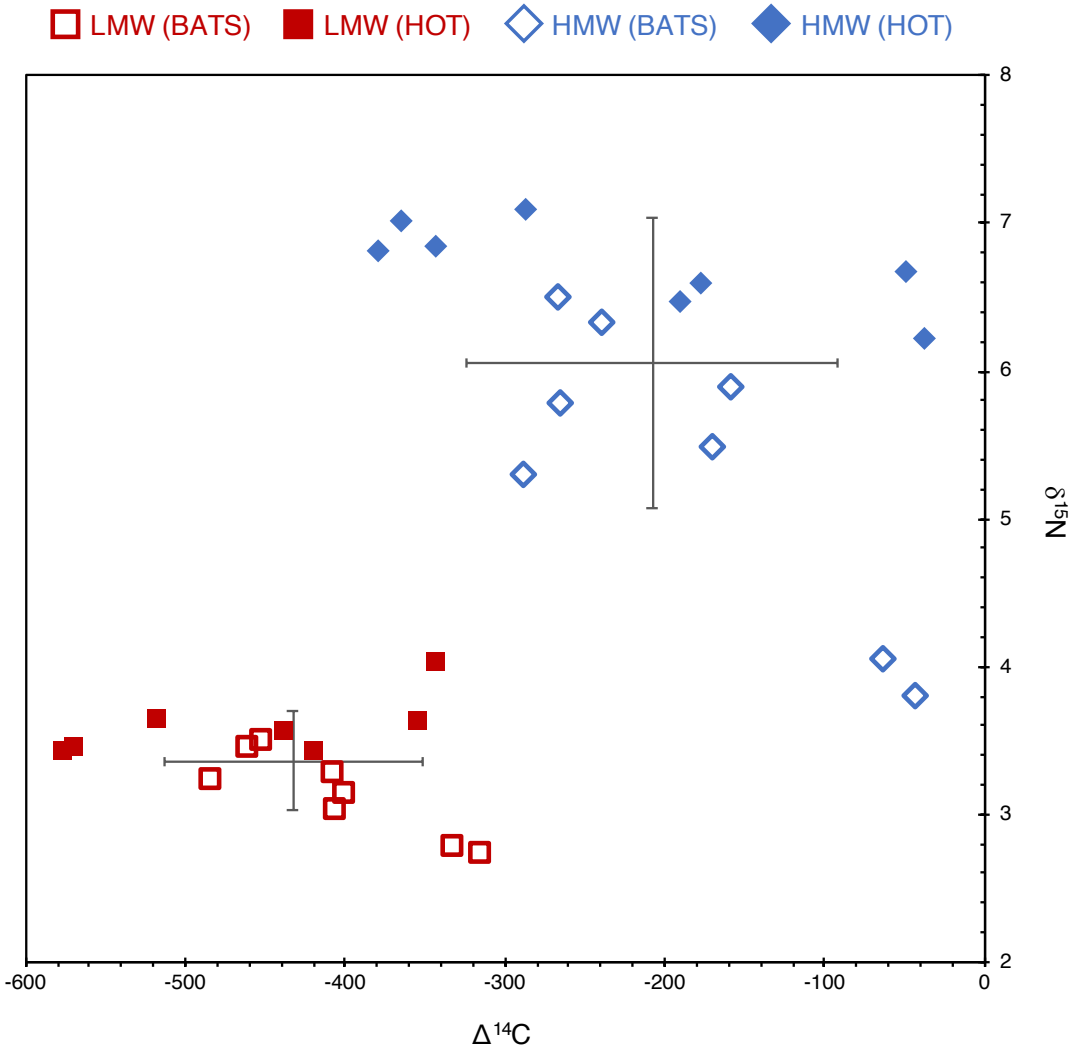

Figure 5.3 $\delta^{15}N$ and $\Delta^{14}C$ values of HMW and LMW DOM fractions. Blue diamonds represent HMW UDOM collected in the North Central Pacific (HOT; filled symbols) and North Central Atlantic (BATS; open symbols). Red squares represent HMW UDOM collected in the North Central Pacific (HOT; filled symbols) and North Central Atlantic (BATS; open symbols). Error bars represent 1 SD of the average $\delta^{15}N$ and $\Delta^{14}C$ values of each fraction. The average $\delta^{15}N$ of HMW DON is significantly different (t-test, $t = 10.1$, $df = 29$, $p < 0.001$) than that of LMW DON and the average $\Delta^{14}C$ of HMW DOC is significantly different (t-test, $t = 6.2$, $df = 29$, $p<0.001$) than that of LMW DOC demonstrating that the two fractions likely represent separate pools without a clear linkage.

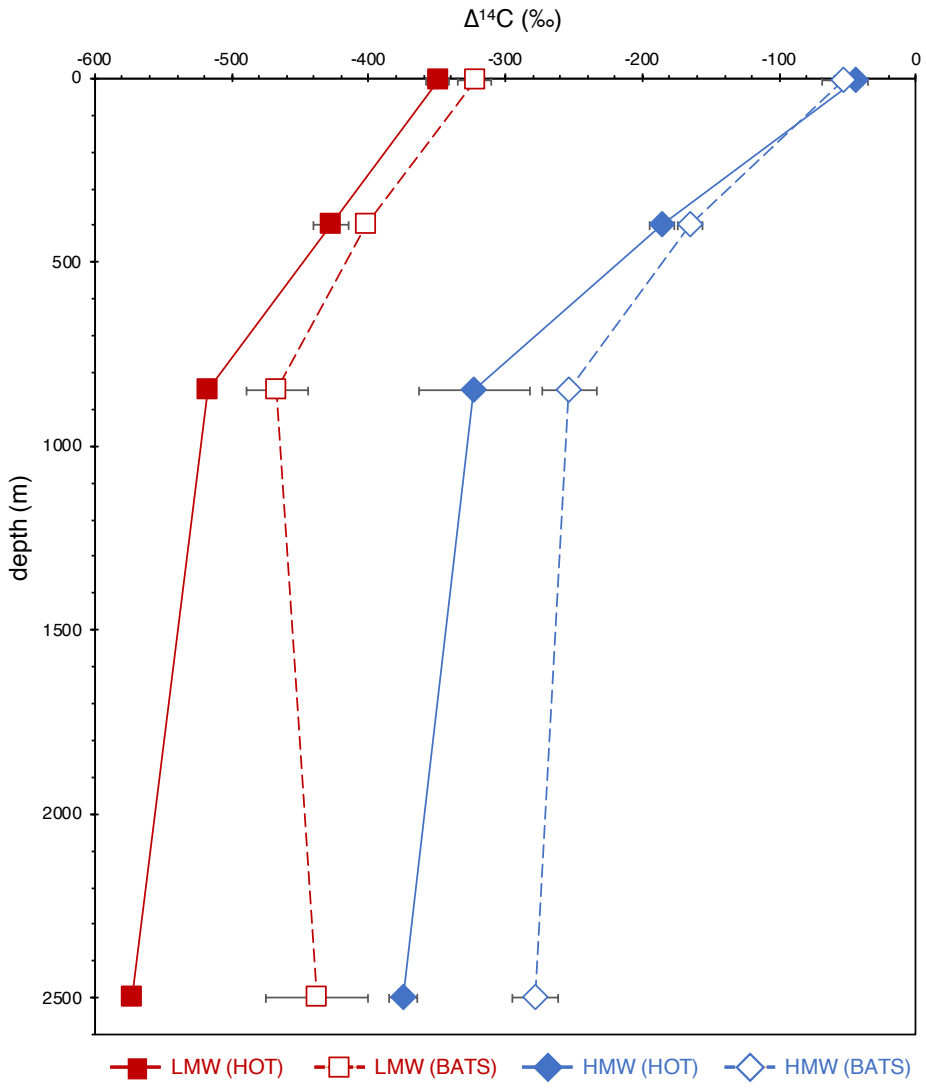

Figure 5.4 Depth profiles of $\Delta^{14}C$ of HMW and LMW DOM isolates. Blue diamonds represent HMW UDOM collected in the North Central Pacific (HOT; filled symbols; solid line) and North Central Atlantic (BATS; open symbols; dashed line). Red squares represent HMW UDOM collected in the North Central Pacific (HOT; filled symbols; solid line) and North Central Atlantic (BATS; open symbols; dashed line). Each point represents the average value of samples collected on 2 separate cruises in Summer and Spring, error bars are 1 SD and represent the propagated uncertainty of measurement error and averaging of the two seasons. In all cases, LMW DOC is significantly ($p<0.01$) depleted in ^{14}C relative to HMW DOC. At 850 m and 2500 m there are significant ($p<0.01$) offsets between basins within each fraction with more depleted values in the North Central Pacific compared to the North Central Atlantic, consistent with ageing of DOM during deep ocean circulation.

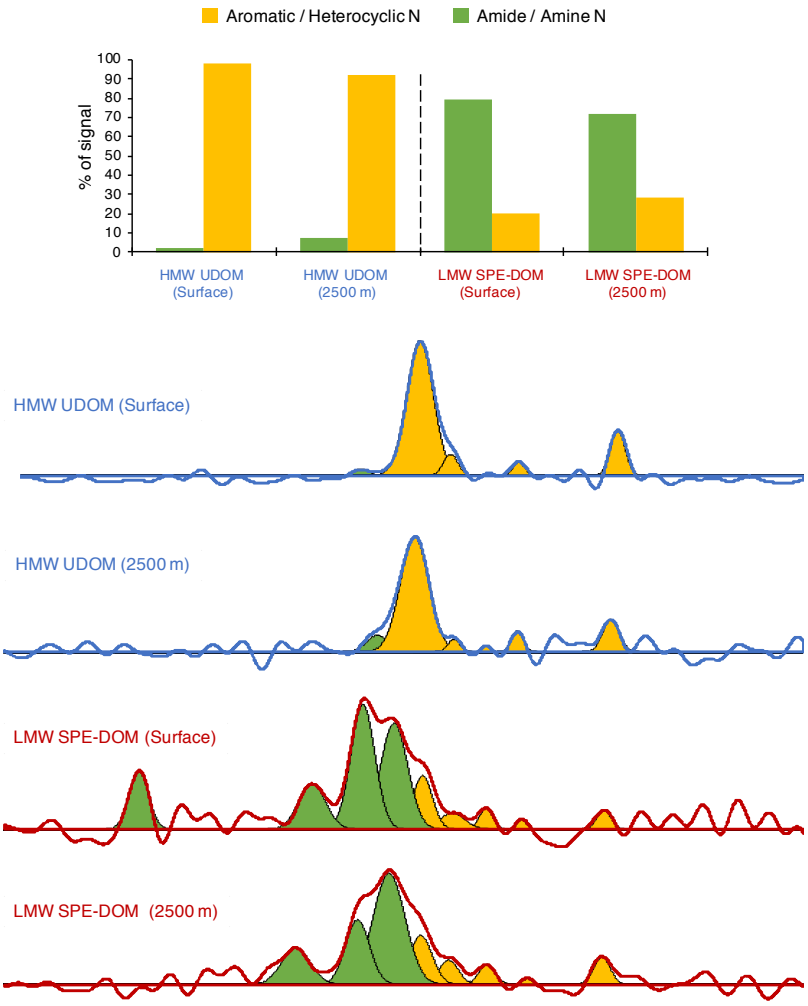

Figure 5.5 Deconvolution and Integration of ^{15}N NMR Spectra. Spectra were deconvoluted by assigning peak centers at chemical shifts of 240 (pyridine), 170, 145, 130 (indoles and pyrroles), 120, 105, 90, 70 (amides), and 35 (amine) ppm. Peaks centers were chosen based on clear maxima and shoulders within individual spectra, consistent with expected chemical shifts and in agreement between spectra. Yellow peak shading and bars represent heterocyclic functional groups. Green shading and bars represent amide and amine functional groups. The HMW material is dominated by amide and amine functionality throughout the water column with some depth-based variability (average = 95%; surface = 98%; 2500 m = 92%). The remaining signal represents a small contribution from heterocyclic-N (average = 5%; surface = 2%; 2500 m = 8%). In contrast, the LMW fraction is dominated by heterocyclic-N functionality throughout the water column with some depth-based variability (average = 76%; surface = 80%; 2500 m = 72%). The remaining LMW signal arises from amide and amine-N (average = 25%; surface = 20%; 2500 m = 28%).

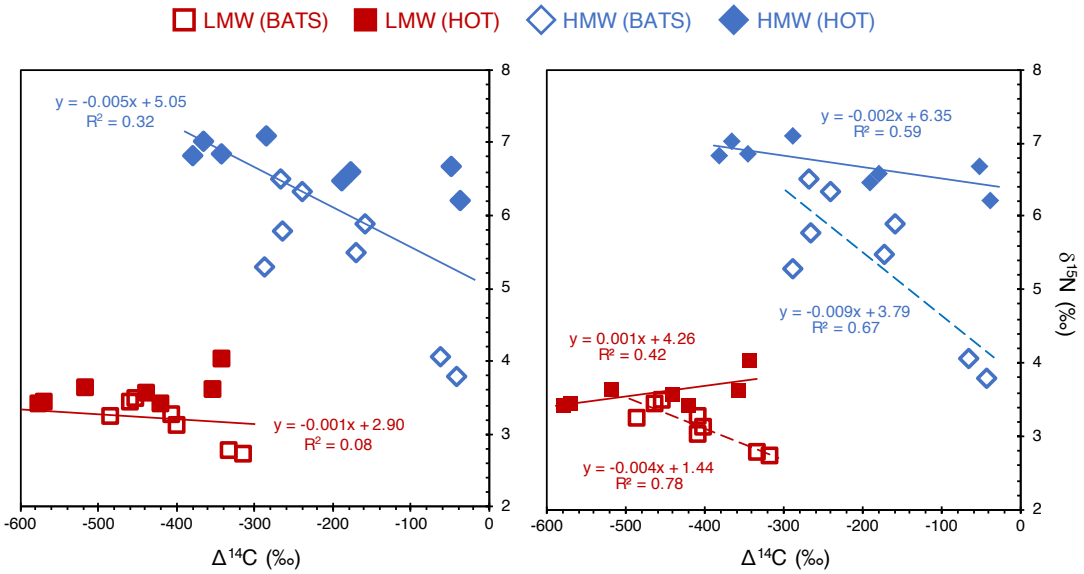

Figure 5.6 Regressions of $\Delta^{14}C$ and $\delta^{15}N$. Blue diamonds represent HMW UDOM collected in the North Central Pacific (HOT; filled symbols; solid line) and North Central Atlantic (BATS; open symbols; dashed line). Red squares represent HMW UDOM collected in the North Central Pacific (HOT; filled symbols; solid line) and North Central Atlantic (BATS; open symbols; dashed line). Panel A displays a linear regression of all data points in each fraction. There is a strong relationship ($R^2 = 0.32$, $t = 2.6$, $df = 14$, $p = 0.01$) between $\delta^{15}N$ and $\Delta^{14}C$ within the HMW DON fraction with a negative slope indicating an increase in $\delta^{15}N$ with increasing age (decreasing $\Delta^{14}C$). In contrast, there is no significant relationship ($R^2 = 0.09$, $t = 1.1$, $df = 13$, $p = 0.15$) between $\delta^{15}N$ and $\Delta^{14}C$ within refractory LMW, demonstrating that average age is not a key predictor of the $\delta^{15}N$ value in refractory DON. Panel B displays separate linear regressions for each basin. Regressions in the HMW fraction show similar trends in both basins with negative slopes indicating an increase in $\delta^{15}N$ with age. Regressions of the LMW fraction have *opposite* slopes in each basin, showing that slightly different surface-derived $\delta^{15}N$ values from each basin converge on an equivalent value in the oldest samples, potentially representing a global averaging of different source $\delta^{15}N$ signals via physical mixing of refractory material.

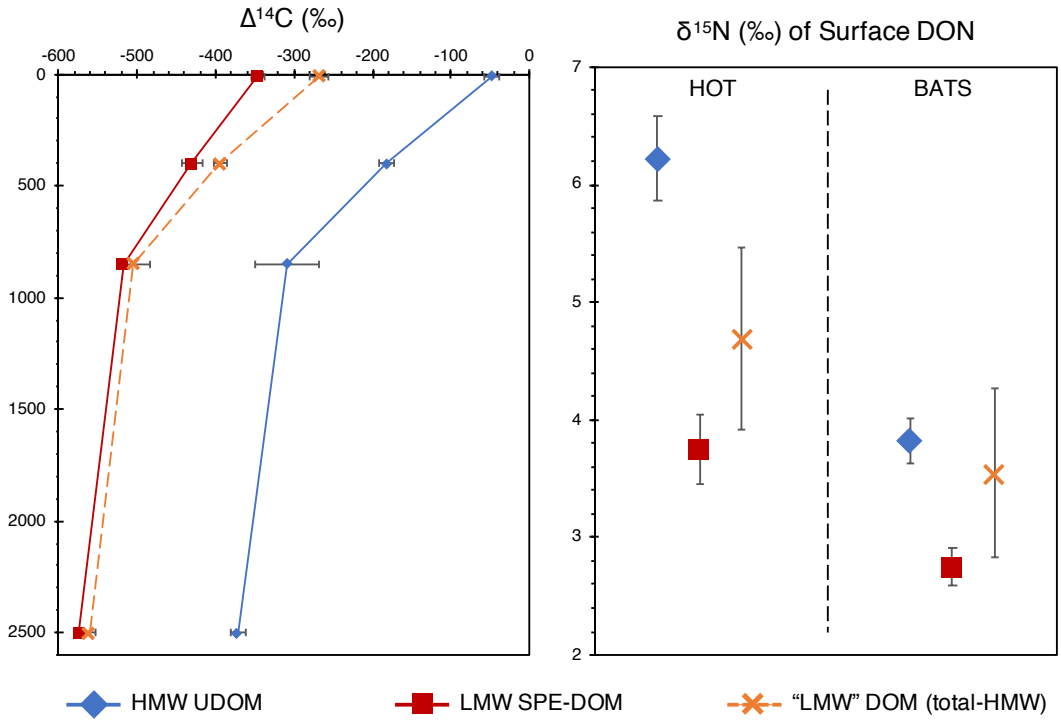

Figure 5.7 Comparison of "LMW" (Total minus HMW) properties with LMW SPE-DOM and UDOM isolates. Left panel; The average $\Delta^{14}C$ of the LMW SPE-DOM fraction is similar to that of the total LMW pool (i.e. Total DOM – HMW UDOM), with an average offset of 45 ± 40 ‰ (600 ± 450 years older). In contrast the HMW UDOM fraction is offset by 440 ± 80 ‰ from the LMW pool (3400 ± 2000 years younger). Right panel; at both BATS and HOT the $\delta^{15}N$ of surface LMW SPE-DON is statistically indistinguishable from the LMW DON pool (Total DON – HMW UDON), whereas the $\delta^{15}N$ of HMW UDON at HOT is significantly higher than LMW DON. Together these data demonstrate that LMW material recovered by SPE is generally representative of the UF permeate from which it was isolated.

Appendix I

Evidence for the Representativeness of Solid Phase Extracted LMW DOM: Comparison of LMW SPE-DOM and LMW DOM (i.e., Total DOM – HMW UDOM)

An important aspect of the sample set discussed in this dissertation is the representativeness of the LMW SPE-DOM fraction relative to the total pool of LMW DOM which permeates the ultrafiltration system. Because SPE was not able to retain the entire LMW pool (average extraction efficiency = 33 ± 6% of LMW DOC), in order to extrapolate the information gained from analyzing the LMW SPE-DOM fraction it is necessary to consider the properties of LMW SPE-DOM in comparison all LMW DOM. This can be accomplished by comparing the LMW SPE-DOM fraction to either the calculated LMW DOM values (i.e., mass weighted subtraction of the HMW UDOM fraction from the total DOM pool) or the non-retained material (i.e., Total DOM minus both the HMW UDOM and LMW SPE-DOM fractions). A comparison of LMW SPE-DOM to the calculated LMW DOM properties allows a direct way to determine the representativeness of the SPE extractable LMW material, whereas comparing properties of the non-retained DOM to the LMW SPE-DOM fraction demonstrates differences between the SPE extractable and non-extractable material. In order to calculate both the LMW DOM and non-retained DOM properties, it is necessary to be able to measure the desired property in the total DOM pool. In our data, these values were only measured for a few parameters such as $\Delta^{14}C$ and DOC concentration. However, a number of other studies have investigated the properties of the LMW pool using unique methods not available to us (refs: Koprivnjak 2009, Knapp 2012, Kaiser and Benner 2008?). The data presented in

these studies allowed us to make direct comparisons of functional group distribution (^{13}C NMR), AA enantiomeric ratios, and DON δ^{15}N. The results of 5 different comparisons are presented below.

Radiocarbon (Δ^{14}C) Profiles

The Δ^{14}C values of our LMW SPE-DOM isolates are similar to the calculated value of the LMW DOM pool (Appendix Fig. 1.1). In the surface ocean, the values are offset by an average of approximately 100 ‰, demonstrating that SPE does discriminate against some fraction of younger LMW material. However, in the deep ocean of both basins (≥ 850 m), the values are statistically indistinguishable (p-values ≥ 0.6).

Deep Ocean Basin Offsets – [DOC] & Δ^{14}C

The [DOC] and Δ^{14}C offsets in deep ocean waters of the North Central Atlantic and North Pacific Subtropical Gyre are statistically indistinguishable for both the LMW SPE-DOC fraction and the non-retained DOC material (Fig. 2.6; [DOC] p = 0.98; Δ^{14}C p = 0.8). As discussed in Chapter 2, this suggests that the utilization of the SPE extractable LMW DOC is the same as the non-retained LMW material, demonstrating that these two pools have similar reactivity, and are therefore likely composed of similar material.

Functional Composition (^{13}C NMR)

As discussed in Chapter 2, two studies have used the difference in the solid-

state ^{13}C NMR spectra of different samples to investigate the composition of specific components of the marine DOC pool (refs; Hertkorn 2006, Koprivnjak 2009). Koprivnjak and co-authors subtracted an averaged spectrum ^{13}C NMR of UF material (representing HMW DOC) from an averaged spectrum of material isolated by RO/ED (non-selective recovery; ≥ 75% of total DOC; generally representative of the total DOC pool) in order to investigate the functional composition of the LMW DOC pool. This calculated spectrum is remarkably similar to that of our LMW SPE-DOM fraction (Appendix Fig. 1.2), demonstrating that the functional group distribution of LMW SPE-DOC is representative of the total LMW DOC pool.

DON Stable Isotope Ratios ($\delta^{15}N$)

In addition to the apparent representativeness of DOC detailed above, there is isotopic evidence that this extends to the N-containing fraction of DOM. The $\delta^{15}N$ values of LMW DON calculated by subtracting measurements of HMW UDOM collected for this study from total DON measured by Knapp et al., (2011) shows that the N isotopic ratios of LMW SPE-DOM are similar to that of the total LMW DON pool, especially in the Pacific basin where the values are equivalent within error (Appendix Fig. 1.3). Because of analytical challenges with measuring the $\delta^{15}N$ of DON, it is currently only possible in the oligotrophic surface ocean where inorganic N concentrations are negligible, therefore this comparison is only possible for the surface LMW SPE-DOM samples. If the comparisons between LMW SPE-DOC and LMW DOC described above are similar to the behavior of the DON pool, it would be expected that the largest deviations would be seen in the surface ocean where SPE is

more discriminative. Therefore, it is likely that LMW SPE-DOM would be more representative of the total LMW DON pool in the deep ocean.

Amino Acid Enantiomeric Ratios

The representativeness of our LMW SPE-DOM fraction is also evident at the molecular level. The D/L enantiomeric ratios of LMW SPE-DOM and LMW DOM values calculated by subtracting measurements of HMW DOM from total DOM from Kaiser and Benner (2008) are similar, although only statistically indistinguishable (p-values ≥ 0.1) for Serine and Glutamic Acid (Appendix Fig. 1.4).

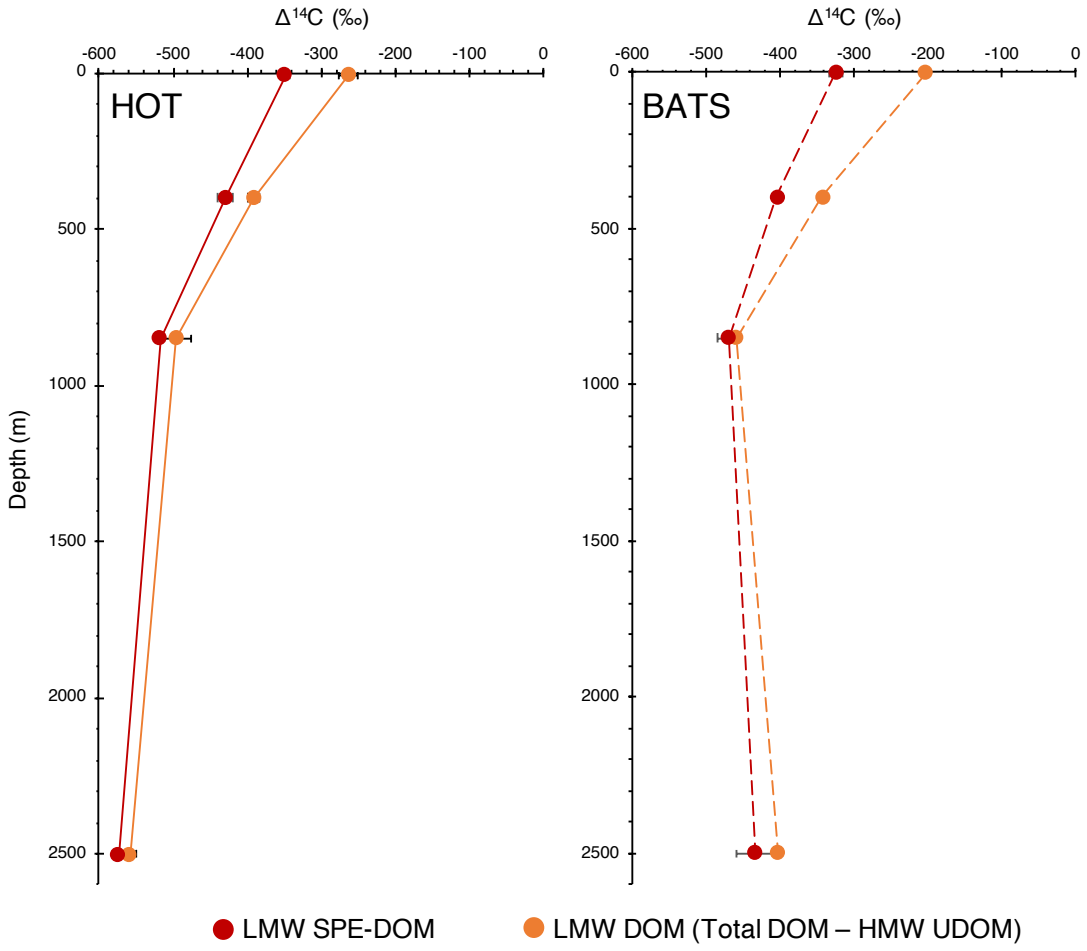

Appendix Figure 1.1 Radiocarbon content ($\Delta^{14}C$) of LMW SPE-DOM (red) and LMW DOM (orange; calculated by subtracting HMW UDOM from total DOM). Points connected by solid lines (left panel) represent samples collected in the North Pacific Subtropical Gyre (HOT), and dotted lines (right panel) represent samples collected in the Central North Atlantic. Points represent the error weighted average of values from 2 repeat cruise samplings in spring and summer, and error bars represent the standard deviation. In the surface ocean, the values are offset by an average of 100 ‰, demonstrating that SPE does discriminate against some fraction of younger LMW material. However, in the deep ocean (≥ 850 m), the values are statistically indistinguishable (p-values ≥ 0.6) demonstrating that the cycling rate of deep ocean LMW SPE-DOM is representative of the total LMW DOM pool.

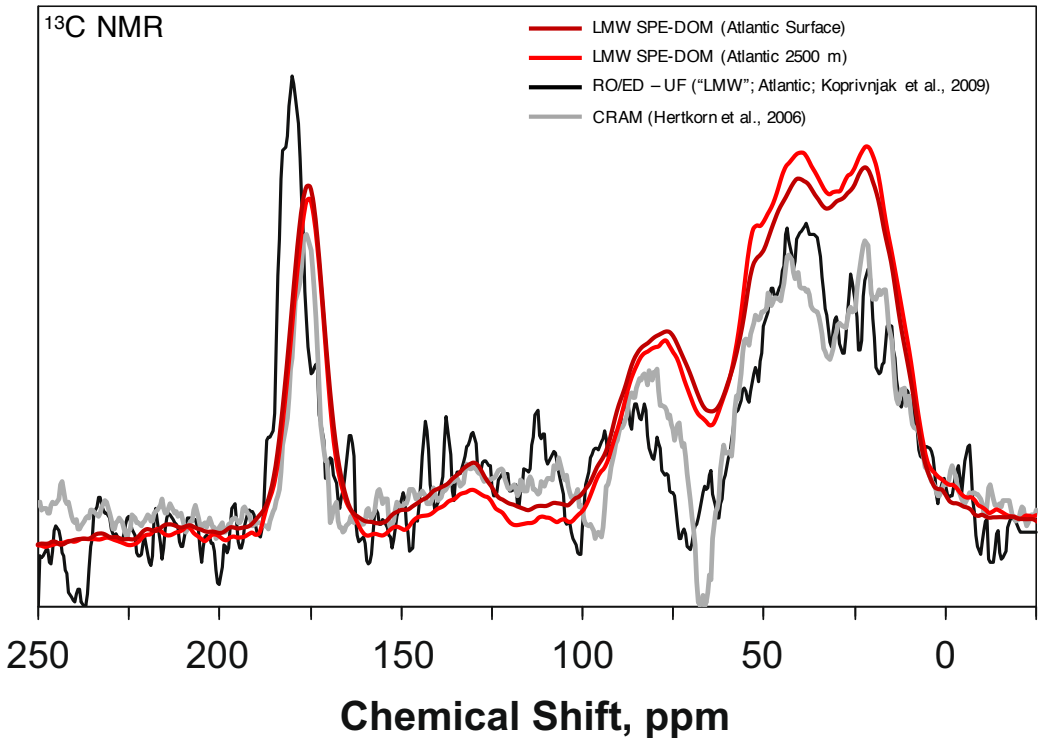

Appendix Figure 1.2 Solid-state ^{13}C NMR spectra of LMW SPE-DOM isolated from surface and deep (2500 m) waters of the Central North Atlantic (red lines) compared to both LMW DOM (black line; calculated by subtracting UDOM spectra from RO/ED spectra; Koprivnjak et al., 2009) and hypothetical HMW CRAM spectra (grey line) generated by subtracting surface minus deep HMW spectra from deep HMW spectra (e.g., Hertkorn et al., 2006). The similarity of LMW SPE-DOM spectra and calculated LMW DOM spectra demonstrates that the functional group distribution of our LMW SPE-DOM fraction is representative of the total LMW DOM pool.

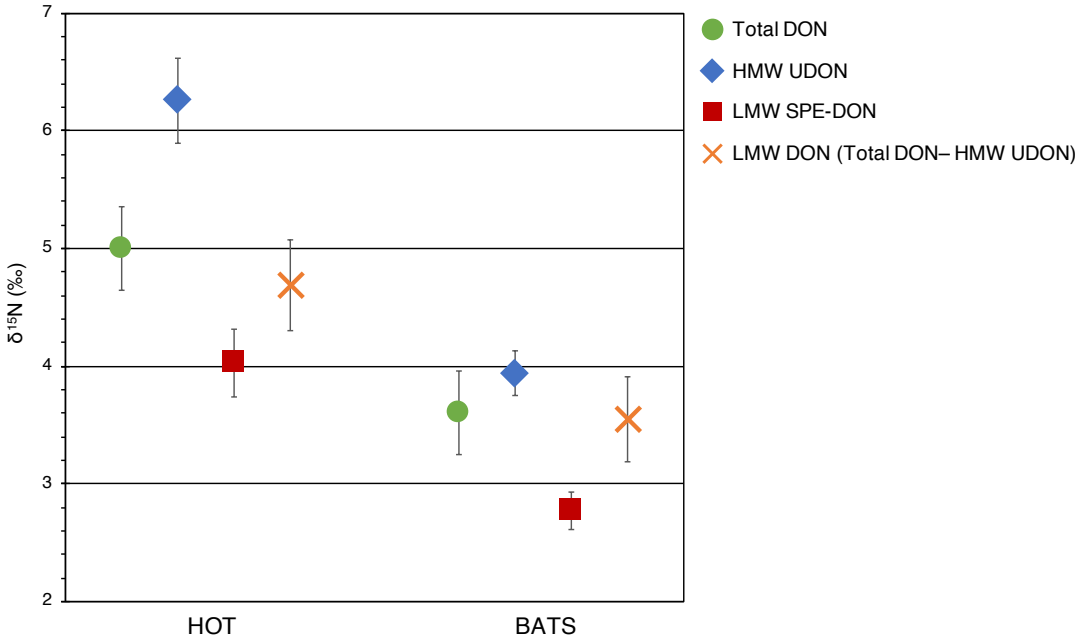

Appendix Figure 1.3 DON Stable Isotope Ratios ($\delta^{15}N$) of total DON (green circle; Knapp et al., 2011), HMW UDON (blue diamonds), LMW SPE-DON (red squares), and LMW DON (orange Xs; calculated by subtracting HMW UDON from total DON) in both the Atlantic (BATS) and Pacific (HOT) basins. The $\delta^{15}N$ similarity between LMW SPE-DOM and calculated $\delta^{15}N$ of LMW, especially in the Pacific basin where the values are equivalent within error, demonstrates that the representativeness of LMW SPE-DON extends to the N-containing fraction of DOM.

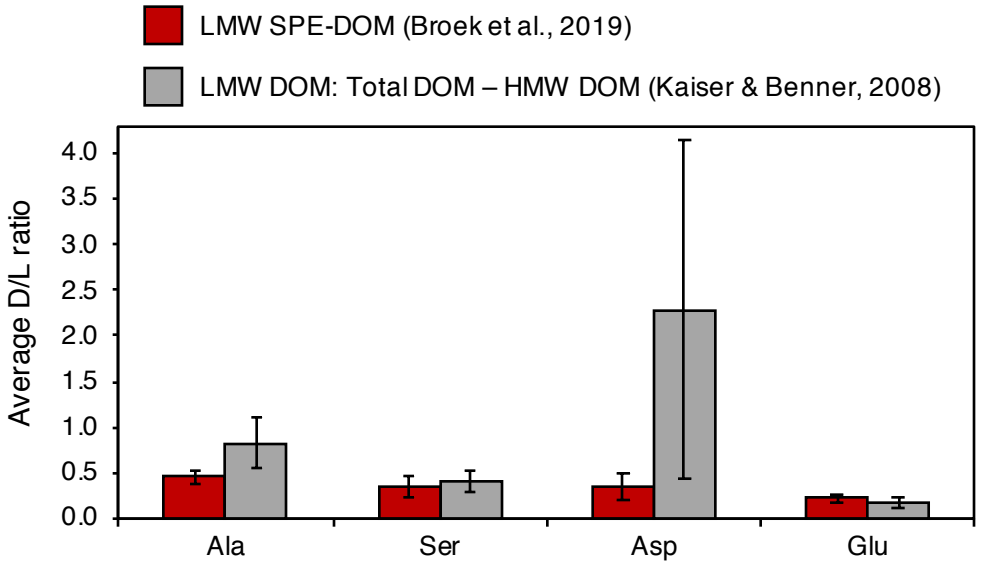

Appendix Figure 1.4 Comparison of measured D/L ratios of LMW SPE-DOM (red bars) to previously published LMW DOM data (grey bars; calculated by subtracting HMW values from total DOM; Kaiser and Benner, 2008) to demonstrate repetitiveness of LMW SPE-DOM fraction at the molecular level. LMW SPE-DOM values represent the average D/L ratio and standard deviation of all samples throughout the full water column. Calculated LMW D/L ratios from Kaiser and Benner (2008) represent the average and standard deviation of all measurements made in the upper 300 m of the water column. Below 300 m the error in calculated values is high due to select AAs (or specific enantiomers of each AA) below the limit of detection. Because of the lack of D/L variability throughout the water column for these AAs, the use of only upper ocean samples for this comparison is valid. *(modified from appendix Fig. 2 of Broek et al., 2019).*

Appendix II

Compilation of Dissertation Data

The following tables represent all of the numerical data presented and discussed within this dissertation. Raw data and values derived from the integration of spectroscopic (NMR) and chromatographic (HPLC-ELSD) measurements are excluded.

Appendix Table 1.1 Total DOC and DON concentrations. DOC and TDN concentration measurements were made using the high temperature oxidation method. DOC concentration measurement errors represent the standard deviation of n = 3 replicate measurements. For some samples, DOC concentrations measurements were also determined via UV oxidation, cryogenic purification and manometric determination. DOC concentrations were similar between the two methods and the presented values represent the error weighted mean of both measurements and propagated uncertainty. Total DON concentrations were determined by subtracting the sum of dissolved inorganic nitrogen (DIN) species (nitrate, nitrite, ammonia) from TDN. DON error represents the propagated analytical uncertainty from the subtraction of [DIN] from [TDN].

location	year	season	depth (m)	[DOC] (µmol/L)	±	[DON] (µmol/L)	±
HOT	2014	Summer	7.5	79.81	0.60	5.67	0.62
HOT	2014	Summer	400	47.24	2.76	3.58	0.40
HOT	2014	Summer	850	40.97	1.08	2.08	0.52
HOT	2014	Summer	2500	34.82	5.31	1.96	0.44
HOT	2015	Spring	7.5	75.90	1.20	5.32	0.68
HOT	2015	Spring	400	45.48	7.81	3.47	0.84
HOT	2015	Spring	850	41.80	4.61	1.78	0.42
HOT	2015	Spring	2500	38.58	5.32	2.10	0.48
BATS	2015	Summer	2	94.26	4.90	5.05	0.92
BATS	2015	Summer	400	69.04	8.60	4.88	1.53
BATS	2015	Summer	850	50.55	1.07	3.32	0.36
BATS	2015	Summer	2500	49.68	1.89	4.21	1.00
BATS	2016	Spring	2	74.05	7.78	4.84	0.63
BATS	2016	Spring	400	52.88	1.05	5.76	2.56
BATS	2016	Spring	850	45.13	1.61	1.81	0.88
BATS	2016	Spring	2500	47.08	1.16	4.28	1.05

Appendix Table 1.2 Filtration volumes, ultrafiltration and solid phase extraction parameters, and recovery of HMW UDOM and LMW SPE-DOM. Percentages represent relative amount of total DOC or DON recovered in each sample type. CF = concentration factor.

location	year	season	sample type	depth (m)	volume (L)	CF	total (mg)	mgC	µmolC/L	%C	mgN	µmolN/L	%N
HOT	2014	Summer	HMW UDOM	7.5	3220	1073	2141	548	14.2	18	50	1.1	20
HOT	2014	Summer	HMW UDOM	400	3880	1293	689	171	3.7	8	17	0.3	9
HOT	2014	Summer	HMW UDOM	850	3100	1033	806	163	4.4	11	15	0.3	17
HOT	2014	Summer	HMW UDOM	2500	4300	1433	865	171	3.3	9	16	0.3	14
HOT	2015	Spring	HMW UDOM	7.5	3319	1037	1537	492	12.4	16	40	0.9	16
HOT	2015	Spring	HMW UDOM	400	2945	998	770	170	4.8	11	15	0.4	10
HOT	2015	Spring	HMW UDOM	850	3330	1189	674	154	3.9	9	13	0.3	15
HOT	2015	Spring	HMW UDOM	2500	3939	1358	603	117	2.5	6	9	0.2	8
BATS	2015	Summer	HMW UDOM	2	2549	850	1988	327	10.7	11	24	0.7	13
BATS	2015	Summer	HMW UDOM	400	2500	833	1513	163	5.4	8	14	0.4	8
BATS	2015	Summer	HMW UDOM	850	1170	390	1221	66	4.7	9	6	0.3	10
BATS	2015	Summer	HMW UDOM	2500	1750	583	1223	75	3.6	7	6	0.2	6
BATS	2015	Summer	HMW UDOM	2500	1750	583	1621	110	5.3	11	9	0.4	9
BATS	2016	Spring	HMW UDOM	2	2999	1000	2240	336	9.3	13	27	0.6	13
BATS	2016	Spring	HMW UDOM	400	2999	1000	1804	188	5.2	10	16	0.4	7
BATS	2016	Spring	HMW UDOM	850	3001	1000	1726	156	4.3	10	13	0.3	17
BATS	2016	Spring	HMW UDOM	2500	3007	1074	1659	144	4.0	8	12	0.3	6

location	year	season	sample type	depth (m)	volume (L)	loading (L/g)	total (mg)	mgC	µmolC/L	%C	mgN	µmolN/L	%N
HOT	2014	Summer	LMW SPE-DOM	7.5	796	2.7	257	138	14.5	18	5	0.4	8
HOT	2014	Summer	LMW SPE-DOM	400	1050	3.5	312	162	12.9	25	6	0.4	12
HOT	2014	Summer	LMW SPE-DOM	850	800	2.7	230	117	12.2	29	5	0.4	21
HOT	2014	Summer	LMW SPE-DOM	2500	1000	3.3	248	128	10.7	25	5	0.3	18
HOT	2015	Spring	LMW SPE-DOM	7.5	2200	4.4	805	409	15.5	20	15	0.5	9
HOT	2015	Spring	LMW SPE-DOM	400	2500	5.0	738	375	12.5	23	14	0.4	12
HOT	2015	Spring	LMW SPE-DOM	2500	3180	6.4	806	445	11.7	29	16	0.4	17
BATS	2015	Summer	LMW SPE-DOM	2	1500	5.0	791	404	22.4	24	15	0.7	14
BATS	2015	Summer	LMW SPE-DOM	400	1500	5.0	640	333	18.5	27	13	0.6	13
BATS	2015	Summer	LMW SPE-DOM	850	800	2.7	362	165	17.2	34	8	0.7	21
BATS	2015	Summer	LMW SPE-DOM	2500	1000	3.3	366	185	15.4	31	9	0.6	14
BATS	2016	Spring	LMW SPE-DOM	2	2000	6.7	1014	508	21.2	29	19	0.7	14
BATS	2016	Spring	LMW SPE-DOM	400	2000	6.7	895	428	17.8	34	17	0.6	10
BATS	2016	Spring	LMW SPE-DOM	850	2000	6.7	873	423	17.6	39	17	0.6	33
BATS	2016	Spring	LMW SPE-DOM	2500	2000	6.7	829	396	16.5	35	16	0.6	13
HOT	2014	Summer	PPL SPE-DOM	7.5	20.5	0.4	32	8	33.7	42	0.5	1.6	28
HOT	2014	Summer	PPL SPE-DOM	2500	20.5	0.4	13	4	17.5	41	0.2	0.8	42
HOT	2015	Spring	PPL SPE-DOM	7.5	20.0	0.4	26	9	36.3	48	0.5	1.7	32
HOT	2015	Spring	PPL SPE-DOM	2500	20.0	0.4	10	4	16.9	47	0.2	0.7	35
HOT	2014	Summer	HP-20 SPE-DOM	7.5	20.5	0.4	81	7	30.1	38	0.3	1.1	20
HOT	2014	Summer	HP-20 SPE-DOM	2500	20.5	0.4	13	4	16.9	40	0.2	0.6	29
HOT	2015	Spring	HP-20 SPE-DOM	2500	20.0	0.4	16	2	10.1	28	0.1	0.3	14

Appendix Table 1.3 Carbon and nitrogen content (wt%C, wt%N), elemental ratios (C/N) and stable isotopic ratios ($\delta^{13}C$, $\delta^{15}N$) of all HMW UDOM and LMW SPE-DOM samples. Error represents standard deviation of n = 3 replicate measurements. All analyses were conducted at the UC Santa Cruz Stable Isotope Lab.

location	year	season	sample type	depth (m)	wt%C	±	wt%N	±	$\delta^{15}N$ (‰)	±	$\delta^{13}C$ (‰)	±	C/N	±
HOT	2014	Summer	HMW UDOM	7.5	25.6	5.9	2.3	0.4	6.2	0.1	-22.1	0.1	12.9	0.1
HOT	2014	Summer	HMW UDOM	400	24.8	1.0	2.5	0.0	6.5	0.1	-21.5	0.0	11.9	0.1
HOT	2014	Summer	HMW UDOM	850	20.3	1.8	1.9	0.1	6.8	0.1	-21.9	0.0	13.1	0.0
HOT	2014	Summer	HMW UDOM	2500	19.7	1.4	1.9	0.1	6.8	0.2	-21.1	0.0	13.1	0.1
HOT	2015	Spring	HMW UDOM	7.5	32.0	1.8	2.6	0.1	6.7	0.3	-22.5	0.0	12.3	0.0
HOT	2015	Spring	HMW UDOM	400	22.1	0.2	1.9	0.0	6.6	0.1	-21.9	0.3	11.5	0.2
HOT	2015	Spring	HMW UDOM	850	22.8	0.4	1.9	0.0	7.1	0.1	-21.5	0.3	12.2	0.0
HOT	2015	Spring	HMW UDOM	2500	19.4	3.2	1.5	0.2	7.0	0.3	-21.5	0.1	12.5	0.1
BATS	2015	Summer	HMW UDOM	2	16.4	0.6	1.2	0.0	3.8	0.1	-22.4	0.1	13.5	0.1
BATS	2015	Summer	HMW UDOM	400	10.8	0.6	0.9	0.0	5.9	0.2	-21.6	0.0	11.8	0.1
BATS	2015	Summer	HMW UDOM	850	5.4	0.1	0.5	0.0	6.5	0.4	-21.4	0.1	12.0	0.1
BATS	2015	Summer	HMW UDOM	2500	6.1	0.4	0.5	0.0	6.1	0.6	-21.3	0.1	12.5	0.2
BATS	2015	Summer	HMW UDOM	2500	6.8	0.5	0.6	0.0	5.3	0.3	-21.4	0.0	12.1	0.1
BATS	2016	Spring	HMW UDOM	2	15.0	0.4	1.2	0.0	4.1	0.1	-22.3	0.0	12.5	0.1
BATS	2016	Spring	HMW UDOM	400	10.4	0.2	0.9	0.0	5.5	0.2	-21.7	0.0	11.7	0.1
BATS	2016	Spring	HMW UDOM	850	9.0	0.2	0.8	0.0	6.3	0.1	-21.3	0.1	12.0	0.1
BATS	2016	Spring	HMW UDOM	2500	8.7	0.3	0.7	0.0	5.8	0.6	-21.3	0.1	12.5	0.3
HOT	2014	Summer	LMW SPE-DOM	7.5	53.7	1.4	1.9	0.1	3.6	0.1	-22.9	0.1	28.2	0.3
HOT	2014	Summer	LMW SPE-DOM	400	52.0	0.4	2.0	0.0	3.4	0.2	-22.5	0.0	26.2	0.1
HOT	2014	Summer	LMW SPE-DOM	850	51.0	1.3	2.1	0.1	3.6	0.1	-22.2	0.0	24.2	0.0
HOT	2014	Summer	LMW SPE-DOM	2500	51.9	1.6	2.0	0.0	3.5	0.2	-22.4	0.1	26.4	0.2
HOT	2015	Spring	LMW SPE-DOM	7.5	50.8	0.8	1.8	0.0	4.0	0.0	-22.6	0.0	27.6	0.1
HOT	2015	Spring	LMW SPE-DOM	400	50.8	2.1	1.9	0.1	3.6	0.4	-22.7	0.4	26.1	1.9
HOT	2015	Spring	LMW SPE-DOM	2500	55.2	1.3	1.9	0.0	3.4	0.2	-22.8	0.1	28.5	0.0
BATS	2015	Summer	LMW SPE-DOM	2	51.1	0.2	1.9	0.0	2.7	0.2	-23.0	0.0	27.2	0.1
BATS	2015	Summer	LMW SPE-DOM	400	52.0	0.1	2.1	0.0	3.0	0.2	-22.7	0.0	24.7	0.1
BATS	2015	Summer	LMW SPE-DOM	850	45.6	1.7	2.1	0.1	3.5	0.1	-22.3	0.1	21.3	0.3
BATS	2015	Summer	LMW SPE-DOM	2500	50.5	0.2	2.3	0.0	3.5	0.1	-22.1	0.0	21.7	0.0
BATS	2016	Spring	LMW SPE-DOM	2	50.1	0.3	1.9	0.0	2.8	0.2	-23.1	0.1	27.1	0.7
BATS	2016	Spring	LMW SPE-DOM	400	47.8	0.2	1.9	0.0	3.1	0.1	-22.9	0.0	25.8	0.0
BATS	2016	Spring	LMW SPE-DOM	850	48.5	0.6	1.9	0.0	3.2	0.1	-22.9	0.0	25.4	0.1
BATS	2016	Spring	LMW SPE-DOM	2500	47.7	0.2	1.9	0.0	3.3	0.1	-22.8	0.0	24.6	0.1
HOT	2014	Summer	PPL SPE-DOM	7.5	26.0	--	1.4	--	5.1	0.2	-23.0	0.1	18.3	0.2
HOT	2014	Summer	PPL SPE-DOM	2500	33.5	--	1.8	--	4.0	0.2	-22.0	0.1	18.2	0.2
HOT	2015	Spring	PPL SPE-DOM	7.5	33.3	--	1.8	--	4.8	0.2	-22.6	0.1	18.4	0.1
HOT	2015	Spring	PPL SPE-DOM	2500	40.9	--	2.1	--	4.2	0.2	-21.7	0.1	19.6	0.1
HOT	2014	Summer	HP-20 SPE-DOM	7.5	9.1	--	0.4	--	4.5	0.2	-22.3	0.1	22.5	0.2
HOT	2014	Summer	HP-20 SPE-DOM	2500	31.4	--	1.2	--	4.0	0.2	-22.4	0.1	25.6	0.2
HOT	2015	Spring	HP-20 SPE-DOM	2500	15.5	--	0.5	--	3.7	0.2	-22.6	0.1	29.3	0.1

Appendix Table 1.4 Radiocarbon content of total DOC determined by UV-oxidation and AMS at the UC Irvine Keck Carbon Cycle AMS Lab. Results are reported as age-corrected $\Delta^{14}C$ (‰) for geochemical samples and have been corrected to the date of collection in accordance with conventions set forth by Stuiver and Polach (1977). All results are background and $\delta^{13}C$ corrected and presented as fraction modern (Fm), $\Delta^{14}C$ (‰), and conventional radiocarbon age (ybp).

location	year	season	sample type	depth (m)	UCIAMS #	Fm	±	$\Delta^{14}C$ (‰)	±	^{14}C age (ybp)	±
HOT	2014	Summer	Total DOC	7.5	158141	0.7911	0.0026	-215.1	2.6	1880	30
HOT	2014	Summer	Total DOC	400	158145	0.6343	0.0023	-370.6	2.3	3655	30
HOT	2014	Summer	Total DOC	850	158144	0.5375	0.0026	-466.7	2.6	4985	40
HOT	2014	Summer	Total DOC	2500	158143	0.4663	0.0020	-537.4	2.0	6130	35
HOT	2015	Spring	Total DOC	7.5	164612	0.7715	0.0019	-234.5	1.9	2085	25
HOT	2015	Spring	Total DOC	400	164613	0.6308	0.0017	-374.1	1.7	3700	25
HOT	2015	Spring	Total DOC	850	168551	0.5140	0.0018	-490.0	1.8	5345	30
HOT	2015	Spring	Total DOC	2500	168540	0.4519	0.0022	-551.6	2.2	6380	40
BATS	2016	Spring	Total DOC	7.5	180280	0.8204	0.0018	-186.1	4.0	1590	20
BATS	2017	Spring	Total DOC	400	180269	0.6793	0.0016	-326.1	4.0	3105	20
BATS	2018	Spring	Total DOC	850	180271	0.5662	0.0016	-438.3	4.0	4570	25
BATS	2019	Spring	Total DOC	2500	180276	0.6129	0.0018	-392.0	4.0	3930	25

Appendix Table 1.5 Radiocarbon content of HMW UDOM, LMW SPE-DOM, and SPE-DOM determined by AMS at the Lawrence Livermore National Laboratory Center for Accelerator Mass Spectrometry. Results are reported as age-corrected $\Delta^{14}C$ (‰) for geochemical samples and have been corrected to the date of collection in accordance with conventions set forth by Stuiver and Polach (1977). All results are background and $\delta^{13}C$ corrected and presented as fraction modern (Fm), $\Delta^{14}C$ (‰), and conventional radiocarbon age (ybp).

location	year	season	sample type	depth (m)	CAMS #	Fm	±	$\Delta^{14}C$ (‰)	±	^{14}C age (ybp)	±
HOT	2014	Summer	HMW UDOM	7.5	169865	0.9703	0.0038	-37.3	3.8	240	35
HOT	2014	Summer	HMW UDOM	400	169866	0.8160	0.0022	-190.4	2.2	1635	25
HOT	2014	Summer	HMW UDOM	850	169867	0.6615	0.0021	-343.7	2.1	3320	30
HOT	2014	Summer	HMW UDOM	2500	169868	0.6252	0.0018	-379.7	1.8	3775	25
HOT	2015	Spring	HMW UDOM	7.5	172708	0.9575	0.0033	-50.0	3.3	350	30
HOT	2015	Spring	HMW UDOM	400	172709	0.8292	0.0029	-177.3	2.9	1505	30
HOT	2015	Spring	HMW UDOM	850	172710	0.7188	0.0028	-286.9	2.8	2655	35
HOT	2015	Spring	HMW UDOM	2500	172711	0.6393	0.0023	-365.7	2.3	3595	30
BATS	2015	Summer	HMW UDOM	2	175978	0.9570	0.0032	-43.0	3.2	355	30
BATS	2015	Summer	HMW UDOM	400	175979	0.8415	0.0029	-158.5	2.9	1385	30
BATS	2015	Summer	HMW UDOM	850	175980	0.7325	0.0022	-267.5	2.2	2500	25
BATS	2015	Summer	HMW UDOM	2500	175981	0.6958	0.0019	-304.2	1.9	2915	25
BATS	2015	Summer	HMW UDOM	2500	175982	0.7118	0.0022	-288.2	2.2	2730	25
BATS	2016	Spring	HMW UDOM	2	175988	0.9359	0.0031	-64.1	3.1	530	30
BATS	2016	Spring	HMW UDOM	400	175989	0.8291	0.0026	-170.9	2.6	1505	30
BATS	2016	Spring	HMW UDOM	850	175990	0.7608	0.0022	-239.2	2.2	2195	25
BATS	2016	Spring	HMW UDOM	2500	175991	0.7349	0.0025	-265.1	2.5	2475	30
HOT	2014	Summer	LMW SPE-DOM	7.5	169869	0.6503	0.0021	-354.8	2.1	3455	30
HOT	2014	Summer	LMW SPE-DOM	400	169870	0.5841	0.0017	-420.4	1.7	4320	25
HOT	2014	Summer	LMW SPE-DOM	850	169871	0.4858	0.0015	-518.0	1.5	5800	30
HOT	2014	Summer	LMW SPE-DOM	2500	169872	0.4337	0.0014	-569.7	1.4	6710	30
HOT	2015	Spring	LMW SPE-DOM	7.5	172712	0.6622	0.0023	-343.0	2.3	3310	30
HOT	2015	Spring	LMW SPE-DOM	400	172713	0.5657	0.0022	-438.8	2.2	4575	35
HOT	2015	Spring	LMW SPE-DOM	2500	172715	0.4257	0.0017	-577.6	1.7	6860	35
BATS	2015	Summer	LMW SPE-DOM	2	175983	0.6839	0.0020	-316.1	2.0	3050	25
BATS	2015	Summer	LMW SPE-DOM	400	175984	0.4922	0.0015	-507.8	1.5	5695	25
BATS	2015	Summer	LMW SPE-DOM	850	175985	0.5464	0.0016	-453.6	1.6	4855	25
BATS	2015	Summer	LMW SPE-DOM	2500	176498	0.5428	0.0016	-461.6	1.6	4910	25
BATS	2016	Spring	LMW SPE-DOM	2	175992	0.6664	0.0026	-333.6	2.6	3260	35
BATS	2016	Spring	LMW SPE-DOM	400	175993	0.5985	0.0019	-401.5	1.9	4125	30
BATS	2016	Spring	LMW SPE-DOM	850	175994	0.5145	0.0019	-485.5	1.9	5340	30
BATS	2016	Spring	LMW SPE-DOM	2500	175995	0.5912	0.0017	-408.8	1.7	4220	25
HOT	2014	Summer	PPL SPE-DOM	7.5	169873	0.7580	0.0021	-248.0	2.1	2225	25
HOT	2014	Summer	PPL SPE-DOM	2500	169874	0.4545	0.0015	-549.1	1.5	6335	30
HOT	2015	Spring	PPL SPE-DOM	7.5	173010	0.7530	0.0027	-253.0	2.7	2280	30
HOT	2015	Spring	PPL SPE-DOM	2500	172716	0.4417	0.0020	-561.8	2.0	6565	40
HOT	2014	Summer	HP-20 SPE-DOM	7.5	169875	0.7261	0.0022	-279.6	2.2	2570	25
HOT	2014	Summer	HP-20 SPE-DOM	2500	169876	0.4519	0.0020	-551.6	2.0	6380	35
HOT	2015	Spring	HP-20 SPE-DOM	2500	172717	0.4532	0.0017	-550.4	1.7	6360	30

Appendix Table 1.6 Radiocarbon content of protein-like (PL) material and molar abundance weighted radiocarbon content of individually purified AAs (ΣAA) from each HMW UDOM and LMW SPE-DOM. PL values were determined by AMS at the Lawrence Livermore National Laboratory Center for Accelerator Mass Spectrometry. Data for ΣAA calculations were determined by AMS at the UC Irvine Keck Carbon Cycle AMS Lab. Results are reported as age-corrected $\Delta^{14}C$ (‰) for geochemical samples and have been corrected to the date of collection in accordance with conventions set forth by Stuiver and Polach (1977). All results are background and $\delta^{13}C$ corrected and presented as fraction modern (Fm), $\Delta^{14}C$ (‰), and conventional radiocarbon age (ybp).

location	year	season	sample type	depth (m)	CAMS #	Fm	±	$\Delta^{14}C$ (‰)	±	^{14}C age (ybp)	±
HOT	2015	Spring	PL (HMW UDOM)	7.5	177037	0.9767	0.0035	-31.2	3.5	190	30
HOT	2015	Spring	PL (HMW UDOM)	2500	177038	0.6725	0.0025	-333.0	2.5	3190	30
HOT	2015	Spring	PL (LMW SPE-DOM)	7.5	177039	0.7113	0.0025	-294.4	2.5	2735	30
HOT	2015	Spring	PL (LMW SPE-DOM)	2500	177040	0.4639	0.0017	-539.8	1.7	6170	30
HOT	2015	Spring	ΣAA (HMW UDOM)	7.5	N/A	--	--	48.9	24.5	-437	195
HOT	2015	Spring	ΣAA (HMW UDOM)	2500	N/A	--	--	-222.5	34.7	2000	422
HOT	2015	Spring	ΣAA (LMW SPE-DOM)	7.5	N/A	--	--	-138.2	23.4	1188	227
HOT	2015	Spring	ΣAA (LMW SPE-DOM)	2500	N/A	--	--	-481.6	30.7	5261	492

Appendix Table 1.7 Radiocarbon content of individual amino acids (AAs) isolated from HMW UDOM and LMW SPE-DOM by semi-preparative high-pressure liquid chromatography. Multiple AAs listed together represent collections of unresolved groups of compounds. Question marks (?) represent the inclusion of unidentified compound peaks in the unresolved groups of compounds. Values were determined by AMS at the UC Irvine Keck Carbon Cycle AMS Lab. Results are reported as age-corrected $\Delta^{14}C$ (‰) for geochemical samples and have been corrected to the date of collection in accordance with conventions set forth by Stuiver and Polach (1977). All results are background and $\delta^{13}C$ corrected and presented as fraction modern (Fm), $\Delta^{14}C$ (‰), and conventional radiocarbon age (ybp).

location	year	season	sample type	amino acid	depth (m)	UCIAMS #	Fm	±	$\Delta^{14}C$ (‰)	±	^{14}C age (ybp)	±
HOT	2015	Spring	HMW UDOM	Ala	7.5	207237	1.0363	0.0071	28.2	7.1	-280	60
HOT	2015	Spring	HMW UDOM	Gly	7.5	207249	1.0306	0.0098	22.5	9.8	-230	80
HOT	2015	Spring	HMW UDOM	Phe	7.5	207253	1.0386	0.0138	30.5	13.8	-290	110
HOT	2015	Spring	HMW UDOM	Pro	7.5	207258	1.0602	0.0118	51.9	11.8	-460	90
HOT	2015	Spring	HMW UDOM	Val	7.5	207265	1.1328	0.0075	124.0	7.5	-990	60
HOT	2015	Spring	HMW UDOM	Asp, Ser	7.5	207244	1.0901	0.0058	81.5	5.8	-690	45
HOT	2015	Spring	HMW UDOM	Ile, Leu, ?	7.5	207233	1.0286	0.0049	20.5	4.9	-220	40
HOT	2015	Spring	HMW UDOM	Thr, Glu, ?	7.5	207263	1.0530	0.0032	44.7	3.2	-410	25
HOT	2015	Spring	HMW UDOM	Ala	2500	207236	0.8862	0.0116	-120.7	11.6	970	110
HOT	2015	Spring	HMW UDOM	Gly	2500	207250	0.7190	0.0125	-286.7	12.5	2650	140
HOT	2015	Spring	HMW UDOM	Phe	2500	207254	0.6447	0.0246	-360.4	24.6	3530	310
HOT	2015	Spring	HMW UDOM	Val	2500	207266	0.6211	0.0112	-383.7	11.2	3830	150
HOT	2015	Spring	HMW UDOM	Asp, Ser	2500	207245	0.7569	0.0090	-249.0	9.0	2240	100
HOT	2015	Spring	HMW UDOM	Ile, Leu, ?	2500	207234	0.5897	0.0085	-414.9	8.5	4240	120
HOT	2015	Spring	HMW UDOM	Thr, Glu, ?	2500	207264	0.7745	0.0056	-231.6	5.6	2050	60
HOT	2015	Spring	LMW SPE-DOM	Ala	7.5	207239	0.7216	0.0118	-284.1	11.8	2620	140
HOT	2015	Spring	LMW SPE-DOM	Gly	7.5	207247	0.9345	0.0112	-72.9	11.2	540	100
HOT	2015	Spring	LMW SPE-DOM	Phe	7.5	207252	0.7807	0.0046	-225.4	4.6	1990	50
HOT	2015	Spring	LMW SPE-DOM	Asp	7.5	207241	1.3905	0.0234	379.6	23.4	-2640	140
HOT	2015	Spring	LMW SPE-DOM	Ser	7.5	207260	0.9678	0.0162	-39.8	16.2	260	140
HOT	2015	Spring	LMW SPE-DOM	Ala	2500	207238	0.4818	0.0194	-522.0	19.4	5870	330
HOT	2015	Spring	LMW SPE-DOM	Gly	2500	207248	0.5314	0.0205	-472.8	20.5	5080	310
HOT	2015	Spring	LMW SPE-DOM	Phe	2500	207257	0.4649	0.0061	-538.8	6.1	6150	110
HOT	2015	Spring	LMW SPE-DOM	Asp 1	2500	207242	0.5927	0.0217	-412.0	21.7	4200	300
HOT	2015	Spring	LMW SPE-DOM	Asp 2	2500	207243	0.5324	0.0267	-471.7	26.7	5060	410
HOT	2015	Spring	LMW SPE-DOM	Ile, Leu, ?	2500	207232	0.4309	0.0033	-572.4	3.3	6760	70
HOT	2015	Spring	LMW SPE-DOM	Thr, Glu, ?	2500	207262	0.5979	0.0099	-406.8	9.9	4130	140
BATS	2016	Spring	HMW UDOM	Ala	2	207240	0.9719	0.0127	-35.7	12.7	230	110
BATS	2016	Spring	HMW UDOM	Gly	2	207251	1.0009	0.0169	-6.9	16.9	0	140
BATS	2016	Spring	HMW UDOM	Phe	2	207256	0.8797	0.0065	-127.2	6.5	1030	60
BATS	2016	Spring	HMW UDOM	Pro	2	207259	0.9219	0.0082	-85.3	8.2	650	80
BATS	2016	Spring	HMW UDOM	Ser	2	207261	0.9688	0.0163	-38.8	16.3	260	140
BATS	2016	Spring	HMW UDOM	Val	2	207267	0.7941	0.0244	-212.1	24.4	1850	250
BATS	2016	Spring	HMW UDOM	Asp, Ser	2	207246	0.9892	0.0077	-18.5	7.7	90	70
BATS	2016	Spring	HMW UDOM	Ile, Leu, ?	2	207235	0.8805	0.0043	-126.4	4.3	1020	40
BATS	2016	Spring	LMW SPE-DOM	Phe	2	207255	0.6872	0.0055	-318.2	5.5	3010	70

Appendix Table 1.8 Enantiomeric ratios (D/L, %D) and relative molar distribution (Mol%) of amino acids in HMW UDOM and LMW SPE-DOM.

location	year	season	sample type	depth (m)	amino acid	Mol%	±	%D	±	D/L	±
HOT	2014	Summer	HMW UDOM	7.5	Ala	23.0	2.3	33.0	0.5	0.49	0.005
HOT	2014	Summer	HMW UDOM	7.5	Asp	15.1	1.5	10.6	1.2	0.12	0.012
HOT	2014	Summer	HMW UDOM	7.5	Glu	8.4	0.8	11.4	0.6	0.13	0.006
HOT	2014	Summer	HMW UDOM	7.5	Gly	14.0	1.4	--	--	--	--
HOT	2014	Summer	HMW UDOM	7.5	Ile	2.5	0.2	--	--	--	--
HOT	2014	Summer	HMW UDOM	7.5	Leu	5.0	0.5	2.6	0.7	0.03	0.007
HOT	2014	Summer	HMW UDOM	7.5	Phe	2.5	0.2	4.4	1.0	0.05	0.010
HOT	2014	Summer	HMW UDOM	7.5	Pro	3.6	0.4	--	--	--	--
HOT	2014	Summer	HMW UDOM	7.5	Ser	12.9	1.3	14.2	0.3	0.17	0.003
HOT	2014	Summer	HMW UDOM	7.5	Thr	6.8	0.7	--	--	--	--
HOT	2014	Summer	HMW UDOM	7.5	Val	3.2	0.3	1.3	1.4	0.01	0.014
HOT	2014	Summer	HMW UDOM	400	Ala	26.8	2.7	41.0	0.5	0.70	0.005
HOT	2014	Summer	HMW UDOM	400	Asp	12.1	1.2	16.2	1.2	0.19	0.012
HOT	2014	Summer	HMW UDOM	400	Glu	8.3	0.8	14.2	0.6	0.17	0.006
HOT	2014	Summer	HMW UDOM	400	Gly	17.0	1.7	--	--	--	--
HOT	2014	Summer	HMW UDOM	400	Ile	3.8	0.4	--	--	--	--
HOT	2014	Summer	HMW UDOM	400	Leu	7.1	0.7	3.6	0.7	0.04	0.007
HOT	2014	Summer	HMW UDOM	400	Phe	3.3	0.3	5.3	1.0	0.06	0.010
HOT	2014	Summer	HMW UDOM	400	Pro	4.6	0.5	--	--	--	--
HOT	2014	Summer	HMW UDOM	400	Ser	8.1	0.8	18.8	0.3	0.23	0.003
HOT	2014	Summer	HMW UDOM	400	Thr	5.0	0.5	--	--	--	--
HOT	2014	Summer	HMW UDOM	400	Val	3.9	0.4	5.5	1.4	0.06	0.014
HOT	2014	Summer	HMW UDOM	850	Ala	22.6	2.3	34.3	0.5	0.52	0.005
HOT	2014	Summer	HMW UDOM	850	Asp	16.5	1.6	7.4	1.2	0.08	0.013
HOT	2014	Summer	HMW UDOM	850	Glu	10.2	1.0	9.5	0.6	0.10	0.006
HOT	2014	Summer	HMW UDOM	850	Gly	17.4	1.7	--	--	--	--
HOT	2014	Summer	HMW UDOM	850	Ile	4.2	0.4	--	--	--	--
HOT	2014	Summer	HMW UDOM	850	Leu	6.7	0.7	2.7	0.7	0.03	0.007
HOT	2014	Summer	HMW UDOM	850	Phe	3.2	0.3	2.7	1.0	0.03	0.010
HOT	2014	Summer	HMW UDOM	850	Pro	5.2	0.5	--	--	--	--
HOT	2014	Summer	HMW UDOM	850	Ser	4.3	0.4	14.8	0.3	0.17	0.003
HOT	2014	Summer	HMW UDOM	850	Thr	5.0	0.5	--	--	--	--
HOT	2014	Summer	HMW UDOM	850	Val	4.6	0.5	2.2	1.4	0.02	0.014
HOT	2014	Summer	HMW UDOM	2500	Ala	38.6	3.9	41.3	0.5	0.70	0.005
HOT	2014	Summer	HMW UDOM	2500	Asp	14.4	1.4	20.7	1.1	0.26	0.012
HOT	2014	Summer	HMW UDOM	2500	Glu	5.6	0.6	15.7	0.6	0.19	0.006
HOT	2014	Summer	HMW UDOM	2500	Gly	18.2	1.8	--	--	--	--
HOT	2014	Summer	HMW UDOM	2500	Ile	2.0	0.2	--	--	--	--
HOT	2014	Summer	HMW UDOM	2500	Leu	3.2	0.3	4.5	0.7	0.05	0.007
HOT	2014	Summer	HMW UDOM	2500	Phe	2.0	0.2	6.2	1.0	0.07	0.010
HOT	2014	Summer	HMW UDOM	2500	Pro	3.1	0.3	--	--	--	--
HOT	2014	Summer	HMW UDOM	2500	Ser	5.2	0.5	19.8	0.3	0.25	0.003
HOT	2014	Summer	HMW UDOM	2500	Thr	4.8	0.5	--	--	--	--
HOT	2014	Summer	HMW UDOM	2500	Val	3.0	0.3	6.6	1.4	0.07	0.014
HOT	2015	Spring	HMW UDOM	7.5	Ala	18.4	1.8	40.4	0.5	0.68	0.005
HOT	2015	Spring	HMW UDOM	7.5	Asp	16.6	1.7	23.5	1.1	0.31	0.011
HOT	2015	Spring	HMW UDOM	7.5	Glu	10.2	1.0	16.2	0.6	0.19	0.006
HOT	2015	Spring	HMW UDOM	7.5	Gly	20.2	2.0	--	--	--	--
HOT	2015	Spring	HMW UDOM	7.5	Ile	1.9	0.2	--	--	--	--
HOT	2015	Spring	HMW UDOM	7.5	Leu	5.5	0.5	4.6	0.7	0.05	0.007
HOT	2015	Spring	HMW UDOM	7.5	Phe	3.5	0.3	7.3	1.0	0.08	0.010
HOT	2015	Spring	HMW UDOM	7.5	Pro	4.3	0.4	--	--	--	--
HOT	2015	Spring	HMW UDOM	7.5	Ser	11.5	1.1	26.7	0.3	0.36	0.003

location	year	season	sample type	depth (m)	amino acid	Mol%	±	%D	±	D/L	±
HOT	2015	Spring	HMW UDOM	7.5	Thr	5.8	0.6	--	--	--	--
HOT	2015	Spring	HMW UDOM	7.5	Val	2.3	0.2	2.3	1.4	0.02	0.014
HOT	2015	Spring	HMW UDOM	400	Ala	28.7	2.9	44.0	0.5	0.79	0.005
HOT	2015	Spring	HMW UDOM	400	Asp	13.6	1.4	23.8	1.1	0.31	0.011
HOT	2015	Spring	HMW UDOM	400	Glu	6.6	0.7	17.7	0.6	0.21	0.006
HOT	2015	Spring	HMW UDOM	400	Gly	26.8	2.7	--	--	--	--
HOT	2015	Spring	HMW UDOM	400	Ile	1.6	0.2	--	--	--	--
HOT	2015	Spring	HMW UDOM	400	Leu	3.2	0.3	5.6	0.6	0.06	0.007
HOT	2015	Spring	HMW UDOM	400	Phe	1.7	0.2	9.1	1.0	0.10	0.010
HOT	2015	Spring	HMW UDOM	400	Pro	3.7	0.4	--	--	--	--
HOT	2015	Spring	HMW UDOM	400	Ser	8.0	0.8	28.0	0.3	0.39	0.003
HOT	2015	Spring	HMW UDOM	400	Thr	3.7	0.4	--	--	--	--
HOT	2015	Spring	HMW UDOM	400	Val	2.3	0.2	5.8	1.4	0.06	0.014
HOT	2015	Spring	HMW UDOM	850	Ala	24.1	2.4	44.3	0.5	0.79	0.005
HOT	2015	Spring	HMW UDOM	850	Asp	16.6	1.7	26.0	1.1	0.35	0.011
HOT	2015	Spring	HMW UDOM	850	Glu	8.4	0.8	19.8	0.6	0.25	0.006
HOT	2015	Spring	HMW UDOM	850	Gly	25.8	2.6	--	--	--	--
HOT	2015	Spring	HMW UDOM	850	Ile	1.6	0.2	--	--	--	--
HOT	2015	Spring	HMW UDOM	850	Leu	3.0	0.3	6.5	0.6	0.07	0.006
HOT	2015	Spring	HMW UDOM	850	Phe	1.7	0.2	9.4	1.0	0.10	0.010
HOT	2015	Spring	HMW UDOM	850	Pro	4.4	0.4	--	--	--	--
HOT	2015	Spring	HMW UDOM	850	Ser	7.6	0.8	28.4	0.3	0.40	0.003
HOT	2015	Spring	HMW UDOM	850	Thr	4.3	0.4	--	--	--	--
HOT	2015	Spring	HMW UDOM	850	Val	2.4	0.2	7.4	1.3	0.08	0.014
HOT	2015	Spring	HMW UDOM	2500	Ala	14.0	1.4	43.0	0.5	0.75	0.005
HOT	2015	Spring	HMW UDOM	2500	Asp	21.7	2.2	24.2	1.1	0.32	0.011
HOT	2015	Spring	HMW UDOM	2500	Glu	13.2	1.3	17.5	0.6	0.21	0.006
HOT	2015	Spring	HMW UDOM	2500	Gly	22.8	2.3	--	--	--	--
HOT	2015	Spring	HMW UDOM	2500	Ile	1.8	0.2	--	--	--	--
HOT	2015	Spring	HMW UDOM	2500	Leu	4.7	0.5	5.5	0.6	0.06	0.007
HOT	2015	Spring	HMW UDOM	2500	Phe	3.3	0.3	8.7	1.0	0.10	0.010
HOT	2015	Spring	HMW UDOM	2500	Pro	5.2	0.5	--	--	--	--
HOT	2015	Spring	HMW UDOM	2500	Ser	7.4	0.7	27.8	0.3	0.39	0.003
HOT	2015	Spring	HMW UDOM	2500	Thr	3.9	0.4	--	--	--	--
HOT	2015	Spring	HMW UDOM	2500	Val	2.0	0.2	5.4	1.4	0.06	0.014
HOT	2014	Summer	LMW SPE-DOM	7.5	Ala	12.2	1.2	24.4	0.5	0.32	0.005
HOT	2014	Summer	LMW SPE-DOM	7.5	Asp	14.5	1.5	15.1	1.2	0.18	0.012
HOT	2014	Summer	LMW SPE-DOM	7.5	Glu	11.2	1.1	11.5	0.6	0.13	0.006
HOT	2014	Summer	LMW SPE-DOM	7.5	Gly	19.6	2.0	--	--	--	--
HOT	2014	Summer	LMW SPE-DOM	7.5	Ile	4.2	0.4	--	--	--	--
HOT	2014	Summer	LMW SPE-DOM	7.5	Leu	6.5	0.7	10.1	0.6	0.11	0.006
HOT	2014	Summer	LMW SPE-DOM	7.5	Phe	4.4	0.4	10.9	1.0	0.12	0.010
HOT	2014	Summer	LMW SPE-DOM	7.5	Pro	7.6	0.8	--	--	--	--
HOT	2014	Summer	LMW SPE-DOM	7.5	Ser	8.9	0.9	17.7	0.3	0.21	0.003
HOT	2014	Summer	LMW SPE-DOM	7.5	Thr	5.7	0.6	--	--	--	--
HOT	2014	Summer	LMW SPE-DOM	7.5	Val	5.3	0.5	10.2	1.3	0.11	0.013
HOT	2014	Summer	LMW SPE-DOM	400	Ala	15.0	1.5	30.1	0.5	0.43	0.005
HOT	2014	Summer	LMW SPE-DOM	400	Asp	14.1	1.4	23.3	1.1	0.30	0.011
HOT	2014	Summer	LMW SPE-DOM	400	Glu	7.7	0.8	18.8	0.6	0.23	0.006
HOT	2014	Summer	LMW SPE-DOM	400	Gly	28.2	2.8	--	--	--	--
HOT	2014	Summer	LMW SPE-DOM	400	Ile	4.0	0.4	--	--	--	--
HOT	2014	Summer	LMW SPE-DOM	400	Leu	5.5	0.5	18.2	0.6	0.22	0.006
HOT	2014	Summer	LMW SPE-DOM	400	Phe	2.3	0.2	12.1	0.9	0.14	0.010

location	year	season	sample type	depth (m)	amino acid	Mol%	±	%D	±	D/L	±
HOT	2014	Summer	LMW SPE-DOM	400	Pro	6.3	0.6	--	--	--	--
HOT	2014	Summer	LMW SPE-DOM	400	Ser	7.6	0.8	27.6	0.3	0.38	0.003
HOT	2014	Summer	LMW SPE-DOM	400	Thr	3.7	0.4	--	--	--	--
HOT	2014	Summer	LMW SPE-DOM	400	Val	5.6	0.6	16.7	1.3	0.20	0.013
HOT	2014	Summer	LMW SPE-DOM	850	Ala	16.9	1.7	31.3	0.5	0.46	0.005
HOT	2014	Summer	LMW SPE-DOM	850	Asp	6.4	0.6	21.0	1.1	0.27	0.012
HOT	2014	Summer	LMW SPE-DOM	850	Glu	6.9	0.7	18.7	0.6	0.23	0.006
HOT	2014	Summer	LMW SPE-DOM	850	Gly	31.8	3.2	--	--	--	--
HOT	2014	Summer	LMW SPE-DOM	850	Ile	4.3	0.4	--	--	--	--
HOT	2014	Summer	LMW SPE-DOM	850	Leu	7.2	0.7	14.3	0.6	0.17	0.006
HOT	2014	Summer	LMW SPE-DOM	850	Phe	2.8	0.3	6.5	1.0	0.07	0.010
HOT	2014	Summer	LMW SPE-DOM	850	Pro	9.6	1.0	--	--	--	--
HOT	2014	Summer	LMW SPE-DOM	850	Ser	3.7	0.4	30.8	0.3	0.45	0.003
HOT	2014	Summer	LMW SPE-DOM	850	Thr	4.0	0.4	--	--	--	--
HOT	2014	Summer	LMW SPE-DOM	850	Val	6.3	0.6	15.2	1.3	0.18	0.013
HOT	2014	Summer	LMW SPE-DOM	2500	Ala	13.1	1.3	30.7	0.5	0.44	0.005
HOT	2014	Summer	LMW SPE-DOM	2500	Asp	14.8	1.5	18.1	1.2	0.22	0.012
HOT	2014	Summer	LMW SPE-DOM	2500	Glu	14.9	1.5	18.1	0.6	0.22	0.006
HOT	2014	Summer	LMW SPE-DOM	2500	Gly	25.9	2.6	--	--	--	--
HOT	2014	Summer	LMW SPE-DOM	2500	Ile	3.7	0.4	--	--	--	--
HOT	2014	Summer	LMW SPE-DOM	2500	Leu	6.1	0.6	16.3	0.6	0.20	0.006
HOT	2014	Summer	LMW SPE-DOM	2500	Phe	3.1	0.3	9.7	1.0	0.11	0.010
HOT	2014	Summer	LMW SPE-DOM	2500	Pro	6.8	0.7	--	--	--	--
HOT	2014	Summer	LMW SPE-DOM	2500	Ser	3.0	0.3	18.3	0.3	0.22	0.003
HOT	2014	Summer	LMW SPE-DOM	2500	Thr	3.4	0.3	--	--	--	--
HOT	2014	Summer	LMW SPE-DOM	2500	Val	5.2	0.5	17.1	1.3	0.21	0.013
HOT	2015	Spring	LMW SPE-DOM	7.5	Ala	14.0	1.4	35.3	0.5	0.55	0.005
HOT	2015	Spring	LMW SPE-DOM	7.5	Asp	15.3	1.5	35.1	1.1	0.54	0.011
HOT	2015	Spring	LMW SPE-DOM	7.5	Glu	9.8	1.0	19.5	0.6	0.24	0.006
HOT	2015	Spring	LMW SPE-DOM	7.5	Gly	23.4	2.3	--	--	--	--
HOT	2015	Spring	LMW SPE-DOM	7.5	Ile	2.9	0.3	--	--	--	--
HOT	2015	Spring	LMW SPE-DOM	7.5	Leu	6.7	0.7	15.4	0.6	0.18	0.006
HOT	2015	Spring	LMW SPE-DOM	7.5	Phe	4.8	0.5	18.1	0.9	0.22	0.009
HOT	2015	Spring	LMW SPE-DOM	7.5	Pro	7.9	0.8	--	--	--	--
HOT	2015	Spring	LMW SPE-DOM	7.5	Ser	7.6	0.8	35.2	0.3	0.54	0.003
HOT	2015	Spring	LMW SPE-DOM	7.5	Thr	3.4	0.3	--	--	--	--
HOT	2015	Spring	LMW SPE-DOM	7.5	Val	4.1	0.4	13.8	1.3	0.16	0.013
HOT	2015	Spring	LMW SPE-DOM	400	Ala	14.7	1.5	35.4	0.5	0.55	0.005
HOT	2015	Spring	LMW SPE-DOM	400	Asp	17.0	1.7	33.5	1.1	0.50	0.011
HOT	2015	Spring	LMW SPE-DOM	400	Glu	9.8	1.0	21.6	0.6	0.28	0.006
HOT	2015	Spring	LMW SPE-DOM	400	Gly	29.8	3.0	--	--	--	--
HOT	2015	Spring	LMW SPE-DOM	400	Ile	2.2	0.2	--	--	--	--
HOT	2015	Spring	LMW SPE-DOM	400	Leu	4.0	0.4	19.6	0.6	0.24	0.006
HOT	2015	Spring	LMW SPE-DOM	400	Phe	1.8	0.2	16.7	0.9	0.20	0.009
HOT	2015	Spring	LMW SPE-DOM	400	Pro	6.0	0.6	--	--	--	--
HOT	2015	Spring	LMW SPE-DOM	400	Ser	6.9	0.7	32.3	0.3	0.48	0.003
HOT	2015	Spring	LMW SPE-DOM	400	Thr	4.2	0.4	--	--	--	--
HOT	2015	Spring	LMW SPE-DOM	400	Val	3.6	0.4	18.1	1.2	0.22	0.013
HOT	2015	Spring	LMW SPE-DOM	850	Ala	14.0	1.4	29.0	0.5	0.41	0.005
HOT	2015	Spring	LMW SPE-DOM	850	Asp	14.6	1.5	23.5	1.1	0.31	0.011
HOT	2015	Spring	LMW SPE-DOM	850	Glu	9.3	0.9	15.6	0.6	0.18	0.006
HOT	2015	Spring	LMW SPE-DOM	850	Gly	24.1	2.4	--	--	--	--
HOT	2015	Spring	LMW SPE-DOM	850	Ile	3.4	0.3	--	--	--	--

location	year	season	sample type	depth (m)	amino acid	Mol%	±	%D	±	D/L	±
HOT	2015	Spring	LMW SPE-DOM	850	Leu	6.6	0.7	14.5	0.6	0.17	0.006
HOT	2015	Spring	LMW SPE-DOM	850	Phe	3.4	0.3	11.2	1.0	0.13	0.010
HOT	2015	Spring	LMW SPE-DOM	850	Pro	7.4	0.7	--	--	--	--
HOT	2015	Spring	LMW SPE-DOM	850	Ser	7.6	0.8	22.6	0.3	0.29	0.003
HOT	2015	Spring	LMW SPE-DOM	850	Thr	4.1	0.4	--	--	--	--
HOT	2015	Spring	LMW SPE-DOM	850	Val	5.5	0.5	14.7	1.3	0.17	0.013
HOT	2015	Spring	LMW SPE-DOM	2500	Ala	12.2	1.2	34.4	0.5	0.52	0.005
HOT	2015	Spring	LMW SPE-DOM	2500	Asp	15.1	1.5	32.9	1.1	0.49	0.011
HOT	2015	Spring	LMW SPE-DOM	2500	Glu	8.7	0.9	20.4	0.6	0.26	0.006
HOT	2015	Spring	LMW SPE-DOM	2500	Gly	26.8	2.7	--	--	--	--
HOT	2015	Spring	LMW SPE-DOM	2500	Ile	2.8	0.3	--	--	--	--
HOT	2015	Spring	LMW SPE-DOM	2500	Leu	5.5	0.5	16.8	0.6	0.20	0.006
HOT	2015	Spring	LMW SPE-DOM	2500	Phe	2.3	0.2	13.2	0.9	0.15	0.010
HOT	2015	Spring	LMW SPE-DOM	2500	Pro	6.2	0.6	--	--	--	--
HOT	2015	Spring	LMW SPE-DOM	2500	Ser	13.6	1.4	23.2	0.3	0.30	0.003
HOT	2015	Spring	LMW SPE-DOM	2500	Thr	2.4	0.2	--	--	--	--
HOT	2015	Spring	LMW SPE-DOM	2500	Val	4.4	0.4	18.5	1.2	0.23	0.013

Bibliography

Abdullah, H. A., Burdige, D. J., Komada, T., 2017. Accumulation of deaminated peptides in anoxic sediments of the Santa Barbara basin. Geochimica et Cosmochimca Acta 223, 245-258.

Alkhatib, M., Schubert, C. J., del Giorgio, P. A., Gelinas, Y. and Lehmann, M. F., 2012. Organic matter reactivity indicators in sediments of the St. Lawrence Estuary. Estuary, Coastal, and Shelf Science 102-103, 36–47.

Aluwihare, L. I., Meador, T., 2008. Chemical composition of marine dissolved organic nitrogen, in: Capone, D. G., Bronk, D. A., Mulholland, M. R., Carpenter, E. J. (Eds.), Nitrogen in the Marine Environment, 95–140.

Aluwihare, L. I., Repeta, D. J. and Pantoja, S., 2005. Two chemically distinct pools of organic nitrogen accumulate in the ocean. Science 308, 1007–1010.

Aluwihare, L. I., Repeta, D. J., Chen, R. F., 1997. A major biopolymeric component to dissolved organic carbon in surface sea water. Nature 387, 166–169.

Amador, J. A., Milne, P. J., Moore, C. A., Zika, R. G., 1990. Extraction of chromophoric humic substances from seawater. Marine Chemistry 29, 1–17.

Amon, R. M. W., Benner, R., 1996. Bacterial utilization of different size classes of dissolved organic matter. Limnology and Oceanography 41, 41–51.

Amon, R. M. W., Benner, R., 1994. Rapid cycling of high-molecular-weight dissolved organic matter in the ocean. Nature 369, 549–552.

Arrieta, J. M., Mayol, E., Hansman, R. L., Herndl, G. J., Dittmar, T., Duarte, C. M., 2015. Dilution limits dissolved organic carbon utilization in the deep ocean. Science 348, 331–333.

Batista, F. C., Ravelo, A. C., Crusius, J., Casso, M. A., McCarthy, M. D., 2014, Compound specific amino acid $\delta^{15}N$ in marine sediments: a new approach for studies of the marine nitrogen cycle. Geochimica et Cosmochimica Acta 142, 553–569.

Bauer, J. E., Williams, P.M., Druffel, E., 1992. C-14 activity of dissolved organic carbon fractions in the north-central Pacific and Sargasso Sea. Nature 357, 667–670.

Beaupré, S. R., Druffel, E. R. M., 2009. Constraining the propagation of bomb-radiocarbon through the dissolved organic carbon (DOC) pool in the northeast Pacific Ocean. Deep-Sea Research Part I – Oceanography Research Papers 56, 1717–1726.

Beaupré, S. R., Druffel, E. R. M., Griffin, S., 2007. A low-blank photochemical extraction system for concentration and isotopic analyses of marine dissolved organic carbon. Limnology and Oceanography Methods 5, 174–184.

Benner, R., Amon, R. M. W., 2015. The size-reactivity continuum of major bioelements in the ocean. Annual Reviews of Marine Science 7, 185–205.

Benner, R., 2002. Chemical composition and reactivity, in: Hansel, D.A., Carlson, C.A. (Eds.), The Biogeochemistry of Marine Dissolved Organic Matter. Academic Press, pp. 59–87.

Benner, R. and Ziegler, S., 1999. Do photochemical transformations of dissolved organic matter produce biorefractory as well as bioreactive substrates. in: Bell, C.R., Brylinsky, M., Johnson-Green, P. (Eds.), Microbial Biosystems: New Frontiers. Proceedings of the 8th International Symposium on Microbial Ecology. Atlantic Canada Society for Microbial Ecology, Halifax, pp 181-192.

Benner, R., Biddanda, B., Black, B., McCarthy, M. D., 1997. Abundance, size distribution, and stable carbon and nitrogen isotopic compositions of marine organic matter isolated by tangential-flow ultrafiltration. Marine Chemistry 57, 243–263.

Benner R., Bodungen, V. B., Farrington, J., Hedges, J., Lee, C., Mantoura, F., Suzuki, Y., Williams, P. M., 1993. Measurement of dissolved organic carbon and nitrogen in natural waters: Workshop report. Marine Chemistry 41, 5–10.

Benner, R., Pakulski, J. D., McCarthy, M. D., Hedges, J. I., Hatcher, P. G., 1992. Bulk chemical characteristics of dissolved organic matter in the ocean. Science 255, 1561–1564.

Bercovici, S. K., McNichol, A. P., Xu, L. and Hansell, D. A., 2018. Radiocarbon Content of Dissolved Organic Carbon in the South Indian Ocean. Geophysical Research Letters 45, 872–879.

Broek, T. A. B., Bour, A. L., Ianiri, H. L., Guilderson, T. P., McCarthy, M. D., 2019. Amino acid enantiomers in old and young dissolved organic matter: implications for a microbial nitrogen pump. Geochimica et Cosmochimica Acta 247, 207–219.

Broek, T. A. B., Walker, B. D., Guilderson, T. P., McCarthy, M. D., 2017. Coupled ultrafiltration and solid phase extraction approach for the targeted study of semi-labile high molecular weight and refractory low molecular weight dissolved organic matter. Marine Chemistry 194, 146-157.

Broek, T. A. B., McCarthy, M.D., 2014. A new approach to $\delta^{15}N$ compound-specific amino acid trophic position measurements: preparative high pressure liquid chromatography technique for purifying underivatized amino acids for stable isotope analysis. Limnology and Oceanography; Methods 12, 840-852.

Broek, T. A. B., Walker, B. D., Andreasen, D. H, McCarthy, M. D., 2013. High-precision measurement of phenylalanine δ15N values for environmental samples: A new approach coupling high-pressure liquid chromatography purification and elemental analyzer isotope ratio mass spectrometry. Rapid Communications in Mass Spectrometry 27, 2327- 2337.

Bronk, D. A., See, J. H., Bradley, P. and Killberg, L., 2007. DON as a source of bioavailable nitrogen for phytoplankton. Biogeosciences 4, 283–296.

Buesseler, K. O., Lamborg, C. H., Boyd, P. W., Lam, P. J., Trull, T. W., Bidigare, R. R., Bishop, J. K. B., Casciotti, K. L., Dehairs, F., Elskens, M., Honda, M., Karl, D. M., Siegel, D. A., Silver, M. W., Steinberg, D. K., Valdes, J., Van Mooy, B. and Wilson, S., 2007. Revisiting Carbon Flux Through the Ocean's Twilight Zone. Science 316, 567–570.

Calleja, M. L., Peacock, M., Kudela, R. and Batista, F. C., 2013. Changes in compound specific $\delta^{15}N$ amino acid signatures and d/l ratios in marine dissolved organic matter induced by heterotrophic bacterial reworking. Marine Chemistry 149, 32–44.

Cardoza, L. A., Korir, A. K., Otto, W. H., Wurrey, C. J. & Larive, C. K., 2004. Applications of NMR spectroscopy in environmental science. Progress in Nuclear Magnetic Resonance Spectroscopy 45, 209–238.

Carlson, C. A., Hansell, D. A., 2014. DOM sources, sinks, reactivity, and budgets, in: Hansel, D. A., Carlson, C. A. (Eds.), The Biogeochemistry of Marine Dissolved Organic Matter. Academic Press, pp. 65–126.

Carstens, D., Schubert, C. J., 2012. Amino acid and amino sugar transformation during sedimentation in lacustrine systems. Organic Geochemistry 50, 26–35.

Carstens, D., Köllner, K. E., Bürgmann, H., Wehrli, B. Schubert, C. J., 2012. Contribution of bacterial cells to lacustrine organic matter based on amino sugars and d-amino acids. Geochimica et Cosmochimica Acta 89, 159–172.

Chen, M., Kim, S., Park, J. E., Jung, H. J., Hur, J., 2016. Structural and compositional changes of dissolved organic matter upon solid-phase extraction tracked by multiple analytical tools. Analytical and Bioanalytical Chemistry 408, 6249–6258.

Chin, W. C., Orellana, M. V., Verdugo, P., 1998. Spontaneous assembly of marine dissolved organic matter into polymer gels. Nature 391, 568–572.

Coppola, A. I., Walker, B. D., Druffel, E. R. M., 2015. Solid phase extraction method for the study of black carbon cycling in dissolved organic carbon using radiocarbon. Marine Chemistry 177, 697–705.

Cowie, G. L., Hedges, J. I., 1992. Sources and reactivities of amino acids in a coastal marine environment. Limnology and Oceanography 37, 703–724.

Dauwe, B., Middelburg, J. J., Herman, P. M. J., Heip, C. H. R., 1999. Linking diagenetic alteration of amino acids and bulk organic matter reactivity. Limnology and Oceanography 44, 1809–1814.

Décima, M., Landry, M. R., Popp, B. N., 2013. Environmental perturbation effects on baseline $\delta^{15}N$ values and zooplankton trophic flexibility in the southern California Current Ecosystem. Limnology and Oceanography 58, 624–634.

Décima, M., Landry, M. R., Bradley, C. J., Fogel, M. L., 2017. Alanine $\delta^{15}N$ trophic fractionation in heterotrophic protists. Limnology and Oceanography 62, 2308–2322.

Dittmar, T., 2014. Reasons Behind the Long-Term Stability of Dissolved Organic Matter, in: Hansel, D.A., Carlson, C.A. (Eds.), Biogeochemistry of Marine Dissolved Organic Matter. Academic Press, pp. 369–388.

Dittmar, T., Koch, B., Hertkorn, N., Kattner, G., 2008. A simple and efficient method for the solid-phase extraction of dissolved organic matter (SPE-DOM) from seawater. Limnology and Oceanography Methods 6, 230–235.

Dittmar, T., Stubbins, A., 2014. Dissolved Organic Matter in Aquatic Systems, in: Treatise on Geochemistry. Elsevier, pp. 125–156.

Druffel, E. R. M., Griffin, S., Coppola, A. I., Walker, B. D., 2016. Radiocarbon in dissolved organic carbon of the Atlantic Ocean. Geophysical Research Letters 43, 5279–5286.

Druffel, E. R. M., Griffin, S., Walker, B. D., Coppola, A. I., Glynn, D. S., 2013. Total Uncertainty of Radiocarbon Measurements of Marine Dissolved Organic Carbon and Methodological Recommendations. Radiocarbon 55, 1135–1141.

Druffel, E., Williams, P. M., Bauer, J. E., Ertel, J. R., 1992. Cycling of dissolved and particulate organic-matter in the open ocean. Journal of Geophysical Research 97, 15639–15659.

Eglinton, T.I., Repeta, D.J., 2006. Organic matter in the contemporary ocean, in: Elderfield, H (Ed.), Treatise on Geochemistry, Volume 6: The Oceans and Marine Geochemistry. Elsevier, Amsterdam, pp 145-180.

Flerus, R., Lechtenfeld, O. J., Koch, B. P., McCallister, S. L., Schmitt-Kopplin, P., Benner, R., Kaiser, K., Kattner, G., 2012. A molecular perspective on the ageing of marine dissolved organic matter. Biogeosciences 9, 1935–1955.

Green, N. W., Perdue, E. M., Aiken, G. R., Butler, K. D., Chen, H., Dittmar, T., Niggemann, J., Stubbins, A., 2014. An intercomparison of three methods for the large-scale isolation of oceanic dissolved organic matter. Marine Chemistry 161, 14–19.

Green, S. A., Blough, N. V., 1994. Optical absorption and fluorescence properties of chromophoric dissolved organic matter in natural waters. Limnology and Oceanography 39, 1903–1916.

Grutters, M., van Raaphorst, W., Epping, E., Helder, W., de Leeuw, J. W., Glavin, D. P., Bada J., 2002. Preservation of amino acids from in situ-produced bacterial cell wall peptidoglycans in northeastern Atlantic continental margin sediments. Limnology and Oceanography 47, 1521–1524.

Guo, L., Santschi, P. H., Cifuentes, L. A., Trumbore, S. E., Southon, J., 1996. Cycling of high-molecular-weight dissolved organic matter in the Middle Atlantic Bight as revealed by carbon isotopic (^{13}C and ^{14}C) signatures. Limnology and Oceanography 41, 1242–1252.

Gweon, L. B., Fisher, N. S., 1992. Degradation and elemental release rates from phytoplankton debris and their geochemical implications. Limnology and Oceanography 37, 1345–1360.

Hansell, D. A., 2013. Recalcitrant dissolved organic carbon fractions. Annual Review of Marine Science 5, 421–445.

Hansell, D. A., Carlson, C. A., 2013. Localized refractory dissolved organic carbon sinks in the deep ocean. Global Biogeochemical Cycles 27, 705–710.

Hansell, D. A., Carlson, C. A., Repeta, D. J., Schlitzer, R., 2009. Dissolved organic matter in the ocean: A controversy stimulates new insights. Oceanography 22, 202–211.

Hansman, R. L., Dittmar, T., Herndl, G. J., 2015. Conservation of dissolved organic matter molecular composition during mixing of the deep water masses of the northeast Atlantic Ocean. Marine Chemistry 177, 288–297.

Hayes, J. M., 2001. Fractionation of carbon and hydrogen isotopes in biosynthetic processes. Reviews of Mineral Geochemistry 43, 225–277.

Hedges, J. I., 1992. Global biogeochemical cycles: progress and problems. Marine Chemistry 39, 67–93.

Hedges, J. I., Eglinton, G., Hatcher, P. G., Kirchman, D. L., Arnosti, C., Derenne, S., Evershed, R. P., Kögel-Knabner, I., de Leeuw, J. W., Littke, R., Michaelis, W., Rullkötter, J., 2000. The molecularly-uncharacterized component of nonliving organic matter in natural environments. Organic Geochemistry 31, 945–958.

Hertkorn, N., Harir, M., Koch, B.P., Michalke, B., Schmitt-Kopplin, P., 2013. High-field NMR spectroscopy and FTICR mass spectrometry: powerful discovery tools for the molecular level characterization of marine dissolved organic matter. Biogeosciences 10, 1583–1624.

Hertkorn, N., Benner, R., Frommberger, M., Schmitt-Kopplin, P., Witt, M., Kaiser, K., Kettrup, A., Hedges, J. I., 2006. Characterization of a major refractory component of marine dissolved organic matter. Geochimica et Cosmochimica Acta 70, 2990–3010.

Higgins, M. B., Wolfe-Simon, F., Robinson, R. S., Qin, Y., Saito, M. A., Pearson, A, 2011. Paleoenvironmental implications of taxonomic variation among delta N-15 values of chloropigments. Geochimica et Cosmochimica Acta 75, 7351–7363.

Hwang, J., 2003. Lipid-like material as the source of the uncharacterized organic carbon in the ocean? Science 299, 881–884.

Ingalls, A. E., Shah, S. R., Hansman, R. L., Aluwihare, L. I., Santos, G. M., Druffel, E. R. M., Pearson, A., 2006. Quantifying archaeal community autotrophy in the mesopelagic ocean using natural radiocarbon. Proceedings of the National Academy of Sciences 103, 6442-6447.

Jiao, N., Herndl, G. J., Hansell, D. A., Benner, R., Kattner, G., Wilhelm, S. W., Kirchman, D. L., Weinbauer, M. G., Luo, T., Chen, F., Azam, F., 2010. Microbial production of recalcitrant dissolved organic matter: long-term carbon storage in the global ocean. Nature Publishing Group 8, 593–599.

Jørgensen, N. O. G., Engel, P., Jellison, R., Hollibaugh, J. T., 2008. Contribution of Bacterial Cell Wall Components to DOM in Alkaline, Hypersaline Mono Lake, California. Geomicrobiology Journal 25, 38–55.

Jørgensen, L., Lechtenfeld, O. J., Benner, R., Middelboe, M., Stedmon, C. A., 2014. Production and transformation of dissolved neutral sugars and amino acids by bacteria in seawater. Biogeosciences 11, 5349–5363.

Kaiser, K., Benner, R., 2012. Organic matter transformations in the upper mesopelagic zone of the North Pacific: Chemical composition and linkages of microbial community structure. Journal of Geophysical Research 117, C01023.

Kaiser, K., Benner, R., 2009. Biochemical composition and size distribution of organic matter at the Pacific and Atlantic time-series stations. Marine Chemistry 113, 63–77.

Kaiser, K., Benner, R., 2008. Major bacterial contribution to the ocean reservoir of detrital organic carbon and nitrogen. Limnology and Oceanography 53, 99–112.

Kaiser, K., Benner, R., 2005. Hydrolysis-induced racemization of amino acids. Limnology and Oceanography - Methods 3, 318–325.

Kilduff, J., Weber, W. J., Jr, 1992. Transport and separation of organic macromolecules in ultrafiltration processes. Environmental Science and Technology 26, 569–577.

Kirchman, D. L., 2004. A Primer on Dissolved Organic Material and Heterotrophic Prokaryotes in the Oceans, in: The Ocean Carbon Cycle and Climate. Springer, Dordrecht, Dordrecht. pp. 31–63.

Kitayama, K., Hama, T., Yanagi, K., 2007. Bioreactivity of peptidoglycan in seawater. Aquatic Microbial Ecology 46, 85–93.

Knapp, A. N., Casciotti, K. L. & Prokopenko, M. G., 2018. Dissolved Organic Nitrogen Production and Consumption in Eastern Tropical South Pacific Surface Waters. Global Biogeochemical Cycles 32, 769–783.

Knapp, A. N., Sigman, D. M., Kustka, A. B., Sañudo-Wilhelmy, S. A., Capone, D. G., 2012. The distinct nitrogen isotopic compositions of low and high molecular weight marine DON. Marine Chemistry 136-137, 24–33.

Knapp, A. N., Sigman, D. M., Lipschultz, F., Kustka, A. B., Capone, D. G., 2011. Interbasin isotopic correspondence between upper-ocean bulk DON and subsurface nitrate and its implications for marine nitrogen cycling. Global Biogeochemical Cycles 25, 4004.

Knicker, H., 2010. 'Black nitrogen' – an important fraction in determining the recalcitrance of charcoal. Organic Geochemistry 41, 947–950.

Knicker, H., 2007. How does fire affect the nature and stability of soil organic nitrogen and carbon? A review. Biogeochemistry 85, 91–118.

Knicker, H., 2004. Stabilization of N-compounds in soil and organic-matter-rich sediments—what is the difference? Marine Chemistry 92, 167–195.

Knicker, H., Scaroni, A. W. & Hatcher, P. G., 1996. ^{13}C and ^{15}N NMR spectroscopic investigation on the formation of fossil algal residues. Organic Geochemistry 24, 661–669.

Knicker, H., Fründ, R. & Lüdemann, H. D., 1993. The chemical nature of nitrogen in native soil organic matter. Naturwissenschaften 80, 219–221.

Koch, B. P., Witt, M., Engbrodt, R., Dittmar, T. and Kattner, G., 2005. Molecular formulae of marine and terrigenous dissolved organic matter detected by electrospray ionization Fourier transform ion cyclotron resonance mass spectrometry. Geochimica et Cosmochimica Acta 69, 3299–3308.

Koprivnjak, J. F., Pfromm, P. H., Ingall, E., Vetter, T. A., Schmitt-Kopplin, P., Hertkorn, N., Frommberger, M., Knicker, H., Perdue, E. M., 2009. Chemical and spectroscopic characterization of marine dissolved organic matter isolated using coupled reverse osmosis–electrodialysis. Geochimica et Cosmochimica Acta 73, 4215–4231.

Lechtenfeld, O. J., Hertkorn, N., Shen, Y., Witt, M., Benner, R., 2015. Marine sequestration of carbon in bacterial metabolites. Nature Communications 6, 6711.

Lechtenfeld, O. J., Kattner, G., Flerus, R., 2014. Molecular transformation and degradation of refractory dissolved organic matter in the Atlantic and Southern Ocean. Geochimica et Cosmochimica Acta 126, 321–337.

Lee, C., Wakeham, S. G., Hedges, J. I., 2000. Composition and flux of particulate amino acids and chloropigments in equatorial Pacific seawater and sediments. Deep-Sea Research Part I 47, 1535–1568.

Lehmann, M. F., Bernasconi, S. M., Barbieri, A., McKenzie, J. A., 2002. Preservation of organic matter and alteration of its carbon and nitrogen isotope composition during simulated and in situ early sedimentary diagenesis. Geochimica et Cosmochimica Acta 66, 3573–3584.

Li, S., Zhang, Y., Hong, M., 2010. 3D ^{13}C–^{13}C–^{13}C correlation NMR for de novo distance determination of solid proteins and application to a human A-defensin. Journal of Magnetic Resonance 202, 203–210.

Li, Y., Harir, M., Lucio, M., Kanawati, B., Smirnov, K., Flerus, R., Koch, B. P., Schmitt-Kopplin, P., Hertkorn, N., 2016. Proposed Guidelines for Solid Phase Extraction of Suwannee River Dissolved Organic Matter. Analytical Chemistry 88, 6680–6688.

Loh, A. N., Bauer, J. E., Druffel, E. R. M., 2004. Variable ageing and storage of dissolved organic components in the open ocean. Nature 430, 877–881.

Maie, N., Parish, K. J., Watanabe, A., Knicker, H., Benner, R., Abe, T., Kaiser, K., Jaffé, R., 2006. Chemical characteristics of dissolved organic nitrogen in an oligotrophic subtropical coastal ecosystem. Geochimica et Cosmochimica Acta 70, 4491-4506.

Mao, J., Kong, X., Schmidt-Rohr, K., Pignatello, J. J., Perdue E. M., 2012. Advanced solid-state NMR characterization of marine dissolved organic matter isolated using the coupled reverse osmosis/electrodialysis method. Environmental Science and Technology 46, 5806–5814.

McCarthy, M. D., Beaupré, S. R., Walker, B. D., Voparil, I., Guilderson, T. P., Druffel, E. R. M., 2010. Chemosynthetic origin of ^{14}C-depleated dissolved organic matter in a ridge-flank hydrothermal system. Nature Geoscience 3, 1–5.

McCarthy, M. D., Bronk, D. A., 2008. Analytical methods for the study of nitrogen, in: Capone, D. G., Bronk, D. A., Mulholland, M. R., Carpenter, E. J. (Eds.), Nitrogen in the Marine Environment. Elsevier, pp. 1219–1275.

McCarthy, M. D., Benner, R., Lee, C., Fogel, M. L., 2007. Amino acid nitrogen isotopic fractionation patterns as indicators of heterotrophy in plankton, particulate, and dissolved organic matter. Geochimica et Cosmochimica Acta 71, 4727–4744.

McCarthy, M. D., Benner, R., Lee, C., Hedges, J. I., Fogel, M. L., 2004. Amino acid carbon isotopic fractionation patterns in oceanic dissolved organic matter: an unaltered photoautotrophic source for dissolved organic nitrogen in the ocean? Marine Chemistry 92, 123–134.

McCarthy, M. D., Hedges, J. I., Benner, R., 1998. Major bacterial contribution to marine dissolved organic nitrogen. Science 281, 231–234.

McCarthy, M. D., Pratum, T., Hedges,, J. I., Benner, R., 1997. Chemical composition of dissolved organic nitrogen in the ocean. Nature 390, 150–154.

McCarthy, M., Hedges, J., Benner, R., 1996. Major biochemical composition of dissolved high molecular weight organic matter in seawater. Marine Chemistry 55, 281–297.

McCarthy, M. D., Hedges, J. I., Benner, R., 1993. The chemical composition of dissolved organic matter in seawater. Chemical Geology 107, 503–507.

Medeiros, P. M., Seidel, M., Powers, L. C., Dittmar, T., Hansell, D. A., Miller, W. L., 2015a. Dissolved organic matter composition and photochemical transformations in the northern North Pacific Ocean. Geophysical Research Letters 42, 863–870.

Medeiros, P. M., Seidel, M., Ward, N. D., Carpenter, E. J., Gomes, H. R., Niggemann, J., Krusche, A. V., Richey, J. E., Yager, P. L., Dittmar, T., 2015b. Fate of the Amazon River dissolved organic matter in the tropical Atlantic Ocean. Global Biogeochemical Cycles 29, 677–690.

Moore, C. M., Mills, M. M., Arrigo, K. R., Berman-Frank, I., Bopp, L., Boyd, P. W., Galbraith, E. D., Geider, R. J., Guieu, C., Jaccard, S. L., Jickells, T. D., La Roche, J., Lenton, T. M., Mahowald, N. M., Marañón, E., Marinov, I., Moore, J. K., Nakatsuka, T., Oschlies, A., Saito, M. A., Thingstad, T. F., Tsuda, A., Ulloa, O., 2013. Processes and patterns of oceanic nutrient limitation. Nature Geoscience 6, 701–710.

Mopper, K., Stubbins, A., Ritchie, J. D., Bialk, H. M., Hatcher, P. G., 2007. Advanced instrumental approaches for characterization of marine dissolved organic matter: extraction techniques, mass spectrometry, and nuclear magnetic resonance spectroscopy. Chemistry Reviews 107, 419–442.

Mortazavi, B., Chanton, J. P., 2004. Use of Keeling plots to determine sources of dissolved organic carbon in nearshore and open ocean systems. Limnology and Oceangraphy 49, 102-108.

Nagata, T., Kirchman, D.L., 1999. Bacterial mortality: A pathway for the formation of refractory DOM, in: Bell, C.R., Brylinsky, M., Johnson-Green, P. (Eds.), Microbial Biosystems: New Frontiers. Proceedings of the 8th International Symposium on Microbial Ecology. Atlantic Canada Society for Microbial Ecology, Halifax, pp 153-158.

Nagata, T., Meon, B., L Kirchman, D., 2003. Microbial degradation of peptidoglycan in seawater. Limnology and Oceanography 48, 745–754.

Niggemann, J., Lomstein, B. A., Schubert, C. J., 2018. Diagenesis of amino compounds in water column and sediment of Lake Baikal. Org Geochem 115, 67–77.

Ogawa, H., 2001. Production of Refractory Dissolved Organic Matter by Bacteria. Science 292, 917–920.

Ohkouchi, N. & Takano, Y., 2014. Organic Nitrogen: Sources, Fates, and Chemistry. Treatise on Geochemistry 251–289.

Olsen, A., Key, R. M., van Heuven, S., Lauvset, S. K., Velo, A., Lin, X., Schirnick, C., Kozyr, A., Tanhua, T., Hoppema, M., Jutterström, S., Steinfeldt, R., Jeansson, E., Ishii, M., Pérez, F. F., Suzuki, T., 2016. The Global Ocean Data Analysis Project version 2 (GLODAPv2) - an internally consistent data product for the world ocean, Earth System Science Data 8, 297-323.

Orellana, M. V., Hansell, D. A., 2012. Ribulose-1,5-bisphosphate carboxylase/oxygenase (RuBisCO): A long-lived protein in the deep ocean. Limnology and Oceanography 57, 826–834.

Pèrez, M. T., Pausz, C., Herndl G. J., 2003. Major shift in bacterioplankton utilization of enantiomeric amino acids between surface waters and the ocean's interior. Limnology and Oceanography 48, 755–763.

Radkov, A. D., Moe, L. A., 2014. Bacterial synthesis of d-amino acids. Applied Microbiology and Biotechnology 98, 5363–5374.

Repeta, D. J., 2014. Chemical Characterization and Cycling of Dissolved Organic Matter, in: Hansel, D.A., Carlson, C.A. (Eds.), The Biogeochemistry of Marine Dissolved Organic Matter. Academic Press, pp. 21–63.

Repeta, D. J., Aluwihare, L. I., 2006. Radiocarbon analysis of neutral sugars in high-molecular-weight dissolved organic carbon: Implications for organic carbon cycling. Limnology and Oceanography 51, 1045–1053.

Roland, L. A., McCarthy, M. D., Peterson, T. D., Walker, B. D., 2009. A large-volume microfiltration system for isolating suspended particulate organic matter: fabrication and assessment versus GFF filters in central North Pacific. Limnology and Oceanography: Methods 7, 64–80.

Osterholz, H., Kirchman, D. L., Niggemann, J., Dittmar, T., 2016. Environmental Drivers of Dissolved Organic Matter Molecular Composition in the Delaware Estuary. Frontiers in Earth Science 4, 231.

Sachs, J. P., Repeta, D. J. & Goericke, R., 1999. Nitrogen and carbon isotopic ratios of chlorophyll from marine phytoplankton. Geochimica et Cosmochimica Acta 63, 1431–1441.

Sannigrahi, P., Ingall, E. D., Benner, R., 2005. Cycling of dissolved and particulate organic matter at station aloha: insights from ^{13}C NMR spectroscopy coupled with elemental, isotopic and molecular analyses. Deep-Sea Research Part I 52, 1429–1444.

Santos, G. M., Southon, J. R., Griffin, S., Beaupré, S. R., Druffel, E. R. M., 2007. Ultra small-mass AMS ^{14}C sample preparation and analyses at KCCAMS/UCI Facility. Nuclear Instrumental Methods in Physical Research Section B: Beam Interactions with Materials and Atoms 259, 293–302.

Santschi, P. H., Guo, L., Baskaran, M., Trumbore, S., Southon, J., Bianchi, T. S., Honeyman, B., Cifuentes, L., 1995. Isotopic evidence for the contemporary origin of high-molecular weight organic matter in oceanic environments. Geochimica et Cosmochimica Acta 59, 625–631.

Schleifer, K. H., Kandler, O., 1972. Peptidoglycan types of bacterial cell walls and their taxonomic implications. Bacteriological Reviews 36, 407.

Schwede-Thomas, S. B., Chin, Y. P., Dria, K. J., Hatcher, P., Kaiser, E., Sulzberger, B., 2005. Characterizing the properties of dissolved organic matter isolated by XAD and C-18 solid phase extraction and ultrafiltration. Aquatic Science 67, 61–71.

Silfer, J. A., Engel, M. H. & Macko, S. A., 1992. Kinetic fractionation of stable carbon and nitrogen isotopes during peptide-bond hydrolysis - experimental-evidence and geochemical implications. Chemical Geology 101, 211–221.

Silfer, J. A., Engel, M. H., Macko, S. A., Jumeau, E. J., 1991. Stable carbon isotope analysis of amino acid enantiomers by conventional isotope ratio mass spectrometry and combined gas chromatography/isotope ratio mass spectrometry. Analytical Chemistry 63, 370–374.

Simjouw, J. P., Minor, E. C., Mopper, K., 2005. Isolation and characterization of estuarine dissolved organic matter: Comparison of ultrafiltration and C18 solid-phase extraction techniques. Marine Chemistry 96, 219–235.

Simon, M., Alldredge, A. L., Azam, F., 1990. Bacterial carbon dynamics on marine snow. Marine Ecology Progress Series 65, 205–211.

Sipler, R. E., Bronk, D. A., 2014. Dynamics of dissolved organic nitrogen, in: Hansel, D.A., Carlson, C.A. (Eds.), The Biogeochemistry of Marine Dissolved Organic Matter. Academic Press, pp. 128–232.

Smernik, R. J. & Baldock, J. A., 2005. Does Solid-state ^{15}N NMR Spectroscopy Detect all Soil Organic Nitrogen? Biogeochemistry 75, 507–528.

Smith, D. C., Simon, M., Alldredge, A. L., Azam, F., 1992. Intense hydrolytic enzyme activity on marine aggregates and implications for rapid particle dissolution. Nature 359, 139–142.

Stubbins, A., Niggemann, J., Dittmar, T., 2012. Photo-lability of deep ocean dissolved black carbon. Biogeosciences 9, 1661-1670.

Stuiver, M., Polach, H. A., 1977. Discussion reporting of ^{14}C data. Radiocarbon 19, 355–363.

Takano, Y., Kashiyama, Y., Ogawa, N. O., Chikaraishi, Y., Ohkouchi, N., 2010. Isolation and desalting with cation-exchange chromatography for compound-specific nitrogen isotope analysis of amino acids: application to biogeochemical samples. Rapid Communications in Mass Spectrometry 24, 2317–2323.

Town, R. M., Powell, H., 1993. Limitations of XAD resins for the isolation of the noncolloidal humic fraction in soil extracts and aquatic samples. Analytical Chimica Acta 271, 195–202.

Tremblay, L., Benner, R., 2006. Microbial contributions to N-immobilization and organic matter preservation in decaying plant detritus. Geochimica et Cosmochimica Acta 70, 133–146.

Verdugo, P., Alldredge, A. L., Azam, F., Kirchman, D. L., Passow, U., Santschi, P. H., 2004. The oceanic gel phase: a bridge in the DOM–POM continuum. Marine Chemistry 92, 67–85.

Vetter, T. A., Perdue, E. M., Ingall, E., Koprivnjak, J. F., Pfromm, P. H., 2007. Combining reverse osmosis and electrodialysis for more complete recovery of dissolved organic matter from seawater. Separation and Purification Technology 56, 383–387.

Vetter, T. A., Perdue, E. M., Ingall, E., Koprivnjak, J. F., Pfromm, P. H., 2007. Combining reverse osmosis and electrodialysis for more complete recovery of dissolved organic matter from seawater. Separation and Purification Technology 56, 383–387.

Vogel, J. S., Southon, J. R., Nelson, D. E., Brown, T. A., 1984. Performance of catalytically condensed carbon for use in accelerator mass-spectrometry. Nuclear Instrumental Methods in Physical Research Section B: Beam Interactions with Materials and Atoms 5, 289–293.

Walker, B. D., Xu, X., 2019. An improved method for the sealed-tube zinc graphitization of microgram carbon samples and ^{14}C AMS measurement. Nuclear Instruments and Methods in Physics Research Section B: Beam Interactions with Materials and Atoms 438, 58-65.

Walker, B. D., Beaupré, S. R., Guilderson, T. P., McCarthy, M. D., Druffel, E. R. M., 2016a. Pacific carbon cycling constrained by organic matter size, age and composition relationships. Nature Geoscience 9, 888-891.

Walker, B. D., Griffin, S., Druffel, E. R. M., 2016b. Effect of acidified versus frozen storage on marine dissolved organic carbon concentration and isotopic composition. Radiocarbon 59, 843-857.

Walker, B. D., Primeau, F. W., Beaupré, S. R., Guilderson, T. P., Druffel, E. R. M., McCarthy, M. D., 2016c. Linked changes in marine dissolved organic carbon molecular size and radiocarbon age. Geophysical Research Letters 43, 10,385–10,393.

Walker, B. D., Guilderson, T. P., Okimura, K. M., 2014. Radiocarbon signatures and size–age–composition relationships of major organic matter pools within a unique California upwelling system. Geochimica et Cosmochimica Acta 126, 1–17.

Walker, B. D., McCarthy, M. D., 2012. Elemental and isotopic characterization of dissolved and particulate organic matter in a unique California upwelling system: Importance of size and composition in the export of labile material. Limnology and Oceanography 57, 1757.

Walker, B. D., Beaupré, S. R., Guilderson, T. P., Druffel, E. R. M., McCarthy, M. D., 2011. Large-volume ultrafiltration for the study of radiocarbon signatures and size vs. age relationships in marine dissolved organic matter. Geochimica et Cosmochimica Acta 75, 5187–5202.

Wang, X. C., Chen, R. F., Whelan, J., Eglinton, L., 2001. Contribution of "old" carbon from natural marine hydrocarbon seeps to sedimentary and dissolved organic carbon pools in the Gulf of Mexico. Geophysical Research Letters 28, 3313–3316.

Williams, P. J. leB., 1995. Evidence for the seasonal accumulation of carbon-rich dissolved organic material, its scale in comparison with changes in particulate material and the consequential effect on net C/N assimilation ratios. Marine Chemistry 51, 17-29.

Williams, P. M., Druffel, E. R. M., 1987. Radiocarbon in dissolved organic matter in the central North Pacific Ocean. Nature 330, 246–248.

Woodward, F. I., 2007. Global primary production. Current Biology 17, R269–R273.

Yamaguchi, Y. T., McCarthy, M. D., 2018. Sources and transformation of dissolved and particulate organic nitrogen in the North Pacific Subtropical Gyre indicated by compound-specific $\delta^{15}N$ analysis of amino acids. Geochimica et Cosmochimica Acta 220, 329–347.

Yamashita, Y., Tanoue, E., 2003. Distribution and alteration of amino acids in bulk DOM along a transect from bay to oceanic waters. Marine Chemistry 82, 145–160.

Zhao, Z., Gonsior, M., Luek, J., Timko, S., Ianiri, H., Hertkorn, N., Schmitt-Kopplin, P., Fang, X., Zeng, Q., Jiao, N., Chen, F., 2017. Picocyanobacteria and deep-ocean fluorescent dissolved organic matter share similar optical properties. Nature Communications 8, 15284.

Zigah, P. K., McNichol, A. P., Xu, L., Johnson, C., Santinelli, C., Karl, D. M., Repeta D. J., 2017. Allochthonous sources and dynamic cycling of ocean dissolved organic carbon revealed by carbon isotopes. Geophysical Research Letters 49, 4421–9.

Ziolkowski, L. A., Druffel, E. R. M., 2010. Aged black carbon identified in marine dissolved organic carbon. Geophysical Research Letters 37, L16601.